NUCLEAR MEDICINE IN THE CONTEXT OF PERSONALIZED MEDICINE

EDITED BY: Françoise Kraeber-Bodéré, Francesco Cicone, Pierre Payoux and Myriam Bernaudin

PUBLISHED IN: Frontiers in Medicine

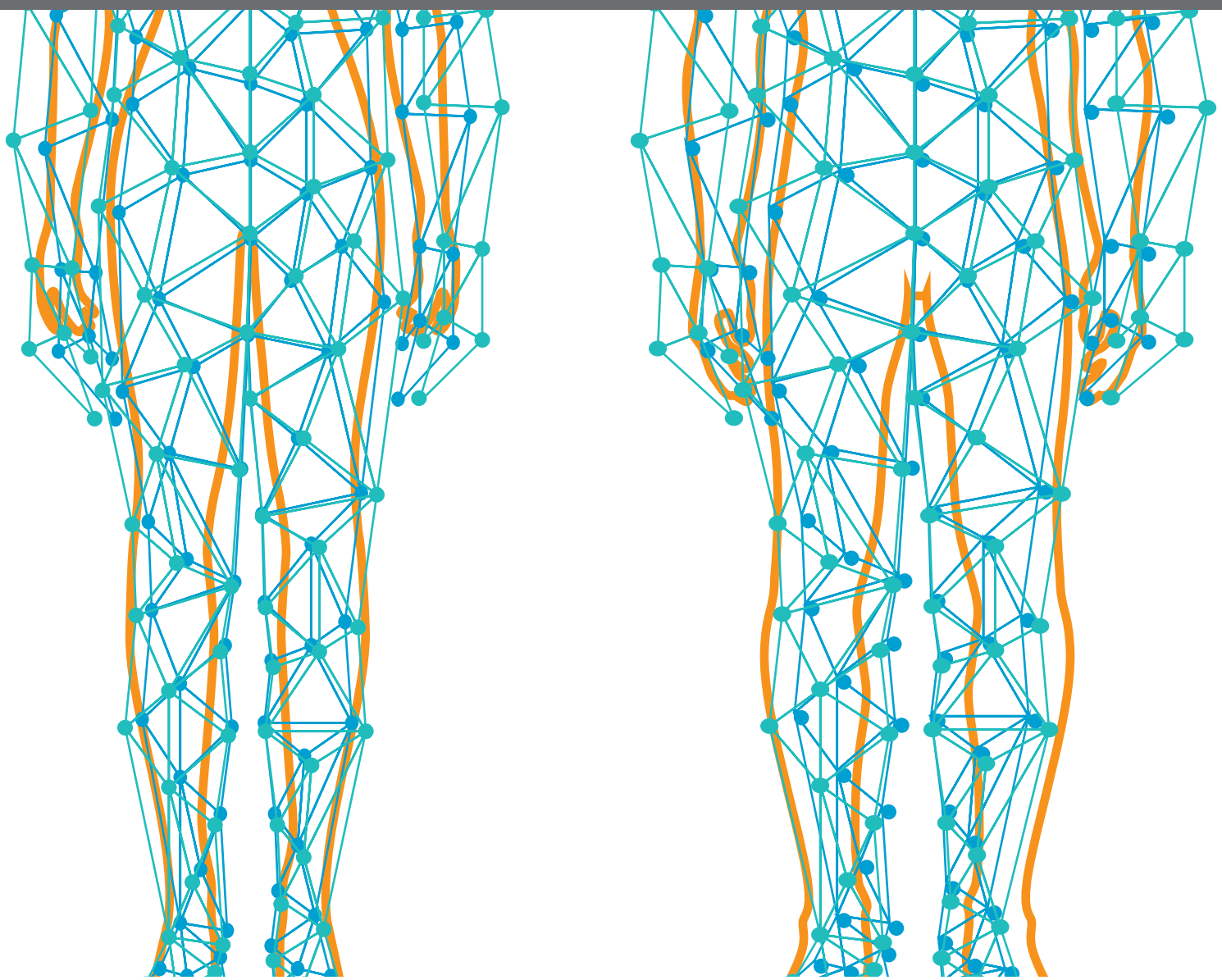

frontiers Research Topics

frontiers

ISSN 1664-8714
ISBN 978-2-88963-861-1
DOI 10.3389/978-2-88963-861-1

About Frontiers

Frontiers is more than just an open-access publisher of scholarly articles: it is a pioneering approach to the world of academia, radically improving the way scholarly research is managed. The grand vision of Frontiers is a world where all people have an equal opportunity to seek, share and generate knowledge. Frontiers provides immediate and permanent online open access to all its publications, but this alone is not enough to realize our grand goals.

Frontiers Journal Series

The Frontiers Journal Series is a multi-tier and interdisciplinary set of open-access, online journals, promising a paradigm shift from the current review, selection and dissemination processes in academic publishing. All Frontiers journals are driven by researchers for researchers; therefore, they constitute a service to the scholarly community. At the same time, the Frontiers Journal Series operates on a revolutionary invention, the tiered publishing system, initially addressing specific communities of scholars, and gradually climbing up to broader public understanding, thus serving the interests of the lay society, too.

Dedication to Quality

Each Frontiers article is a landmark of the highest quality, thanks to genuinely collaborative interactions between authors and review editors, who include some of the world's best academicians. Research must be certified by peers before entering a stream of knowledge that may eventually reach the public - and shape society; therefore, Frontiers only applies the most rigorous and unbiased reviews.
Frontiers revolutionizes research publishing by freely delivering the most outstanding research, evaluated with no bias from both the academic and social point of view. By applying the most advanced information technologies, Frontiers is catapulting scholarly publishing into a new generation.

What are Frontiers Research Topics?

Frontiers Research Topics are very popular trademarks of the Frontiers Journals Series: they are collections of at least ten articles, all centered on a particular subject. With their unique mix of varied contributions from Original Research to Review Articles, Frontiers Research Topics unify the most influential researchers, the latest key findings and historical advances in a hot research area! Find out more on how to host your own Frontiers Research Topic or contribute to one as an author by contacting the Frontiers Editorial Office: researchtopics@frontiersin.org

NUCLEAR MEDICINE IN THE CONTEXT OF PERSONALIZED MEDICINE

Topic Editors:
Françoise Kraeber-Bodéré, Centre de Recherche en Cancérologie Nantes Angers, France
Francesco Cicone, University of Catanzaro, Italy
Pierre Payoux, INSERM U1214 Centre d'Imagerie Neuro Toulouse (ToNIC), France
Myriam Bernaudin, Centre National de la Recherche Scientifique (CNRS), France

Citation: Kraeber-Bodéré, F., Cicone, F., Payoux, P., Bernaudin, M., eds. (2020). Nuclear Medicine in the Context of Personalized Medicine. Lausanne: Frontiers Media SA. doi: 10.3389/978-2-88963-861-1

Table of Contents

frontiers in Medicine

EDITORIAL
published: 09 June 2020
doi: 10.3389/fmed.2020.00252

Editorial: Nuclear Medicine in the Context of Personalized Medicine

Jacques Barbet[1], *Myriam Bernaudin*[2], *Pierre Payoux*[3,4], *Francesco Cicone*[5,6], *Marie-Hélène Gaugler*[7] *and Françoise Kraeber-Bodéré*[8]*

[1] GIP Arronax, Saint-Herblain, France, [2] Université de Normandie, UNICAEN, CEA, CNRS, ISTCT/CERVOxy Group, GIP CYCERON, Caen, France, [3] Service de Médecine Nucléaire, CHU de Toulouse, Toulouse, France, [4] ToNIC, Toulouse NeuroImaging Center, UMR1214 Inserm, Toulouse, France, [5] Department of Experimental and Clinical Medicine, "Magna Graecia" University of Catanzaro, Catanzaro, Italy, [6] Department of Nuclear Medicine and Molecular Imaging, Lausanne University Hospital, Lausanne, Switzerland, [7] Université de Nantes, CNRS, Inserm, CRCINA, Nantes, France, [8] Université de Nantes, CHU de Nantes, ICO Gauducheau, CNRS, Inserm, CRCINA, Nantes, France

Keywords: PET, theranostics, radionuclide therapy, solid tumors, hematological malignancies

Editorial on the Research Topic

Nuclear Medicine in the Context of Personalized Medicine

Nuclear Medicine has been at the heart of theranostics even before the term was coined. It provides effective tools for precision medicine particularly with positron emission tomography (PET), and radioligand therapy. It allows the investigation of phenotypes and functions in all areas of medicine and provides innovative tools to kill cancer cells. This Research Topic for Frontiers in Medicine focuses on the role of Nuclear Medicine in the context of Personalized Medicine.

Three reviews reported the growing interest of PET in onco-hematological diseases. Jamet et al. have demonstrated the interest of 2-[^{18}F]fluoro-2-deoxy-D-glucose ([^{18}F]FDG) PET in the management of patients with multiple myeloma (MM). [^{18}F]FDG-PET is highly sensitive and specific for bone lesions detection at baseline. The presence of extra-medullary disease, the number of bone focal lesions and the maximum standardized uptake value [SUVmax] have independent pejorative prognostic value on progression-free survival and overall survival. For therapy response assessment, [^{18}F]FDG-PET is considered as the reference imaging technique. [^{18}F]FDG-PET and bone marrow flow cytometry are complementary for detection of minimal residual disease before maintenance therapy. New PET tracers such as [^{11}C]methionine, choline or acetate,[^{68}Ga]Ga-pentixafor, which targets CXCR4, and immuno-PET targeting CD138 and CD38, also show promising results.

As discussed by Bailly et al., [^{18}F]FDG-PET changed response assessment and therapy strategy in diffuse large B-cell lymphoma (DLBCL) and Hodgkin lymphoma. [^{18}F]FDG-PET might also have a significant impact in the management of mantle cell lymphoma (MCL). [^{18}F]FDG-PET at baseline in MCL patients has good sensitivity for staging and SUVmax provides prognostic information. They conclude that [^{18}F]FDG-PET results should be integrated in the definition of MCL treatment strategy to identify patients who might benefit from more intensive therapy.

The specificity of [^{18}F]FDG uptake has been questioned. Thus, new tracers such as [^{18}F]Fludarabine, a nucleoside analog, have been developed. Early results with [^{18}F]Fludarabine have been reviewed by Barré et al.. Favorable preclinical results in murine models (follicular and central nervous system lymphoma, MM) have prompted a "first in man" study. In DLBCL patients, increased uptake was observed in sites considered abnormal by CT and [^{18}F]FDG. In chronic lymphocytic leukemia patients, increased uptake coincided with lymph-nodal sites expected to be involved by the disease. [^{18}F]Fludarabine uptake was also high in the spleen and bone marrow. No uptake was observed in the cardiac muscle and brain. They conclude that [^{18}F]Fludarabine might correctly quantify the disease burden, in the presence of confounding inflammatory processes.

Edited and reviewed by:
Ronan Abgral,
Centre Hospitalier Regional Universitaire (CHU) de Brest, France

***Correspondence:**
Françoise Kraeber-Bodéré
francoise.bodere@chu-nantes.fr

Specialty section:
This article was submitted to Nuclear Medicine, a section of the journal Frontiers in Medicine

Received: *27 March 2020*
Accepted: *12 May 2020*
Published: *09 June 2020*

Citation:
Barbet J, Bernaudin M, Payoux P, Cicone F, Gaugler M-H and Kraeber-Bodéré F (2020) Editorial: Nuclear Medicine in the Context of Personalized Medicine. Front. Med. 7:252. doi: 10.3389/fmed.2020.00252

Monoclonal antibody (mAb)-based therapies and immunotherapy have experienced considerable growth in cancer management. Labeled mAbs also show promise for theranostics. While PET can be performed using directly radiolabeled mAbs, pretargeting improves imaging contrast. The development of pretargeted immuno-PET in tumors expressing carcinoembryonic antigen (CEA; CEACAM5) has been reviewed by Bodet-Milin et al., focusing on medullary thyroid carcinoma. They conclude that pretargeted PET imaging has a high potential for antibody-based diagnostics and theranostics.

Immunotherapy relies on *in situ* activation or inhibition of immune cells or on the administration of immune cells selected, activated, or transformed *ex vivo*. It is most important to delineate, by *in vivo* imaging, the distribution, activation and migration of immunologically active cells. Methods designed to monitor the fate of these cells and to define their immunological status have been reviewed by Perrin et al., focusing on cell tracking in cancer immunotherapy, particularly CAR (Chimeric Antigen Receptor) T-cell therapy, and on its potential impact on these new therapeutic modalities.

Severe hypoxia, frequent in glioblastoma multiforme, is associated with resistance to ionizing radiation. It contributes to treatment failures after external-beam radiation therapy (EBRT). It would be logical to deliver higher radiation doses to hypoxic tumor regions. This calls for the delineation of hypoxic zones as examined by Gérard et al. Preliminary *in silico* studies investigate the conversion of hypoxia maps into dose-distribution objectives for EBRT dose painting in view of future clinical trials.

The ability to monitor the distribution of radioactivity inside the body is a major advantage of nuclear medicine procedures. Rhenium-188 (^{188}Re) is an attractive candidate for therapy and has a favorable gamma emission for imaging purposes. It is readily extracted from ^{188}W/^{188}Re generators and exhibits chemical properties similar to those of technetium-99m, which might constitute an additional, purely diagnostic companion radionuclide. The development of radiopharmaceuticals based on ^{188}Re, including peptides, mAbs, and particles has been reviewed by Lepareur et al., demonstrating that ^{188}Re is a cost-effective alternative for routine clinical use.

In neuroscience, carbon-11 or fluorine-18 can be used to label molecules that cross the blood brain barrier, the latter being considered preferable for clinical use. Molecular imaging has focused on receptors, neurotransmitter transporters, and other proteins and PET and SPECT biomarkers have become indispensable for clinical research and the selection of treatment options in a number of pathologies, notably neurodegenerative diseases. They can be used for assessing patients' eligibility for new treatments, or for treatment follow-up. The review by Beaurain et al. describes some radiotracers used in neuroscience according to their target: dopaminergic, cholinergic or serotoninergic systems, β-amyloid plaques, tau protein, neuroinflammation, glutamate or GABA receptors, or α-synuclein.

Targeting the membrane dopamine transporter (DAT) proves useful in the follow-up and treatment assessment of brain diseases. Carbon-11 and fluorine-18 labeled tracers have been derived from the chemical structure of cocaine. The review by Chalon et al. focuses on the development of one such tracer, LBT-999. [^{18}F]LBT-999 proved capable of exploring *in vivo* the localization of DAT at the dopaminergic nerve endings as well as at the mesencephalic cell bodies in lesion-induced rat models of Parkinson's disease. Recent clinical data demonstrated the efficiency of [^{18}F]LBT-999 in the diagnosis of Parkinson's disease.

To complete this overview, risk management has been discussed by Lonceint et al. as a major concern for health organizations. In hospitals, medical personnel may be exposed to ionizing radiation and the highest doses (up to a few mSv) are recorded in nuclear medicine departments. The review aims at understanding the attitude of health professionals toward the risks of exposure and how they combine patient care with self-protection. The coexistence of care and radiation protection logics was shown to be a source of contradictions for nuclear medicine professionals and of differences in risk regulation strategies according to occupational groups.

AUTHOR CONTRIBUTIONS

JB wrote the editorial, which was revised, proofed, and accepted by all authors.

FUNDING

This work has been supported in part by grants from the French National Agency for Research called Investissements d'Avenir Labex IRON no. ANR-11-LABX-0018-01 and Equipex ArronaxPlus no. ANR-11-EQPX-0004.

Conflict of Interest: The authors declare that the research was conducted in the absence of any commercial or financial relationships that could be construed as a potential conflict of interest.

frontiers in Medicine

REVIEW
published: 09 April 2019
doi: 10.3389/fmed.2019.00070

Interest of FDG-PET in the Management of Mantle Cell Lymphoma

Clément Bailly[1,2], *Thomas Carlier*[1,2], *Cyrille Touzeau*[3], *Nicolas Arlicot*[1], *Françoise Kraeber-Bodéré*[1,2,4], *Steven Le Gouill*[3] *and Caroline Bodet-Milin*[1,2]*

[1] CRCINA, INSERM, CNRS, Université d'Angers, Université de Nantes, Nantes, France, [2] Department of Nuclear Medicine, CHU de Nantes, Nantes, France, [3] Department of Hematology, CHU de Nantes, Nantes, France, [4] Department of Nuclear Medicine, ICO-René Gauducheau, Saint-Herblain, France

FDG-PET changed response assessment and therapy strategy in diffuse large B-cell lymphoma and Hodgkin disease lymphoma. The value of FDG-PET evaluation in MCL has not been extensively studied and a recent expert consensus highlighted the need for more studies addressing this question. Data of the literature show the value of FDG-PET at baseline in patients with MCL, underlining the good sensitivity of this examination for the initial staging of this pathology, but also the potential impact of semi-quantitative analysis in this indication. The determination of SUVmax at diagnosis might indeed provide important prognostic information. Some studies also suggest the potential value of early and end-of-treatment metabolic assessment in MCL, but these results need to be validated in standardized prospective studies. These results also underlie the need to integrate FDG-PET results into MCL treatment strategy to improve disease management in identifying patients who might benefit from more intensive therapy.

Keywords: mantle cell lymphoma, FDG-PET, staging, therapeutic evaluation, SUV

OPEN ACCESS

Edited by:
Ronan Abgral, Centre Hospitalier Regional Universitaire (CHU) de Brest, France

Reviewed by:
Umberto Vitolo, University Hospital of the City of Health and Science of Turin, Italy
Xavier Palard-Novello, University of Rennes 1, France

***Correspondence:**
Caroline Bodet-Milin
caroline.milin@chu-nantes.fr

Specialty section:
This article was submitted to Nuclear Medicine, a section of the journal Frontiers in Medicine

Received: *28 January 2019*
Accepted: *20 March 2019*
Published: *09 April 2019*

Citation:
Bailly C, Carlier T, Touzeau C, Arlicot N, Kraeber-Bodéré F, Le Gouill S and Bodet-Milin C (2019) Interest of FDG-PET in the Management of Mantle Cell Lymphoma. Front. Med. 6:70. doi: 10.3389/fmed.2019.00070

INTRODUCTION

The use of positron emission tomography with 18Fluoro-deoxyglucose (FDG-PET) in patients with malignant lymphomas has increased dramatically in the last decade, both for initial staging and for therapeutic evaluation. FDG-PET has indeed become an essential tool in the management of these patients, and regular meetings of international expert committees, such as those held annually in Menton or Lugano, have allowed standardization of practices (1–3). Currently, the role of FDG-PET in rarer histological subtypes of lymphomas such as mantle cell lymphoma (MCL) is less well-defined. MCL is an aggressive subtype of non-Hodgkin lymphoma (NHL) which accounts for ∼5% of all NHLs (4, 5). The majority of patients presents with advanced-stage disease and often has extra-nodal sites of involvement such as the gastrointestinal (GI) tract and bone marrow. Patients diagnosed with this disorder generally have poor prognosis and even if the introduction of novel approaches combining rituximab and chemotherapy increased the median overall survival (OS), most patients still experience relapse (6–8). However, a small minority of patients seems to have a longer survival than would be expected and achieve long lasting remissions. The lack of early biomarkers has become a major issue in MCL. Recent advances in the understanding of the clinical, molecular, and genetic characteristics of MCL have identified prognostic factors that might be useful to develop risk-adapted therapies (6, 8). These prognostic factors include, inter alia, splenomegaly, performance status, mitotic index, and the Mantle Cell International Prognostic

Index (MIPI) (9). The role of FDG-PET and its prognostic value in MCL remain debatable as contradictory results regarding its utility for assessing disease burden and response to therapy. In this era of personalized medicine, a non-invasive method for assessing tumor heterogeneity and predicting survival or response to therapy could permit a better selection of worse prognosis patients who might benefit from more intensive therapy. A recent expert consensus highlighted the need for more studies addressing this question (2).

METHODOLOGY OF THE LITERATURE REVIEW

The literature search entailed a systematic search of MEDLINE and PUBMED for publications that were published between 2000 and 2018 using the following key words: mantle cell lymphoma, PET, FDG, SUV.

FDG-Pet at Diagnosis In MCL

FDG-PET is recommended by international guidelines for initial staging in all FDG-avid histological subtypes of lymphomas including MCL (2, 3).

The first correlation between FDG uptake and the histopathological subtype of lymphoma as defined by the WHO classification was published in 2003 (10). This retrospective study showed that FDG-PET detected at least one pathological site in all cases of MCL Indeed, existing data in the literature confirm this observation and show that FDG-PET at diagnosis in patients with MCL has a high sensitivity in the detection of lesions in nodes and spleen (11–14). However, the sensitivity for bone marrow and gastrointestinal (GI) involvement is inadequate to replace routine bone marrow and GI biopsy in disease staging (11).

Besides, despite this significant uptake of FDG in all patients with MCL, most of the literature show a significant intra-individual and inter-individual heterogeneity with uptake. Indeed, the values of SUVmax, the metric widely adopted as a surrogate of the overall net rate of FDG uptake, varied between 2.5 and 36.7 and between 1.0 and 18.8 in the series of Mato et al. (15) and Bodet-Milin et al. (11), respectively. In this latter, a calculated intra-patient SUVmax gradient was $\geq$5 in 46% of cases and $\geq$10 in 13%. Thus, intra- and inter-individual differences might reflect heterogeneity in tumor cell biology, especially since the study by Schöder et al. (16) reported that the value of SUVmax is potentially correlated with histological aggressiveness. Oncogenesis of MCL being a multistep process (17), progressing from a less to a more aggressive form, it can therefore be postulated that low SUVmax value is related to less aggressive MCL cells while high SUVmax values reflects a more aggressive behavior or a more advanced disease. Existence of intra-individual SUVmax variation in MCL might be similar to what is observed in Richter's syndrome where aggressive transformation is located to a specific tumor tissue area. The results of the retrospective study published by Karam et al. confirmed this findings, showing an adverse impact on both event-free-survival (PFS) and overall survival (OS) for MCL patients presenting with SUVmax >4.8 (18). This is also supported by the results of the LyMa-PET study (19). In this prospective ancillary study of the multicentric LyMa trial (NCT00921414), studying the predictive value of FDG-PET at diagnosis in young previously untreated MCL patients, high SUVmax (>10.3) was associated with shorter PFS ($p = 0.0003$) and OS ($p = 0.0003$). This observation at diagnosis was not found in works by Schaffel et al. (ASH 2009), Mato et al. (15) and Bodet-Milin et al. (11) even if this latter reported a negative trend of an SUV max> 6 on the overall survival ($p = 0.07$). In addition, this close relation between tumor cell biology and SUVmax in MCL is also supported by the relationship between SUV max, blastoid variant considered as the most aggressive form of MCL and high percentage of Ki67 positive MCL cells (19). SUVmax measurement could therefore be used to assess tumor cell aggressiveness as FDG-PET has the advantage to be a whole-body non-invasive technique, not restricted as Ki-67 immunostaining to tissue biopsies. The prognostic value of SUVmax seems even reinforced when associated with clinical and biological factors, as shown by Bodet-Milin et al. (11). Used together, IPI and SUVmax allowed to separate MCL patients into three groups with different PFS duration: low (29%; no relapse/progression), intermediate (42%; median PFS: 37 months) and high risk (29%, median PFS: 22 months) ($p = 0.004$) (11). Preliminary results of the LyMa-PET study (19) seem to confirm this observation. This approach clearly identified a subset of patients with a very high risk of early progression after first line treatment, who might benefit from more intensive therapy.

FDG-Pet for Response Assessment In MCL

Response Assessment During Treatment

The most recent international recommendations for the use of imaging in malignant lymphoma does not mandate FDG-PET-based response assessment in MCL outside the context of a clinical trial (2). These conclusions based on a limited number of publications are due to the lack of prospective data, the heterogeneity of patient populations/treatment strategies, and most importantly, the lack of uniformity in the way 18FDG-PET imaging is obtained and interpreted. Thus, although some studies showed no significant predictive value for interim FDG-PET in terms of PFS or OS (14, 15, 20, 21), some reported higher progression rate for patients exhibiting a positive interim FDG-PET, irrespective of therapy applied and particularly before autologous stem-cell transplant (ASCT) (22–25). The preliminary results of the Lyma-PET study seem to confirm these data by demonstrating the potential prognostic value of the variation of SUVmax called ΔSUVmax (defined as the percentage of reduction of SUVmax between PET at baseline and PET before ASCT) on OS and PFS (19).

Interestingly, in the Nordic MCL3 study (22) and the work by Htet et al. (25), the authors described inferior PFS and OS predicted by FDG-PET positivity before-ASCT and detectable minimal residual disease (MRD) after transplant. Because these techniques were reported as having independent prognostic values, both may be of importance to guide treatment decisions. Yet, in the Czech Lymphoma Study Group-MCL1

observational study (26), only achievement of FDG-PET–negativity independently correlated with PFS. In this prospective analysis, the safety and efficacy of alternation of R-CHOP and R-cytarabine for elderly/comorbid MCL patients ineligible for high dose therapy or ASCT was explored, with initiation of Rituximab maintenance (RM) in most of them. In this group, a survival benefit of RM was observed for patients achieving response by FDG-PET response criteria regardless of their MRD-status (26, 27).

If all of these data suggest the potential value of early metabolic assessment in MCL patients, prospective studies are warranted to validate these results.

Response Assessment After Treatment

FDG-PET is the standard of care for remission assessment in FDG-avid lymphoma, yet its value in MCL is debatable. In their retrospective series of 44 patients, Bodet-Milin et al had shown significantly lower PFS for patients with residual FDG-uptake at the end of treatment, according to the IHP criteria (11). Mato et al. confirmed this prognostic value of negative FDG-PET at the end of treatment, again using the IHP criteria, in 53 patients with MCL, with better PFS at 3 years and a trend for OS ($p = 0.07$) (15). Similar results have also been reported by Brepoels et al who demonstrated better PFS at 2 years for patients who achieved a complete response at end-of-treatment FDG-PET (57 vs. 22%, $p = 0.011$) (20). However, some studies have also shown contradictory results such as Kedmi et al. (21) and Hosein et al. (14), who found no significant difference on survival between MCL patients with positive or negative FDG-PET findings at the end of treatment.

Thus, even if these different results seem to show a certain prognostic impact of FDG-PET at the end of treatment, published data are currently too heterogeneous to allow definitive conclusions to be drawn. In addition, some of these publications suffer from many methodological biases. Particularly, none of these latter used the Deauville Score, as actually validated and recommended by Lugano's Recommendations in Lymphoma (2), except for Lamonica et al. (28) yet in patients with relapsed or refractory MCL. Recent guidelines enacted to standardize PET protocols and to ensure more reproducible analyses between scans and centers will hopefully soon lead to the full integration of these interpretation criteria into future prospective investigations.

CONCLUSION

FDG-PET changed response assessment and therapy strategy in diffuse large B-cell lymphoma and Hodgkin disease lymphoma. The value of FDG-PET evaluation in MCL has not been extensively studied and a recent expert consensus highlighted the need for more studies addressing this question. Data of the literature show the value of FDG-PET at baseline in patients with MCL, underlining the good sensitivity of this examination for the initial staging of this pathology, but also the potential impact of semi-quantitative analysis in this indication. The determination of SUVmax at diagnosis might indeed provide important prognostic information. Some studies also suggest the potential value of early and end-of-treatment metabolic assessment in MCL, but these results need to be validated in standardized prospective studies. These results also underlie the need to integrate FDG-PET results into MCL treatment strategy to improve disease management in identifying patients who might benefit from more intensive therapy.

AUTHOR CONTRIBUTIONS

All authors listed have made a substantial, direct and intellectual contribution to the work, and approved it for publication.

ACKNOWLEDGMENTS

This work has been supported in part by grants from the French National Agency for Research called, Investissements d'Avenir IRON Labex n° ANR-11-LABX-0018-01 and ArronaxPlus Equipex n° ANR-11-EQPX-0004.

REFERENCES

1. Nanni C, Cottereau AS, Lopci E, Bodet-Milin C, Coronado M, Pro B, et al. Report of the 6th International Workshop on PET in lymphoma. *Leuk. Lymphoma*. (2017) 58:2298–303. doi: 10.1080/10428194.2017.1298752
2. Barrington SF, Mikhaeel NG, Kostakoglu L, Meignan M, Hutchings M, Müeller SP, et al. Role of imaging in the staging and response assessment of lymphoma: consensus of the international conference on malignant lymphomas imaging working group. *J Clin Oncol.* (2014) 32:3048–58. doi: 10.1200%2FJCO.2013.53.5229
3. Cheson BD, Fisher RI, Barrington SF, Cavalli F, Schwartz LH, Zucca E, et al. Recommendations for initial evaluation, staging, and response assessment of hodgkin and non-hodgkin lymphoma: the lugano classification. *J Clin Oncol.* (2014) 32:3059–67. doi: 10.1200/JCO.2013.54.8800
4. Vose JM. Mantle cell lymphoma: 2012 update on diagnosis, risk-stratification, and clinical management. *Am J Hematol.* (2012) 87:604–9. doi: 10.1002/ajh.23176
5. Swerdlow SH, Campo E, Pileri SA, Harris NL, Stein H, Siebert R, et al. The 2016 revision of the World Health Organization classification of lymphoid neoplasms. *Blood*. (2016) 127:2375–90. doi: 10.1182/blood-2016-01-643569
6. McKay P, Leach M, Jackson B, Robinson S, Rule S. Guideline for the management of mantle cell lymphoma. *Br J Haematol.* (2018) 182:46–62. doi: 10.1111/bjh.15283
7. McKay P, Leach M, Jackson B, Robinson S, Rule S. A british society for haematology good practice paper on the diagnosis and investigation of patients with mantle cell lymphoma. *Br J Haematol.* (2018) 182:46–62. doi: 10.1111/bjh.15281
8. Dreyling M, Campo E, Hermine O, Jerkeman M, Le Gouill S, Rule S, et al. Newly diagnosed and relapsed mantle cell lymphoma: ESMO clinical practice guidelines for diagnosis, treatment and follow-up. *Ann Oncol.* (2017) 28(Suppl. 4):iv62–71. doi: 10.1093/annonc/mdx223r
9. Hoster E, Dreyling M, Klapper W, Gisselbrecht C, van Hoof A, Kluin-Nelemans HC, et al. A new prognostic index (MIPI) for patients with advanced-stage mantle cell lymphoma. *Blood.* (2008) 111:558–65. doi: 10.1182/blood-2007-06-095331

10. Elstrom R, Guan L, Baker G, Nakhoda K, Vergilio JA, Zhuang H, et al. Utility of FDG-PET scanning in lymphoma by WHO classification. *Blood*. (2003) 101:3875–6. doi: 10.1182/blood-2002-09-2778
11. Bodet-Milin C, Touzeau C, Leux C, Sahin M, Moreau A, Maisonneuve H, et al. Prognostic impact of 18F-fluoro-deoxyglucose positron emission tomography in untreated mantle cell lymphoma: a retrospective study from the GOELAMS group. *Eur J Nucl Med Mol Imaging*. (2010) 37:1633–42. doi: 10.1007/s00259-010-1469-2
12. Gill S, Hicks RJ, Seymour JF. What is the role of 18 F-fluorodeoxyglucose positron emission tomography in mantle cell lymphoma? *Leukemia Lymphoma*. (2008) 49:1653–6. doi: 10.1080/10428190802311433
13. Alavi A, Shrikanthan S, Aydin A, Talanow R, Schuster S. Fluorodeoxyglucose-Positron-emission tomography findings in mantle cell lymphoma. *Clin Lymphoma Myeloma Leukemia*. (2011) 11:261–6. doi: 10.1016/j.clml.2011.03.013
14. Hosein PJ, Pastorini VH, Paes FM, Eber D, Chapman JR, Serafini AN, et al. Utility of positron emission tomography scans in mantle cell lymphoma. *Am J Hematol*. (2011) 86:841–5. doi: 10.1002/ajh.22126
15. Mato AR, Svoboda J, Feldman T, Zielonka T, Agress H, Panush D, et al. Post-treatment (not interim) positron emission tomography-computed tomography scan status is highly predictive of outcome in mantle cell lymphoma patients treated with R-HyperCVAD. *Cancer*. (2012) 118:3565–70. doi: 10.1002/cncr.26731
16. Schöder H, Noy A, Gönen M, Weng L, Green D, Erdi YE, et al. Intensity of 18fluorodeoxyglucose uptake in positron emission tomography distinguishes between indolent and aggressive non-Hodgkin's lymphoma. *J Clin Oncol*. (2005) 23:4643–51. doi: 10.1200/JCO.2005.12.072
17. Jares P, Colomer D, Campo E. Genetic and molecular pathogenesis of mantle cell lymphoma: perspectives for new targeted therapeutics. *Nat Rev Cancer*. (2007) 7:750–62. doi: 10.1038/nrc2230
18. Karam M, Ata A, Irish K, Feustel PJ, Mottaghy FM, Stroobants SG, et al. FDG positron emission tomography/computed tomography scan may identify mantle cell lymphoma patients with unusually favorable outcome. *Nucl Med Commun*. (2009) 30:770–8. doi: 10.1097/MNM.0b013e32832e0c13
19. Bodet-Milin C, Bailly C, Meignan M, Beriollo-Riedinger A, Casasnovas R-O, Devillers A, et al. Predictive power of FDG-PET parameters at diagnosis and after induction in patients with mantle cell lymphoma, interim results from the LyMa-PET project, conducted on behalf of the lysa group. *Blood*. (2015) 126:335. Available online at: http://www.bloodjournal.org/content/126/23/335
20. Brepoels L, Stroobants S, De Wever W, Vandenberghe P, Thomas J, Mortelmans L, et al. Positron emission tomography in mantle cell lymphoma. *Leukemia Lymphoma*. (2008) 49:1693–701. doi: 10.1080/10428190802216707
21. Kedmi M, Avivi I, Ribakovsky E, Benyamini N, Davidson T, Goshen E, et al. Is there a role for therapy response assessment with 2-[fluorine-18] fluoro-2-deoxy-D-glucose-positron emission tomography/computed tomography in mantle cell lymphoma? *Leuk. Lymphoma*. (2014) 55:2484–9. doi: 10.3109/10428194.2014.882506
22. Kolstad A, Laurell A, Jerkeman M, Grønbæk K, Elonen E, Räty R, et al. Nordic MCL3 study: 90Y-ibritumomab-tiuxetan added to BEAM/C in non-CR patients before transplant in mantle cell lymphoma. *Blood*. (2014) 123:2953–9. doi: 10.1182/blood-2013-12-541953
23. Magnusson E, Cao Q, Linden MA, Frolich J, Anand V, Burns LJ, et al. Hematopoietic cell transplantation for mantle cell lymphoma: predictive value of pretransplant positron emission tomography/computed tomography and bone marrow evaluations for outcomes. *Clin Lymphoma Myeloma Leuk*. (2014) 14:114–21. doi: 10.1016/j.clml.2013.10.007
24. Bachanova V, Burns LJ, Ahn KW, Laport GG, Akpek G, Kharfan-Dabaja MA, et al. Impact of pretransplantation (18)F-fluorodeoxy glucose-positron emission tomography status on outcomes after allogeneic hematopoietic cell transplantation for non-hodgkin lymphoma. *Biol Blood Marrow Transplant*. (2015) 21:1605–11. doi: 10.1016/j.bbmt.2015.05.007
25. Htet S, Lane S, Kipp D, Rose H, Campbell P. PET-CT confirmed complete remission and MRD negativity in mantle cell lymphoma patients treated with R-hyper-CVAD results in excellent outcome in the absence of autologous stem cell transplantation: a single-centre case for a transplant-free approach. *Intern Med J*. (2016) 46:1113–4. doi: 10.1111/imj.13179
26. Klener P, Fronkova E, Belada D, Forsterova K, Pytlik R, Kalinova M, et al. Alternating R-CHOP and R-cytarabine is a safe and effective regimen for transplant-ineligible patients with a newly diagnosed mantle cell lymphoma. *Hematol Oncol*. (2018) 36:110–5. doi: 10.1002/hon.2483
27. Klener P, Fronkova E, Kalinova M, Belada D, Forsterova K, Pytlik R, et al. Potential loss of prognostic significance of minimal residual disease assessment after R-CHOP-based induction in elderly patients with mantle cell lymphoma in the era of rituximab maintenance. *Hematol Oncol*. (2018) 36:773–8. doi: 10.1002/hon.2550
28. Lamonica D, Graf DA, Munteanu MC, Czuczman MS. 18F-FDG PET for measurement of response and prediction of outcome to relapsed or refractory mantle cell lymphoma therapy with bendamustine-rituximab. *J Nucl Med*. (2017) 58:62–8. doi: 10.2967/jnumed.116.173542

Conflict of Interest Statement: The authors declare that the research was conducted in the absence of any commercial or financial relationships that could be construed as a potential conflict of interest.

frontiers in Medicine

REVIEW
published: 09 April 2019
doi: 10.3389/fmed.2019.00069

Interest of Pet Imaging in Multiple Myeloma

Bastien Jamet[1], Clément Bailly[1,2], Thomas Carlier[1,2], Cyrille Touzeau[2,3], Cristina Nanni[4], Elena Zamagni[5], Louisa Barré[6], Anne-Victoire Michaud[1], Michel Chérel[2], Philippe Moreau[2,3], Caroline Bodet-Milin[1,2] and Françoise Kraeber-Bodéré[1,2,7]*

[1] Nuclear Medicine Unit, University Hospital, Nantes, France, [2] CRCINA, INSERM, CNRS, Nantes University, Nantes, France, [3] Haematology Department, University Hospital, Nantes, France, [4] Nuclear Medicine, Azienda Ospedaliero-Universitaria di Bologna, Bologna, Italy, [5] Seràgnoli Institute of Hematology, Bologna University School of Medicine, Bologna, Italy, [6] Unicaen-CEA-CNRS, UMR6030, Caen, France, [7] Nuclear Medicine Unit, ICO-Gauducheau, Nantes-Saint-Herblain, France

The interest of 18Fluoro-deoxyglucose (FDG) positron emission tomography (PET) imaging in the management of patients with multiple myeloma (MM) for the workup at diagnosis and for therapeutic evaluation has recently been demonstrated. FDG-PET is a powerful imaging tool for bone lesions detection at initial diagnosis with high sensitivity and specificity values. The independent pejorative prognostic value on progression-free survival (PFS) and overall survival (OS) of baseline PET-derived parameters (presence of extra-medullary disease (EMD), number of focal bone lesions (FLs), and maximum standardized uptake values [SUV_{max}]) has been reported in several large independent prospective studies. During therapeutic evaluation, FDG-PET is considered as the reference imaging technique, because it can be performed much earlier than MRI which lacks specificity. Persistence of significant FDG uptake after treatment, notably before maintenance therapy, is an independent pejorative prognostic factor, especially for patients with a complete biological response. So FDG-PET and medullary flow cytometry are complementary tools for detection of minimal residual disease before maintenance therapy. However, the definition of PET metabolic complete response should be standardized. In patients with smoldering multiple myeloma, the presence of at least one hyper-metabolic lytic lesions on FDG-PET may be considered as a criterion for initiating therapy. FDG-PET is also indicated for initial staging of a solitary plasmacytoma so as to not disregard other bone or extra-medullary localizations. Development of nuclear medicine offer new perspectives for MM imaging. Recent PET tracers are willing to overcome limitations of FDG. (11)C-Methionine, which uptake reflects the increased protein synthesis of malignant cells seems to correlate well with bone marrow infiltration. Lipid tracers, such as Choline or acetate, and some peptide tracers, such as (68) Ga-Pentixafor, that targets CXCR4 (chemokine receptor-4, which is often expressed with high density by myeloma cells), are other promising PET ligands. 18F-fludarabine and immuno-PET targeting CD138 and CD38 also showed promising results in preclinical models.

Keywords: multiple myeloma, PET/CT imaging, FDG-PET/CT, review, prognosis

OPEN ACCESS

Edited by:
Ronan Abgral, Centre Hospitalier Regional Universitaire (CHU) De Brest, France

Reviewed by:
Pierre-Yves Le Roux, Centre Hospitalier Regional Universitaire (CHU) De Brest, France
Ramin Sadeghi, Mashhad University of Medical Sciences, Iran
Constantin Lapa, University of Wuerzburg, Germany

****Correspondence:***
Bastien Jamet
bastien.jamet@chu-nantes.fr

Specialty section:
This article was submitted to Nuclear Medicine, a section of the journal Frontiers in Medicine

Received: *05 February 2019*
Accepted: *20 March 2019*
Published: *09 April 2019*

Citation:
Jamet B, Bailly C, Carlier T, Touzeau C, Nanni C, Zamagni E, Barré L, Michaud A-V, Chérel M, Moreau P, Bodet-Milin C and Kraeber-Bodéré F (2019) Interest of Pet Imaging in Multiple Myeloma. Front. Med. 6:69. doi: 10.3389/fmed.2019.00069

INTRODUCTION

Multiple myeloma (MM) is a hematological neoplasm characterized by the clonal proliferation of malignant plasma cells in the bone marrow. It is almost always preceded by an initial monoclonal gammopathy of undetermined significance (MGUS), that then develops into asymptomatic or Smoldering MM (SMM), which constitutes an intermediate clinical stage between MGUS and MM.

The rate of progression from MGUS to MM is 0.5–1% per year, and that of SMM to MM 10% per year for the first 5 years, with the thresholds of serum M protein and spinal plasmacytosis differing between both classifications. SMM is a heterogeneous classification including patients with a very slow progression to proven MM (several years) and patients progressing very rapidly to symptomatic MM in <2 years (high-risk SMM). The definition of symptomatic MM, a clinical stage requiring treatment, typically based on the presence of CRAB criteria (HyperCalcemia, Renal failure, Anemia, and Bone disease) (1) was revised in 2014 by the International Myeloma Working Group (IMWG) by integrating new prognostic biomarkers (2), with the aim of not delaying the initiation of treatment for patients classified as high risk SMM and to avoid progression to harmful bone lesions or renal insufficiency. Indeed, medullary plasmacytosis ≥60%, serum free light chain ratio ≥100 and more than 1 focal MRI bone lesion were predictive of an 80% progression to a CRAB-positive MM within 2 years in several studies, confirming a stage of the disease requiring treatment.

In addition, the 2014 IMWG criteria for the diagnosis of MM highlighted the importance of new imaging in the management of MM in order to detect bone disease, which is considered as a symptomatic MM criterion requiring treatment even when asymptomatic. Studies conducted over the past 10 years have shown better performance using low-dose whole-body CT and MRI scans (3, 4) than standard skeletal radiographs, formerly considered as the reference technique for detecting bone disease.

Recent data suggest that positron emission tomography (PET) using ^{18}F-deoxyglucose (FDG) is a reliable imaging for initial staging, therapeutic monitoring and relapse workup in MM, especially because of its prognostic potential (5). Moreover, as shown recently in a prospective comparison between size of biopsied focal bone lesions (FL) depicted by FDG-PET and genomic profiles, the extent of spatial heterogeneity is positively associated with the size of FL, resulting coexistence of different disease clones (6). More recent PET tracers (Methionine, lipid and peptide tracers) are available to overcome limitations of FDG.

PERFORMANCE OF FDG-PET FOR THE DETECTION OF MEDULLARY AND EXTRA-MEDULLARY DISEASE AT INITIAL DIAGNOSIS

PET-FDG allows whole-body exploration and has a global sensitivity of 90% for the detection of medullary disease with a specificity varying from 70 to 100% according to several studies (7–9). Medullary abnormalities detected by PET are focal lesions (**Figure 1**), para-medullary lesions (PML, **Figure 2**) and diffuse medullary involvement with variable glucose uptake, resulting in variable SUV_{max} values (5–13). FDG-PET also allows the detection of extra-medullary disease (EMD, **Figure 3**), in <10% of patients at diagnosis (14). FL are most often defined as foci of uptake above the surrounding background noise on two successive sections with or without osteolysis opposite the CT image. PML are soft tissue invasions with contiguous bone involvement. Diffuse bone marrow involvement is usually defined as heterogeneous or homogenous diffuse uptake of the axial (that may extend to the peripheral) skeleton, of greater intensity than the liver (**Figure 4**). MM related disease abnormalities to be incorporated in the baseline FDG-PET report are presented in the **Table 1**.

The Bologna group recently proposed the "IMPETUS" criteria (15) to standardize the interpretation of PET in MM. It showed that the use of a standardized visual scale of interpretation (Deauville 5-level scale) in the description of the number of FL, EMD as well as diffuse medullary involvement makes it possible to improve the reproducibility of inter-observer interpretation (with however, a very great disparity in interpretation of skull lesions). The pathological positivity cut-offs for bone lesions, especially on therapeutic evaluation examinations, are still to be determined however, especially when comparing with sensitive biological techniques (CMF) for detection of MRD.

The sensitivity of FDG-PET is greater than whole-body radiology to detect bone lesions and comparable to or less than that of pelvic-spinal MRI (7, 12, 16–19). In the first small series of patients comparing FDG-PET and MRI, sensitivity of FDG-PET was less than that of pelvic-spinal MRI (PR-MRI) for diffuse medullary involvement but allowed detection of additional FL, especially outside the field of the MRI view (17). More recently, the French Imajem study (14) prospectively compared PR-MRI and FDG-PET at initial diagnosis and after therapy. In this cohort of 134 patients with symptomatic MM, PR-MRI was positive in 94.7% of cases and FDG-PET in 91% of cases, revealing an equivalent detection sensitivity.

FDG-PET also demonstrated interest in patients with solitary plasmacytoma (SP), allowing detection of additional lesions, with sensitivity, and specificity greater than MRI (5–7, 20). In addition, Fouquet et al. showed that the presence of at least 2 hypermetabolic lesions by FDG-PET was predictive of rapid progression to MM (21).

According to recent update data of the Southeastern Minnesota cohort (22) with a long-term follow-up, there are adversely risk factors for MGUS to active MM progression including an M-protein of 15 g/L or more and an abnormal free light chain ratio in patients with non-IgM MGUS. Patients with 2 risk factors showed a significantly higher progression rate to MM of 30% in 20 years than patients with no (7%) or 1 risk factor (20%). Therefore, there is a need of imaging for patients with high risk MGUS. To date, there are unfortunately no published data on FDG-PET findings in MGUS patients.

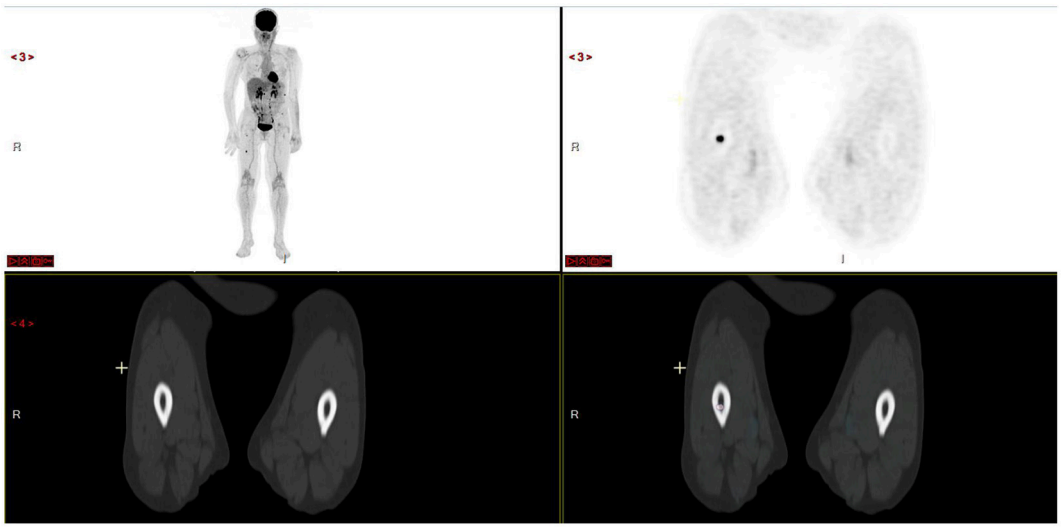

FIGURE 1 | Patient with more than 10 focal lesions of the axial and appendicular skeleton. Note absence of osteolysis on opposite CT scan of right femur focal lesion.

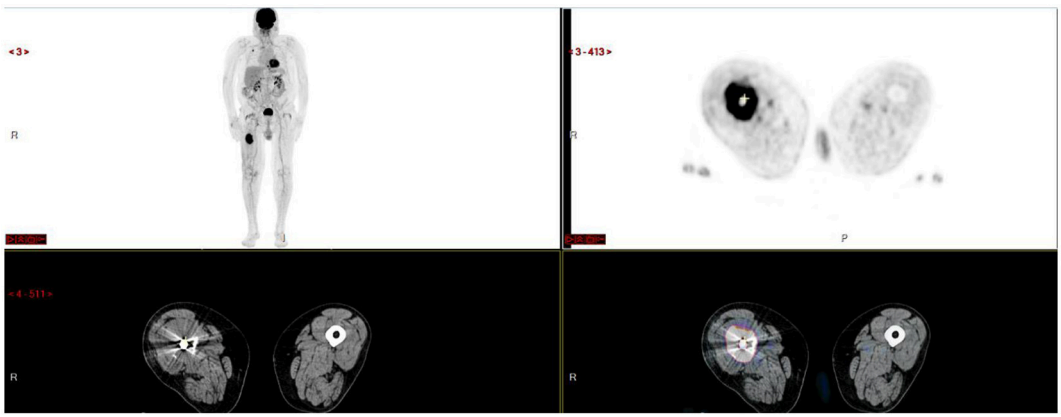

FIGURE 2 | Voluminous hypermetabolic lytic lesion of the right femoral shaft contiguously invading adjacent soft tissues.

PROGNOSTIC VALUE OF FDG-PET IN SMM AND SYMPTOMATIC MM AT BASELINE EVALUATION

FDG-PET showed prognostic value in patients with SMM and symptomatic MM.

Even if the latest international recommendations of the IMWG (1) indicate that the presence of one or more FL with osteolysis on FDG-PET is considered a criterion for treatment at initial diagnosis, all prospective studies lead from 2009 defined FL as foci of uptake with or without osteolysis cause metabolic could precede morphological abnormalities.

Moreover, in SMM, a positive FDG-PET defined by the presence of FL without underlying osteolytic lesions is associated with a rapid progression to symptomatic MM. Indeed, in a cohort of 122 SMM patients, Siontis et al. (23) showed that the probability of progression to MM within 2 years for positive FDG-PET patients was 75 vs. 30% for patients with a negative PET, without therapy. In another prospective study of 120 SMM patients, the group of Bologna (24) reported a rate of progression to symptomatic MM at 2 years of 58% for patients with positive PET vs. 33% for patients with a negative PET.

In symptomatic MM baseline evaluation, three large prospective studies have demonstrated important prognostic impact of FDG-PET results, which is particularly important at age of precision medicine and risk-based therapies. First of all, Bartel et al. in a large cohort ($n = 239$) treated using the Total Therapy 3 strategy (25) showed that the only imaging examination (between FDG-PET and MRI) significantly associated with an adverse prognosis for both overall survival (OS) and event-free survival (EFS) was FDG-PET when the number of FL was >3. Then, the Bologna group, in a large series of 192 MM patients also enrolled in a double autologous

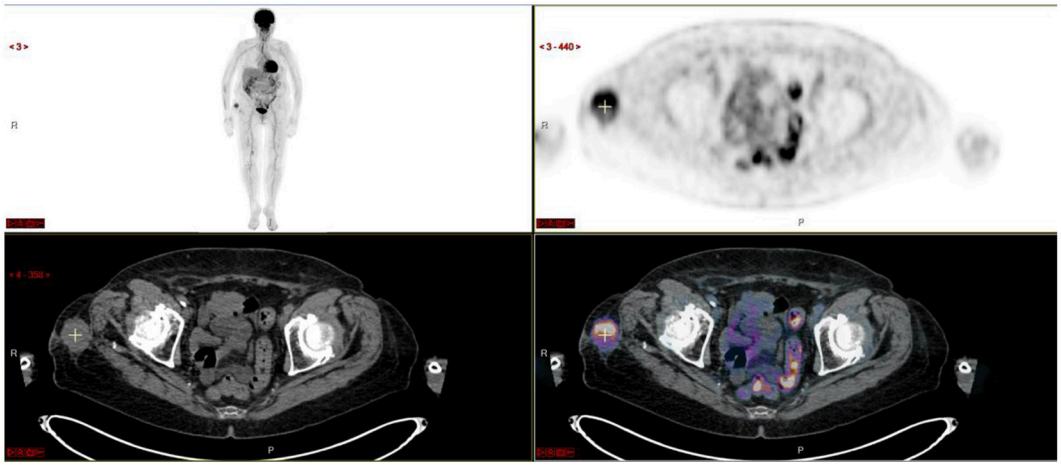

FIGURE 3 | Extra-medullary disease histologically proven in this subcutaneous mass.

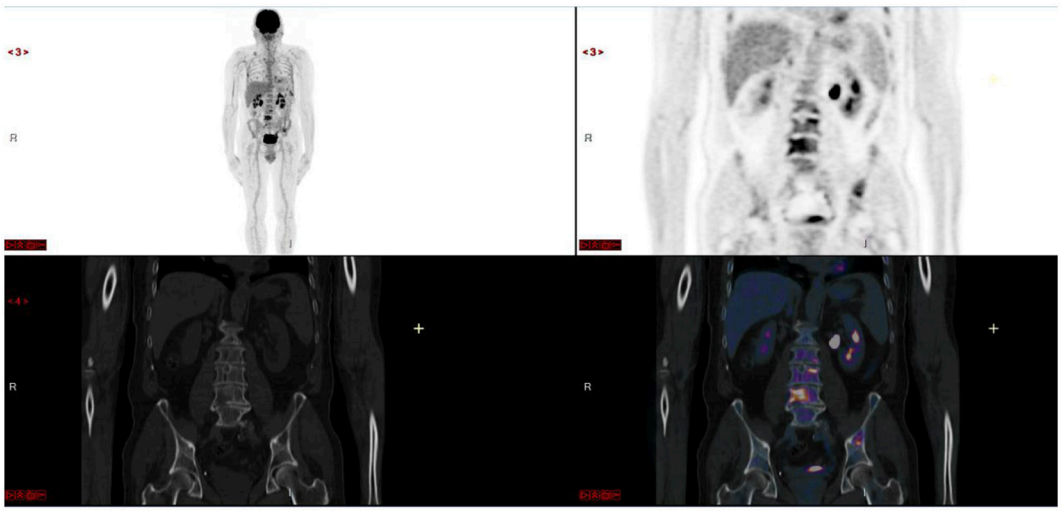

FIGURE 4 | Diffuse medullary involvement (and superimposed lesions).

stem cell transplantation (ASCT) program after induction (26), confirmed the pejorative prognostic impact of more than 3 FL on progression-free survival (PFS) at 4 years as well as an SUV > 4.2 and the presence of EMD. SUV > 4.2 and the presence of EMD were also associated with a shorter OS. The prognostic value of EMD on PFS and OS was recently confirmed by the French Imajem study (14).

Two large retrospective studies found equal results about prognostic value of FDG-PET in symptomatic MM baseline evaluation. The Mayo Clinic team, in a 313 patient cohort showed that the presence of at least 3 FL and EMD predicted inferior OS (only by univariate analysis), with no clear SUVmax cutoff predictive of PFS or OS (27). In a smaller series of patients ($n = 167$), Jung et al. (28) confirmed (in multivariate analyses) that presence of more than three FL or EMD was associated with significantly inferior PFS and OS, especially in Revised International Staging System (R-ISS) II and III subgroups of patients.

More complex PET biomarkers, such as functional volumes and tumor heterogeneity, have also been studied or are being evaluated with promising results. First pre-therapeutic assessment of the whole-body total metabolic volume of FL and EMD (MTVWB) in 47 patients showed a poor prognostic value of high values on PFS and OS (29), with best discriminant cut-offs of 42.2 cm^3 for the PFS and 77.6 cm^3 for the OS. A second larger study of 192 patients confirmed the poor prognostic value of a high MTVWB, which was also similar for a high Total lesion glycolysis (TLG) WB (30). Indeed, by multivariate analysis, TLGWB > 620 g or MTVWB > 210 cm^3 at baseline significantly decreased PFS and OS after adjustment for known prognostic factors. Combined with the gene expression profiling prognostic score (GEP70), a TLGWB > 205 g identified a high-risk subgroup

TABLE 1 | What should be provided in the FDG-PET report at baseline?

MM related disease abnormalities
• **Focal Lesion (FL):** With or without osteolysis on CT: Total Number: 0, 1–3, >3; Intensity: Hottest SUV_{max} (Most intense FDG uptake identified among all foci determined by the nuclear physician);
• **Bone Marrow diffuse involvement (BMI):** Evaluation of the bone marrow diffuse uptake, regardless focal lesions: Visual analysis (Deauville 5-level scale): Positive if diffuse uptake of the axial (that may extend to the peripheral) skeleton is greater intensity than the liver (Deauville 4 or 5).
• **Extramedullary disease (EMD):** Soft tissue or nodal mass not directly adjacent to MM bone localization: Presence or not and localization.
• **Paramedullary disease (PMD):** Bone lesion involving surrounding soft tissues with bone cortical interruption: Presence or not, localization, clinical risk?

MM, multiple myeloma; CT, computed tomography; SUV, standardized uptake value.

and separated ISS II patients into two subgroups, with a similar outcome to ISS I and ISS III patients.

Finally, as described by Carlier et al. (31) for 66 patients of the Imajem study, intra-tumoral textural features (e.g., reflecting of tumor heterogeneity), especially energy, also seem to be of prognostic value (independent prognostic value of energy on PFS and OS). More work is in progress on this subject.

PROGNOSTIC VALUE OF FDG-PET IN THERAPEUTIC EVALUATION

FDG-PET is considered as the reference imaging technique for therapeutic evaluation in MM with a strong independent prognostic value (5). FDG-PET allows evaluation of the response earlier than standard MRI but new MRI functional approaches, such as diffusion weighted imaging (DWI) measuring the apparent diffusion coefficient (ADC) influenced by tissue microarchitecture and related to marrow cellularity could be interesting tools to evaluate the disease after therapy (32, 33). However, homogeneous and prospective data about comparison between FDG-PET and WB-DWIMRI are lacking (34).

FDG-PET, coupled with a biological technique for the detection of minimal residual disease (MRD), makes it possible to improve the definition of complete response (35) clearly correlated with long-term outcomes.

All large prospective studies above mentioned have demonstrated the strong and independent prognostic impact of FDG-PET results after therapy of symptomatic MM.

The Little Rock team first showed in 2009 that normalization of FDG uptake of FL after chemotherapy induction cycles (before the transplant procedure) was associated with better EFS and OS (25). The same team reported in 2013 in a larger series of 302 patients (277 of them were also the object of a gene expression profile study) (36) treated according to the same intensive protocol that 3 FL on FDG-PET performed at Day 7 of induction was associated with lower PFS and OS, even in the high-risk group in relation to genetic profiling. FDG-PET could be considered as a tool for early therapeutic adaptation. They finally confirmed these results in 2018 from data collected in their TT4–TT6 clinical trials, in a very large cohort of more than 500 patients, showing patients achieving 100% suppression of FL signal following treatment at each time point studied (day 7, end of induction, post transplantation, and maintenance) had PFS and OS values that were not significantly different from cases with no FL present at baseline (37).

The Bologna group then showed that after induction therapy, a SUV > 4.2 was associated with a reduced PFS (26). Three months after ASCT, complete metabolic response (CMR) was achieved in 65% of patients, with PFS and OS at 4 years higher than those in PET-positive patients. Interestingly, 23% of patients achieving CR in accordance with conventional criteria were considered PET-positive. Multivariate analysis showed that post ASCT PET status was an independent prognostic factor of PFS. In 2015, the same group confirmed these results in 282 patients undergoing front line treatment between 2002 and 2012 (38). After treatment, a CMR was obtained in 70% of patients, whereas the conventional biological methods concluded at 53% of CR. The FDG-PET negativity affected the PFS and the OS positively.

The Imajem study more recently confirmed the major benefit of FDG-PET in therapeutic evaluation (14). Whereas, normalization of MRI after three cycle of combined induction therapy or before maintenance did not significantly affect either PFS or OS, FDG-PET normalization before maintenance was strongly associated with better PFS and OS. The PFS and OS of PET-negative patients were better than those of PET-positive patients (24-months PFS by 72 vs. 56.8%: $p = 0.01$; OS at 24 months of 94.2 vs. 72.9%: $p = 0.03$). In addition, multivariate analysis revealed that normalization of pre-maintenance FDG-PET was independently associated with longer PFS, such as absence of EMD at diagnosis and at least a very good partial biological response after three cycles of induction therapy.

Moreover, for the Imajem patients presenting a FDG-avid MM defined by lesion intensity higher than liver background, the prognostic value of FDG-PET after three cycles of induction therapy was also reported (39). Indeed, by multivariate analysis, only ΔSUVmax ($p < 0.001$) and biochemical response ($p = 0.025$) appeared as independent prognostic factors, with a more discriminative hazard ratio for ΔSUVmax analysis (>−25 vs. ≤−25%) which identified patients with improved median PFS.

The benefit of post-ASCT FDG-PET was also reported in 2013 in a prospective series of 77 patients assessed by FDG-PET 3 months after ASCT, and then every 6–12 months during follow-up (40). The duration of the response was longer when the PET scan was negative (27.6 months) than when it was positive (18 months, $p = 0.05$), whereas in patients with positive PET, SUVmax was inversely correlated with the duration of the response ($P < 0.01$).

However, the definition of CMR was not the same in these different clinical studies and a standardization of FDG-PET interpretation criteria should be done. Definition of cut-offs for FDG-PET positivity/negativity after therapy for MRD evaluation is currently underway. Preliminary results of a combined analysis of two European prospective trials have been presented by Zamagni et al. at the 2018 annual meeting of the ASH (41). In this joint analysis of 236 patients, attaining FL and bone marrow Deauville score <4 prior to maintenance therapy was the strongest independent predictor for prolonged PFS and OS

and could be identified as the most representative cut-off value for PET negativity after therapy. Moreover, the CASSIOPET study is on-going, aiming to determine the best CMR threshold (mediastinal vs. hepatic background) on FDG-PET and try to establish the concordance between CMR and MRD negativity in the bone marrow (by flow cytometry or sequencing) to confirm the complementary role of functional imaging with modern biological tools for the detection of MRD inside and outside the bone marrow.

PROGNOSTIC VALUE OF FDG-PET AT RELAPSE SETTING

Although existing data are less available, FDG-PET seems to have also a prognostic impact at relapse workup. In a small series of 37 MM patients suspected of relapse after ASCT, it was shown that the absence of FL was a favorable prognostic factor for time to progression (TTP) and OS (42). The presence of more than 10 FL correlated with a shorter TTP and OS whilst a high SUV_{max} and the presence of EMD resulted in a longer TTP.

More recently, in a retrospective series of 40 confirmed relapsed patients, Nantes' group have described that the presence of at least 6 FL in the peripheral skeleton was an independent pejorative prognostic factor on both the PFS and the OS by multivariate analysis (43). Moreover, a high SUV_{max} (>15.9) was an independent negative prognostic factor on the PFS as was a high TLG of the hottest lesion (>98.1 g). Interestingly, 15% of the patients were FDG-PET positive without re-ascending the monoclonal peak and no change in the level of serum free-light chains.

Finally, scarce data on the value of FDG-PET before or after allo-SCT are available but two retrospective studies of heavily pre-treated MM patients showed FDG-PET results prior to and after allo-SCT were strongly associated with the outcome (44, 45).

NEW PET TRACERS

It has been recently reported in a 227 patients study with an initial diagnosis of symptomatic MM a FDG-PET negativity rate of 11% (13). It was found in this subgroup of patients a low expression of the hexokinase 2 gene (which catalyzes the first step of glycolysis) and consequently a FDG trapping in the cells. Indeed, for these patients FDG-PET is not an appropriate tool to evaluate MRD. Development of nuclear medicine offer new perspectives for MM imaging and other PET tracers, preliminarily investigated in limited series of MM patients, targeting other metabolic pathways or plasma cell receptors, could be potentially more sensitive and specific than FDG.

11C-Methionine, which uptake reflects the increased protein synthesis of malignant cells seems to correlate well with bone marrow infiltration and could be more sensitive than FDG to detect intra- and extra-medullary MM lesions (46).

Choline is a lipid PET tracer clinically used for the evaluation of relapse of prostate cancer. This tracer labeled with C^{11} was proposed years ago in a preliminary study in comparison to FDG on 10 patients affected by symptomatic MM (47) and showed Choline would reveal more lesions. Another study on the comparison of FDG and ^{18}F-Choline presented similar results on 21 patients with symptomatic MM (48). Then it seems that Choline (either C^{11}- or ^{18}F-) has a better detection rate as compared to FDG in MM patients at staging. However, unfavorable physiological biodistribution (increased background of the liver parenchyma and of the bone marrow) is a limitation.

Pilot study comparing other lipid tracer (^{11}C-Acetate) and FDG at diagnosis of symptomatic MM also showed acetate would reveal more lesions (49).

Another new and potentially interesting tracer is CXCR4. C – X – C chemokine receptor 4 (CXCR4) is a G-protein-coupled chemokine receptor family implicated in the process of cell migration as well as in the homing process of hematopoietic stem cells to the bone marrow, angiogenesis and cell proliferation.

In multiple myeloma, CXCR4 expression is associated to disease progression and poor prognosis (50). Most experience with CXCR4-directed PET imaging has been gained in MM and around two thirds of patients could overexpress the receptor on the myeloma cell surface.

^{68}Ga-Pentixafor, that targets CXCR4 is a promising PET ligand (51) especially as potential target for myeloma specific treatment (for CXCR4-positive tumors) in a theranostic approach with preliminary encouraging results with good tolerance of the treatment, high initial response rates in advanced-stage MM cases (52). However, it has been reported that, in a non-negligible number of cases, FDG provided better detectability so further studies would be important to clarify this aspect (53). Moreover, receptor expression seems to be a dynamic process that could be highly influenced by preceding or concomitant chemotherapy (53).

^{18}F-fludarabine (54) and immuno-PET targeting CD138 (55) and CD38 (56, 57) also showed promising results in preclinical models.

However, pending issues with these new tracers are willingness, inter-patient tumor heterogeneity for specific targets and the lack of prognostic data reported.

CONCLUSION

FDG-PET is a powerful diagnostic tool for the detection of medullary and extra-medullary disease at the initial diagnosis of symptomatic MM with a pejorative prognostic value for the presence of EMD. Moreover, FDG-PET is the reference imaging technique to assess therapeutic response of symptomatic MM, evaluation being available much earlier than by MRI. The negativity of pre-ASCT FDG-PET is a favorable prognostic factor and the positivity of FDG-PET after ASCT, especially in patients with complete biological response, is an independent pejorative prognostic factor. The negativity of FDG-PET, intramedullary flow cytometry, and the ratio of serum free light chains would make it possible to define an optimal complete response (eradication of monoclonal plasma cells in all compartments). Ongoing prospective trials will try to

establish the concordance between CMR and MRD negativity in the bone marrow to confirm the complementary role of functional imaging with modern biological tools for the detection of MRD inside and outside the bone marrow. We recommend to perform FDG-PET at initial work-up and after therapy (before maintenance) for detection of EMD, for patients with oligo/non-secretory MM and if a MRD assessment is performed. At relapse it is probably the best imaging technique to differentiate active disease from morphological scars and remodeling. Other PET tracers may also show interest in FDG-negative patients but should be evaluated in prospective clinical trials.

AUTHOR CONTRIBUTIONS

BJ and FK-B wrote the paper. CB, TC, CT, CN, EZ, LB, A-VM, MC, PM, and CB-M critically revised and improved the paper.

ACKNOWLEDGMENTS

This work has been supported in part by grants from the French National Agency for Research called Investissements d'Avenir IRON Labex n○ ANR-11-LABX-0018-01 and ArronaxPlus Equipex n○ ANR-11-EQPX-0004, and by a grant INCa-DGOS-Inserm_12558 (SIRIC ILIAD).

REFERENCES

1. Kyle RA, Rajkumar SV. Criteria for diagnosis, staging, risk stratification and response assessment of multiple myeloma. *Leukemia.* (2009) 23:3–9. doi: 10.1038/leu.2008.291
2. Rajkumar SV, Dimopoulos MA, Palumbo A, Blade J, Merlini G, Mateos MV, et al. International myeloma working group updated criteria for the diagnosis of multiple myeloma. *Lancet Oncol.* (2014) 15:538–48. doi: 10.1016/S1470-2045(14)70442-5
3. Dimopoulos M, Hillengass J, Usmani S, Zamagni E, Lentzsch S, Davies FE, et al. Role of magnetic resonance imaging in the management of patients with multiple myeloma: a consensus statement. *J Clin Oncol.* (2015) 33:657–64. doi: 10.1200/JCO.2014.57.9961
4. Terpos E, Kleber M, Engelhardt M, Zweegman S, Gay F, Kastritis E, et al. European Myeloma Network guidelines for the management of multiple myeloma-related complications. *Haematologica.* (2015) 100:1254-66. doi: 10.3324/haematol.2014.117176
5. Cavo M, Terpos E, Nanni C, Moreau P, Lentzsch S, Zweegman S, et al. Role of 18F-FDG PET/CT in the diagnosis and management of multiple myeloma and other plasma cell disorders: a consensus statement by the international myeloma working group. *Lancet Oncol.* (2017) 18:e206–17. doi: 10.1016/S1470-2045(17)30189-4
6. Rasche L, Chavan SS, Stephens OW, Patel PH, Tytarenko R, Ashby C, et al. Spatial genomic heterogeneity in multiple myeloma revealed by multi-region sequencing. *Nat Commun.* (2017) 18:268. doi: 10.4324/9781315080932
7. Dammacco F, Rubini G, Ferrari C, Vacca A, Racanelli V, et al. 18F-FDG PET/CT: a review of diagnostic and prognostic features in multiple myeloma and related disorders. *Clin Exp Med.* (2015) 15:1–18. doi: 10.1007/s10238-014-0308-3
8. Weng W-W, Dong M-J, Zhang J, Yang J, Xu Q, Zhu YJ, et al. A systematic review of MRI, scintigraphy, FDG-PET and PET/CT for diagnosis of multiple myeloma related bone disease-which is best? *Asian Pac J Cancer Prev.* (2014) 15:9879-84.
9. Lu YY, Chen JH, Lin WY, Liang JA, Wang HY, Tsai SC, et al. FDG PET or PET/CT for detecting intramedullary and extramedullary lesions in multiple Myeloma: a systematic review and meta-analysis. *Clin Nucl Med.* (2012) 37:833–7. doi: 10.1097/RLU.0b013e31825b2071
10. Walker RC, Brown TL, Jones-Jackson LB, De Blanche L, Bartel T, et al. Imaging of multiple myeloma and related plasma cell dyscrasias. *J Nucl Med.* (2012) 53:1091–101. doi: 10.2967/jnumed.111.098830
11. Sager S, Ergul N, Ciftci H, Cetin G, Güner SI, Cermik TF. The value of FDG PET/CT in the initial staging and bone marrow involvement of patients with multiple myeloma. *Skeletal Radiol.* (2011) 40:843–7. doi: 10.1007/s00256-010-1088-9
12. Mesguich C, Fardanesh R, Tanenbaum L, Chari A, Jagannath S, Kostakoglu L. State of the art imaging of multiple myeloma: comparative review of FDG PET/CT imaging in various clinical settings. *Eur J Radiol.* (2014) 83:2203–23. doi: 10.1016/j.ejrad.2014.09.012
13. Rasche L, Angtuaco E, McDonald JE, Buros A, Stein C, Pawlyn C, et al. Low expression of hexokinase-2 is associated with false-negative FDG-positron emission tomography in multiple myeloma. *Blood.* (2017) 130:30-4. doi: 10.1182/blood-2017-03-774422
14. Moreau P, Attal M, Caillot D, Macro M, Karlin L, Garderet L, et al. Prospective evaluation of magnetic resonance imaging and [18F]fluorodeoxyglucose positron emission tomography-computed tomography at diagnosis and before maintenance therapy in symptomatic patients with multiple myeloma included in the IFM/DFCI 2009 trial: results of the IMAJEM study. *J Clin Oncol.* (2017) 35:2911-8. doi: 10.1200/JCO.2017.72.2975
15. Nanni C, Versari A, Chauvie S, Bertone E, Bianchi A, Rensi M, et al. Interpretation criteria for FDG PET/CT in multiple myeloma (IMPeTUs): final results. IMPeTUs (Italian myeloma criteria for PET USe). *Eur J Nucl Med Mol Imaging.* (2018) 45:712-9. doi: 10.1007/s00259-017-3909-8
16. Van Lammeren-Venema D, Regelink JC, Riphagen II, Zweegman S, Hoekstra OS, Zijlstra JM, et al. 18F-fluoro-deoxyglucose positron emission tomography in assessment of myeloma-related bone disease: a systematic review. *Cancer.* (2012) 118:1971–81. doi: 10.1002/cncr.26467
17. Zamagni E, Nanni C, Patriarca F, Englaro E, Castellucci P, Geatti O, et al. A prospective comparison of 18F-fluorodeoxyglucose positron emission tomography-computed tomography, magnetic resonance imaging and whole-body planar radiographs in the assessment of bone disease in newly diagnosed multiple myeloma. *Haematologica.* (2007) 92:50–5. doi: 10.3324/haematol.10554
18. Fonti R, Salvatore B, Quarantelli M, Sirignano C, Segreto S, Petruzziello F, et al. 18F-FDG PET/CT, 99mTc-MIBI, and MRI in evaluation of patients with multiple myeloma. *J Nucl Med.* (2008) 49:195–200. doi: 10.2967/jnumed.107.045641
19. Fonti R, Pace L, Cerchione C, Catalano L, Salvatore B, De LS, et al. 18F-fdg pet/ct, 99mtc-mibi, and mri in the prediction of outcome of patients with multiple myeloma: a comparative study. *Clin Nuclear Med.* (2015) 40:303–8. doi: 10.1097/RLU.0000000000000696
20. Salaun P-Y, Gastinne T, Frampas E, Bodet-Milin C, Moreau P, Bodéré-Kraeber F. FDG-positron-emission tomography for staging and therapeutic assessment in patients with plasmacytoma. *Haematologica.* (2008) 93:1269-71. doi: 10.3324/haematol.12654
21. Fouquet G, Guidez S, Herbaux C, Van de Wyngaert Z, Bonnet S, Beauvais D, et al. Impact of initial FD G-PET/CT and serum-free light chain on transformation of conventionally defined solitary plasmacytoma to multiple myeloma. *Clin Cancer Res.* (2014) 20:3254–60. doi: 10.1158/1078-0432.CCR-13-2910
22. Kyle RA, Larson DR, Therneau TM, Dispenzieri A, Kumar S, Cerhan JR, et al. Long- term follow-up of monoclonal gammopathy of undetermined significance. *N Engl J Med.* (2018) 378:241–9. doi: 10.1056/NEJMoa1709974
23. Siontis, B, Kumar S, Dispenzieri A, Drake MT, Lacy MQ, Buadi F, et al. Positron emission tomography-computed tomography in the diagnostic evaluation of smoldering multiple myeloma: identification of patients needing therapy. *Blood.* (2015) 2015:e364. doi: 10.1038/bcj.2015.87

24. Zamagni E, Nanni C, Gay F, Pezzi A, Patriarca F, Bellò M, et al. 18F-FDG PET/CT focal, but not osteolytic, lesions predict the progression of smoldering myeloma to active disease. *Leukemia.* (2016) 30:417–22. doi: 10.1038/leu.2015.291
25. Bartel TB, Haessler J, Brown TL, Shaughnessy JD Jr, van Rhee F, Anaissie E, et al. F18-fluorodeoxyglucose positron emission tomography in the context of other imaging techniques and prognostic factors in multiple myeloma. *Blood.* (2009) 114:2068–76. doi: 10.1182/blood-2009-03-213280
26. Zamagni E, Patriarca F, Nanni C, Zannetti B, Englaro E, Pezzi A, et al. Prognostic relevance of 18-F FDG PET/CT in newly diagnosed multiple myeloma patients treated with up-front autologous transplantation.[Erratum appears in Blood. 2012 Sep 13;120:2349]. *Blood.* (2011) 118:5989–95. doi: 10.1182/blood-2011-06-361386
27. Aljama MA, Sidiqi MH, Buadi FK, Lacy MQ, Gertz MA, Dispenzieri A, et al. Utility and prognostic value of 18 F-FDG positron emission tomography-computed tomography scans in patients with newly diagnosed multiple myeloma. *Am J Hematol.* (2018) 93:1518–23. doi: 10.1002/ajh.25279
28. Jung S-H, Kwon SY, Min J-J, Bom H-S, Ahn S-Y, Jung S-Y, et al. 18F-FDG PET/CT is useful for determining survival outcomes of patients with multiple myeloma classified as stage II and III with the Revised International Staging System. *Eur J Nucl Med Mol Imaging.* (2019) 46:107–15. doi: 10.1007/s00259-018-4114-0
29. Fonti R, Larobina M, Del Vecchio S, De Luca S, Fabbricini R, Catalano L, et al. Metabolic tumor volume assessed by 18F-FDG PET/CT for the prediction of outcome in patients with multiple myeloma. *J Nuclear Med.* (2012) 53:1829–35. doi: 10.2967/jnumed.112.106500
30. McDonald JE, Kessler MM, Gardner MW, Buros AF, Ntambi JA, Waheed S, et al. Assessment of total lesion glycolysis by 18F FDG PET/CT significantly improves prognostic value of GEP and ISS in myeloma. *Clin Cancer Res.* (2017) 23:1981–7. doi: 10.1158/1078-0432.CCR-16-0235
31. Carlier T, Jamet B, Bailly C, Touzeau C, Moreau P, Bodet-Milin C, et al. Preliminary results of prognostic added value of PET textural features at diagnosis in multiple myeloma with a long-term follow-up Oral communication. In *7th International Workshop on PET in Lymphoma and Myeloma.* Menton (2018).
32. Messiou C, Giles S, Collins DJ, West S, Davies FE, Morgan GJ, et al. Assessing response of myeloma bone disease with diffusion-weighted MRI. *Br J Radiol.* (2012) 85:e1198–203. doi: 10.1259/bjr/52759767
33. Hillengass J, Merz M, Delorme S. Minimal residual disease in multiple myeloma: use of magnetic resonance imaging. *Semin Hematol.* (2018) 55:19–21. doi: 10.1053/j.seminhematol.2018.02.001
34. Zamagni E, Tacchetti P, Cavo M. Imaging in multiple myeloma: which? when? *Blood.* (2018) 133:644–51. doi: 10.1182/blood-2018-08-825356
35. Kumar S, Paiva B, Anderson KC, Durie B, Landgren O, Moreau P, et al. International myeloma working group consensus criteria for response and minimal residual disease assessment in multiple myeloma. *Lancet Oncol.* (2016) 17:e328–46. doi: 10.1016/S1470-2045(16)30206-6
36. Usmani SZ, Mitchell A, Waheed S, Crowley J, Hoering A, Petty N, et al. Prognostic implications of serial 18-fluoro-deoxyglucose emission tomography in multiple myeloma treated with total therapy 3. *Blood.* (2013) 121:1819–23. doi: 10.1182/blood-2012-08-451690
37. Davies FE, Rosenthal A, Rasche L, Petty NM, McDonald JE, Ntambi JA, et al. Treatment to suppression of focal lesions on positron emission tomography-computed tomography is a therapeutic goal in newly diagnosed multiple myeloma. *Haematologica.* (2018) 103:1047-53. doi: 10.3324/haematol.2017.177139
38. Zamagni E, Nanni C, Mancuso K, Tacchetti P, Pezzi A, Pantani L, et al. PET/CT improves the definition of complete response and allows to detect otherwise unidentifiable skeletal progression in multiple Myeloma. *Clin Cancer Res.* (2015) 21:4384-90. doi: 10.1158/1078-0432.CCR-15-0396
39. Bailly C, Carlier T, Jamet B, Eugene T, Touzeau C, Attal M, et al. Interim PET analysis in first line therapy of multiple myeloma: prognostic value of ΔSUVmax in the FDG-avid patients of the IMAJEM study. *Clin Cancer Res.* (2018) 24:521–224. doi: 10.1158/1078-0432.CCR-18-0741
40. Nanni C, Zamagni E, Celli M, Caroli P, Ambrosini V, Tacchetti P, et al. The value of 18F-FDG PET/CT after autologous stem cell transplantation (ASCT) in patients affected by multiple myeloma (MM): experience with 77 patients. *Clin. Nuclear Med.* (2013) 38:e74–9. doi: 10.1097/RLU.0b013e318266cee2
41. Zamagni E, Nanni C, Dozza L, Carlier T, Tacchetti P, Versari A, et al. Standardization of 18F-FDG PET/CT according to deauville criteria for MRD Evaluation in newly diagnosed transplant eligible multiple myeloma patients: joined analysis of two prospective randomized phase III trials. In *Oral communication ASH Annual Meeting.* San Diego, CA (2018).
42. Lapa C, Lückerath K, Malzahn U, Samnick S, Einsele H, Buck AK, et al. 18 FDG-PET/CT for prognostic stratification of patients with multiple myeloma relapse after stem cell transplantation. *Oncotarget.* (2014) 5:7381–91. doi: 10.18632/oncotarget.2290
43. Jamet B, Bailly C, Carlier T, Planche L, Touzeau C, Kraeber-Bodéré F, et al. Added prognostic value of FDG-PET/CT in relapsing multiple myeloma patients. *Leuk Lymphoma.* (2018) 60:222–5. doi: 10.1080/10428194.2018.1459602
44. Stolzenburg A, Lückerath K, Samnick S, Speer M, Kneer K, Schmid J-S, et al. Prognostic value of [18F] FDG-PET/CT in multiple myeloma patients before and after allogeneic hematopoietic cell transplantation. *Eur J Nucl Med Mol Imaging.* (2018) 45:1694–704. doi: 10.1007/s00259-018-3997-0
45. Patriarca F, Carobolante F, Zamagni E, Montefusco V, Bruno B, Englaro E, et al. The role of positron emission tomography with 18F-fluorodeoxyglucose integrated with computed tomography in the evaluation of patients with multiple myeloma undergoing allogeneic stem cell transplantation. *Biol Blood Marrow Transplant.* (2015) 21:1068–73. doi: 10.1016/j.bbmt.2015.03.001
46. Lapa C, Garcia-Velloso MJ, Lückerath K, Samnick S, Schreder M, Otero PR, et al. 11C-methionine-PET in multiple myeloma: a combined study from two different Institutions. *Theranostics.* (2017) 7:2956–64. doi: 10.7150/thno.20491
47. Nanni C, Zamagni E, Cavo M, Rubello D, Tacchetti P, Pettinato C, et al. 11C-choline vs. 18F-FDG PET/CT in assessing bone involvement in patients with multiple myeloma. *World J Surg Oncol.* (2007) 5:68. doi: 10.1186/1477-7819-5-68
48. Cassou-Mounat T, Balogova S, Nataf V, Calzada M, Huchet V, Kerrou K, et al. 18F-fluorocholine versus 18F-fluorodeoxyglucose for PET/CT imaging in patients with suspected relapsing or progressive multiple myeloma: a pilot study. *Eur J Nucl Med Mol Imaging.* (2016) 43:1995–2004. doi: 10.1007/s00259-016-3392-7
49. Ho C, Chen S, Leung YL, Cheng T, Wong K, Cheung SK, et al. 11C-acetate PET/CT for metabolic characterization of multiple myeloma: a comparative study with 18F-FDG PET/CT. *J Nucl Med.* (2014) 55:749–52. doi: 10.2967/jnumed.113.131169
50. Vande Broek I, Leleu X, Schots R, Facon T, Vanderkerken K, Van Camp B, et al. Clinical significance of chemokine receptor (CCR1, CCR2 and CXCR4) expression in human myeloma cells: the association with disease activity and survival. *Haematologica.* (2006) 91:200–6.
51. Lapa C, Schreder M, Schirbel A, Samnick S, Kortüm KM, Herrmann K, et al. [68Ga]Pentixafor-PET/CT for imaging of chemokine receptor CXCR4 expression in multiple myeloma - Comparison to [18F]FDG and laboratory values. *Theranostics.* (2017) 7:205–12. doi: 10.7150/thno.16576
52. Herrmann K, Schottelius M, Lapa C, Osl T, Poschenrieder A, Hänscheid H, et al. First-in-human experience of CXCR4-directed endoradiotherapy with 177Lu- and 90Y-labeled pentixather in advanced-stage multiple myeloma with extensive intra- and extramedullary disease. *J Nucl Med.* (2016) 57:248-51. doi: 10.2967/jnumed.115.167361
53. Lapa C, Lückerath K, Kircher S, Hänscheid H, Grigoleit GU, Rosenwald A, et al. Potential influence of concomitant chemotherapy on CXCR4 expression in receptor directed endoradiotherapy. *Br J Haematol.* (2019) 184:440–3. doi: 10.1111/bjh.15096
54. Hovhannisyan N, Dhilly M, Fidalgo M, Fillesoye F, Guillouet S, Sola B, et al. [18F]Fludarabine-PET in a murine model of multiple myeloma. *PLoS ONE.* (2017) 12:e0177125. doi: 10.1371/journal.pone.0177125

55. Bailly C, Gouard S, Lacombe M, Remaud-Le Saëc P, Chalopin B, Bourgeois M, et al. Comparison of Immuno-PET of CD138 and PET imaging with 64CuCl2 and 18F-FDG in a preclinical syngeneic model of multiple myeloma. *Oncotarget*. (2018) 9:9061-72. doi: 10.18632/oncotarget.23886
56. Caserta E, Chea J, Minnix M, Viola D, Vonderfecht S, Yazaki P, et al. Copper 64-labeled daratumumab as a PET/CT imaging tracer for multiple myeloma. *Blood*. (2018) 131:741-5. doi: 10.1182/blood-2017-09-807263
57. Pandit-Taskar N. Functional imaging methods for assessment of minimal residual disease in multiple myeloma: current status and novel immunoPET based methods. *Semin Hematol*. (2018) 55:22-32. doi: 10.1053/j.seminhematol.2018.02.009

Conflict of Interest Statement: The authors declare that the research was conducted in the absence of any commercial or financial relationships that could be construed as a potential conflict of interest.

frontiers in Medicine

MINI REVIEW
published: 17 April 2019
doi: 10.3389/fmed.2019.00077

[^{18}F]-Fludarabine for Hematological Malignancies

Louisa Barré[1], Narinée Hovhannisyan[1], Caroline Bodet-Milin[2], Françoise Kraeber-Bodéré[2] and Gandhi Damaj[3]*

[1] LDM-TEP Group, UMR6030 Imagerie et Stratégies Thérapeutiques des Pathologies Cérébrales et Tumorales, Caen, France, [2] Service de Médecine Nucléaire, Centre Hospitalier Universitaire de Nantes, Nantes, France, [3] Department of Hematology, University Hospital Center of Caen, Caen, France

With the emergence of PET/CT using ^{18}F-FDG, molecular imaging has become the reference for lymphoma lesion detection, tumor staging, and response assessment. According to the response in some lymphoma subtypes it has also been utilized for prognostication of disease. Although ^{18}F-FDG has proved useful in the management of patients with lymphoma, the specificity of ^{18}F-FDG uptake has been critically questioned, and is not without flaws. Its dependence on glucose metabolism, which may indiscriminately increase in benign conditions, can affect the ^{18}F-FDG uptake in tumors and may explain the causes of false-positive imaging data. Considering these drawbacks, ^{18}F-fludarabine, an adenine nucleoside analog, was developed as a novel PET imaging probe. An efficient and fully automated radiosynthesis has been implemented and, subsequently preclinical studies in xenograft murine models of hematological maligancies (follicular lymphoma, CNS lymphoma, multiple myeloma) were conducted with this novel PET probe in parallel with ^{18}F-FDG. The results demonstrated several crucial points: tumor-specific targeting, weaker uptake in inflammatory processes, stronger correlation between quantitative values extracted from [^{18}F]-fludarabine and histology when compared to ^{18}F-FDG-PET, robustness during immunotherapy with rituximab, divergent responses between CNS lymphoma and glioblastoma (GBM). All these favorable findings permitted to establish a "first in man" study where 10 patients were enrolled. In DLBCL patients, increased uptake was observed in sites considered abnormal by CT and [^{18}F]FDG; in two patients discrepancies were observed in comparison with ^{18}F-FDG. In CLL patients, the uptake coincided with sites expected to be involved and displayed a significant uptake in hematopoietic bone marrow. No uptake was observed, whatever the disease group, in the cardiac muscle and brain. Moreover, its mean effective dose was below the effective dose reported for ^{18}F-FDG. These preclinical and clinical findings revealed a marked specificity of ^{18}F-fludarabine for lymphoma tissues. Furthermore, it might well be a robust tool for correctly quantifying the disease, in the presence of confounding inflammatory processes, thus avoiding false-positive results, and an innovative approach for imaging hematological malignancies.

Keywords: ^{18}F-fludarabine, lymphoma, PET—positron emission tomography, imaging, diagnosis

OPEN ACCESS

Edited by:
Anil Kumar Mishra, Institute of Nuclear Medicine & Allied Sciences (DRDO), India

Reviewed by:
George K. Loudos, Technological Educational Institute of Athens, Greece
Serge Goldman, Free University of Brussels, Belgium
Baljinder Singh, Post Graduate Institute of Medical Education and Research (PGIMER), India

****Correspondence:***
Louisa Barré
barre@cyceron.fr

Specialty section:
This article was submitted to Nuclear Medicine, a section of the journal Frontiers in Medicine

Received: *07 February 2019*
Accepted: *29 March 2019*
Published: *17 April 2019*

Citation:
Barré L, Hovhannisyan N, Bodet-Milin C, Kraeber-Bodéré F and Damaj G (2019) [^{18}F]-Fludarabine for Hematological Malignancies Front. Med. 6:77. doi: 10.3389/fmed.2019.00077

INTRODUCTION

Cancer diagnosis has significantly been improved over the past decades, due to novel imaging agents that enable earlier detection. The challenge of an imaging technique is to demonstrate with accuracy the morphology and functional status of a tumor tissue. Historically, the staging and restaging of lymphoma have been established using CT. The higher accuracy of PET/CT using ^{18}F-FDG in baseline lymphoma staging compared with traditional anatomical imaging techniques such as CT or MRI has profoundly changed the management of patients. This investigation appears as the most efficient in the initial assessment and appreciation of the therapeutic response. In addition, this approach affords important information in terms of prognosis and can lead to an optimization of the therapeutic strategy. Although PET/CT is a non-invasive imaging technique, which constitutes one of its major advantages, the findings using ^{18}F-FDG may be misinterpreted to differentiate uptake within a site of cancer from uptake in a site of inflammation or infection. In fact, false-positives occur because ^{18}F-FDG is taken up in any process associated with increased glycolysis such as inflammation, infection, or granulomatous disease. On the other hand, it is to highlight that normal physiological uptake of ^{18}F-FDG into the brain, heart, digestive tract will mask the lesion, and hence downgrade the disease falsely. A consensus exists to consider ^{18}F-FDG-PET more valuable in Hodgkin's disease and early-stage aggressive non-Hodgkin's lymphoma (NHL) and less useful in indolent NHL which represent 40% of all non-Hodgkin lymphoma subtypes (1–3).

Based on the characteristics of ^{18}F-FDG-PET, novel imaging probe must be developed to fulfill the need of a more specific radiopharmaceutical for a better tumor delineation and a more precise evaluation of the response to therapy. To improve the diagnostic accuracy, in particular in lymphoma with a fluctuating ^{18}F-FDG avidity, ^{18}F-fludarabine was introduced as a novel PET probe. Though, ^{18}F-fludarabine appears to be an appealing tool in evaluation of suspicious finding on ^{18}F-FDG PET both before or after treatment (4).

Our approach was based on the therapeutic activity of fludarabine, alone or in combination with other active drugs, in the clinical treatment of lymphoid malignancies and more particularly in the treatment of lymphoma that have a low proliferative index. Fludarabine is transported into the cells and phosphorylated intracellularly into its triphosphate form, by the deoxycytidine kinase, the principal active compound. One of the characteristics of this drug is its cellular accumulation, which is cell-cycle-independent (5). This nucleoside analog which has a fluorine atom is resistant to deamination resulting in a therapeutic activity. To elaborate a probe for PET imaging, the fluorine atom was replaced by a fluorine-18. The manufacturing process, which includes efficiency of radiolabeling, purification, and stability of the final product, automation, was subject to various quality control tests prior to ^{18}F-fludarabine implementation for *in vivo* studies (6).

RADIOSYNTHESIS OF ^{18}F-FLUDARABINE

The most reliable radiosynthesis of ^{18}F-fludarabine involved a simple two-step procedure. The strategy reported for the radiolabeling was based on a nucleophilic substitution of a nitro group at the two-position on the purine ring to act as a leaving group. The protected nitro precursor, described as a 2-nitro-pentabenzoyl adenosine derivative, was involved in a classical fluorination reaction using K^{18}F/K222 followed by an intermediate purification on a Sep-Pak silica.

To generate ^{18}F-fludarabine, hydrolysis of benzoyl groups using a mixture of methanol/aqueous ammonia was applied before a final HPLC purification. The robustness of the described process (radiochemical yield 48 $\pm$ 3%, specific activity 310 $\pm$ 72 GBq/μmol, radiochemical purity up to 99%) allowed us to initiate several preclinical studies and a first-in-man clinical trial (6).

PRECLINICAL STUDIES

In preliminary studies biodistribution or pharmacokinetic properties, metabolism, and dosimetry were established on control animals which are important prerequisites, before testing ^{18}F-fludarabine on animal models of hematological malignancies.

^{18}F-Fludarabine in Control Animals

The accumulated activity of ^{18}F-fludarabine, over 1 h period and after i.v. injection (5–12 MBq), was preferentially in the spleen and the kidneys which, respectively, confirmed the selectivity for lymphoid organ, and demonstrated its renal excretion (7). Moreover, our *in vivo* findings indicated no degradation of the probe 60 min post injection, which is an ideal characteristic for an imaging agent. To estimate the maximum dosage of ^{18}F-fludarabine that could be safely administrated to patients, radiation dose was calculated in major organs; the results revealed that the urinary bladder wall, considered as a limiting organ, received the highest dose. Nevertheless, the effective dose obtained by extrapolation of animal data to humans, was consistent (7.3 mSv) with the previously reported values of ^{18}F-FDG (3.8–10.7 mSv) (8).

^{18}F-Fludarabine in a Xenograft Model of Human Follicular Lymphoma

Follicular lymphoma is the most common subtype of indolent lymphoma. This lymphoma is FDG-avid and PET/CT using ^{18}F-FDG is the current standard tool in its management in humans (9). To determine the potential of ^{18}F-fludarabine and to acquire comparative preclinical data with ^{18}F-FDG, biodistribution was carried out in parallel on a SCID xenografted tumor model. A marked difference in their behavior was observed which was in favor of ^{18}F-fludarabine: in the tumor, its accumulation increased rapidly to reach a plateau within 20 min and its specific binding led to high-contrast images by comparison with ^{18}F-FDG (**Figure 1A**). The clear positive correlation ($p < 0.001$) between the tracer uptake in the tumor and the density of lymphoid cells (determined by histological

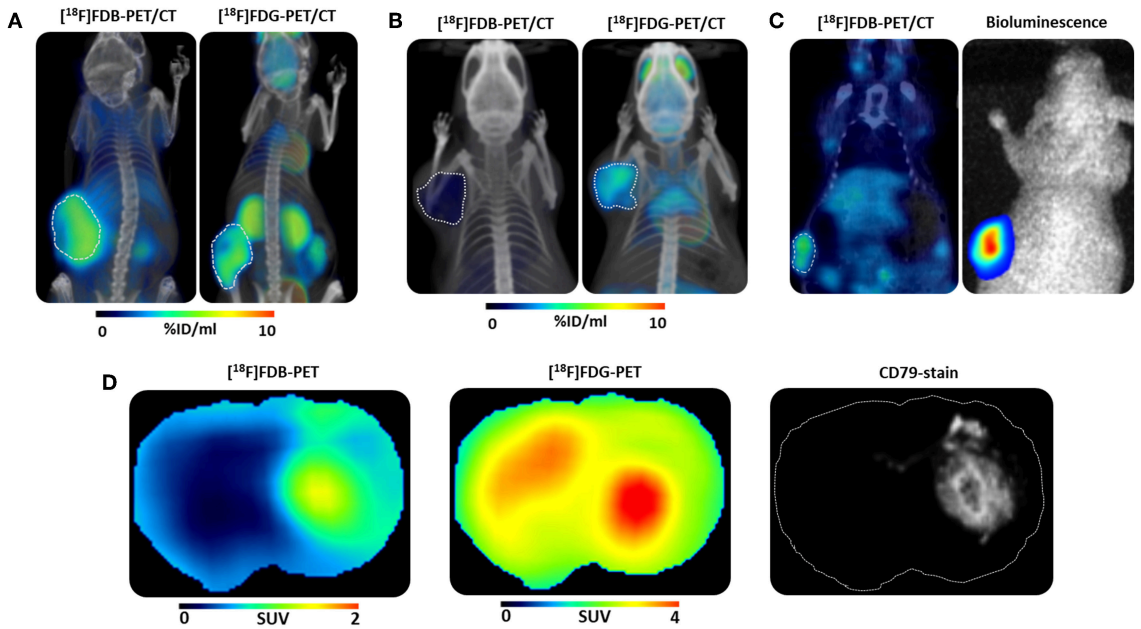

FIGURE 1 | Preclinical studies. 3D illustration of μPET/CT fused scans with [^{18}F]Fludarabine ([^{18}F]FDB) and [^{18}F]Fluorodeoxyglucose ([^{18}F]FDG) in **(A)** mice bearing human follicular lymphoma xenograft, reproduced from Hovhannisyan et al. (10), no permission required **(B)** inflammation-bearing mouse, reproduced from Hovhannisyan et al. Copyright 2016 American Chemical Society (11), permission obtained **(C)** μPET/CT scan with [^{18}F]FDB and corresponding bioluminescence image of a mouse bearing human multiple myeloma xenograft, reproduced from Hovhannisyan et al. (12), no permission required **(D)** Representative co-registered μPET scans and corresponding immunohistochemistry image of a mouse bearing human CNS lymphoma xenograft, reproduced from Hovhannisyan et al. (13), no permission required.

analysis) highlighted, the sensitivity of ^{18}F-fludarabine. It was also important to demonstrate that the treatment with the anti-CD20 antibody rituximab did not have any negative influence on the tumor-targeting ability and, we hypothesized that ^{18}F-fludarabine could be able to detect residual disease under treatment (10).

^{18}F-Fludarabine in a Murine Model of Inflammation

The major drawback of ^{18}F-FDG is its uptake in inflammatory tissue providing false-positives which could lead to a misinterpretation and perhaps an overtreatment of the patient. For this purpose, our reflex was to test ^{18}F-fludarabine and compare to ^{18}F-FDG in a previously described murine model of inflammation (14). The PET image analysis revealed that the uptake of this novel radiopharmaceutical in the inflamed tissue is negligible compared to ^{18}F-FDG (**Figure 1B**). These results enhance the potential of ^{18}F-fludarabine as a more specific probe (11).

^{18}F-Fludarabine in Brain Tumors (CNS Lymphoma vs. Glioblastoma)

Primary central nervous system lymphoma (PCNSL) account for 5% of primary brain tumors and are predominantly diffuse large B cell lymphoma (90% of cases). MRI is the reference imaging for the diagnosis and monitoring (15). The evaluation of the therapeutic response, based on MRI, is perfectible. This imaging modality can miss atypical forms not enhanced by gadolinium and the significance of contrast enhancement occurring under or after treatment is sometimes ambiguous (16). ^{18}F-FDG is established as the reference imaging in systemic lymphomas, but its applications in PSNCL are restricted by the limited specificity of cerebral fixations, and high uptake in healthy brain tissue (17). Taken into account the limitations of ^{18}F-FDG, we demonstrated in a human CNS lymphoma model the pertinence to use ^{18}F-fludarabine to detect brain lesions and we established its superiority over^{18}F-FDG in differentiating brain tumors (13).

In the CNS lymphoma model, which closely mimics disseminated lesions, a marked retention was observed with ^{18}F-fludarabine in accordance with histological findings (CD79 staining) representative of cells lymphoma ($p < 0.001$). ^{18}F-Fludarabine exhibited tumor to background ratio (TBR) 2 to 3-fold higher than ^{18}F-FDG, this made delineation of the tumor more precise. ^{18}F-FDG, on the other hand, is poor in accurate delineation of the lesion due to its normal physiological brain uptake and poor specificity (**Figure 1D**). Considering high-grade glioma (GBM) and CNS lymphoma differentiation, the diagnostic accuracy is uncertain due to a similar imaging appearance on MRI or the previously described limitations of ^{18}F-FDG. The scenario to use ^{18}F-fludarabine is relevant taking into consideration that this probe has a rapid clearance from glioblastoma and this feature can help to discriminate between both brain tumors.

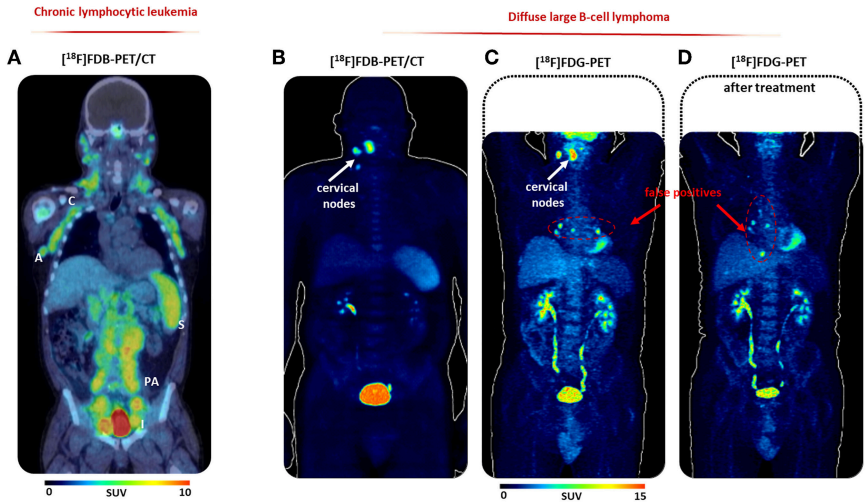

FIGURE 2 | First-in-man study. **(A)** [^{18}F]FDB-PET/CT (30–50 min scan period) of a representative CLL patient; **(B)** [^{18}F]FDB-PET (30–50 min scan period), **(C)** [^{18}F]FDG-PET (60–80 min), and **(D)** post-treatment (60–80 min) of a representative DLBCL patient, reproduced from Chantepie et al. (18), no permission required. A, axillary nodes; C, cervical nodes; I, iliac nodes; PA, paraaortic nodes; S, spleen.

^{18}F-Fludarabine in Multiple Myeloma (MM)

Multiple myeloma (MM) is a clonal plasma cells that accounts for 15% of all hematological malignancies. ^{18}F-FDG is an accepted imaging technique to assess and monitor myeloma therapy. Despite the fact that ^{18}F-FDG is reasonably sensitive and specific for bone disease, the detection of diffuse infiltration of plasma-cells in bone marrow, and lytic lesions in the skull is underestimated (1, 19). Based on our previous results in the animal models, ^{18}F-fludarabine was then considered in a xenograft MM murine model. The tumor growth was followed by bioluminescence (BLI), after injection of a luciferase reporter MM cell line and characterized by immunohistochemistry (IHC, CD 138 staining) (**Figure 1C**). To compare with ^{18}F-FDG, the metabolically active tumor was defined for both radiotracers (12). Although the ^{18}F-FDG uptake was superior, the quantitative data extracted from IHC or BLI are in better agreement with the ^{18}F-fludarabine uptake. These findings enforce the hypothesis that this radiopharmaceutical could be more suitable to detect MM disease.

CLINICAL STUDY

The reported preclinical studies revealed the real potential of ^{18}F-fludarabine to detect hematological malignancies and have resulted in the design of a clinical research protocol. This novel PET probe has been evaluated in human to better identify pathological from physiological or inflammatory uptake at initial staging of the disease and, in the future to enhance PET performance for therapeutic evaluation. Ten untreated patients with either B-cell chronic lymphocytic leukemia (B-CLL, $n = 5$) or diffuse large B-cell lymphoma (DLBCL, $n = 5$) were included in the study (18). CLL imaging with ^{18}F-FDG-PET is not recommended, except in the case of suspected disease transformation (Richter syndrome), in contrast to DLBCL disease where it is being included as part of clinical practice. Nevertheless, despite an excellent sensitivity, the analysis of some areas remains difficult due to the lack of ^{18}F-FDG specificity (bone marrow or spleen for example). Despite new criteria (20), the interpretation of ^{18}F-FDG-PET positivity after therapy remains difficult, partly due to tumor-, and/or treatment-associated inflammation leading to false positives (4).

The design of the pilot clinical trial was to acquire six successive partial body scans for 250 min (0–10, 15–25, 30–50, 90–100, 180–190, 240–250 min) after i.v. injection of ^{18}F-fludarabine (4 MBq/kg) in both groups. In all patients, any side effects were observed to the radiopharmaceutical injection. The average activity received by the patients was 305 ± 76 MBq with a ^{18}F-fludarabine mass of 0.23 ± 0.14 μg. The results with conventional modalities CT and [^{18}F]FDG-PET (for DLBCL) were investigated. The imaging session was performed 60–80 min after injection of 335 ± 77MBq of ^{18}F-FDG. In DLBCL patients, increased uptake of ^{18}F-fludarabine was observed in sites deemed suspicious by CT and/or ^{18}F-FDG. At 50 min, SUVs were significantly higher in involved lesions (SUVmax = 7.1) in comparison with histologically normal bone marrow (SUVmax = 2.3) or ascending aorta considered as reference (SUVmax = 1.4). In this group, aged 57–73 years, divergence was observed in two patients. In one patient a positivity with ^{18}F-FDG was detected and not with ^{18}F-fludarabine in bilateral hilar foci. These foci persisted at subsequent evaluation with ^{18}F-FDG and were considered as false positives (**Figures 2B–D**). Indeed this patient was free from relapse more than 2 years after the end of treatment. In the second patient, unilateral testicular lymphomatous infiltration was not observed with ^{18}F-fludarabine and could be attributed to the role of the testis barrier (21). In CLL patients, aged 51–70 years, ^{18}F-fludarabine revealed all involved lymph nodes, with also a marked accumulation in the spleen and bone marrow

involvement. At 50 min, SUVmax was 1.5 on the mediastinal vascular noise (taken as reference) against 6.05 in the affected lymph nodes, 7.7 for the spleen, and 4.4 in bone marrow, indicating a very good tumor/tissue contrast (**Figure 2A**). In both groups, no physiological uptake was noted in heart and brain.

CONCLUSION

This recent study as a "proof of concept" in human paved the way to several underway national clinical trials including a larger cohort of patients to define the role and prognostic impact of ^{18}F-fludarabine-PET/CT in the management of hematological malignancies. An exploratory, multicenter prospective clinical trial to evaluate the interest of PET images using ^{18}F-fludarabine for initial staging and therapeutic evaluation in three subtypes of newly diagnosed lymphomas (DLBCL, Hodgkin lymphoma, and follicular lymphoma) is ongoing.

AUTHOR CONTRIBUTIONS

LB prepared a first draft of the manuscript. NH, CB-M, FK-B, and GD critically reviewed the manuscript. All authors conceived the idea of this review article and approved the final version.

FUNDING

All this research was supported by a grant from Commissariat à l'Energie Atomique et aux Energies Alternatives (CEA), the French National Agency for Research (ANR-11 LABEX-0018-01) and the Region Basse-Normandie.

ACKNOWLEDGMENTS

The authors gratefully acknowledge the team Laboratoire de Développements Méthodologiques en TEP.

REFERENCES

1. Valls L, Badve C, Avril S, Herrmann K, Faulhaber P, O'Donnell J, et al. FDG-PET imaging in hematological malignancies. *Blood Rev*. (2016) 30:317–31. doi: 10.1016/j.blre.2016.02.003
2. Ayers EC, Fardin S, Gholami S, Alavi A, Mato AR. Personalized management approaches in lymphoma: utility of fluorodeoxyglucose-PET imaging. *PET Clin*. (2016) 11:209–18. doi: 10.1016/j.cpet.2016.02.001
3. Alobthani G, Romanov V, Isohashi K, Matsunaga K, Watabe T, Kato H, et al. Value of 18F-FDG PET/CT in discrimination between indolent and aggressive non-Hodgkin's lymphoma: a study of 328 patients. *Hell J Nucl Med*. (2018) 21:7–14. doi: 10.1967/s002449910701
4. Barrington SF, Friedman K. PET/MRI in lymphoma. In: Iagaru A, Hope T, Veit-Haibach P, editors. *PET/MRI in Oncology*. Cham: Springer (2018). p. 373–400.
5. Grégoire V, Van NT, Stephens LC, Brock WA, Milas L, Plunkett W, et al. The role of fludarabine-induced apoptosis and cell cycle synchronization in enhanced murine tumor radiation response *in vivo*. *Cancer Res*. (1994) 54:6201–9.
6. Guillouet S, Patin D, Tirel O, Delamare J, Gourand F, Deloye JB, et al. Fully automated radiosynthesis of 2-[18F]fludarabine for PET imaging of low-grade lymphoma. *Mol Imaging Biol*. (2014) 16:28–35. doi: 10.1007/s11307-013-0657-4
7. Dhilly M, Guillouet S, Patin D, Fillsoye F, Abbas A, Gourand F, et al. 2-[18F]Fludarabine, a novel positron emission tomography (PET) tracer for imaging lymphoma: a micro-PET study in murine models. *Mol Imaging Biol*. (2014) 16:118–26. doi: 10.1007/s11307-013-0659-2
8. Deloar HM, Fujiwara T, Shidahara M, Nakamura T, Watabe H, Narita Y, et al. Estimation of absorbed dose for 2-[F-18]fluoro-2-deoxy-D-glucose using whole-body positron emission tomography and magnetic resonance imaging. *Eur J Nucl Med*. (1998) 25:565–74. doi: 10.1007/s002590050257
9. Wirth A, Foo M, Seymour JF, Macmanus MP, Hicks RJ. Impact of [18f]fluorodeoxyglucose positron emission tomography on staging and management of early-stage follicular non-Hodgkin lymphoma. *Int J Radiat Oncol Biol Phys*. (2008) 71:213–9. doi: 10.1016/j.ijrobp.2007.09.051
10. Hovhannisyan N, Guillouet S, Fillesoye F, Dhilly M, Patin D, Galateau F, et al. Evaluation of the specificity of [18F]fludarabine PET/CT in a xenograft model of follicular lymphoma: comparison with [18F]FDG and impact of rituximab therapy. *EJNMMI Res*. (2015) 5:23. doi: 10.1186/s13550-015-0101-7
11. Hovhannisyan N, Dhilly M, Guillouet S, Leporier M, Barré L. Comparative analysis between [18F]Fludarabine-PET and [18F]FDG-PET in a murine model of iInflammation. *Mol Pharm*. (2016) 13:2136–9. doi: 10.1021/acs.molpharmaceut.6b00050
12. Hovhannisyan N, Dhilly M, Fidalgo M, Fillesoye F, Guillouet S, Sola B, et al. [18F]Fludarabine-PET in a murine model of multiple myeloma. *PLoS ONE*. (2017) 12:e0177125. doi: 10.1371/journal.pone.0177125
13. Hovhannisyan N, Fillesoye F, Guillouet S, Ibazizene M, Toutain J, Gourand F, et al. [18 F]Fludarabine-PET as a promising tool for differentiating CNS lymphoma and glioblastoma: comparative analysis with [18F]FDG in human xenograft models. *Theranostics*. (2018) 8:4563–73. doi: 10.7150/thno.26754
14. Yamada S, Kubota K, Kubota R, Ido T, Tamahashi N. High accumulation of fluorine-18-fluorodeoxyglucose in turpentine-induced inflammatory tissue. *J Nucl Med*. (1995) 36:1301–6.
15. Hoang-Xuan K, Bessell E, Bromberg J, Hottinger AF, Preusser M, Rudà R, et al. Diagnosis and treatment of primary CNS lymphoma in immunocompetent patients: guidelines from the European Association for Neuro-Oncology. *Lancet Oncol*. (2015) 16:e322–32. doi: 10.1016/S1470-2045(15)00076-5
16. Valles FE, Perez-Valles CL, Regalado S, Barajas RF, Rubenstein JL, Cha S. Combined diffusion and perfusion MR imaging as biomarkers of prognosis in immunocompetent patients with primary central nervous system lymphoma. *Am J Neuroradiol*. (2013) 34:35–40. doi: 10.3174/ajnr.A3165
17. Kawai N, Miyake K, Okada M, Yamamoto Y, Nishiyama Y, Tamiya T. Usefulness and limitation of FDG-PET in the diagnosis of primary central nervous system lymphoma. *No Shinkei Geka*. (2013) 41:117–26. doi: 10.11477/mf.1436101928
18. Chantepie S, Hovhannisyan N, Guillouet S, Pelage J-P, Ibazizene M, Bodet-Milin C, et al. 18F-Fludarabine-PET for lymphoma imaging: first-in-man study in DLBCL and CLL patients. *J Nucl Med*. (2018) 59:1380–5. doi: 10.2967/jnumed.117.206920
19. Cavo M, Terpos E, Nanni C, Moreau P, Lentzsch S, Zweegman S. Role of 18F-FDG PET/CT in the diagnosis and management of multiple myeloma and other plasma cell disorders: a consensus statement by the International Myeloma Working Group. *Lancet Oncol*. (2017) 18:e206–17. doi: 10.1016/S1470-2045(17)30189-4
20. Cheson BD, Fisher RI, Barrington SF, Cavalli F, Schwartz LH, Zucca E, et al. Andrew lister recommendations for initial evaluation, staging, and response assessment of Hodgkin and non-hodgkin lymphoma: the Lugano classification. *J Clin Oncol*. (2014) 32:3059–67. doi: 10.1200/JCO.2013.54.8800
21. Horne MJ, Adeniran AJ. Primary diffuse large B-cell lymphoma of the testis. *Arch Pathol Lab Med*. (2011) 135:1363–7. doi: 10.5858/arpa.2010-0158-RS

Conflict of Interest Statement: The authors declare that the research was conducted in the absence of any commercial or financial relationships that could be construed as a potential conflict of interest.

frontiers in Medicine

REVIEW
published: 03 May 2019
doi: 10.3389/fmed.2019.00090

The Story of the Dopamine Transporter PET Tracer LBT-999: From Conception to Clinical Use

Sylvie Chalon[1]*, *Johnny Vercouillie*[1,2], *Pierre Payoux*[3,4], *Jean-Bernard Deloye*[5], *Cécile Malherbe*[1], *Florence Le Jeune*[6,7], *Nicolas Arlicot*[1,2,8], *Anne-Sophie Salabert*[3,4], *Denis Guilloteau*[1,8], *Patrick Emond*[1,8] and *Maria-Joao Ribeiro*[1,2,8]

[1] UMR 1253, iBrain, Université de Tours, Inserm, Tours, France, [2] Inserm CIC 1415, University Hospital, Tours, France, [3] ToNIC, Toulouse NeuroImaging Center, Université de Toulouse, Inserm, UPS, Toulouse, France, [4] University Hospital, Nuclear Medicine Unit, Toulouse, France, [5] Zionexa, 42 avenue de la Grande Armée, Paris, France, [6] University of Rennes 1, Rennes, France, [7] Department of Nuclear Medicine, Centre Eugène Marquis, Rennes, France, [8] CHRU Tours, Tours, France

The membrane dopamine transporter (DAT) is involved in a number of brain disorders and its exploration by positron emission tomography (PET) imaging is highly relevant for the early and differential diagnosis, follow-up and treatment assessment of these diseases. A number of carbon-11 and fluor-18 labeled tracers are to date available for this aim, the majority of them being derived from the chemical structure of cocaine. The development of such a tracer, from its conception to its use, is a long process, the expected result being to obtain the best radiopharmaceutical adapted for clinical protocols. In this context, the cocaine derivative *(E)-N*-(4-fluorobut-2-enyl)2β-carbomethoxy-3β-(4′-tolyl)nortropane, or LBT-999, has passed all the required stages of the development that makes it now a highly relevant imaging tool, particularly in the context of Parkinson's disease. This review describes the different steps of the development of LBT-999 which initially came from its non-fluorinated derivative (*E*)-*N*-(3-iodoprop-2-enyl)-2-carbomethoxy-3-(4-methylphenyl) nortropane, or PE2I, because of its high promising properties. [^{18}F]LBT-999 has been extensively characterized in rodent and non-human primate models, in which it demonstrated its capability to explore *in vivo* the DAT localized at the dopaminergic nerve endings as well as at the mesencephalic cell bodies, in physiological conditions. In lesion-induced rat models of Parkinson's disease, [^{18}F]LBT-999 was able to precisely quantify *in vivo* the dopaminergic neuron loss, and to assess the beneficial effects of therapeutic approaches such as pharmacological treatment and cell transplantation. Finally recent clinical data demonstrated the efficiency of [^{18}F]LBT-999 in the diagnosis of Parkinson's disease.

Keywords: PET, dopaminergic neuron, Parkinson's disease, radiopharmaceutical, basal ganglia

OPEN ACCESS

Edited by:
Thierry M. L. B. Vander Borght, Catholic University of Louvain, Belgium

Reviewed by:
Ramin Sadeghi, Mashhad University of Medical Sciences, Iran
Serge Goldman, Free University of Brussels, Belgium

***Correspondence:**
Sylvie Chalon
sylvie.chalon@univ-tours.fr

Specialty section:
This article was submitted to Nuclear Medicine, a section of the journal Frontiers in Medicine

Received: *25 February 2019*
Accepted: *10 April 2019*
Published: *03 May 2019*

Citation:
Chalon S, Vercouillie J, Payoux P, Deloye J-B, Malherbe C, Le Jeune F, Arlicot N, Salabert A-S, Guilloteau D, Emond P and Ribeiro M-J (2019) The Story of the Dopamine Transporter PET Tracer LBT-999: From Conception to Clinical Use. Front. Med. 6:90. doi: 10.3389/fmed.2019.00090

IN VIVO IMAGING OF THE DAT: A HIGHLY POTENT TOOL FOR BRAIN DISORDERS

The dopaminergic neurotransmission is strongly involved in the regulation of multiple brain functions such as locomotion, cognition and reward, and then plays a major role in a great number of brain disorders such as Parkinson's disease (PD) (1) but also several neuropsychiatric disorders (2). In this context, *in vivo* exploration of this system through molecular imaging methods is a

real added value for the diagnosis, follow-up, and treatment of such disorders. Several molecular targets of the dopaminergic neurotransmission can be explored *in vivo*, at both the pre- and post-synaptic level. These explorations require the use of specific radiotracers able to bind specifically to each target and then to quantify it as accurately as possible. For this aim a high number of tracers have been developed, either labeled with γ emitters such as ^{123}I or ^{99m}Tc for single photon emission tomography (SPECT), or with β+ emitters such as ^{11}C or ^{18}F for positron emission tomography (PET). Several tracers are yet available for the different types of post-synaptic dopaminergic receptors (3). Regarding pre-synaptic dopaminergic neurons, SPECT and/or PET exploration of three main molecular targets are to date available. The 6-[^{18}F]-fluoro-L-dopa or [^{18}F]DOPA uptake, which reflects both the conversion of Dopa into dopamine (DA) and the storage of DA into synaptic vesicles, has been the first gold standard tool (4). Besides, the vesicular monoamine transporter 2 (VMAT2) and the membrane dopamine transporter (DAT) can also be explored. The respective advantages and drawbacks related to imaging these different pre-synaptic molecular targets have mainly been compared in the context of PD, and prominent conclusions are summarized in **Table 1**.

For a long time, the DAT has been identified as a target of choice because its localization makes it a marker of neuron integrity and density, and also because it is a key-actor in the regulation of synaptic dopamine levels (13). A high number of SPECT and PET tracers have been developed for DAT imaging. In all cases, they were derived from known ligands of the DAT, and most of them from the tropane structure characteristic of cocaine (14). The first of these tracers which demonstrated its potency in the field of PD using SPECT imaging was the 2β-carbomethoxy-3β-(4-iodophenyl)tropane (β-CIT) (15), which bound to the DAT with a high affinity (around 3 nM) and accumulated significantly in dopaminergic brain areas when labeled with iodine-123. Although β-CIT demonstrated its usefulness for the detection of DAT loss in PD, it had several drawbacks such as a similar affinity for the dopamine and serotonin transporters (16), a poor signal/noise ratio and an *in vivo* kinetics requiring as long as 24 h to reach equilibrium state allowing the DAT quantification in the striatum (17).

A number of new β-CIT derivatives were then proposed to overcome these weaknesses. Among them, the N-(3-iodopro-2*E*-enyl)-2β-carbomethoxy-3β-(4-methylphenyl)nortropane (PE2I) is structurally characterized by the presence of a methyl group on the phenyl ring of the β-CIT structure instead of an iodine, and

TABLE 1 | Presynaptic molecular PET imaging targets of the dopaminergic neurotransmission.

Molecular target	Examples of tracer	Advantages	Drawbacks	References
DOPA decarboxylase	[^{18}F]F-DOPA	– Distinguishes patients with advanced PD from patients with *de novo* PD	– Reflects both the conversion of Dopa into DA and pre-synaptic storage of DA – Possible under-estimation of DA neurons loss in *de novo* PD patients due to an up-regulation of DA synthesis	(5–7)
Vesicular monoamine transporter 2 (VMAT2)	[^{11}C]DTBZ [^{18}F]AV-133	– Detects early PD vs. healthy controls – Improves diagnostic accuracy in clinically uncertain parkinsonian syndrome	– Present on all monoaminergic neurons	(8–10)
Membrane dopamine transporter (DAT)	[^{18}F]FP-CIT [^{11}C]PE2I [^{18}F]FE-PE2I	– Distinguishes patients with advanced PD from patients with *de novo* PD – Greater sensitivity than F-DOPA for detecting motor severity in PD – Identification of patients at risks for developing PSP or FTD	– Possible over-estimation of DA neurons loss due to a down-regulation of the DAT	(5, 11, 12)

AV-133, fluoropropyldihydrotetrabenazine; DA, dopamine; F-DOPA, 6-fluoro-dopa; DTBZ, dihydrotetrabenazine, FDT, frontotemporal dementia; PSP, progressive supranuclear palsy.

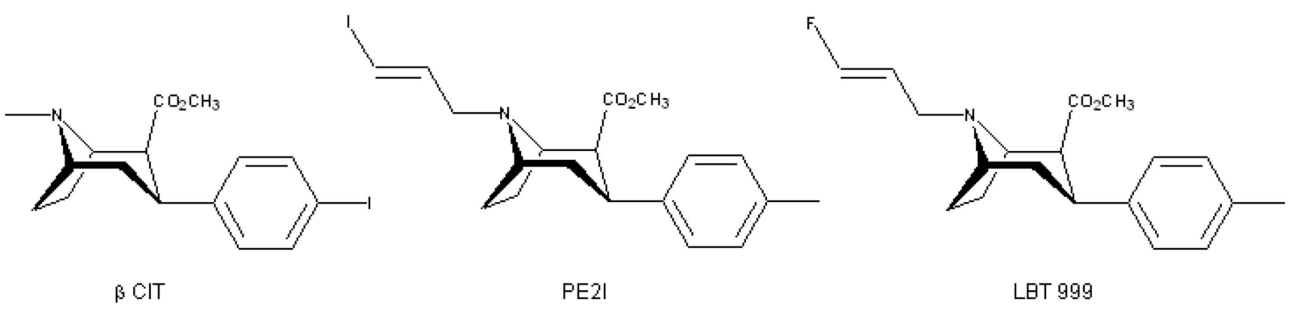

FIGURE 1 | Chemical structures of β-CIT, PE2I, and LBT-999.

a 3-iodopro-2E-enyl group at the tropane nitrogen instead of a methyl carried by β-CIT (18). These chemical modifications have led to a significant improvement in the pharmacological profile of this ligand (19, 20), showing a high selectivity for the DAT toward the serotonin transporter (SERT). The high affinity and selectivity made PE2I a highly potent tracer to image the DAT *in vivo* either by SPECT when labeled with ^{123}I and by PET when labeled with ^{11}C. In this context, [^{123}I]PE2I demonstrated its usefulness for the differential diagnosis between patients suffering from PD and atypical parkinsonian syndromes without degeneration of striatal dopaminergic nerve endings (21). The PET imaging with [^{11}C]PE2I has also been successfully used in this same disease (11, 22) but also in schizophrenia (23, 24), attention deficit / hyperactivity disorders (25) and more recently in the exploration of the reward dopaminergic pathway (26).

DEVELOPMENT OF LBT-999

Regarding the high potency of binding of PE2I for the DAT and because PET imaging enables *in vivo* exploration at high resolution and high sensitivity, we developed the fluorinated derivative of PE2I, i.e., 8-((E)-4-fluoro-but-2-enyl)-3β-p-tolyl-8-aza-bicyclo[3.2.1]octane-2β-carboxylic acid methyl ester (LBT-999) (**Figure 1**).

The *in vitro* pharmacological evaluation of LBT-999 demonstrated that its properties was close to that of PE2I, with a good affinity for the DAT (9 nM) and a Ki > 1 μM for different ligands of the serotonin and norepinephrine transporters (27). Firstly, LBT-999 was labeled with carbon-11 (28) by methylation of the acid precursor that can be obtained in an easier way compared to a precursor useable for fluorine labeling. The [^{11}C]LBT-999 shown to have a high *in vivo* accumulation in brain areas containing high levels of DAT both in rats and monkeys (27, 28). Based on these results, the development of the radiolabeling with [^{18}F] was then realized, first using a two-step methodology (29) followed by a one-step approach (30) required for rapid and reproducible radiofluorination dedicated to preclinical and clinical studies. As for the [^{11}C]LBT-999, [^{18}F]LBT-999 rapidly, and highly entered the rat brain where its distribution was in agreement with the DAT density. Importantly, 1 h post-injection, the *in vivo* specific binding represented by the ratio of accumulation in the striatum to cerebellum, was 10 times higher for LBT-999 (ratio of 25) (27) compared to that we obtained previously with PE2I in same experimental conditions (31). For LBT as for PE2I, the striatal accumulation at 1 h post-injection was around 70% decreased in the presence of a saturating dose of the DAT inhibitor GBR12909, whereas no significant effect was observed with a pre-injection of paroxetine (SERT ligand) or nisoxetine (NET ligand). In monkey, LBT-999 was also able to bind specifically to the DAT, either labeled with [^{11}C] (27) or with [^{18}F] (32). This last study demonstrated that LBT was also suitable for DAT exploration in extra-striatal regions, and that the estimated dosimetry was acceptable for human use.

PRECLINICAL EXPERIMENTS IN ANIMAL MODELS

As the final aim of the development of a new PET tracer is its use for human health improvement, it is of high value to explore the properties of such a candidate tracer in animal models of human diseases. For this purpose, we performed in a first step in rats, an extensive test-retest study that demonstrated the ability of [^{18}F]LBT-999 to quantify the DAT with high reproducibility (variability of 8–14%) and reliability (intra-class correlation coefficient, ICC, of 0.9) in the striatum, whereas these parameters were less accurate in the substantia nigra, in relation with the small size of this brain structure (33). In a rat model of early PD induced by a moderate unilateral striatal lesion using 6-hydroxydopamine (6-OHDA), we showed that [^{18}F]LBT-999 was

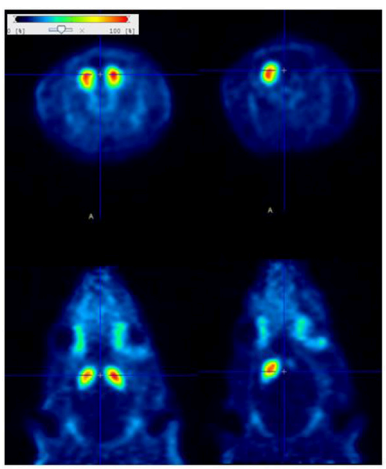

FIGURE 2 | Coronal (upper side) and axial (lower side) PET static images (30–50 min post-injection) obtained with [^{18}F]LBT-999 in a normal rat (left) and in a rat lesioned with 6-OHDA in the right striatum. The quantitative analysis revealed a decreased of 70% in the tracer accumulation in the lesioned vs. intact striatum.

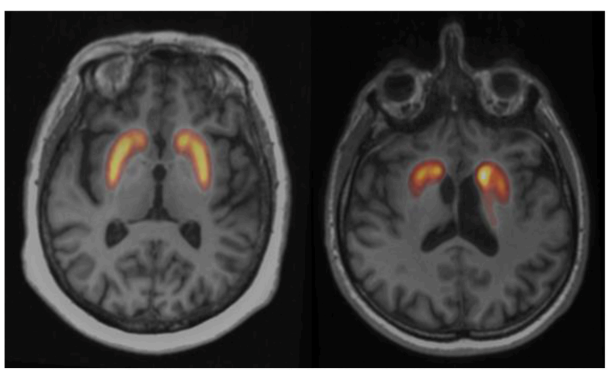

FIGURE 3 | Fusion axial slices between PET and MRI of the [^{18}F]LBT-999 uptake at the level of the striatum in a control subject (left) and a drug-naïve patient with early Parkinson disease (right). The radiopharmaceutical uptake is asymmetrically decreased in Parkinson patient.

able to accurately quantify *in vivo* the dopaminergic endings loss (**Figure 2**), in full agreement with the results obtained by *in vitro* autoradiography with [125I]PE2I on brain sections (34).

It was also important to assess the potency of [18F]LBT-999 to evaluate the efficacy of various therapeutic approaches aiming at the preservation or replacement of dopaminergic neurons *in vivo* in the rat model of 6-OHDA lesions. This property was demonstrated in the case of a pharmacological therapeutic approach (35) as well as for the graft of human embryonic stem cells-derived midbrain dopaminergic neurons (36). These whole findings provided strong preclinical support for clinical translation of [18F]LBT-999.

THE USE OF [18F]LBT-999 IN HUMAN

[18F]LBT-999 has recently been evaluated in clinical setting (37, 38). Preliminary results on a small sample of 6 subjects with early Parkinson's disease and 8 healthy controls demonstrated that injection of [18F]LBT-999 is feasible and pharmacologically safe. [18F]LBT-999 distribution was consistent with DAT density in human brain and PET images in both caudate and putamen nuclei indicate that this tracer may successfully differentiate the two groups of subjects (**Figure 3**). On the basis of these initial findings, [18F]LBT-999 might be a suitable radiopharmaceutical for PET assessment of DAT in future clinical studies.

CONCLUSIONS

After the identification of a brain molecular target whose PET exploration would be crucial for improvement of the diagnosis and/or treatment of a particular disease, it is a long way to make available an optimal radiotracer. A very high number of tracers have been developed as potential DAT imaging agents, the most promising being based on the tropane scaffold derived from the structure of cocaine. Several SPECT compounds are used in clinical protocols, such as ^{99m}Tc-TRODAT (39) and [123I]FP-CIT (40). However, they suffer from many disadvantages such as poor sensitivity, spatial resolution, and slow kinetic uptake, and PET ligands should be a good alternative. We described in this paper the development of one of these tracers, [18F]LBT-999, which has the particularity to be highly specific for its target, and which is now ready to be used for clinical purpose.

AUTHOR CONTRIBUTIONS

All authors listed have made a substantial, direct and intellectual contribution to the work, and approved it for publication.

ACKNOWLEDGMENTS

This work was supported by Labex IRON (ANR-11-LABX-18-01).

REFERENCES

1. Meder D, Herz DM, Rowe JB, Lehéricy S, Siebner HR. The role of dopamine in the brain – lessons learned from Parkinson's disease. *NeuroImage.* (2018) 190:79–93. doi: 10.1016/j.neuroimage.2018.11.021
2. Thal LB, Tomlinson ID, Quinlan MA, Kovtun O, Blakely RD, Rosenthal SJ. Single quantum dot imaging reveals PKCβ-dependent alterations in membrane diffusion and clustering of an attention-deficit hyperactivity disorder / autism / bipolar disorder-associated dopamine transporter variant. *ACS Chem Neurosci.* (2019) 10:460–71. doi: 10.1021/acschemneuro.8b00350
3. Niccolini F, Su P, Politis M. Dopamine receptor mapping with PET imaging in Parkinson's disease *J Neurol.* (2014) 261:2251–63. doi: 10.1007/s00415-014-7302-2
4. Gjegge A, Reith J, Dyve S, Leger G, Guttman M, Diksic M, et al. Dopa decarboxylase activity of the living human brain. *Proc Natl Acad Sci USA.* (1991) 88:2721–5.
5. Eshuis SA, Maguire RP, Leenders KL, Jonkman S, JagerPL. Comparison of FP-CIT SPECT with F-DOPA PET in patients with de novo and advanced Parkinson's disease. *Eur J Nucl Med Mol Imaging.* (2006) 33:200–9. doi: 10.1007/s00259-005-1904-y
6. Lee CS, Samii A, Sossi V, Ruth TJ, Schulzer M, Holden JE, et al. *In vivo* positron emission tomographic evidence for compensatory changes in presynaptic dopaminergic nerve terminals in Parkinson's disease. *Ann Neurol.* (2000) 47:493–503. doi: 10.1002/1531-8249(200004)47:4<493::AID-ANA13>3.0.CO;2-4
7. Ribeiro M-J, Vidailhet M, Loc'h C, Dupel C, Nguyen J-P, Ponchant M, et al. Dopaminergic function and dopamine transporter binding assessed with positron emission tomography in Parkinson disease. *Arch Neurol.* (2002) 59:580–6. doi: 10.1001/archneur.59.4.580
8. Martin WR, Wieler M, Stoessl AJ, Schulzer M. Dihydrotetrabenazine positron emission tomography imaging in early, untreated Parkinson's disease. *Ann Neurol.* (2008) 63:388–94. doi: 10.1002/ana.21320
9. Okamura N, Villemagne VL, Drago J, Pejoska S, Dhamija RK, Mulligan RS, et al. *In vivo* measurement of vesicular monoamine transporter type 2 density in Parkinson disease with 18F-AV-133. *J Nucl Med.* (2010) 51:223–8. doi: 10.2967/jnumed.109.070094
10. Xu SS, Alexander PK, Lie Y, Dore V, Bozinovski S, Mulligan RS, et al. Diagnostic accuracy of imaging brain vesicular monoamine transporter type 2 (VMAT2) in clinically uncertain parkinsonian syndrome (CUPS): a 3-year follow-up study in community patients. *BMJ Open.* (2018) 8:e025533. doi: 10.1136/bmjopen-2018-025533.
11. Li W, Lao-Kaim NP, Roussakis AA, Martín-Bastida A, Valle-Guzman N, Paul G, et al. 11C-PE2I and 18F-Dopa PET for assessing progression rate in Parkinson's: a longitudinal study. *Mov Dis.* (2018) 33:117–27. doi: 10.1002/mds.27183
12. Yoo HS, Chung SJ, Kim S-J, Oh JS, Kim JS, Ye BS, et al. The role of 18F-FP-CIT PET in differentiation of progressive supranuclear palsy and frontotemporal dementia in the early stage. *Eur J Nucl Med Mol Imaging.* (2018) 45:1585–95. doi: 10.1007/s00259-018-4019-y
13. Mulvihill KG. Presynaptic regulation of dopamine release: Role of the DAT and VMAT2 transporters. *Neurochem Int.* (2019) 122:94–105. doi: 10.1016/j.neuint.2018.11.004
14. Brooks DJ Molecular imaging of dopamine transporter. *Aging Res Rev.* (2016) 30:114–21. doi: 10.1016/j.arr.2015.12.009
15. Innis RB, Seibyl JP, Scanley BE, Laruelle M, Abi-Dargham A, Wallace E, et al. Single photon emission computed tomographic imaging demonstrates loss of striatal dopamine transporters in Parkinson disease. *Proc Natl Acad Sci USA.* (1993) 90: 11965–9.
16. Boja JW, Mitchell WM, Patel A, Kopajtic TA, Carroll FI, Lewin AH, et al. High-affinity binding of [125I]RTI-55 to dopamine and serotonin transporters in rat brain. *Synapse.* (1992) 12:27–36.
17. Laruelle M, Wallace E, Seibyl JP, Baldwin RM, Zea-Ponce Y, Zoghbi SS, et al. Graphical, kinetic, and equilibrium analyses of in vivo [123I] beta-CIT binding to dopamine transporters in healthy human subjects. *J Cereb Blood Flow Metab.* (1994) 14:982–94.
18. Emond P, Garreau L, Chalon S, Boazi M, Caillet M, Bricard J, et al. Synthesis and ligand binding of nortropane derivatives: N-substituted

2β-Carbomethoxy-3β-(4′-iodophenyl)nortropane and *N*-(3-Iodoprop-(2*E*)-enyl)-2β-carbomethoxy-3β-(3′,4′-disubstituted phenyl)nortropane. New high-affinity and selective compounds for the dopamine transporter. *J Med Chem.* (1997) 40:1366–72.

19. Chalon S, Garreau L, Emond P, Zimmer L, Vilar MP, Besnard JC, et al. Pharmacological characterization of (*E*)-*N*-(3-iodoprop-2-enyl)-2β-Carbomethoxy-3β-(4′-methylphenyl)nortropane as a selective and potent inhibitor of the neuronal dopamine transporter. *J Pharmacol Exp Ther.* (1999) 291:648–54.
20. Emond P, Guilloteau D, Chalon S. PE2I: a radiopharmaceutical for in vivo exploration of the dopamine transporter. *CNS Neurosci Ther.* (2008) 14:47–64. doi: 10.1111/j.1527-3458.2007.00033.x
21. Ziebell M, Andersen BB, Thomsen G, Pinborg LH, Karlsborg M, Hasselbalch SG, et al. Predictive value of dopamine SPECT imaging with [123I]PE2I in patients with subtle parkinsonian symptoms. *Eur J Nucl Med Mol Imaging.* (2012) 39:242–50. doi: 10.1007/s00259-011-1976-9
22. Appel L, Jonasson M, Danfors T, Nyholm D, Askmark H, Lubberink M, et al. Use of [11C]PE2I PET in differential diagnosis of Parkinsonian disorders. *J Nucl Med.* (2015) 56:234–42. doi: 10.2967/jnumed.114.148619
23. Arakawa R, Ichimiya T, Ito H, Takano A, Okumura M, Takahashi H et al. Increase in thalamic binding of [11C]PE2I in patients with schizophrenia: a positron emission tomography study of dopamine transporter. *J Psychiatr Res.* (2009) 43:1219–23. doi: 10.1016/j.jpsychires.2009.04.009
24. Artiges E, Leroy C, Dubol M, Prat M, Pepin A, Mabondo A et al. Striatal and extrastriatal dopamine transporter availability in schizophrenia and its clinical correlates: a voxel-based and high-resolution PET study. *Schizophrenia Bull.* (2017) 43:1134–42. doi: 10.1093/schbul/sbw192
25. Jucaite A, Fernell E, Halldin C, Forssberg H, Farde L. Reduced midbrain dopamine transporter binding in male adolescents with attention-deficit/hyperactivity disorder: association between striatal dopamine markers and motor hyperactivity. *Biol Psychiatry.* (2005) 57:229–38. doi: 10.1016/j.biopsych.2004.11.009
26. Dubol M, Trichard C, Leroy C, Sandu AL, Rahim M, Granger B, et al. Dopamine transporter and reward anticipation in a dimensional perspective: a multimodal brain imaging study. *Neuropsychopharmacology.* (2018) 43:820–7. doi: 10.1038/npp.2017.183
27. Chalon S, Hall H, Saba W, Garreau L, Dollé F, Halldin C, et al. Pharmacological characterization of (E)-N-(4-fluorobut-2-enyl)-2beta-carbomethoxy-3beta-(4'-tolyl)nortropane (LBT-999) as a highly promising fluorinated ligand for the dopamine transporter. *J Pharmacol Exp Ther.* (2006) 317:147–52. doi: 10.1124/jpet.105.096792
28. Dollé F, Emond P, Mavel S, Dezmphel S, Hinnen F, Mincheva Z, et al. Synthesis, radiosynthesis and *in vivo* preliminary evaluation of [11C]LBT-999, a selective radioligand for the visualization of the dopamine transporter with PET. *Bioorg Med Chem.* (2006) 14:1115–25. doi: 10.1016/j.bmc.2005.09.035
29. Dollé F, Hinnen F, Emond P, Mavel S, Mincheva Z, Saba W, et al. Radiosynthesis of [18F]LBT-999, a selective radioligand for the visualization of the dopamine transporter with PET. *J. Labelled Compd Rad.* (2006) 49:687–98. doi: 10.1002/jlcr.1092
30. Dollé F, Helfenbein J, Hinnen F, Mavel S, Mincheva Z, Saba W, et al. One-step radiosynthesis of [18F]LBT-999: a selective radioligand for the visualization of the dopamine transporter with PET. *J. Labelled Compd Rad.* (2007) 50:716–23. doi: 10.1002/jlcr.1412
31. Guilloteau D, Emond P, Baulieu JL, Garreau L, Frangin Y, Pourcelot L, et al. Exploration of the Dopamine Transporter: *in vitro* and *in vivo* characterization of a high-affinity and high-specificity iodinated tropane Derivative (*E*)-*N*-(3-iodoprop-2-enyl)-2β-carbomethoxy-3β-(4′-methylphenyl) nortropane (PE2I). *Nucl Med Biol.* (1998) 25:331–7.
32. Varrone A, Stepanov V, Nakao R, Toth M, Gulyas B, Emond P, et al. Imaging of the striatal and extrastriatal dopamine transporter with 18F-LBT-999: quantification, biodistribution, and radiation dosimetry in nonhuman primates. *J Nucl Med.* (2011) 52:1313–21. doi: 10.2967/jnumed.111.089953
33. Sérrière S, Tauber C, Vercouillie J, Guilloteau D, Deloye JB, Garreau L, et al. *In vivo* PET quantification of the dopamine transporter in rat brain with [18F]LBT-999. *Nucl Med Biol.* (2014) 41:106–13. doi: 10.1016/j.nucmedbio.2013.09.007
34. Vetel S, Sérrière S, Vercouillie J, Vergote J, Chicheri G, Deloye JB, et al. Extensive exploration of a novel rat model of Parkinson's disease using partial 6-hydroxydopamine lesion of dopaminergic neurons suggests new therapeutic approaches. *Synapse.* (2018) 73:e22077. doi: 10.1002/syn.22077
35. Sérrière S, Doméné A, Vercouillie J, Mothes C, Bodard S, Rodrigues N, et al. Assessment of the protection of dopaminergic neurons by an alpha7 nicotinic receptor agonist, PHA 543613 using [(18)F]LBT-999 in a Parkinson's disease rat model. *Front Med.* (2015) 2:61. doi: 10.3389/fmed.2015.00061
36. Grealish S, Diguet E, Kirkeby A, Mattson B, Heuer A, Bramoulle Y, et al. Human ESC-derived dopamine neurons show similar preclinical efficacy and potency to fetal neurons when grafted in a rat model of Parkinson's disease. *Cell Stem Cell.* (2014) 15:653–65. doi: 10.1016/j.stem.2014.09.017
37. Arlicot N, Vercouillie J, Malherbe C, Bidault R, Gissot V, Maia S, et al. PET imaging of Dopamine Transporter with 18F-LBT999: first human exploration. *J Nucl Med.* (2017) 58:276.
38. Ribeiro MJ, Vercouillie J, Arlicot N, Mondon K, Gissot V, Maia S, et al. A simplified method for the diagnosis of striatal dopaminergic dysfunction using PET with a new fluorine DAT tracer, the 18F-LBT-999. *J Nucl Med.* (2017) 58:413.
39. Gupta V, Ranjan R, Verma R, Belho ES, Malik D, Mahajan H. Correlation of 99mTc-TRODAT-1 SPECT imaging findings and clinical staging of Parkinson's disease. *Clin Nucl Med.* (2019) 44:347–50. doi: 10.1097/RLU.0000000000002529
40. Jakobson Mo S, Axelsson J, Jonasson L, Larsson A, Ögren MJ, Ögren M, et al. Dopamine transporter imaging with [18F]FE-PE2I PET and [123I]FP-CIT SPECT-a clinical comparison. *EJNMMI Res.* (2018) 8:100. doi: 10.1186/s13550-018-0450-0

Conflict of Interest Statement: J-BD was employed by company Zionexa, Paris, France.

The remaining authors declare that the research was conducted in the absence of any commercial or financial relationships that could be construed as a potential conflict of interest.

frontiers in Medicine

REVIEW
published: 04 June 2019
doi: 10.3389/fmed.2019.00124

Clinical Results in Medullary Thyroid Carcinoma Suggest High Potential of Pretargeted Immuno-PET for Tumor Imaging and Theranostic Approaches

*Caroline Bodet-Milin[1,2], Clément Bailly[1,2], Yann Touchefeu[2,3], Eric Frampas[1,4], Mickael Bourgeois[1,2], Aurore Rauscher[2,5], Franck Lacoeuille[6], Delphine Drui[7], Nicolas Arlicot[8], David M. Goldenberg[9,10], Alain Faivre-Chauvet[1,2], Jacques Barbet[11], Caroline Rousseau[2,5] and Françoise Kraeber-Bodéré[1,2,5]**

[1] Nuclear Medicine, University Hospital, Nantes, France, [2] CRCINA, INSERM, CNRS, Université d'Angers, Université de Nantes, Nantes, France, [3] Hepato-Gastro-enterology, University Hospital, Nantes, France, [4] Radiology, University Hospital, Nantes, France, [5] Nuclear Medicine, ICO Cancer Center, Saint-Herblain, France, [6] Nuclear Medicine, University Hospital, Angers, France, [7] Endocrinology Department, University Hospital, Nantes, France, [8] Nuclear Medicine, University Hospital, Tours, France, [9] IBC Pharmaceuticals, Inc., Morris Plains, NJ, United States, [10] Immunomedics, Inc., Morris Plains, NJ, United States, [11] GIP Arronax, Saint-Herblain, France

OPEN ACCESS

Edited by:
Ronan Abgral,
Centre Hospitalier Regional Universitaire (CHU) de Brest, France

Reviewed by:
Guus Van Dongen,
University Medical Center Amsterdam, Netherlands
Désirée Deandreis,
University of Turin, Italy

***Correspondence:**
Françoise Kraeber-Bodéré
francoise.bodere@chu-nantes.fr

Specialty section:
This article was submitted to Nuclear Medicine, a section of the journal Frontiers in Medicine

Received: 19 February 2019
Accepted: 17 May 2019
Published: 04 June 2019

Citation:
Bodet-Milin C, Bailly C, Touchefeu Y, Frampas E, Bourgeois M, Rauscher A, Lacoeuille F, Drui D, Arlicot N, Goldenberg DM, Faivre-Chauvet A, Barbet J, Rousseau C and Kraeber-Bodéré F (2019) Clinical Results in Medullary Thyroid Carcinoma Suggest High Potential of Pretargeted Immuno-PET for Tumor Imaging and Theranostic Approaches. Front. Med. 6:124. doi: 10.3389/fmed.2019.00124

Monoclonal antibody (mAb)-based therapies have experienced considerable growth in cancer management. When labeled with radionuclides, mAbs also represent promising probes for imaging or theranostic approaches. Initially, mAbs have been radiolabeled with single-photon emitters, such as ^{131}I, ^{99m}Tc, or ^{111}In, for diagnostic purposes or to improve radioimmunotherapy (RIT) using dosimetry estimations. Today, more accurate imaging is achieved using positron- emission tomography (PET). Thanks to the important technical advances in the production of PET emitters and their related radiolabeling methods, the last decade has witnessed the development of a broad range of new probes for specific PET imaging. Immuno-PET, which combines the high sensitivity and resolution of a PET camera with the specificity of a monoclonal antibody, is fully in line with this approach. As RIT, immuno-PET can be performed using directly radiolabeled mAbs or using pretargeting to improve imaging contrast. Pretargeted immuno-PET has been developed against different antigens, and promising results have been reported in tumor expressing carcinoembryonic antigen (CEA; CEACAM5) using a bispecific mAb (BsmAb) and a radiolabeled peptide. Medullary thyroid carcinoma (MTC) is an uncommon thyroid cancer subtype which accounts for $<$10% of all thyroid neoplasms. Characterized by an intense expression of CEA, MTC represents a relevant tumor model for immuno-PET. High sensitivity of pretargeted immunoscintigraphy using murine or chimeric anti-CEA BsMAb and pretargeted haptens-peptides labeled with ^{111}In or ^{131}I were reported in metastatic MTC patients 20 years ago. Recently, an innovative clinical study reported high tumor uptake and contrast using pretargeted anti-CEA immuno-PET in relapsed MTC patients. This review focuses on MTC as an example, but the same pretargeting technique has been applied with success for clinical PET imaging of other

CEA-expressing tumors and other pretargeting systems. In particular, those exploiting bioorthogonal chemistry also appear interesting in preclinical animal models, suggesting the high potential of pretargeting for diagnostic and theranostic applications.

Keywords: medullary thyroid carcinoma (MTC), immunoPET, theranostic (therapeutic and diagnostic), pretargeted imaging, radioimmunoconjugate

INTRODUCTION

Targeting radionuclides to tumor cells using monoclonal antibodies (mAbs) has emerged for imaging and therapy purposes (1). The production of chimeric or humanized mAbs with lower immunogenicity than murine mAbs prompted the clinical development of immunotherapy, and the anti-tumor effects reported with trastuzumab in breast cancer (BC) expressing HER2 and of the anti-CD20 rituximab in B-cell non-Hodgkin lymphoma demonstrated for the first time the high potential of mAbs for cancer therapy. The clinical successes of rituximab and trastuzumab have accelerated the research for new target membrane proteins in different types of malignant tumors. Some monoclonal antibodies have also been radiolabeled for tumor imaging by scintigraphy with promising initial results. Yet, in spite of mAbs' good specificity, the expected success was limited by the low resolution of the images. Thanks to significant technical progress in the production of positron emitters and their labeling methods, as well as the development of more sensitive detectors and specific software, the last decade has seen the development of a wide range of new PET radiopharmaceuticals. In medical practice, the identification of biomarkers is gradually becoming a prerequisite for any treatment decision, along with the approach of personalized medicine. Immuno-PET, which combines the high sensitivity and resolution of a PET camera with mAb's specificity, is an excellent candidate for this new concept (2, 3). mAbs labeled with radionuclides represent promising probes for theranostic approaches, providing a non-invasive solution for *in vivo* evaluation of target expression, distribution and accessibility, and for obtaining reliable information for diagnosis, prognosis, and therapy. Based on immunoPET, treatment strategies could be adapted to each patient before pricey and potentially toxic treatments are administered (4, 5).

Medullary thyroid carcinoma (MTC) accounts for <10% of all thyroid cancers (6). After initial surgery, serum calcitonin is used to monitor residual disease, which is still detectable in nearly 20% of patients after surgery. Imaging including neck ultrasound, neck and chest computed tomography (CT), liver contrast-enhanced CT or magnetic resonance imaging (MRI), and spine and pelvis bone MRI are recommended when calcitonin exceeds 150 pg/ml (7). Due to their ability to characterize and quantify cancer molecular processes, ^{18}F-DOPA or ^{18}F-FDG PET tracers also have a major interest in patients with recurrent MTC and offer great potential as surrogate biomarkers, useful for early response evaluation and prediction of outcomes (8–11).

MTC is characterized by a high and homogeneous expression of ACE. Several clinical trials have shown pretargeted immunoscintigraphy's sensitivity, performed using the Affinity Enhancement System (AES) based on the injection of murine or chimeric anti-CEA bispecific antibodies (BsMAb) and pretargeted haptenpeptides radiolabeled with ^{111}In or ^{131}I (12, 13). Prolonged tumor efficacy was also observed using therapeutic haptens radiolabeled with ^{131}I (14). These results and the high potential of pretargeting reported in other solid tumors using different radioimmunoconjugates suggested that pretargeted peptides labeled with PET emitters would take advantage of the better sensitivity and resolution of PET compared to SPECT and provide high sensitivity and specificity imaging under good conditions of radiation protection and dosimetry (15–17). However, no clinical study has yet compared pretargeted immuno-PET with pretargeted immuno-SPECT.

This review focuses on MTC as an example, but the same pretargeting technique has been applied with success for clinical PET imaging of other CEA-expressing tumors and, in mice, to other target antigens (18). Other pretargeting systems, in particular those exploiting bio-orthogonal chemistry, also appear interesting in preclinical animal models, suggesting the high potential of pretargeting for diagnostic or theranostic applications (19).

Choice of Radionuclide for Immuno-PET

For nearly 30 years, mAbs have been labeled with gamma-emitting radionuclides, such as ^{131}I, ^{99m}Tc, or ^{111}In for planar or Single Photon Emission Computed Tomography (SPECT) imaging. However, the sensitivity of these techniques is low, the resolution poor and accurate quantitative information cannot be obtained. PET provides quantitative information and has a better spatial resolution that allows for good delineation of tumors and organs. In addition, exact attenuation correction, precise dispersion correction, improved sensitivity, good signal-to-noise ratios, and the ability to perform true whole body imaging within a reasonable time frame are key factors in the outperformance of PET over SPECT.

Marrying mAbs and PET emitters requires an appropriate match between the biologic half-life of the protein and the physical half-life of the isotope to achieve optimal tumor-to-background activity ratios (4, 5). Indeed, intact mAbs have a circulation time of several days, and longer imaging windows allow for both the accumulation of the tracer in the target tissue and the clearance of unbound tracer from the blood pool. This in turn leads to improved image contrast and tumor-to-background activity ratios. ^{89}Zr and ^{124}I are well suited to the labeling of large molecules, such as intact mAbs. The long half-life also offers an advantage for logistics related to transportation. ^{64}Cu, with an intermediate half- life of 12.7 h, can be used for labeling a large number of molecules of different sizes ^{18}F or ^{68}Ga, with their short half-life, may be used to label small-size

molecules, such as peptides or small molecular weight binding proteins, that distribute rapidly in the body. They are appropriate for pretargeted PET imaging, as shown for ^{68}Ga in the studies discussed here. ^{18}F may also be used to label the haptens or small molecular weight tracers for pretargeting and, for example, this was done in preclinical studies with a NOTA-derivatized hapten by the formation of an aluminum-fluoride complex (20, 21).

From a "theranostic" perspective, the pairs of beta+/beta emitting radionuclides (^{124}I/^{131}I, ^{86}Y/^{90}Y, ^{64}Cu/^{67}Cu, ^{44}Sc/^{47} Sc) are very promising as the same distribution is expected both for imaging dosimetry and therapy.

Other considerations must also be taken into account when selecting appropriate radionuclides. In addition to the half-life, the existence of concomitant gamma emissions will have significant effects on the radiation dose received by the patient. Positron range may affect resolution if the positron travels a significant distance before annihilation. Finally, additional factors to consider include cost and availability.

Pretargeting for Immuno-PET

Since the first clinical pretargeted scintigraphy and radioimmunotherapy clinical studies discussed previously (12–14), new pretargeting reagents for the AES method have been designed (20–23). TF2 is an engineered BsMAb composed of anti-hapten Fab-fragment derived from the murine 679 antibody recognizing the histamine-succinyl-glycine (HSG) motif, and two humanized anti-CEA Fab-fragments derived from the hMN-14 antibody, formed into a trivalent 157 kD protein by the Dock-and-Lock® procedure (22). IMP288 is a bivalent HSG hapten that can be labeled with a variety of radionuclides for therapy (^{90}Y and ^{177}Lu), scintigraphy (^{111}In) or PET (^{124}I, ^{68}Ga, and ^{18}F) (20, 21, 23). The clinical implementation of pretargeting requires a first phase to optimize the BsMAb and peptide molar doses and a delay between the two injections (24–27). The first clinical results were reported using TF2/^{177}Lu-IMP288 in colorectal carcinoma patients. Fast tumor uptake and high tumor-to-background activity ratios were observed within a few hours (24, 25). These results using TF2/^{177}Lu-IMP288 were confirmed in a phase I clinical trial performed in patients with CEA-positive lung cancer (27). This phase I study determined that a pretargeting delay of 24 h between the TF2 and the radiolabeled peptide injections was considered the best compromise between the high tumor uptake required to deliver a high irradiation dose to tumor cells and a high tumor-to-background activity ratio to reduce irradiation of normal tissues. Along the same line, high doses of TF2 (75 mg/m^2) were used to deliver sufficient irradiation using a 10:1 TF2: hapten molar ratio. The rapid distribution of the reagents observed in these therapy trials, indicated that that labeling with the short-lived radionuclides, ^{68}Ga or ^{18}F, for PET should be feasible. Whereas, ^{18}F allows PET imaging with better resolution than ^{68}Ga possibly with lower cost, the choice between ^{68}Ga and ^{18}F would mostly depend on the logistics of the clinical centers. With ^{68}Ga having the advantage of availability via a generator (20), the imaging performance of immuno-PET using TF2/^{68}Ga-IMP288 was tested in an orthotopic murine xenograft model of human colonic liver metastases (28). ^{68}Ga-immuno-PET allowed for better tumor/organ ratios compared to ^{18}FDG-PET ($P < 0.05$) for both imaging and biodistribution. Sixty-seven percent of tumors were detected with ^{68}Ga-immuno-PET vs. 31% with ^{18}FDG PET ($P = 0.049$). For tumors <200 mg, the sensitivity was 44% with ^{68}Ga-immuno-PET vs. 0% for ^{18}FDG PET ($P = 0.031$). Finally, tumor uptake measured on PET images was strongly correlated to biodistribution analyses ($r^2 = 0.85$).

Preliminary Results of Pretargeting Immuno-PET in MTC Patients

A pilot clinical study was designed in relapsed MTC patients to transfer TF2 /^{68}Ga-IMP288 pretargeting to the clinic. The first part of the study aimed at determining the best pretargeting parameters. Different cohorts of patients were injected with variable TF2 and IMP288 molar doses at variable pretargeting delays. The second part was designed to assess immuno-PET performance. Adults with a histological diagnosis of MTC treated by complete surgery and presenting a calcitonin serum level ≥150 pg/ml, with at least one lesion ≥10 mm on conventional imaging, were eligible. The results of the first part of the study have been published, and the analysis of the second part is in progress (29). First, the molar doses of TF2 and hapten were reduced as compared to the therapy studies, because the injected activity of short-lived ^{68}Ga was set to 150 MBq, as compared to GBq activities of ^{177}Lu for therapy. According to a PET semi-quantitative analysis and pharmacokinetic studies, the 30-h pretargeting delay between BsMAb and peptide injections was the most favorable for imaging: tumor uptake was not significantly reduced as compared to 24-h and tumor/background ratios were better. Pretargeted immuno-PET detected MTC confirmed foci in all patients except one. Our previous studies showed that CEA expression seemed to be almost constant in MTC, and that high sensitivity PET imaging using CEA as a target would detect the disease independently of the prognosis, in contrast to ^{18}FDG or ^{18}F-DOPA PET/CT (10, 12, 13, 29). The preliminary results obtained in the first 12 MTC patients already suggested that high tumor contrast can be obtained using this novel whole-body imaging (**Figure 1**) (29, 30). In this small cohort of metastatic patients with a median calcitonin of 915 pg/ml (249–5,300) and CEA of 29.5 ng/ml (7.4–257), a total of 110 lesions were detected by immuno-PET, whereas CT detected 59 lesions, bone MRI 12 lesions, liver MRI 13 lesions, and ^{18}F-DOPA-PET/CT 63 lesions. Since pathological confirmation was generally not possible, in the MTC studies and in other pathologies such as colorectal cancer and breast cancer discussed below, the Gold Standard was defined as follow. A lesion detected by immuno-PET was considered to be related to cancer when it was confirmed by histology and/or detected by another imaging method and/or confirmed by follow-up. Complementary imaging (for example CT, MRI, ^{18}F-DOPA PET and ^{18}FDG PET in the MTC study) could be prescribed within 3 months after immuno-PET to confirm anomalies detected by immuno-PET but not visualized on the inclusion imaging assessment. The preliminary analysis then resulted in an overall sensitivity of 89% for immuno-PET, with 100% sensitivity for

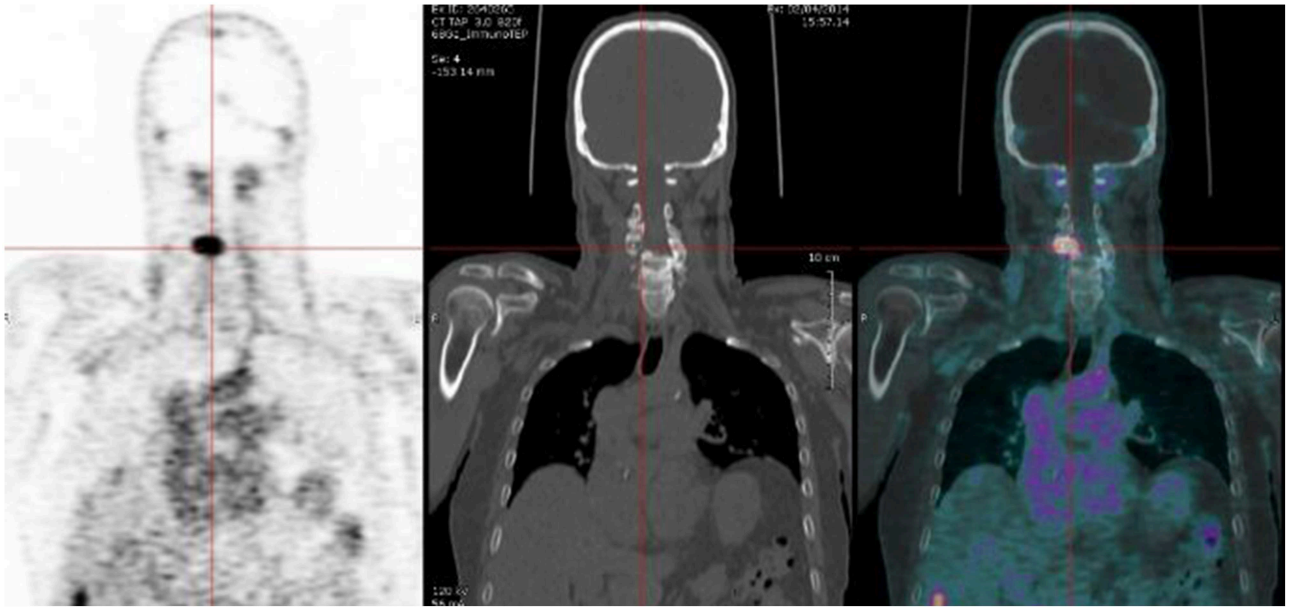

FIGURE 1 | Immuno-PET performed using TF2 BsMAb and ^{68}Ga-IMP288 peptide in a MTC patient with a spinal lesion.

lymph nodes and liver, 87% for bone, and 42% for lungs. Overall sensitivities of CT, bone MRI, liver MRI and ^{18}F-DOPA-PET/CT were 77, 92, 76, and 66%, respectively.

Promising Performance of Pretargeted ^{68}Ga-IMP288 in Other CEA-Positive Tumors

CEA is expressed in other solid tumors, and pretargeted immuno-PET has also been assessed with promising results in BC and colorectal carcinoma (CRC). Preliminary results have been reported at international congresses (31, 32). In the 9 metastatic BC patients enrolled in an optimization immuno-PET study evaluating TF2 /^{68}Ga-IMP288, with median CA15-3 was 249.3 kUI/L (40–2,448) and a median CEA of 76 μg/L (9.5–1359.0), pretargeted anti-CEA immuno-PET allowed the detection of a total of 533 lesions, whereas 245 lesions were detected by CT, 160 by bone MRI, and 425 by ^{18}FDG-PET/CT (**Figure 2**). Immuno-PET showed 92.5% overall sensitivity, with, respectively, 100% sensitivity for bone, liver, skin, and brain, 91% for lymph nodes, and 28.5% for lung. Brain lesions were only seen on immuno-PET imaging and secondly confirmed by MRI.

Another pilot study included 11 patients who received an imaging work-up for the diagnosis of metastases from CEA-expressing CRC, comprising TF2/^{68}Ga-IMP288 immuno-PET, ^{18}FDG-PET, thoraco-abdominopelvic CT, liver MRI, and abdominal ultrasound scanning. In the per-patient analysis, immuno-PET was positive in 9/11 patients. The two negative patients were, respectively, one false-negative (single lung metastasis) and one true-negative (mediastinal sarcoidosis). On a per-lesion analysis, the sensitivity, specificity, positive predictive value and negative predictive value were, respectively, 82, 25, 82, and 25% for the morphological assessment (CT + ultrasound + MRI); 76, 67, 87, and 33% for ^{18}FDG-PET; and 88, 100, 100, 67% for immuno-PET (32).

These data show high performances of pretargeted immuno-PET in tumor detection, except for lung lesions. Several hypotheses can explain the low sensitivity in this organ. On the one hand, the current generations of CT scanners are very sensitive and can diagnose very small pulmonary nodules. Thus, since our Gold standard does not require histological evidence, micronodules considered as discretely progressive on follow up CT scans were validated as related to tumor. The very small size of some of these lesions could explain the low sensitivity of immuno-PET since immuno-PET images were recorded in "spontaneous breathing" thus underestimating the uptake in infra-centimetric pulmonary nodules due to the partial volume effect related to the amplitude of respiratory movements. On the other hand, immunoscintigraphy images recorded 5–10 days after hapten injection showed better sensitivity in lung lesions (10). So, it is possible that immuno-PET images have been recorded too early after hapten injection to allow the visualization of some infra-centimetric pulmonary nodules. Later images may have improved tumor contrast. A longer half-life radionuclide like ^{64}Cu, permitting later images, could improve PET sensitivity to detect lung nodules.

Other Pretargeting Systems

Pretargeted immuno-PET using the AES method also has been successfully assessed against other tumor antigens in preclinical models (18). TF12 is a trivalent BsMAb consisting in two anti-TROP-2 Fab fragments and one anti-HSG Fab fragment. Many epithelial cancers, including prostate cancer (PC) express the TROP-2 antigen. The potential of pretargeted immuno-PET with TF2 /^{68}Ga-IMP288, was studied in mice with

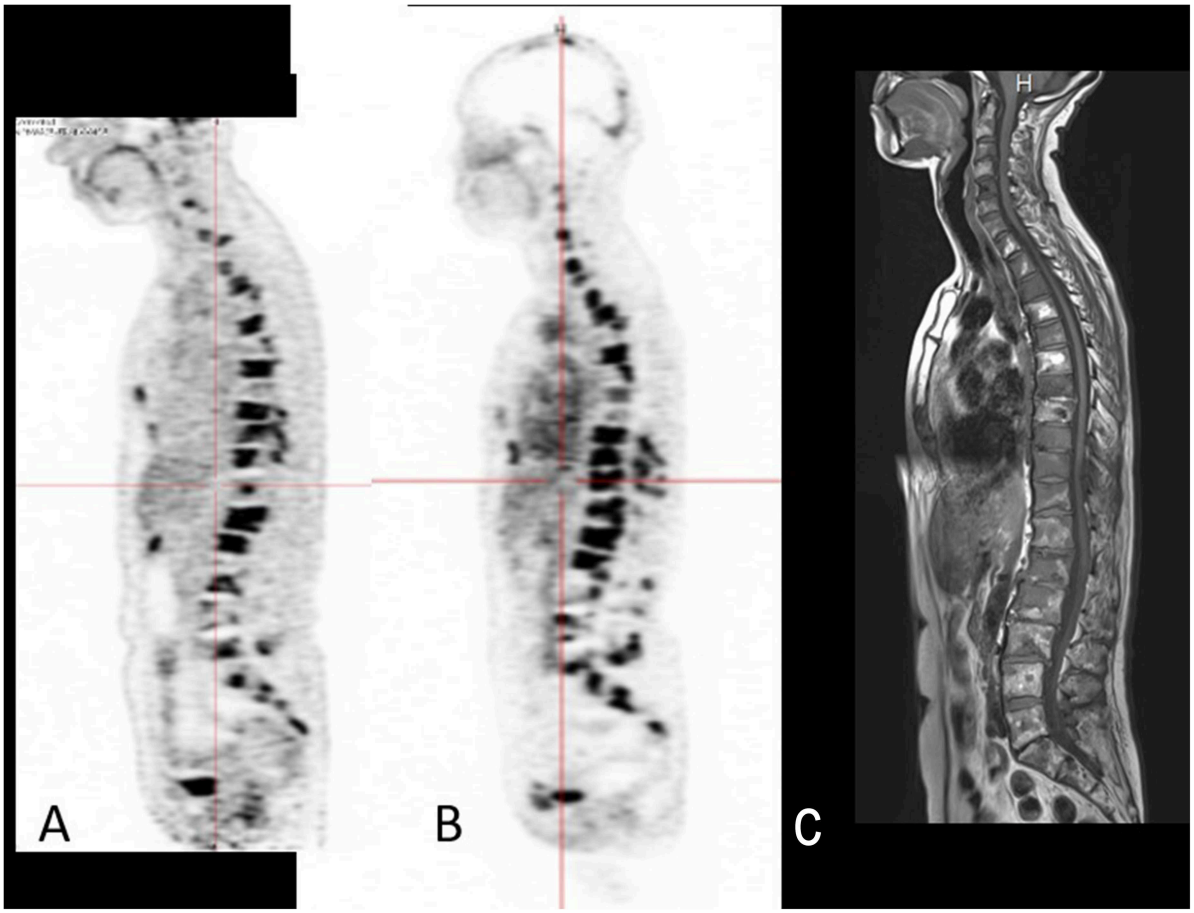

FIGURE 2 | (A) FDG PET/CT, **(B)** Immuno-PET with TF2 and ^{68}Ga-IMP288 peptide showing multiple spine bone foci, and **(C)** STIR TSE bone MRI showing multiple spine bone abnormalities in a BC patient.

subcutaneous and intraperitoneal PC3 human prostate tumors, using ^{18}FDG-PET as a reference. ^{68}Ga-IMP288 demonstrated a rapid accumulation in the TF12 pretargeted subcutaneous tumors (7.2 ± 1.1% ID/g), and low blood levels and kidney uptake resulting in high tumor/blood ratios (17.4 ± 11.2) at 1 h p.i. ^{18}FDG's uptake was significantly lower (3.4 ± 0.9% ID/g, $P = 0.008$), with lower tumor/blood ratios (3.0 ± 1.9, $P = 0.011$). Immuno-PET identified both subcutaneous and intraperitoneal tumors as small as 5 mm^3, suggesting that the method was efficient for rapid, sensitive, and specific imaging of PC.

Recently, entirely different pretargeting approaches have been developed or revisited. One is based on the *in vivo* formation of an oligonucleotide duplex. A first oligonucleotide analog (e.g., peptide nucleic acid or PNA) is coupled to an antibody or binding protein (an anti-HER2 Affibody) for pretargeting of a radiolabeled complementary oligonucleotide analog (33). Good tumor targeting was achieved with a significant reduction in blood and kidney retention 1 h after activity injection, as compared to the directly-labeled Affibody in a human ovarian cancer model in mice. The other approach, which attracts even more interest, is based on bio-orthogonal chemistry, also known as click chemistry. While click chemistry became quite popular about 15 years ago for various coupling reactions *in vitro*, it was soon discovered that these very fast chemical reactions can occur *in vivo* as well with similar efficiency and specificity. They were soon proposed for pretargeting applications (34). The CC49 antibody recognizing the TAG72 antigen derivatized with trans-cyclooctene (TCO) was used for pretargeting ^{111}In-labeled DOTA-dipyridyltetrazine, demonstrating fast and high tumor activity uptake and high tumor-to-muscle ratios in a mouse model. This pioneering work was followed by a large number of preclinical investigations aiming at further improving the pretargeting performance by testing alternative bio-orthogonal chemistry reagents, adding a chase step between the injection of the antibody and that of the labeled compound, and also by applying bio-orthogonal pretargeting to small-binding proteins, such as diabodies or Affibodies. These efforts have been reviewed recently in a broad comparison of all pretargeting approaches by Altai and coworkers (19). Translation of such new pretargeting approaches to the clinic should come soon, both for PET imaging and therapy.

CONCLUSION

An increased interest for immuno-PET is found in the recent literature (17), where targeted therapies using antibodies are experiencing a considerable growth in cancer management. Immuno-PET can offer a non-invasive solution to quantitatively assess whole-body tumor biomarker cartography. Based on immuno-PET, treatment strategies could be adapted to each patient before costly and potentially toxic treatments are administered.

Pretargeted immuno-PET represents a sensitive and specific imaging method, with promising results reported in MTC and also in other solid tumors. Pretargeted immuno-PET could indeed be a specific diagnostic tool for tumor detection, but also a theranostic companion approach to select patients to be treated with radioimmunconjugates or antibody-drug conjugates.

Pretargeting has advantages and limitations. It can be used to visualize or treat tumor lesions, depending on the radionuclide used, for example by using ^{111}In and ^{99m}Tc for SPECT imaging, ^{68}Ga or ^{18}F for PET imaging, or ^{131}I, ^{90}Y, and ^{177}Lu for radioimmunotherapy. Using BsMab as the pretargeting agent has several advantages: BsMAb can be humanized to minimize their immunogenicity and tailored to clear from the circulation more rapidly than intact IgG's. Then, together with the limited affinity of the BsMAb-hapten binding that allows for dissociation of BsMAb -hapten complexes in the circulation, there is no need for a clearing agent. Over the past decade, several improvements have been made to this system, resulting in a flexible, and efficient pretargeting system. However, it requires careful optimization, both for the design of the appropriate pretargeting reagents and for the definition of dosing and administration schedules. In addition, optimal reagents doses and injection schedules are not identical for imaging, where rapidly achieving high tumor to non-tumor activity ratios is the goal, and therapy where sufficient irradiation of tumors is also needed.Several roads of improvement exist. The non-covalent binding between the radiolabeled hapten and BsMAb on the surface of tumor cells limits the retention of the radiolabeled hapten-peptide in the tumor. Recent developments in the use of bio-orthogonal chemistry are very promising and represent an attractive alternative to the use of BsMAb. The question of cost should also be examined. Although these innovative technologies are certainly costly, but this could be acceptable if the advantage in patient selection for expensive therapies and drug development is confirmed. Large-scale, randomized, multicenter clinical trials are warranted.

AUTHOR CONTRIBUTIONS

All authors listed have made a substantial, direct and intellectual contribution to the work, and approved it for publication.

FUNDING

This work has been supported in part by French DHOS INCA,the University Hospital of Nantes, the Fondation Avenir, the French National Agency for Research (Investissements d'Avenir IRON Labex n° ANR-11-LABX-0018-01 and ArronaxPlus Equipex n° ANR-11-EQPX-0004).

REFERENCES

1. Goldenberg DM, DeLand F, Kim E, Bennett S, Primus FJ, van Nagell JR, et al. Use of radiolabeled antibodies to carcinoembryonic antigen for the detection and localization of diverse cancers by external photoscanning. *N Engl J Med*. (1978) 298:1384–6. doi: 10.1056/NEJM197806222982503
2. Wu AM. Antibodies and antimatter: the resurgence of immuno-PET. *J Nucl Med Off Publ Soc Nucl Med*. (2009) 50:2–5. doi: 10.2967/jnumed.108.056887
3. Boerman OC, Oyen WJG. Immuno-PET of cancer: a revival of antibody imaging. *J Nucl Med Off Publ Soc Nucl Med*. (2011) 52:1171–2. doi: 10.2967/jnumed.111.089771
4. Bailly C, Cléry P-F, Faivre-Chauvet A, Bourgeois M, Guérard F, Haddad F, et al. Immuno-PET for clinical theranostic approaches. *Int J Mol Sci*. (2016) 18:57. doi: 10.3390/ijms18010057
5. Kraeber-Bodere F, Bailly C, Chérel M, Chatal J-F. ImmunoPET to help stratify patients for targeted therapies and to improve drug development. *Eur J Nucl Med Mol Imaging*. (2016) 43:2166–8. doi: 10.1007/s00259-016-3458-6
6. Machens A, Schneyer U, Holzhausen H-J, Dralle H. Prospects of remission in medullary thyroid carcinoma according to basal calcitonin level. *J Clin Endocrinol Metab*. (2005) 90:2029–34. doi: 10.1210/jc.2004-1836
7. Wells SA, Asa SL, Dralle H, Elisei R, Evans DB, Gagel RF, et al. Revised American thyroid association guidelines for the management of medullary thyroid carcinoma. *Thyroid Off J Am Thyroid Assoc*. (2015) 25:567–610. doi: 10.1089/thy.2014.0335
8. Luster M, Karges W, Zeich K, Pauls S, Verburg FA, Dralle H, et al. Clinical value of 18-fluorine-fluorodihydroxyphenylalanine positron emission tomography/computed tomography in the follow-up of medullary thyroid carcinoma. *Thyroid Off J Am Thyroid Assoc*. (2010) 20:527–33. doi: 10.1089/thy.2009.0342
9. Kauhanen S, Schalin-Jäntti C, Seppänen M, Kajander S, Virtanen S, Schildt J, et al. Complementary roles of ^{18}F-DOPA PET/CT and 18F-FDG PET/CT in medullary thyroid cancer. *J Nucl Med Off Publ Soc Nucl Med*. (2011) 52:1855–63. doi: 10.2967/jnumed.111.094771
10. Oudoux A, Salaun P-Y, Bournaud C, Campion L, Ansquer C, Rousseau C, et al. Sensitivity and prognostic value of positron emission tomography with F-18-fluorodeoxyglucose and sensitivity of immunoscintigraphy in patients with medullary thyroid carcinoma treated with anticarcinoembryonic antigen-targeted radioimmunotherapy. *J Clin Endocrinol Metab*. (2007) 92:4590–7. doi: 10.1210/jc.2007-0938
11. Verbeek HHG, Plukker JTM, Koopmans KP, de Groot JWB, Hofstra RMW, Muller Kobold AC, et al. Clinical relevance of 18F-FDG PET and 18F-DOPA PET in recurrent medullary thyroid carcinoma. *J Nucl Med Off Publ Soc Nucl Med*. (2012) 53:1863–71. doi: 10.2967/jnumed.112.105940
12. Peltier P, Curtet C, Chatal JF, Le Doussal JM, Daniel G, Aillet G, et al. Radioimmunodetection of medullary thyroid cancer using a bispecific anti-CEA/anti-indium-DTPA antibody and an indium-111-labeled DTPA dimer. *J Nucl Med Off Publ Soc Nucl Med*. (1993) 34:1267–73.
13. Barbet J, Peltier P, Bardet S, Vuillez JP, Bachelot I, Denet S, et al. Radioimmunodetection of medullary thyroid carcinoma using indium-111 bivalent hapten and anti-CEA x anti-DTPA-indium bispecific antibody. *J Nucl Med Off Publ Soc Nucl Med*. (1998) 39:1172–8.
14. Salaun P-Y, Campion L, Bournaud C, Faivre-Chauvet A, Vuillez J-P, Taieb D, et al. Phase II trial of anticarcinoembryonic antigen pretargeted radioimmunotherapy in progressive metastatic medullary thyroid carcinoma: biomarker response and survival improvement. *J Nucl Med Off Publ Soc Nucl Med*. (2012) 53:1185–92. doi: 10.2967/jnumed.111.101865
15. Baum RP, Prasad V, Müller D, Schuchardt C, Orlova A, Wennborg A, et al. Molecular imaging of HER2-expressing malignant tumors in breast cancer

patients using synthetic ^{111}In- or ^{68}Ga-labeled affibody molecules. *J Nucl Med Off Publ Soc Nucl Med*. (2010) 51:892–7. doi: 10.2967/jnumed.109.073239
16. Tamura K, Kurihara H, Yonemori K, Tsuda H, Suzuki J, Kono Y, et al. 64Cu-DOTA-trastuzumab PET imaging in patients with HER2-positive breast cancer. *J Nucl Med Off Publ Soc Nucl Med*. (2013) 54:1869–75. doi: 10.2967/jnumed.112.118612
17. Bensch F, van der Veen EL, Lub-de Hooge MN, Jorritsma-Smit A, Boellaard R, Kok IC, et al. ^{89}Zr-atezolizumab imaging as a non-invasive approach to assess clinical response to PD-L1 blockade in cancer. *Nat Med*. (2018) 24:1852–8. doi: 10.1038/s41591-018-0255-8
18. van Rij CM, Lütje S, Frielink C, Sharkey RM, Goldenberg DM, Franssen GM, et al. Pretargeted immuno-PET and radioimmunotherapy of prostate cancer with an anti-TROP-2 x anti-HSG bispecific antibody. *Eur J Nucl Med Mol Imaging*. (2013) 40:1377–83. doi: 10.1007/s00259-013-2434-7
19. Altai M, Membreno R, Cook B, Tolmachev V, Zeglis BM. Pretargeted imaging and therapy. *J Nucl Med Off Publ Soc Nucl Med*. (2017) 58:1553–9. doi: 10.2967/jnumed.117.189944
20. Schoffelen R, Sharkey RM, Goldenberg DM, Franssen G, McBride WJ, Rossi EA, et al. Pretargeted immuno-positron emission tomography imaging of carcinoembryonic antigen-expressing tumors with a bispecific antibody and a ^{68}Ga- and ^{18}F-labeled hapten peptide in mice with human tumor xenografts. *Mol Cancer Ther*. (2010) 9:1019–27. doi: 10.1158/1535-7163.MCT-09-0862
21. McBride WJ, Sharkey RM, Karacay H, D'Souza CA, Rossi EA, Laverman P, et al. A novel method of 18F radiolabeling for PET. *J Nucl Med Off Publ Soc Nucl Med*. (2009) 50:991–8. doi: 10.2967/jnumed.108.060418
22. Rossi EA, Goldenberg DM, Cardillo TM, McBride WJ, Sharkey RM, Chang C-H. Stably tethered multifunctional structures of defined composition made by the dock and lock method for use in cancer targeting. *Proc Natl Acad Sci USA*. (2006) 103:6841–6. doi: 10.1073/pnas.0600982103
23. McBride WJ, Zanzonico P, Sharkey RM, Norén C, Karacay H, Rossi EA, et al. Bispecific antibody pretargeting PET (immunoPET) with an ^{124}I-labeled hapten-peptide. *J Nucl Med Off Publ Soc Nucl Med*. (2006) 47:1678–88.
24. Schoffelen R, Boerman OC, Goldenberg DM, Sharkey RM, van Herpen CML, Franssen GM, et al. Development of an imaging-guided CEA-pretargeted radionuclide treatment of advanced colorectal cancer: first clinical results. *Br J Cancer*. (2013) 109:934–42. doi: 10.1038/bjc.2013.376
25. Schoffelen R, Woliner-van der Weg W, Visser EP, Goldenberg DM, Sharkey RM, McBride WJ, et al. Predictive patient-specific dosimetry and individualized dosing of pretargeted radioimmunotherapy in patients with advanced colorectal cancer. *Eur J Nucl Med Mol Imaging*. (2014) 41:1593–602. doi: 10.1007/s00259-014-2742-6
26. Kraeber-Bodéré F, Rousseau C, Bodet-Milin C, Ferrer L, Faivre-Chauvet A, Campion L, et al. Targeting, toxicity, and efficacy of 2-step, pretargeted radioimmunotherapy using a chimeric bispecific antibody and ^{131}I-labeled bivalent hapten in a phase I optimization clinical trial. *J Nucl Med Off Publ Soc Nucl Med*. (2006) 47:247–55.
27. Bodet-Milin C, Ferrer L, Rauscher A, Masson D, Rbah-Vidal L, Faivre-Chauvet A, et al. Pharmacokinetics and dosimetry studies for optimization of pretargeted radioimmunotherapy in CEA expressing advanced lung cancer patient. *Front Med Lausanne*. (2015) 2:84. doi: 10.3389/fmed.2015.00084
28. Foubert F, Gouard S, Saï-Maurel C, Chérel M, Faivre-Chauvet A, Goldenberg DM, et al. Sensitivity of pretargeted immunoPET using ^{68}Ga-peptide to detect colonic carcinoma liver metastases in a murine xenograft model: comparison with 18FDG PET-CT. *Oncotarget*. (2018) 9:27502–13. doi: 10.18632/oncotarget.25514
29. Bodet-Milin C, Faivre-Chauvet A, Carlier T, Rauscher A, Bourgeois M, Cerato E, et al. Immuno-PET using anti-CEA bispecific antibody and ^{68}Ga-labeled peptide in metastatic medullary thyroid carcinoma: clinical optimization of the pretargeting parameters in a First-in Human trial. *J Nucl Med Off Publ Soc Nucl Med*. (2016) 57:1505–11. doi: 10.2967/jnumed.116.172221
30. Bodet-Milin C, Rousseau C, Ansquer C, Faivre-Chauvet A, Rauscher A, Carlier T, et al. High sensitivity of pretargeted immuno-PET using anti-carcinoembryonic antigen (CEA) bispecific antibody and Ga-68-labeled peptide in metastatic medullary thyroid carcinoma (MTC) patients. *Eur J Nucl Med Mol Imaging*. 41:S314–5.
31. Rousseau C, Campone M, Rauscher A, Faivre-Chauvet A, Carlier T, Ferrer L, et al. Pretargeted immuno-PET with an anti-carcinoembryonic antigen (CEA) bispecific antibody (BsMAb) and a ^{68}Ga-labeled hapten-peptide compared to conventional imaging and FDG-PET in metastatic breast cancer patients (BC): First results. *Cancer Res*. (2015) 75:P5-01-01-P5-01–01. doi: 10.1158/1538-7445.SABCS14-P5-01-01
32. Touchefeu Y, Bailly C, Frampas E, Eugène T, Rousseau C, Faivre-Chauvet A, et al. Pre-targeted immuno-PET with bispecific anti-CEA antibody and Gallium-68-labeled IMP-288 peptide for imaging of metastates from colorectal cancer. In: *JFHOD Annual Meeting,* Paris (2019).
33. Honarvar H, Westerlund K, Altai M, Sandström M, Orlova A, Tolmachev V, et al. Feasibility of affibody molecule-based PNA-mediated radionuclide pretargeting of malignant tumors. *Theranostics*. (2016) 6:93–103. doi: 10.7150/thno.12766
34. Rossin R, Verkerk PR, van den Bosch SM, Vulders RCM, Verel I, Lub J, et al. *In vivo* chemistry for pretargeted tumor imaging in live mice. *Angew Chem Int Ed Engl*. (2010) 49:3375–8. doi: 10.1002/anie.200906294

Conflict of Interest Statement: At the time the work was conducted, DG was Chairman of the Board, Chief Scientific Officer, and Chief Patent Officer of Immunomedics, Inc., and also Chairman of IBC Pharmaceuticals, Inc.

The remaining authors declare that the research was conducted in the absence of any commercial or financial relationships that could be construed as a potential conflict of interest.

frontiers in Medicine

REVIEW
published: 12 June 2019
doi: 10.3389/fmed.2019.00117

Hypoxia Imaging and Adaptive Radiotherapy: A State-of-the-Art Approach in the Management of Glioma

Michael Gérard[1,2], *Aurélien Corroyer-Dulmont*[1], *Paul Lesueur*[1,2], *Solène Collet*[1,3], *Michel Chérel*[4], *Mickael Bourgeois*[4], *Dinu Stefan*[2], *Elaine Johanna Limkin*[5], *Cécile Perrio*[6], *Jean-Sébastien Guillamo*[1,7], *Bernard Dubray*[8], *Myriam Bernaudin*[1], *Juliette Thariat*[2] *and Samuel Valable*[1]*

[1] Normandie Université, UNICAEN, CEA, CNRS, ISTCT/CERVOxy Group, GIP Cyceron, Caen, France, [2] Department of Radiation Oncology, Centre Lutte Contre le Cancer François Baclesse, Caen, France, [3] Department of Radiophysics, Centre Lutte Contre le Cancer François Baclesse, Caen, France, [4] Team 13–Nuclear Oncology, INSERM U1232 Centre de Recherche en Cancérologie et Immunologie Nantes Angers (CRCINA), Nantes, France, [5] Department of Radiotherapy, Gustave Roussy, Université Paris-Saclay, Villejuif, France, [6] Normandie Université, UNICAEN, CEA, CNRS, ISTCT/LDM-TEP Group, GIP Cyceron, Caen, France, [7] Department of Neurology, Centre Hospitalier Universitaire de Nîmes, Nîmes, France, [8] Département de Radiothérapie et de Physique Médicale, Laboratoire QuantIF–LITIS [EA 4108], Centre de Lutte Contre le Cancer Henri Becquerel, Université de Normandie, Rouen, France

OPEN ACCESS

Edited by:
Samer Ezziddin, Saarland University, Germany

Reviewed by:
Baljinder Singh, Post Graduate Institute of Medical Education and Research (PGIMER), India
Ekaterina Dadachova, University of Saskatchewan, Canada

***Correspondence:**
Samuel Valable
samuel.valable@cnrs.fr

Specialty section:
This article was submitted to Nuclear Medicine, a section of the journal Frontiers in Medicine

Received: *31 January 2019*
Accepted: *13 May 2019*
Published: *12 June 2019*

Citation:
Gérard M, Corroyer-Dulmont A, Lesueur P, Collet S, Chérel M, Bourgeois M, Stefan D, Limkin EJ, Perrio C, Guillamo J-S, Dubray B, Bernaudin M, Thariat J and Valable S (2019) Hypoxia Imaging and Adaptive Radiotherapy: A State-of-the-Art Approach in the Management of Glioma. Front. Med. 6:117. doi: 10.3389/fmed.2019.00117

Severe hypoxia [oxygen partial pressure (pO_2) below 5–10 mmHg] is more frequent in glioblastoma multiforme (GBM) compared to lower-grade gliomas. Seminal studies in the 1950s demonstrated that hypoxia was associated with increased resistance to low–linear energy transfer (LET) ionizing radiation. In experimental conditions, the total radiation dose has to be multiplied by a factor of 3 to achieve the same cell lethality in anoxic situations. The presence of hypoxia in human tumors is assumed to contribute to treatment failures after radiotherapy (RT) in cancer patients. Therefore, a logical way to overcome hypoxia-induced radioresistance would be to deliver substantially higher doses of RT in hypoxic volumes delineated on pre-treatment imaging as biological target volumes (BTVs). Such an approach faces various fundamental, technical, and clinical challenges. The present review addresses several technical points related to the delineation of hypoxic zones, which include: spatial accuracy, quantitative vs. relative threshold, variations of hypoxia levels during RT, and availability of hypoxia tracers. The feasibility of hypoxia imaging as an assessment tool for early tumor response to RT and for predicting long-term outcomes is discussed. Hypoxia imaging for RT dose painting is likewise examined. As for the radiation oncologist's point of view, hypoxia maps should be converted into dose-distribution objectives for RT planning. Taking into account the physics and the radiobiology of various irradiation beams, preliminary *in silico* studies are required to investigate the feasibility of dose escalation in terms of normal tissue tolerance before clinical trials are undertaken.

Keywords: glioblastoma, hypoxia, imaging, PET, MRI, radiation therapy

INTRODUCTION

Brain Tumors and Hypoxia

Brain tissue physiologically has a tissue pO_2 (ptO_2) of ∼40 mmHg, referred to as a normoxic or aerobic state. Hypoxia, generally defined when ptO_2 falls below 10 mmHg, is the result of an imbalance between oxygen consumption and delivery, a common situation in various types of malignancies.

Tumor growth was initially modelized by Gompertzian curves in the 1970s, in which the growth saturates when the tumor volume reaches the carrying capacity (1, 2). However, this model has some limitations and has been improved by incorporating various parameters such as angiogenesis and necrosis. A specific focus was placed on hypoxia, known to play a crucial role in tumor angiogenesis, genetic instability, and tumor invasion (3). More recently, hypoxia has also been shown to induce pro-tumoral activity by macrophage polarization (4). It is evident that hypoxia has a positive role in tumor growth and a negative role in therapeutic response (5) and is ultimately related to poor prognosis (6–8).

In primary brain tumors, hypoxia is also associated with malignant tumor growth. Glioblastoma multiforme (GBM), the most aggressive glioma and most frequent primary brain tumor, is particularly hypoxic. Using the Eppendorf needle electrode, previous works demonstrated that while the oxygenation in the normal brain ranges around 40 mmHg of oxygen, it falls below 10 mmHg in GBM (9, 10). However, hypoxic components are highly heterogeneous both within a single tumor and among patients. It has been proposed that tumors could be separated into three compartments: well oxygenated, acutely hypoxic, and chronically hypoxic (11).

Hypoxia also induces resistance to radiotherapy (RT) (12). In the early 1950s, Gray and colleagues reported that the radiosensitivity of mammalian cells was dependent on oxygen concentration (13). Hypoxia was therefore assumed to contribute to the failures after RT in cancer patients. It has also been suspected to be involved in resistance to various chemotherapies (14, 15). Explored solutions to target hypoxia included the use of hyperbaric oxygen chambers, hypoxic radiosensitizers, and, in recent years, hypoxia image guided radiotherapy (HIGRT) (16).

More recently, various publications have demonstrated that hypoxia changes during tumor growth. Hypoxia is a result of an increased oxygen demand not only from tumor cells but also from immune cells, coupled with a perturbed vasculature (17). While in normal situations, the capillary density allows oxygen to be delivered to the cells with distances ranging from 30 to 60 μm, within a tumor, the distance to the closest capillary dramatically increases and causes a decrease in oxygen pressure. The concept of perfusion-limited hypoxia resulting from vessel obstruction and perturbed blood flow (poorly oxygenated blood) has introduced the concept of dynamic or cycling hypoxia (18–20). Temporal instability of ptO_2 has been observed with intermittent periods of reoxygenation. The kinetics of cycling hypoxia follow a complex timescale and occur with two frequencies: a few cycles per hour and cycles lasting from hours to days (21, 22). At present, no clear distinction exists between chronic and cycling hypoxia.

Hypoxia and Radiobiological Basis

In the presence of molecular oxygen at the time of or within microseconds after exposure, low-LET radiation ionizes water molecules, producing high-energy electrons and highly reactive oxygen species (ROS) (23). DNA damage results from either a direct or an indirect (via ROS) effect of irradiation. In the absence of oxygen, ROS are not produced, and DNA damage is reduced for a given RT dose. *In vitro*, the ratio of the doses yielding the same level of cell mortality in anoxic (100% N_2 atmosphere) vs. oxic (100% O_2 atmosphere) conditions is 2.5–3, corresponding to the oxygen enhancement ratio (OER) (24–26). This "oxygen effect" is not associated with oxygen-dependent differences in DNA repair processes (27). Therefore, oxygen is considered as the strongest existing radiosensitizing agent. Hypoxic tumors are thus considered radioresistant and are harder to control with conventional RT doses.

OER and OER modeling: As a function of pO_2 and LET, OER increases nonlinearly with decreasing pO_2 as described by the Alper and Howard-Flanders formula (28) and with decreasing LET (27–29) (**Figure 1**). Under exposure to low-LET radiation, OER is around 2 for a pO_2 value of around 10–15 mmHg, and a maximum is reached with pO_2 <5 mmHg (30, 31). For high LET (over a few hundred keV/μm), OER remains around 1, whatever the pO_2 (29, 32). Thus, high-LET radiation therapy is supposed to be more efficient than low-LET conventional RT (photons or protons) when treating hypoxic tumors (33, 34). This could be explained by the *in situ* "oxygen production in the heavy ion track" phenomenon (35–38).

For a precise modeling of OER dependence, a rigorous analysis should include several parameters: ptO_2 in both the

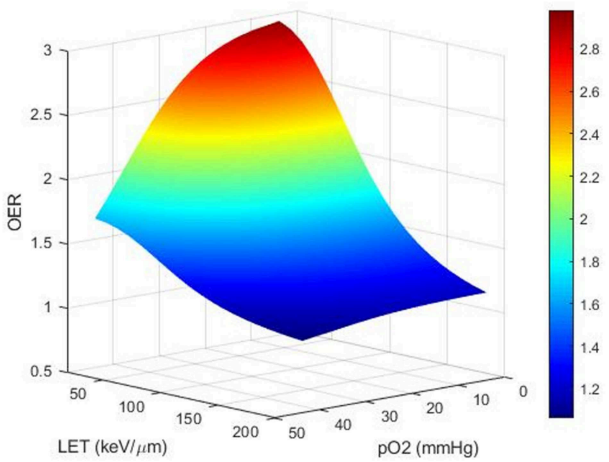

FIGURE 1 | Theoretical computational modeling of the OER as a function of pO_2 and LET (performed on MATLAB). OER increases nonlinearly with increasing degree of hypoxia and decreases with increasing LET. Compared to low-LET conventional RT (photons or protons), high-LET RT, over a few hundreds of keV/μm (carbons), is expected to be less sensitive to hypoxia and could be more efficient for treating hypoxic tumors.

TABLE 1 | Imaging biomarkers to evaluate oxygenation in glioblastoma: advantages and limitations.

	Advantages	Limitations
StO_2	• Easy setup and application in clinical routine • Sensitive • Assuming fully oxygenated arterial blood, the fraction of deoxygenated blood corresponds to the OEF • Spatial resolution is better than PET biomarkers	• Indirect assessment of p_tO_2 • Specificity for hypoxia needs to be validated
OE-MRI	• Showed promising results in the characterization of intratumor hypoxia heterogeneity in one GBM model • Spatial resolution is better than PET biomarkers	• Indirect assessment of p_tO_2 • Specificity for hypoxia needs to be validated • Needs to be validated in other GBM models and in the clinical setting
MOBILE	• No need to inject contrast agent • Spatial resolution better than PET biomarkers	• Indirect and relative assessment of p_tO_2 • No studies in brain tumors
MR fingerprint	• Multi-parametric (vascularization, oxygenation…) characterization with rapid acquisition • Spatial resolution is better than PET biomarkers	• Indirect and relative assessment of p_tO_2 • Needs to be validated in other GBM models and in the clinical setting with multiple slices
^{15}O-oxygen	•Allows direct quantification of OEF	• Very short radioactive decay • No linear relation between oxygen consumption and cellular hypoxia • Spatial resolution
[^{18}F]-FMISO	• Current gold standard for hypoxia imaging • Indicator of cellular hypoxia	• Injection of a radioactive compound • Relatively prolonged time before steady-state acquisition (2h) • Spatial resolution
[^{18}F]-FAZA	• Indicator of cellular hypoxia • More rapid clearance than [^{18}F]-FMISO	• Injection of a radioactive compound • Needs to be validated in a more important number of studies • Spatial resolution
[^{18}F]-HX4	• Indicator of cellular hypoxia • More hydrophilic tracer allowing more rapid clearance than [^{18}F]-FMISO/FAZA	• Injection of a radioactive compound • Not recommended for brain tumors • Spatial resolution
[^{18}F]-DiFA	• Indicator of cellular hypoxia • More hydrophilic tracer allowing more rapid clearance than [^{18}F]-FMISO/FAZA	• Injection of a radioactive contrast agent • Needs to be validated in a more important number of studies • Spatial resolution
[^{62}Cu]/[^{64}Cu]-ATSM	• Characterization of moderate hypoxia • Promising tracer for imaging hypoxia thanks to its high membrane permeability and low redox potential	• Injection of a radioactive compound with long half-life (12.7 h) • Specificity to hypoxia is questionable • Spatial resolution

hypoxic and aerobic conditions, LET, cell survival end point, dose per fraction, particle species, tissue, and cell cycle phase. These variables are derived from *in vitro* survival data and may overestimate or underestimate the effects of hypoxia *in vivo*. Due to the complexity of dependencies, results of experimental data on OER measurements possess significant uncertainty. Improved understanding of the physical and chemical basis of the OER would add useful information on top of current empirical models. An accurate OER model is necessary to calculate doses necessary for RT dose escalation. Numerous mathematical OER models have been proposed, based on a range of experimental data from literature (**Figure 1**). However, the optimal mathematical function remains unknown, and estimation remains empirical. Once known, the model will be of invaluable aid to radiation oncologists in performing "hypoxia dose painting" in treatment planning for photon and ion beam RT.

Characterizing the heterogeneity of hypoxia necessitates tools with good temporal and spatial resolution to enable its eventual use in personalized medicine. Medical imaging is a promising tool, as it allows repeated noninvasive measurements to track both the temporal and spatial heterogeneity of tumor hypoxia. This is particularly relevant in RT, where constant technological advancements may permit treatment personalization based on the local ptO_2. There are, however, numerous points that require validation before using imaging of hypoxia for radiation therapy guidance.

MAPPING OF HYPOXIA IN CLINICAL SITUATIONS: CURRENT DEVELOPMENTS

Various approaches have been designed to assess hypoxia in tissues. The use of implantable probes or needles is still the gold standard for ptO_2 measurement (5). In a clinical environment, however, tissue ptO_2 cannot be mapped with probes (39), and biomedical imaging based on positron-emission tomography (PET) and magnetic resonance imaging (MRI) serves as a surrogate biomarker of hypoxia or of cerebral oxygenation (**Table 1**).

MRI Markers

MRI has the advantage of being nonionizing and can be used to quantify the blood oxygenation level in tissue (StO_2) (40). In particular, a BOLD-based MRI method for the measurement of relative oxygen extraction fraction (rOEF) showed that high rOEF was present in high-grade but not low-grade gliomas.

However, confounding factors such as cerebral blood volume (CBV), tissular T2, and contrast agent leakage need further investigation (41). Oxygen-enhanced MRI (OE-MRI) is likewise useful, based on the correlation between hypoxia and the variation in longitudinal relaxation rate (ΔR1) during oxygen challenge (42). In a preclinical model of GBM, Fan et al. have shown that OE-MRI is able to show intratumoral hypoxic heterogeneity and present an interesting correlation of OE-MRI with hypoxia by histological staining (24). However, OE-MRI still has to be validated in other GBM models and in the clinical setting. Mapping of oxygen by imaging lipids relaxation enhancement (MOBILE) (25) has also been proposed and also needs validation. OE-MRI and MOBILE present the advantage of repeated measurements of oxygenation without the need for exogenous contrast agents. Recently, an original approach termed MR fingerprint has also been proposed, which simultaneously obtains data on CBV, mean vessel radius, and blood oxygen saturation and creates high-resolution parametric maps of the microvascular network of the brain (26).

PET Markers

PET can also be used to map the OEF with radioactive molecular oxygen ($^{15}O_2$) as a tracer. It can also be used to estimate ptO_2 by mapping of tracers trapped in areas with low ptO_2. This approach is achieved with a variety of PET tracers based on an imidazole structure such as 3-[^{18}F]fluoro-1-(2-nitro-1-imidazolyl)-2-propanol ([^{18}F]-FMISO) (43, 44) and [^{18}F]-fluoroazomycin arabinoside ([^{18}F]-FAZA), the uptake of which depends on a ptO_2 threshold (45). After cell penetration by passive diffusion, these tracers are reduced in a two-step process, with the first step being reversed if oxygen is present and with the tracer becoming irreversibly trapped in the absence of oxygen.

It takes time to visualize hypoxic regions using [^{18}F]-FMISO or [^{18}F]-FAZA due to lipophilicity and slow clearance in normoxic tissues. More recently, 3-[^{18}F]fluoro-2-(4-((2-nitro-1H-imidazol-1-yl)methyl)-1H-1,2,3-triazol-1-yl)propan-1-ol ([^{18}F]-HX4 or 18F-flortanidazole) (46) and 1-(2,2-dihydroxymethyl-3-[^{18}F]fluoropropyl)-2-nitroimidazole ([^{18}F]-DiFA) (47) have been developed as more hydrophilic tracers with the potential advantages of shorter acquisition times. However, formal validation in clinical situations is required.

Other radiopharmaceuticals have been described. Cu(II)-diacetyl-bis(N4-methylthiosemicarbazone) (^{64}Cu-ATSM) seems to be a promising tracer for imaging hypoxia thanks to its high membrane permeability and low redox potential. However, the selectivity of Cu-ATSM to hypoxia has been challenged and discussed (48). See **Figure 2** for the chemical structures of the various PET tracers designed for hypoxia imaging.

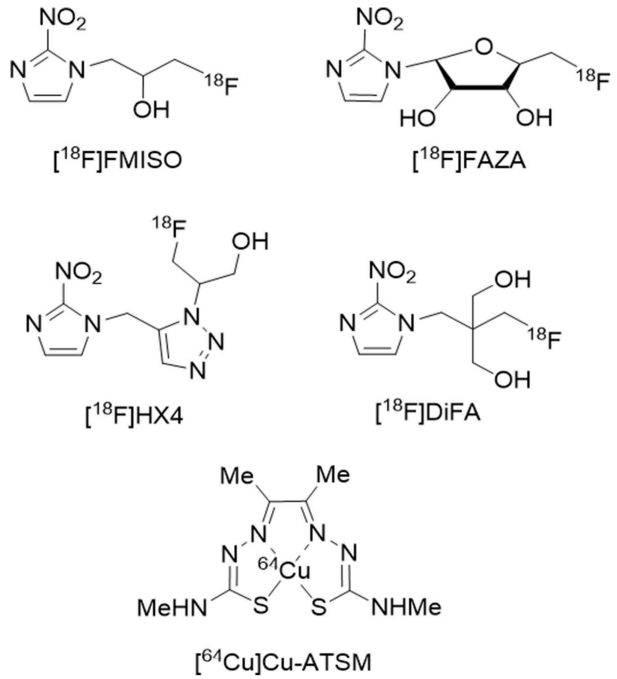

FIGURE 2 | Chemical structure of the various PET tracers designed for hypoxia imaging.

ROBUSTNESS AND ACCURACY OF AVAILABLE TECHNIQUES TO ASSESS HYPOXIA IN THE BRAIN

MRI and PET biomarkers have the advantage of being available and regularly utilized in the clinics; however, in assessing hypoxia, they have several limitations, which presently hinder routine clinical utilization for RT dose modulation (**Table 1**).

Limitation of MRI Markers

Mapping StO_2 or the OEF yields a continuous signal with high temporal and spatial resolutions, but the relationship to ptO_2 is indirect, and vascular changes indirectly reflect tissue changes. In particular, their relationship depends on the dissociation curve of hemoglobin, which itself depends on pH and temperature, among other factors. For example, a lower blood pH or a higher blood temperature would lead to a higher blood ptO_2 for the same blood oxygen saturation.

In addition, OE-MRI and MOBILE have to be validated in various GBM models and in the clinical setting. MR fingerprint has been validated in patients but only for a single slice; thus, further developments are necessary.

Limitation of PET Markers

Accessibility: One of the main drawbacks of the extensive use of PET tracers of hypoxia in oncology is that tracer production is cost-intensive and only available at selected centers, in part due to limited manufacturers.

Poor Spatial Resolution

As discussed in the review of Grimes et al. (49) the molecular effect of oxygen is in the range of nm to μm, while PET resolution is about 3–4 mm. This raises various concerns about the interpretation of the PET results. It was shown that the PET signal would be similar between two voxels if 25% of a voxel

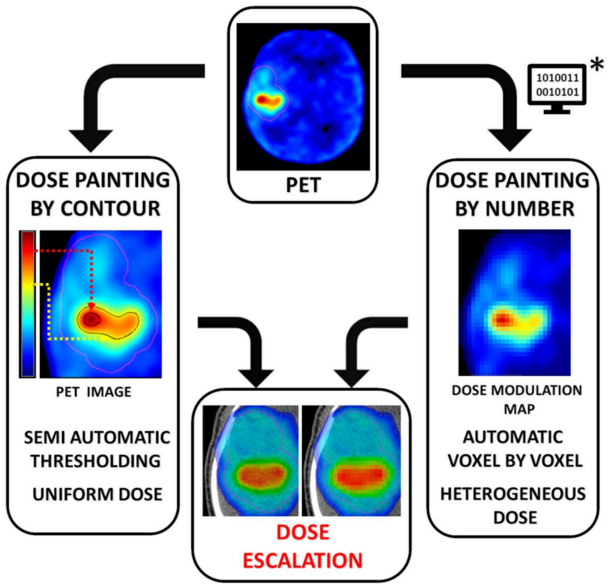

FIGURE 3 | The two main approaches of dose painting: by contour (DPBC) or by number (DPBN). For DPBC, added to the standard clinical dose level (in pink), the radiation oncologist manually delineates a uniform HTV (in black) corresponding to a subjective PET-uptake level threshold (dashed line). Note that both methods use PET images, but DPBN requires a mathematical data pre-processing step (*) that computes PET image into a "dose modulation map." When performed, dose painting allows RT dosimetric simulation for optimal dose escalation.

was anoxic (but viable) and the remainder well oxygenated, if the voxel was 50%/50% split between 1.4 mmHg and oxic, or if the whole voxel was at 4.2 mmHg (49).

Impact of Altered Blood Flow in Tracer Uptake

PET tracers are delivered to the hypoxic tumor cells via the bloodstream. However, GBM vascularization is highly perturbed, which could impact the tracer biodistribution, notably in anoxic areas without any functional vascularization where delivery of the tracer might not be achieved (50). This could result in a very low tracer uptake in highly hypoxic areas. Vessel permeability may also have an impact in tissue biodistribution if more hydrophilic tracers have to be used. Dynamic PET has been proposed as an alternative to address the issues of both tumor perfusion and hypoxia, but the increased duration of the examination is a limitation for its routine use.

Poor Temporal Resolution

The 109-min half-life of ^{18}F is hardly ideal for examining temporal resolution. In general, the radioactive nature and short half-lives of PET tracers make it difficult to assess the evolution of hypoxia over hours or days. For instance, a study on head and neck cancers demonstrated that variability in spatial uptake can occur between repeated ^{18}F-FMISO PET scans (51). These results could be either a reflection of the poor reproducibility of FMISO PET due to confounding influences (perfusion, permeability) or a reflection of cycling hypoxia.

Molecular oxygen, with its very short half-life, would in theory address the dynamic nature of tissue oxygenation. However, its access is limited to a few centers worldwide, and ^{15}O has a poor intrinsic spatial resolution in comparison to ^{18}F.

In summary, while being of major importance for tumor growth and resistance to treatment, the mapping and routine assessment of hypoxia remains a challenge. Among the various markers, [^{18}F]-FMISO PET remains the most extensively studied and most accurate approach to map hypoxia in the clinical situation (52), but for brain tumors where PET imaging is not standard practice, MRI may provide surrogate biomarkers of oxygenation.

HYPOXIA FROM THE RADIATION ONCOLOGIST'S POINT OF VIEW

Hypoxia and the Dose Painting Concept

At present, the same radiation dose is delivered to all subregions of the tumor volume regardless of their individual biology and radiosensitivity. The RT concept of dose painting involves adapting the dose prescriptions for tumor subvolumes as a function of the tumor's heterogeneous biology. This could be done with functional imaging that maps different dose–response levels (53) over anatomic contours provided by morphological imagery, resulting in a "biological target volume" (BTV), where dose escalation could be applied. Hypoxia imaging could be used to provide the level of ptO_2 and, subsequently, the spatial distribution of potentially radioresistant regions (54). These hypoxic target volumes (HTVs) are given a higher dose to achieve better tumor control (54), taking care not to compromise normal tissue tolerance (55, 56). To counteract radioresistance associated with hypoxic tumors, radiation oncologists need accurate calculations of the biologically optimal RT doses. The technical feasibility of optimizing RT plans has been well documented, mostly in head and neck cancers (57, 58). A similar study has never been done in gliomas.

To define the HTV, there are two main approaches: dose painting by contour (DPBC) or by number (DPBN) based on PET images (**Figure 3**).

Dose Painting by Contour

Also called multilevel or subvolume boosting, DPBC defines the HTV by segmenting a volume based on an uptake threshold on hypoxia functional images. This approach delivers a uniform boost dose to hypoxic subvolumes (59). Pixels with intensities higher than a defined value are considered as potentially hypoxic volumes. The cutoff is based on an empirical uptake threshold relative to a well-oxygenated reference, such as tumor-to-muscle and tumor-to-blood ratios (>95% of normal tissue voxels had a tissue/blood ratio of $\leq$1.2) or SUV>1.4 (60, 61).

DPBC is the most common approach in studies for several reasons. First, it is easier to integrate into conventional clinical workflows using commercial RT treatment planning systems (TPS). Second, it is easier to prescribe uniform dose boost regions. Lastly, it is more robust to spatial errors (62). In practice, dose escalation is achievable for the vast majority of

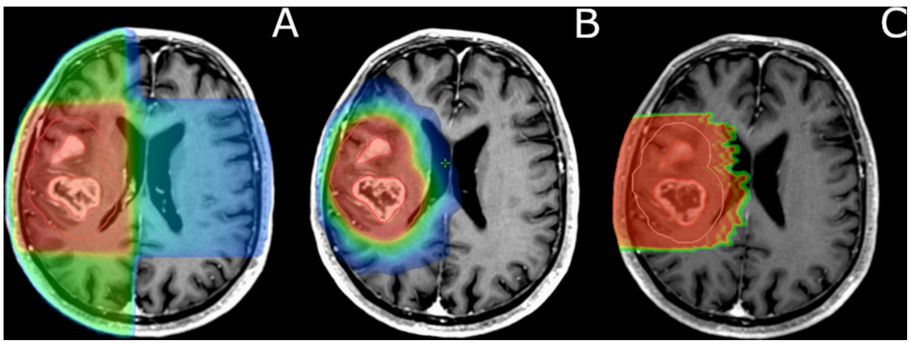

FIGURE 4 | Comparison of dose distribution and target coverage (GBM) in 3D-CRT **(A)**, IMRT **(B)**, and protontherapy **(C)**. **(B,C)** show finer target coverage with increased normal tissue sparing. For clinical implementation of dose painting, these accurate RT techniques are needed **(B,C)**. In current routine clinical practice, the target volume receives a homogeneous dose prescription and distribution regardless of potential hypoxic subvolumes.

cases (63, 64). However, the absence of consensus on the most appropriate threshold cutoff, the fact that high values can be found outside the tumor, and disparate tracer characteristics (intrinsic biochemical, uptake, clearance, etc.) make this method clinically debatable.

Dose Painting by Numbers

DPBN is a voxel-by-voxel level dose prescription based on a relationship between the intensities of neighboring voxels integrated in a "dose modulation map." This is achieved through a mathematical transformation of the spatial distribution of hypoxia from noninvasive methods such as PET scans, named "ptO_2map." The ptO_2 and OER levels enable algorithms to compute the heterogeneous doses to be prescribed (65, 66).

Several attempts have been made to estimate ptO_2 and include OER in RT treatment planning. However, these methods are much more complex than DPBC and require specific algorithms and software for numerical processing steps (67). Some methods are proposed (68) but remain subject to discussion (69). Some authors consider a linear transformation of the image intensity into a prescribed dose (65, 67), whereas others assume a "dose redistribution" between hypoxic and normoxic pixels resulting in the same average dose as a conventional RT plan (58, 62, 70).

For head and neck tumors, Toma-Dasu et al. used a nonlinearity approach, which considers that the relationship between [^{18}F]-FMISO uptake and ptO_2 follows a hyperbolic function (65). This equation was adapted for brain tumors and fine-tuned patient by patient using two healthy regions of interest for calibration of the model (68). This approach enables the computation of ptO_2 maps. However, once ptO2 maps are calculated, dose modulation maps must also be computed. To do this, authors reported an equation that links dose modulation to ptO_2 by incorporating the OER effect (65). Another approach used was to compute an inverted dose prescription map that can be directly imported into the RT TPS without any modifications (71). To the best of our knowledge, these dose modulation maps have never been proposed for brain tumors.

To conclude, the adaption in clinical practice of both DPBC and DPBN to address tumor hypoxia remains to be validated before becoming a clinical routine.

Intensity-Modulated Radiation Therapy

In GBM, the standard RT dose prescription is 60 Gray, in 1.8–2 Gray daily fractions, administered 5 days per week for 6 weeks. However, radioresistance is almost constant, inevitably leading to subsequent tumor relapse (72). RT dose escalation is one of the avenues of research being explored to improve local control (73). Because GBMs are infiltrative, diffuse, and often diagnosed late, these usually require irradiation of large volumes encompassing normal brain tissue. Thus, increased doses may potentially lead to unacceptable radiation-induced toxicities (edema, inflammation, necrosis, etc.) and severe sequelae.

Several methods have been identified to overcome the dose-limiting tolerance of the brain, especially in the era of constant technological medical advancements. The improved resolution of MRIs allows better visualization of the brain anatomy and, in consequence, a more accurate delineation of organs at risk (OARs). Furthermore, newer RT planning techniques such as intensity-modulated radiation therapy (IMRT) make dose painting feasible. Compared to 3-D conformational radiotherapy (3D-CRT), IMRT allows highly conformal dose distributions of X-rays in target volumes with low levels of radiation to the surrounding normal tissues (74) (**Figures 1–4**). Using IMRT, very steep dose gradients in tumor subvolumes without unacceptable increased doses to OARs are achievable (53, 63, 64, 75).

Boron neutron capture therapy (BNCT) is another way to enhance the dose delivery in the tumor while preserving surrounding tissues. It can be done by boron administration into the tumor via the intravenous route or by perioperative intratumoral injection. BNCT relies on epithermal neutrons, which below 10 keV are not toxic to healthy tissues. Excellent spatial distribution is, however, critical due to their lack of spatial selectivity, with depth distribution profiles like photons but with a 3-fold biological efficacy, which can thus turn into a drawback if

not targeted properly. Also, obtaining only a low energy spectrum of neutrons (below 10 keV to protect healthy tissues) can be quite challenging, and specific equipment has been designed that might only be adequate for superficial tumors (10 cm deep). Recent approaches suggest that proton and carbon ion beams could also be used to produce epithermal neutrons at the site of boron capture within the tumor (76–80). Thus, the need for specific neutron therapy machines, which are likely inadequate for the treatment of deep-seated tumors, might be surpassed by the use of proton and carbon ion accelerators. BCNT techniques are being investigated by a few teams worldwide, mostly in Japan and Sweden.

While being relevant from a radiobiological point of view, the concept of HIGRT has not entered clinical routine utilization, with some limiting factors being the difficulties tied to OER modeling, ptO_2 mapping, and evolution of hypoxia during the course of RT.

REOXYGENATION STRATEGIES TO IMPROVE RT EFFICACY

Reoxygenation During the Course of RT

The adaptation of RT based on hypoxia imaging also raises some questions about the evolution of hypoxia during the course of RT. Tumor reoxygenation is a phenomenon wherein cells that are hypoxic before RT become oxygenated during or after RT (81). For example, in head and neck cancers, it was recently published that during the course of RT, tumor hypoxia decreases (82). In this review, authors also discuss oxygenation in various tumor types, namely, lung, cervical, and rectal carcinomas. For these tumors, a decrease in hypoxia was likewise seen during RT. Thus, existing OER models do not incorporate variations of a tumor's radiosensitivity or reoxygenation during the course of treatment.

Rapid reoxygenation affects acutely hypoxic cells, while slow reoxygenation affects chronically hypoxic cells. These two processes may provide specific windows of opportunity. The RT fraction should be delivered when tumor reoxygenation is expected to be at its maximum so as to optimize the OER. Consequently, the HTV may not be spatially fixed over time, and a single pre-treatment PET may not be pertinent, especially for adaptive RT (83). PET scans may be repeated (over 5–7 days) to monitor hypoxia dynamics during RT (84). To this aim, numerous studies, mostly in head and neck cancers, have been published (82). Consistent with the reoxygenation model, results show that PET hypoxia uptake decreases during RT (82). Increasing PET uptake during RT has been correlated with loco-regional failure (85–87); however, disappearance of hypoxia was not correlated with better prognosis (88, 89).

With regard to the reproducibility of intratumor uptake among repeated scans during RT, results are ambiguous, with a study reporting highly reproducible uptake (90) and another reporting high uptake variability (51). Nevertheless, repeat imaging during the course of treatment might improve measurements (83). It is clear that further work is required to understand the spatio-temporal intratumor distribution of radiotracers before and during RT.

External Reoxygenation Strategies

New radiosensitizing drugs and radio-enhancing nanoparticles may be delivered into the tumor to improve oxygenation. Among the radiosensitizers, some have been designed so as to overcome the effect of hypoxia by inducing reoxygenation of the tumor [reviewed in Graham and Unger (91)]. Of these, fluorochemicals can dissolve considerable amounts of oxygen and could be considered to deliver oxygen through passive diffusion in hypoxic regions. As an example, NVX-108 is a radiosensitizer composed of dodecafluoropentane (DDFP) exhibiting 200 times the oxygen carrying capacity compared to human hemoglobin (92), that demonstrated its promise in preclinical studies, with a clinical study ongoing for GBM.

Breathing of oxygen under normobaric or hyperbaric conditions has also been investigated. As discussed by Graham et al. hyperbaric oxygenation has an overall positive effect on RT but has not been adapted and remains to be validated as standard treatment. To further improve the reoxygenation, the use of carbogen has been proposed for GBM. However, overall results were unsatisfactory, and we recently demonstrated using advanced MRI that this failure was attributable to facilitated reoxygenation in the normal brain relative to the tumor (93).

In endogenous reoxygenation or external reoxygenation strategies, one can observe that hypoxia remains highly dynamic during the course of treatment. This reinforces the need for accurate imaging strategies that quantify temporal variations in tumor hypoxia to be able to adapt the RT regimen based on the hypoxic component of the tumor.

INNOVATIVE RADIATION THERAPY MODALITIES TO OVERCOME HYPOXIA-INDUCED RADIORESISTANCE IN GBM

The efficacy of photon-based RT critically depends on the presence of molecular oxygen. To achieve higher equivalent doses into the tumor, hadrontherapy such as proton therapy has also been proposed, advantageous due to its better spatial distribution and normal tissue sparing (and thus potential for accurate dose escalation). Carbon ion therapy is also a promising option, representing an increase in the biological efficacy of RT by a factor of 3 to 4 relative to photons, thus potentially overcoming radioresistance and achieving better tumor control while sparing healthy tissues.

Proton Therapy

The depth dose distribution of a proton beam, represented by the Bragg peak, can be used to reduce radiation exposure of healthy tissues beyond the tumor (94) (**Figure 4**). These properties are particularly relevant to pediatric malignancies and benign/low-grade intracranial tumors. However, GBMs are rapidly progressive, poorly limited tumors. Thus, proton therapy should be used carefully to avoid marginal misses, with careful monitoring of tumor volumes over the weeks of RT. The process of rescanning, and replanning if necessary, is called adaptive RT. Provided that such caution is employed, proton therapy may be used to perform dose escalation. Proton therapy has a relative

biological effectiveness (RBE) relative to high-energy photons of 1.1. Thus, protons are 10% more biologically efficient than high-energy photons. Although the OER of protons is similar to that of photons, the increased RBE might partially counteract the radioresistance of hypoxic areas. A dosimetric study indicated that for a subpopulation of patients with GBM, at least 90 Gray RBE (Gy RBE) could be delivered to the tumor with proton therapy, with only small volumes of normal brain structures receiving more than 70 Gy RBE. In a phase I–II proton therapy–based dose escalation study by Mizumoto et al. patients received photon-based RT or 250 MeV proton therapy (50.4 Gy RBE in 28 fractions) to a large tumor volume with a concomitant proton therapy boost (23.1 Gy RBE in 14 fractions) to MRI gadolinium-enhanced areas, which included hypoxic zones (95, 96). Overall, patients received a total dose of 96.6 Gy RBE in 56 fractions. The 1- and 2-year overall survival rates were 78% (95% CI, 61%−95%) and 43% (95% CI, 23%−63%), respectively, with a median survival of 21.0 months (range, 5.5–81.0 months; 95% CI, 16.1–25.9 months). This proof-of-concept study shows an overall survival gain of 6 months in comparison with historical series, but results have yet to be reproduced.

Carbon Ion Beam Irradiation

Carbon ions have, to an even higher degree, the spatial selectivity of protons and can exhibit a very high LET of ∼100 keV/μm. Carbon ions are densely ionizing, releasing their energy in a constant and very close manner, contrary to photons or protons. They possess, physical doses being equal, a higher RBE (around 3), as they more likely interact with DNA and produce complex damage that is difficult or impossible to repair (97). This direct effect of carbon ions is less influenced by the presence of oxygen. OER values of hypoxic cells are, respectively, 1.5 for high-LET ions and 3.0 for X-rays. For a similar effect in hypoxic conditions, the dose needed for conventional RT is three times higher than in normoxic conditions, but such increase in dose is not achievable without compromising OAR dose limits. For carbon ions, the 1.5× increase needed is achievable. Preclinical studies have reported that accelerated heavy ion particles may have an advantage over X-rays in overcoming GBM radioresistance (98, 99). A phase I–II study combined 50 Gy X-ray RT with chemotherapy, followed by a carbon ion boost in the contrast enhancing region with doses from 16.8 to 24.8 Gray (RBE) (100). For the 32 GBM patients included, the median survival time was 17 months and reached 26 months for the high-dose group, with dose escalation having a significant impact. In line with these results, the randomized CLEOPATRA trial compares low- and high-LET irradiation in GBM patients (101).

Spatial Fractionation, Hypofractionation, and Flash Dose

Alternative approaches also include modulation of radiation delivery to deliver tumoricidal doses to large volumes, using adaptations that allow an enhanced differential effect between normal tissues and the tumor. Spatial fractionation has been identified as a promising approach to such aim. This is particularly relevant to GBMs because of the large volumes irradiated and the radiosensitivity of the brain (102–104). Specific devices are being designed and adapted on various types of treatment machines using different radiation modalities, including synchrotron radiation, very-high-energy electrons, and proton beams (either double scattering with a grid or with modified pencil beam scanning).

Hypofractionation has been originally defined as the use of doses above 2.5 Gy per fraction. However, the concept of hypofractionation has now been extended to very high doses per fraction using photon-based stereotactic irradiation. Fraction doses commonly use 3 times 20 Gy (in lung cancers) but may even use 90 Gy in a single fraction for conditions such as trigeminal neuralgia. An extension of the concept is a flash (ultra-high) dose that combines hypofractionation with a very high dose rate (105, 106). Animal models have consistently shown excellent skin sparing and tumor response equivalent to standard regimens (107, 108).

CONCLUSIONS

It is widely accepted that hypoxia is a poor prognostic factor in GBM. Among the key effects of hypoxia, radioresistance is a promising and potentially actionable factor. Imaging offers the opportunity to map tumor hypoxia or oxygenation before and during the course of RT and consequently opens an avenue for treatment adaptation. These adaptations can be by modulating doses based on ptO_2 and OER measurements, by introducing reoxygenation strategies in combination with conventional RT, or by adapting the RT techniques. All these developments require accurate characterization of hypoxia. In this review, we argue that while various strategies are being developed, at present, PET remains the most relevant strategy with the most evidence.

AUTHOR CONTRIBUTIONS

All authors listed have made a substantial, direct and intellectual contribution to the work, and approved it for publication.

FUNDING

This work has been supported by the French national agency for research Investissements d'Avenir via grant Labex IRON n°ANR-11-LABX-0018-01 and Institut National du Cancer (INCa).

ACKNOWLEDGMENTS

The authors wish to thank Elmostafa Fadaili, Nicolas Pirault, and Yann Lauzin for their technical help.

REFERENCES

1. Simpson-Herren L, Lloyd HH. Kinetic parameters and growth curves for experimental tumor systems. *Cancer Chemother. Rep.* (1970) 54:143–74.
2. Norton L, Simon R, Brereton HD, Bogden AE. Predicting the course of Gompertzian growth. *Nature*. (1976) 264:542–5. doi: 10.1038/264542a0
3. Pouysségur J, Dayan F, Mazure NM. Hypoxia signalling in cancer and approaches to enforce tumour

regression. *Nature*. (2006) 441:437–43. doi: 10.1038/nature 04871
4. Leblond MM, Gérault AN, Corroyer-Dulmont A, MacKenzie ET, Petit E, Bernaudin M, et al. Hypoxia induces macrophage polarization and re-education toward an M2 phenotype in U87 and U251 glioblastoma models. *Oncoimmunology*. (2016) 5:e1056442. doi: 10.1080/2162402X.2015.1056442
5. Corroyer-Dulmont A, Chakhoyan A, Collet S, Durand L, MacKenzie ET, Petit E, et al. Imaging modalities to assess oxygen status in glioblastoma. *Front Med.* (2015) 2:57. doi: 10.3389/fmed.2015.00057
6. Evans SM, Jenkins KW, Chen HI, Jenkins WT, Judy KD, Hwang W-T, et al. The relationship among hypoxia, proliferation, and outcome in patients with de novo glioblastoma: a pilot study. *Transl Oncol.* (2010) 3:160–9. doi: 10.1593/tlo.09265
7. Spence AM, Muzi M, Swanson KR, O'Sullivan F, Rockhill JK, Rajendran JG, et al. Regional hypoxia in glioblastoma multiforme quantified with [18F]fluoromisonidazole positron emission tomography before radiotherapy: correlation with time to progression and survival. *Clin. Cancer Res.* (2008) 14:2623–30. doi: 10.1158/1078-0432.CCR-07-4995
8. Gerstner E, Zhang Z, Fink J, Muzi M, Hanna L, Greco E, et al. ACRIN 6684: Assessment of tumor hypoxia in newly diagnosed GBM using 18F-FMISO PET and MRI. *Clin Cancer Res.* (2016). doi: 10.1158/1078-0432.CCR-15-2529
9. Rampling R, Cruickshank G, Lewis AD, Fitzsimmons SA, Workman P. Direct measurement of pO2 distribution and bioreductive enzymes in human malignant brain tumors. *Int J Radiat Oncol Biol Phys.* (1994) 29:427–31. doi: 10.1016/0360-3016(94)90432-4
10. Collingridge DR, Piepmeier JM, Rockwell S, Knisely JP. Polarographic measurements of oxygen tension in human glioma and surrounding peritumoural brain tissue. *Radiother Oncol.* (1999) 53:127–31. doi: 10.1016/S0167-8140(99)00121-8
11. Popple RA, Ove R, Shen S. Tumor control probability for selective boosting of hypoxic subvolumes, including the effect of reoxygenation. *Int J Radiat Oncol Biol Phys.* (2002) 54:921–7. doi: 10.1016/S0360-3016(02)03007-9
12. Horsman MR, Overgaard J. The impact of hypoxia and its modification of the outcome of radiotherapy. *J Radiat Res.* (2016) 57(Suppl. 1):i90–8. doi: 10.1093/jrr/rrw007
13. Gray LH, Conger AD, Ebert M, Hornsey S, Scott OC. The concentration of oxygen dissolved in tissues at the time of irradiation as a factor in radiotherapy. *Br J Radiol.* (1953) 26:638–48. doi: 10.1259/0007-1285-26-312-638
14. Rohwer N, Cramer T. Hypoxia-mediated drug resistance: novel insights on the functional interaction of HIFs and cell death pathways. *Drug Resist Updat.* (2011) 14:191-201. doi: 10.1016/j.drup.2011.03.001
15. Harris AL. Hypoxia—a key regulatory factor in tumour growth. *Nat Rev Cancer*. (2002) 2:38–47. doi: 10.1038/nrc704
16. Dische S. Chemical sensitizers for hypoxic cells: a decade of experience in clinical radiotherapy. *Radiother Oncol.* (1985) 3:97–115. doi: 10.1016/S0167-8140(85)80015-3
17. Ostergaard L, Tietze A, Nielsen T, Drasbek KR, Mouridsen K, Jespersen SN, et al. The relationship between tumor blood flow, angiogenesis, tumor hypoxia, and aerobic glycolysis. *Cancer Res.* (2013) 73:5618–24. doi: 10.1158/0008-5472.CAN-13-0964
18. Dewhirst MW, Cao Y, Moeller B. Cycling hypoxia and free radicals regulate angiogenesis and radiotherapy response. *Nat Rev Cancer*. (2008) 8:425–37. doi: 10.1038/nrc2397
19. Bristow RG, Hill RP. Hypoxia and metabolism. Hypoxia, DNA repair and genetic instability. *Nat Rev Cancer*. (2008) 8:180–92. doi: 10.1038/nrc2344
20. Dewhirst MW. Relationships between cycling hypoxia, HIF-1, angiogenesis and oxidative stress. *Radiat Res.* (2009) 172:653–65. doi: 10.1667/RR 1926.1
21. Trotter MJ, Chaplin DJ, Olive PL. Effect of angiotensin II on intermittent tumour blood flow and acute hypoxia in the murine SCCVII carcinoma. *Eur J Cancer*. (1991) 27:887–93. doi: 10.1016/0277-5379(91)90140-9
22. Chaplin DJ, Olive PL, Durand RE. Intermittent blood flow in a murine tumor: radiobiological effects. *Cancer Res.* (1987) 47:597–601.
23. Howard-Flanders P, Moore D. The time interval after pulsed irradiation within which injury to bacteria can be modified by dissolved oxygen. I. A search for an effect of oxygen 0.02 second after pulsed irradiation. *Radiat Res.* (1958) 9:422–37. doi: 10.2307/3570768
24. Fan Q, Tang CY, Gu D, Zhu J, Li G, Wu Y, et al. Investigation of hypoxia conditions using oxygen-enhanced magnetic resonance imaging measurements in glioma models. *Oncotarget*. (2017) 8:31864–75. doi: 10.18632/oncotarget.16256
25. Colliez F, Neveu M-A, Magat J, Cao Pham TT, Gallez B, Jordan BF. Qualification of a noninvasive magnetic resonance imaging biomarker to assess tumor oxygenation. *Clin Cancer Res.* (2014) 20:5403–11. doi: 10.1158/1078-0432.CCR-13-3434
26. Christen T, Pannetier NA, Ni WW, Qiu D, Moseley ME, Schuff N, et al. MR vascular fingerprinting: a new approach to compute cerebral blood volume, mean vessel radius, and oxygenation maps in the human brain. *Neuroimage*. (2014) 89:262–70. doi: 10.1016/j.neuroimage.2013.11.052
27. Zhang H, Koch CJ, Wallen CA, Wheeler KT. Radiation-induced DNA damage in tumors and normal tissues. III. Oxygen dependence of the formation of strand breaks and DNA–protein crosslinks. *Radiat Res.* (1995) 142:163–8. doi: 10.2307/3579024
28. Alper T, Howard-Flanders P. Role of oxygen in modifying the radiosensitivity of *E. coli* B. *Nature*. (1956) 178:978–9. doi: 10.1038/178978a0
29. Tinganelli W, Durante M, Hirayama R, Krämer M, Maier A, Kraft-Weyrather W, et al. Kill-painting of hypoxic tumours in charged particle therapy. *Sci Rep*. (2015) 5:17016. doi: 10.1038/srep17016
30. Wouters BG, Brown JM. Cells at intermediate oxygen levels can be more important than the "hypoxic fraction" in determining tumor response to fractionated radiotherapy. *Radiat Res.* (1997) 147:541–50. doi: 10.2307/3579620
31. Freyer JP, Jarrett K, Carpenter S, Raju MR. Oxygen enhancement ratio as a function of dose and cell cycle phase for radiation-resistant and sensitive CHO cells. *Radiat Res.* (1991) 127:297–307. doi: 10.2307/3577945
32. Furusawa Y, Fukutsu K, Aoki M, Itsukaichi H, Eguchi-Kasai K, Ohara H, et al. Inactivation of aerobic and hypoxic cells from three different cell lines by accelerated (3)He-, (12)C- and (20)Ne-ion beams. *Radiat Res.* (2000) 154:485–96. doi: 10.1667/0033-7587(2000)154[0485:IOAAHC]2.0.CO;2
33. Schlaff CD, Krauze A, Belard A, O'Connell JJ, Camphausen KA. Bringing the heavy: carbon ion therapy in the radiobiological and clinical context. *Radiat Oncol.* (2014) 9:88. doi: 10.1186/1748-717X-9-88
34. Wenzl T, Wilkens JJ. Modelling of the oxygen enhancement ratio for ion beam radiation therapy. *Phys Med Biol.* (2011) 56:3251–68. doi: 10.1088/0031-9155/56/11/006
35. Alper T, Bryant PE. Reduction in oxygen enhancement ratio with increase in LET: tests of two hypotheses. *Int J Radiat Biol Relat Stud Phys Chem Med.* (1974) 26:203–18. doi: 10.1080/09553007414551171
36. Baverstock KF, Burns WG. Primary production of oxygen from irradiated water as an explanation for decreased radiobiological oxygen enhancement at high LET. *Nature*. (1976) 260:316–8. doi: 10.1038/260316a0
37. Michael BD, Prise KM. A multiple-radical model for radiation action on DNA and the dependence of OER on LET. *Int J Radiat Biol.* (1996) 69:351–8. doi: 10.1080/095530096145913
38. Meesungnoen J, Jay-Gerin J-P. High-LET ion radiolysis of water: oxygen production in tracks. *Radiat Res.* (2009) 171:379–86. doi: 10.1667/RR1468.1
39. Valable S, Corroyer-Dulmont A, Chakhoyan A, Durand L, Toutain J, Divoux D, et al. Imaging of brain oxygenation with magnetic resonance imaging: a validation with positron emission tomography in the healthy and tumoural brain. *J Cereb Blood Flow Metab.* (2017) 37:2584–97. doi: 10.1177/0271678X16671965
40. Christen T, Bouzat P, Pannetier N, Coquery N, Moisan A, Lemasson B, et al. Tissue oxygen saturation mapping with magnetic resonance imaging. *J Cereb Blood Flow Metab.* (2014) 34:1550–7. doi: 10.1038/jcbfm.2014.116
41. Tóth V, Förschler A, Hirsch NM, den Hollander J, Kooijman H, Gempt J, et al. MR-based hypoxia measures in human glioma. *J Neurooncol.* (2013) 115:197–207. doi: 10.1007/s11060-013-1210-7
42. O'Connor JPB, Boult JKR, Jamin Y, Babur M, Finegan KG, Williams KJ, et al. Oxygen-enhanced MRI accurately identifies, quantifies, and maps tumor hypoxia in preclinical cancer models. *Cancer Res.* (2016) 76:787–95. doi: 10.1158/0008-5472.CAN-15-2062
43. Corroyer-Dulmont A, Pérès EA, Petit E, Durand L, Marteau L, Toutain J, et al. Noninvasive assessment of hypoxia with 3-[18F]-fluoro-1-(2-nitro-1-imidazolyl)-2-propanol ([18F]-FMISO): a PET study in two experimental models of human glioma. *Biol Chem.* (2013) 394:529–39. doi: 10.1515/hsz-2012-0318

44. Lee ST, Scott AM. Hypoxia positron emission tomography imaging with 18f-fluoromisonidazole. *Semin Nucl Med.* (2007) 37:451–61. doi: 10.1053/j.semnuclmed.2007.07.001
45. Tran L-B-A, Bol A, Labar D, Jordan B, Magat J, Mignion L, et al. Hypoxia imaging with the nitroimidazole 18F-FAZA PET tracer: a comparison with OxyLite, EPR oximetry and 19F-MRI relaxometry. *Radiother Oncol.* (2012) 105:29–35. doi: 10.1016/j.radonc.2012.04.011
46. Wack LJ, Mönnich D, van Elmpt W, Zegers CML, Troost EGC, Zips D, et al. Comparison of [18F]-FMISO, [18F]-FAZA and [18F]-HX4 for PET imaging of hypoxia—a simulation study. *Acta Oncol.* (2015) 54:1370–7. doi: 10.3109/0284186X.2015.1067721
47. Shimizu Y, Zhao S, Yasui H, Nishijima K-I, Matsumoto H, Shiga T, et al. A novel PET probe "[18F]DiFA" accumulates in hypoxic region via glutathione conjugation following reductive metabolism. *Mol Imaging Biol.* (2018) 21:122–9. doi: 10.1007/s11307-018-1214-y
48. Colombié M, Gouard S, Frindel M, Vidal A, Chérel M, Kraeber-Bodéré F, et al. Focus on the controversial aspects of (64)Cu-ATSM in tumoral hypoxia mapping by PET imaging. *Front Med.* (2015) 2:58. doi: 10.3389/fmed.2015.00058
49. Grimes DR, Warren DR, Warren S. Hypoxia imaging and radiotherapy: bridging the resolution gap. *Br J Radiol.* (2017) 90:20160939. doi: 10.1259/bjr.20160939
50. Marcu LG, Moghaddasi L, Bezak E. Imaging of tumor characteristics and molecular pathways with PET: developments over the last decade toward personalized cancer therapy. *Int J Radiat Oncol Biol Phys.* (2018) 102:1165–82. doi: 10.1016/j.ijrobp.2018.04.055
51. Nehmeh SA, Lee NY, Schröder H, Squire O, Zanzonico PB, Erdi YE, et al. Reproducibility of intratumor distribution of (18)F-fluoromisonidazole in head and neck cancer. *Int J Radiat Oncol Biol Phys.* (2008) 70:235–42. doi: 10.1016/j.ijrobp.2007.08.036
52. Inubushi M, Tatsumi M, Yamamoto Y, Kato K, Tsujikawa T, Nishii R. European research trends in nuclear medicine. *Ann Nucl Med.* (2018) 32:579–82. doi: 10.1007/s12149-018-1303-7
53. Ling CC, Humm J, Larson S, Amols H, Fuks Z, Leibel S, et al. Towards multidimensional radiotherapy (MD-CRT): biological imaging and biological conformality. *Int J Radiat Oncol Biol Phys.* (2000) 47:551–60. doi: 10.1016/S0360-3016(00)00467-3
54. Bentzen SM, Gregoire V. Molecular-imaging–based dose painting—a novel paradigm for radiation therapy prescription. *Semin Radiat Oncol.* (2011) 21:101–10. doi: 10.1016/j.semradonc.2010.10.001
55. Chang JH, Wada M, Anderson NJ, Lim Joon D, Lee ST, Gong SJ, et al. Hypoxia-targeted radiotherapy dose painting for head and neck cancer using (18)F-FMISO PET: a biological modeling study. *Acta Oncol.* (2013) 52:1723–9. doi: 10.3109/0284186X.2012.759273
56. Hendrickson K, Phillips M, Smith W, Peterson L, Krohn K, Rajendran J. Hypoxia imaging with [F-18] FMISO-PET in head and neck cancer: potential for guiding intensity modulated radiation therapy in overcoming hypoxia-induced treatment resistance. *Radiother Oncol.* (2011) 101:369–75. doi: 10.1016/j.radonc.2011.07.029
57. Søvik A, Malinen E, Skogmo HK, Bentzen SM, Bruland OS, Olsen DR. Radiotherapy adapted to spatial and temporal variability in tumor hypoxia. *Int J Radiat Oncol Biol Phys.* (2007) 68:1496–504. doi: 10.1016/j.ijrobp.2007.04.027
58. Flynn RT, Bowen SR, Bentzen SM, Mackie TR, Jeraj R. Intensity modulated x-ray (IMXT) vs. proton (IMPT) therapy for theragnostic hypoxia-based dose painting. *Phys Med Biol.* (2008) 53:4153–67. doi: 10.1088/0031-9155/53/15/010
59. Bentzen SM. Theragnostic imaging for radiation oncology: dose-painting by numbers. *Lancet Oncol.* (2005) 6:112–7. doi: 10.1016/S1470-2045(05)01737-7
60. Zegers CML, van Elmpt W, Reymen B, Even AJG, Troost EGC, Ollers MC, et al. *In vivo* quantification of hypoxic and metabolic status of NSCLC tumors using [18F]HX4 and [18F]FDG-PET/CT imaging. *Clin Cancer Res.* (2014) 20:6389–97. doi: 10.1158/1078-0432.CCR-14-1524
61. Thureau S, Dubray B, Modzelewski R, Bohn P, Hapdey S, Vincent S, et al. FDG and FMISO PET-guided dose escalation with intensity-modulated radiotherapy in lung cancer. *Radiat Oncol.* (2018) 13:208. doi: 10.1186/s13014-018-1147-2
62. Malinen E, Søvik A, Hristov D, Bruland ØS, Olsen DR. Adapting radiotherapy to hypoxic tumours. *Phys Med Biol.* (2006) 51:4903–21. doi: 10.1088/0031-9155/51/19/012
63. Choi W, Lee S, Park SH, Ryu JS, Oh SJ, Im KC, et al. Planning study for available dose of hypoxic tumor volume using fluorine-18–labeled fluoromisonidazole positron emission tomography for treatment of the head and neck cancer. *Radiother Oncol.* (2010) 97:176–82. doi: 10.1016/j.radonc.2010.04.012
64. Lee NY, Mechalakos JG, Nehmeh S, Lin Z, Squire OD, Cai S, et al. Fluorine-18–labeled fluoromisonidazole positron emission and computed tomography–guided intensity-modulated radiotherapy for head and neck cancer: a feasibility study. *Int J Radiat Oncol Biol Phys.* (2008) 70:2–13. doi: 10.1016/j.ijrobp.2007.06.039
65. Toma-Dasu I, Uhrdin J, Antonovic L, Dasu A, Nuyts S, Dirix P, et al. Dose prescription and treatment planning based on FMISO-PET hypoxia. *Acta Oncol.* (2012) 51:222–30. doi: 10.3109/0284186X.2011.599815
66. Powathil G, Kohandel M, Milosevic M, Sivaloganathan S. Modeling the spatial distribution of chronic tumor hypoxia: implications for experimental and clinical studies. *Comput Math Methods Med.* (2012) 2012:410602. doi: 10.1155/2012/410602
67. Alber M, Paulsen F, Eschmann SM, Machulla HJ. On biologically conformal boost dose optimization. *Phys Med Biol.* (2003) 48:N31–35. doi: 10.1088/0031-9155/48/2/404
68. Chakhoyan A, Guillamo J-S, Collet S, Kauffmann F, Delcroix N, Lechapt-Zalcman E, et al. FMISO-PET–derived brain oxygen tension maps: application to glioblastoma and less aggressive gliomas. *Sci Rep.* (2017) 7:10210. doi: 10.1038/s41598-017-08646-y
69. Lindblom E, Dasu A, Uhrdin J, Even A, van Elmpt W, Lambin P, et al. Defining the hypoxic target volume based on positron emission tomography for image guided radiotherapy—the influence of the choice of the reference region and conversion function. *Acta Oncol.* (2017) 56:819–25. doi: 10.1080/0284186X.2017.1293289
70. Søvik A, Malinen E, Bruland ØS, Bentzen SM, Olsen DR. Optimization of tumour control probability in hypoxic tumours by radiation dose redistribution: a modelling study. *Phys Med Biol.* (2007) 52:499–513. doi: 10.1088/0031-9155/52/2/013
71. Arnesen MR, Knudtsen IS, Rekstad BL, Eilertsen K, Dale E, Bruheim K, et al. Dose painting by numbers in a standard treatment planning system using inverted dose prescription maps. *Acta Oncol.* (2015) 54:1607–13. doi: 10.3109/0284186X.2015.1061690
72. Wilson TA, Karajannis MA, Harter DH. Glioblastoma multiforme: state of the art and future therapeutics. *Surg Neurol Int.* (2014) 5:64. doi: 10.4103/2152-7806.132138
73. Badiyan SN, Markovina S, Simpson JR, Robinson CG, DeWees T, Tran DD, et al. Radiation therapy dose escalation for glioblastoma multiforme in the era of temozolomide. *Int J Radiat Oncol Biol Phys.* (2014) 90:877–85. doi: 10.1016/j.ijrobp.2014.07.014
74. Connell PP, Hellman S. Advances in radiotherapy and implications for the next century: a historical perspective. *Cancer Res.* (2009) 69:383–92. doi: 10.1158/0008-5472.CAN-07-6871
75. Chao KS, Bosch WR, Mutic S, Lewis JS, Dehdashti F, Mintun MA, et al. A novel approach to overcome hypoxic tumor resistance: Cu-ATSM–guided intensity-modulated radiation therapy. *Int J Radiat Oncol Biol Phys.* (2001) 49:1171–82. doi: 10.1016/S0360-3016(00)01433-4
76. Sato T, Masunaga S-I, Kumada H, Hamada N. Depth distributions of RBE-weighted dose and photon-isoeffective dose for boron neutron capture therapy. *Radiat Prot Dosim.* (2018) 183:247–50. doi: 10.1093/rpd/ncy235
77. Safavi-Naeini M, Chacon A, Guatelli S, Franklin DR, Bambery K, Gregoire M-C, et al. Opportunistic dose amplification for proton and carbon ion therapy via capture of internally generated thermal neutrons. *Sci Rep.* (2018) 8:16257. doi: 10.1038/s41598-018-34643-w
78. Zaidi L, Belgaid M, Taskaev S, Khelifi R. Beam shaping assembly design of 7Li(p,n)7Be neutron source for boron neutron capture therapy of deep-seated tumor. *Appl Radiat Isot.* (2018) 139:316–24. doi: 10.1016/j.apradiso.2018.05.029
79. Cirrone GAP, Manti L, Margarone D, Petringa G, Giuffrida L, Minopoli A, et al. First experimental proof of proton boron capture therapy

(PBCT) to enhance protontherapy effectiveness. *Sci Rep.* (2018) 8:1141. doi: 10.1038/s41598-018-19258-5
80. Jung J-Y, Yoon D-K, Barraclough B, Lee HC, Suh TS, Lu B. Comparison between proton boron fusion therapy (PBFT) and boron neutron capture therapy (BNCT): a Monte Carlo study. *Oncotarget*. (2017) 8:39774–81. doi: 10.18632/oncotarget.15700
81. Kallman RF. The phenomenon of reoxygenation and its implications for fractionated radiotherapy. *Radiology*. (1972) 105:135–42. doi: 10.1148/105.1.135
82. Stieb S, Eleftheriou A, Warnock G, Guckenberger M, Riesterer O. Longitudinal PET imaging of tumor hypoxia during the course of radiotherapy. *Eur J Nucl Med Mol Imaging*. (2018) 45:2201-17. doi: 10.1007/s00259-018-4116-y
83. Thorwarth D, Eschmann S-M, Paulsen F, Alber M. A model of reoxygenation dynamics of head-and-neck tumors based on serial 18F-fluoromisonidazole positron emission tomography investigations. *Int J Radiat Oncol Biol Phys.* (2007) 68:515–21. doi: 10.1016/j.ijrobp.2006.12.037
84. Fleming IN, Manavaki R, Blower PJ, West C, Williams KJ, Harris AL, et al. Imaging tumour hypoxia with positron emission tomography. *Br J Cancer*. (2015) 112:238–50. doi: 10.1038/bjc.2014.610
85. Zips D, Zöphel K, Abolmaali N, Perrin R, Abramyuk A, Haase R, et al. Exploratory prospective trial of hypoxia-specific PET imaging during radiochemotherapy in patients with locally advanced head-and-neck cancer. *Radiother Oncol.* (2012) 105:21–8. doi: 10.1016/j.radonc.2012.08.019
86. Löck S, Perrin R, Seidlitz A, Bandurska-Luque A, Zschaeck S, Zöphel K, et al. Residual tumour hypoxia in head-and-neck cancer patients undergoing primary radiochemotherapy, final results of a prospective trial on repeat FMISO-PET imaging. *Radiother Oncol.* (2017) 124:533–40. doi: 10.1016/j.radonc.2017.08.010
87. Dirix P, Vandecaveye V, De Keyzer F, Stroobants S, Hermans R, Nuyts S. Dose painting in radiotherapy for head and neck squamous cell carcinoma: value of repeated functional imaging with (18)F-FDG PET, (18)F-fluoromisonidazole PET, diffusion-weighted MRI, and dynamic contrast-enhanced MRI. *J Nucl Med.* (2009) 50:1020–7. doi: 10.2967/jnumed.109.062638
88. Kikuchi M, Koyasu S, Shinohara S, Usami Y, Imai Y, Hino M, et al. Prognostic value of pretreatment 18F-fluorodeoxyglucose positron emission tomography/CT volume-based parameters in patients with oropharyngeal squamous cell carcinoma with known p16 and p53 status. *Head Neck*. (2015) 37:1524–31. doi: 10.1002/hed.23784
89. Eschmann S-M, Paulsen F, Reimold M, Dittmann H, Welz S, Reischl G, et al. Prognostic impact of hypoxia imaging with 18F-misonidazole PET in non–small cell lung cancer and head and neck cancer before radiotherapy. *J Nucl Med.* (2005) 46:253–60.
90. Okamoto S, Shiga T, Yasuda K, Ito YM, Magota K, Kasai K, et al. High reproducibility of tumor hypoxia evaluated by 18F-fluoromisonidazole PET for head and neck cancer. *J Nucl Med.* (2013) 54:201–7. doi: 10.2967/jnumed.112.109330
91. Graham K, Unger E. Overcoming tumor hypoxia as a barrier to radiotherapy, chemotherapy and immunotherapy in cancer treatment. *Int J Nanomed.* (2018) 13:6049–58. doi: 10.2147/IJN.S140462
92. Johnson JLH, Dolezal MC, Kerschen A, Matsunaga TO, Unger EC. *In vitro* comparison of dodecafluoropentane (DDFP), perfluorodecalin (PFD), and perfluoroctylbromide (PFOB) in the facilitation of oxygen exchange. *Artif Cells Blood Substit Immobil Biotechnol.* (2009) 37:156–62. doi: 10.1080/10731190903043192
93. Chakhoyan A, Corroyer-Dulmont A, Leblond MM, Gérault A, Toutain J, Chazaviel L, et al. Carbogen-induced increases in tumor oxygenation depend on the vascular status of the tumor: A multiparametric MRI study in two rat glioblastoma models. *J Cereb Blood Flow Metab.* (2017) 37:2270–82. doi: 10.1177/0271678X16663947
94. Lesueur P, Calugaru V, Nauraye C, Stefan D, Cao K, Emery E, et al. Proton therapy for treatment of intracranial benign tumors in adults: a systematic review. *Cancer Treat Rev.* (2019) 72:56–64. doi: 10.1016/j.ctrv.2018.11.004
95. Mizumoto M, Tsuboi K, Igaki H, Yamamoto T, Takano S, Oshiro Y, et al. Phase I/II trial of hyperfractionated concomitant boost proton radiotherapy for supratentorial glioblastoma multiforme. *Int J Radiat Oncol Biol Phys.* (2010) 77:98–105. doi: 10.1016/j.ijrobp.2009.04.054
96. Mizumoto M, Yamamoto T, Takano S, Ishikawa E, Matsumura A, Ishikawa H, et al. Long-term survival after treatment of glioblastoma multiforme with hyperfractionated concomitant boost proton beam therapy. *Pract Radiat Oncol.* (2015) 5:e9–16. doi: 10.1016/j.prro.2014.03.012
97. Orecchia R, Krengli M, Jereczek-Fossa BA, Franzetti S, Gerard JP. Clinical and research validity of hadrontherapy with ion beams. *Crit Rev Oncol Hematol.* (2004) 51:81–90. doi: 10.1016/j.critrevonc.2004.04.005
98. Takahashi M, Hirakawa H, Yajima H, Izumi-Nakajima N, Okayasu R, Fujimori A. Carbon ion beam is more effective to induce cell death in sphere-type A172 human glioblastoma cells compared with X-rays. *Int J Radiat Biol.* (2014) 90:1125–32. doi: 10.3109/09553002.2014.927933
99. Combs SE, Zipp L, Rieken S, Habermehl D, Brons S, Winter M, et al. *In vitro* evaluation of photon and carbon ion radiotherapy in combination with chemotherapy in glioblastoma cells. *Radiat Oncol.* (2012) 7:9. doi: 10.1186/1748-717X-7-9
100. Mizoe J-E, Tsujii H, Hasegawa A, Yanagi T, Takagi R, Kamada T, et al. Phase I/II clinical trial of carbon ion radiotherapy for malignant gliomas: combined X-ray radiotherapy, chemotherapy, and carbon ion radiotherapy. *Int J Radiat Oncol Biol Phys.* (2007) 69:390–6. doi: 10.1016/j.ijrobp.2007.03.003
101. Combs SE, Kieser M, Rieken S, Habermehl D, Jäkel O, Haberer T, et al. Randomized phase II study evaluating a carbon ion boost applied after combined radiochemotherapy with temozolomide versus a proton boost after radiochemotherapy with temozolomide in patients with primary glioblastoma: the CLEOPATRA trial. *BMC Cancer*. (2010) 10:478. doi: 10.1186/1471-2407-10-478
102. Prezado Y, Jouvion G, Hardy D, Patriarca A, Nauraye C, Bergs J, et al. Proton minibeam radiation therapy spares normal rat brain: long-term clinical, radiological and histopathological analysis. *Sci Rep.* (2017) 7:14403. doi: 10.1038/s41598-017-14786-y
103. Prezado Y, Fois G, Le Duc G, Bravin A. Gadolinium dose enhancement studies in microbeam radiation therapy. *Med Phys.* (2009) 36:3568–74. doi: 10.1118/1.3166186
104. Bräuer-Krisch E, Serduc R, Siegbahn EA, Le Duc G, Prezado Y, Bravin A, et al. Effects of pulsed, spatially fractionated, microscopic synchrotron X-ray beams on normal and tumoral brain tissue. *Mutat Res.* (2010) 704:160–6. doi: 10.1016/j.mrrev.2009.12.003
105. Patriarca A, Fouillade C, Auger M, Martin F, Pouzoulet F, Nauraye C, et al. Experimental set-up for FLASH proton irradiation of small animals using a clinical system. *Int J Radiat Oncol Biol Phys.* (2018) 102:619–26. doi: 10.1016/j.ijrobp.2018.06.403
106. Durante M, Bräuer-Krisch E, Hill M. Faster and safer? FLASH ultra-high dose rate in radiotherapy. *Br J Radiol*. (2018) 91:20170628. doi: 10.1259/bjr.20170628
107. Vozenin M-C, De Fornel P, Petersson K, Favaudon V, Jaccard M, Germond J-F, et al. The advantage of FLASH radiotherapy confirmed in mini-pig and cat-cancer patients. *Clin Cancer Res.* (2019) 25:35–42. doi: 10.1158/1078-0432.CCR-17-3375
108. Montay-Gruel P, Petersson K, Jaccard M, Boivin G, Germond J-F, Petit B, et al. Irradiation in a flash: unique sparing of memory in mice after whole brain irradiation with dose rates above 100Gy/s. *Radiother Oncol.* (2017) 124:365–9. doi: 10.1016/j.radonc.2017.05.003

Conflict of Interest Statement: The authors declare that the research was conducted in the absence of any commercial or financial relationships that could be construed as a potential conflict of interest.

frontiers in Medicine

REVIEW
published: 14 June 2019
doi: 10.3389/fmed.2019.00132

Rhenium-188 Labeled Radiopharmaceuticals: Current Clinical Applications in Oncology and Promising Perspectives

Nicolas Lepareur[1,2], Franck Lacœuille[3,4], Christelle Bouvry[1,5], François Hindré[4,6], Emmanuel Garcion[4,6], Michel Chérel[4,7], Nicolas Noiret[5,8], Etienne Garin[1,2] and F. F. Russ Knapp Jr.[9]*

[1] Comprehensive Cancer Center Eugène Marquis, Rennes, France, [2] Univ Rennes, Inra, Inserm, Institut NUMECAN (Nutrition, Métabolismes et Cancer)—UMR_A 1341, UMR_S 1241, Rennes, France, [3] Angers University Hospital, Angers, France, [4] Univ Angers, Univ Nantes, Inserm, CNRS, CRCINA (Centre de Recherche en Cancérologie et Immunologie Nantes—Angers)—UMR 1232, ERL 6001, Nantes, France, [5] Univ Rennes, CNRS, ISCR (Institut des Sciences Chimiques de Rennes)—UMR 6226, Rennes, France, [6] Univ Angers, PRIMEX (Plateforme de Radiobiologie et d'Imagerie EXperimentale), Angers, France, [7] ICO (Institut de Cancérologie de l'Ouest), Comprehensive Cancer Center René Gauducheau, Saint-Herblain, France, [8] ENSCR (Ecole Nationale Supérieure de Chimie de Rennes), Rennes, France, [9] Emeritus, Medical Radioisotopes Program, ORNL (Oak Ridge National Laboratory), Oak Ridge, TN, United States

OPEN ACCESS

Edited by:
Francesco Cicone, Lausanne University Hospital (CHUV), Switzerland

Reviewed by:
Ekaterina Dadachova, University of Saskatchewan, Canada
Adriano Duatti, University of Ferrara, Italy

****Correspondence:***
Nicolas Lepareur
n.lepareur@rennes.unicancer.fr

Specialty section:
This article was submitted to Nuclear Medicine, a section of the journal Frontiers in Medicine

Received: *31 January 2019*
Accepted: *29 May 2019*
Published: *14 June 2019*

Citation:
Lepareur N, Lacœuille F, Bouvry C, Hindré F, Garcion E, Chérel M, Noiret N, Garin E and Knapp FFR Jr (2019) Rhenium-188 Labeled Radiopharmaceuticals: Current Clinical Applications in Oncology and Promising Perspectives. Front. Med. 6:132. doi: 10.3389/fmed.2019.00132

Rhenium-188 (^{188}Re) is a high energy beta-emitting radioisotope with a short 16.9 h physical half-life, which has been shown to be a very attractive candidate for use in therapeutic nuclear medicine. The high beta emission has an average energy of 784 keV and a maximum energy of 2.12 MeV, sufficient to penetrate and destroy targeted abnormal tissues. In addition, the low-abundant gamma emission of 155 keV (15%) is efficient for imaging and for dosimetric calculations. These key characteristics identify ^{188}Re as an important therapeutic radioisotope for routine clinical use. Moreover, the highly reproducible on-demand availability of ^{188}Re from the ^{188}W/^{188}Re generator system is an important feature and permits installation in hospital-based or central radiopharmacies for cost-effective availability of no-carrier-added (NCA) ^{188}Re. Rhenium-188 and technetium-99 m exhibit similar chemical properties and represent a "theranostic pair." Thus, preparation and targeting of ^{188}Re agents for therapy is similar to imaging agents prepared with ^{99m}Tc, the most commonly used diagnostic radionuclide. Over the last three decades, radiopharmaceuticals based on ^{188}Re-labeled small molecules, including peptides, antibodies, Lipiodol and particulates have been reported. The successful application of these ^{188}Re-labeled therapeutic radiopharmaceuticals has been reported in multiple early phase clinical trials for the management of various primary tumors, bone metastasis, rheumatoid arthritis, and endocoronary interventions. This article reviews the use of ^{188}Re-radiopharmaceuticals which have been investigated in patients for cancer treatment, demonstrating that ^{188}Re represents a cost effective alternative for routine clinical use in comparison to more expensive and/or less readily available therapeutic radioisotopes.

Keywords: bone pain palliation, oncology, peptides, radioembolization, radionuclide therapy, radiopharmaceuticals, Rhenium-188

INTRODUCTION

During the last decades, new radionuclide-based targeted therapies have arisen as efficient tools for cancer and inflammatory lesions treatment. They are based on the use of unsealed radioactive sources emitting β^- or α particles, or Auger or low energy conversion electrons and aim at delivering tumoricidal ionizing radiation to tumor cells, while sparing healthy tissues (1–8). Several therapeutic radionuclides, essentially β^- emitters, are routinely used in clinics or actively investigated in clinical trials. Some of them are summarized in **Table 1**. Among them, ^{188}Re is particularly attractive, thanks to its ideal properties [$t_{1/2}$ = 16.9 h, $E_{\beta max}$ = 2.12 MeV, E_γ = 155 keV (15%)] and its on-demand availability at high-specific activity through its generator mode of production.

Rhenium is the 3rd-row congener of transition metal elements in Group VIIB, after manganese and technetium, which, with its isotope technetium-99 m ($t_{1/2}$ = 6 h, E_γ = 141 keV), has been the workhorse of nuclear medicine for more than half a century (9–11). It has a rich chemistry, with oxidation states ranging from −1 to +7 and coordination numbers up to nine. Rhenium is able to complex with a variety of ligands and bifunctional chelating agents (12–16). It possesses two potentially useful therapeutic isotopes, ^{186}Re and ^{188}Re (1). Both can be produced non-carrier-added (nca), but ^{188}Re is produced with high specific activities, thanks to its generator mode of production, while ^{186}Re is essentially reactor-produced with low specific activity, but research is currently conducted on cyclotron production of nca ^{186}Re (17, 18). Likewise, both possess γ emissions which allow for imaging and dosimetry calculations. ^{186}Re has a lower β^- emission with a maximum tissue penetration of 4.5 mm, which is more or less half that of ^{188}Re (11 mm), making ^{186}Re particular suitable for treating small to mid-sized tumors while ^{188}Re is a better match for larger-sized tumors. Considering half-lives, ^{188}Re has a relatively short one (17 h) which restricts its use to agents with rapid target uptake and non-target tissue clearance, while ^{186}Re can also be employed in targeting agents with longer biological half-lives, like antibodies. Based on chemical similarities and the availability of non-radioactive isotopes—which is not the case for technetium—rhenium has been used as a surrogate for technetium-99 m to elucidate structures and mechanisms (19–21). On the other hand, ^{99m}Tc-labeled radiopharmaceuticals likewise serve as a model to prepare $^{186/188}$Re-radiotracers using similar labeling methods (22, 23). However, despite close properties, there are notable differences in the reactivity of technetium and rhenium, particularly concerning their reaction kinetics and redox behaviors (24, 25). Perrhenate is much more difficult to reduce than pertechnetate, which is of prime importance, since this is the form obtained from the generators. This rich but difficult chemistry—which has been thoroughly reviewed recently and do not enter the scope of this review (26), coupled with the current limited availability of pharmaceutical-grade rhenium-188, may explain why ^{188}Re-radiopharmaceuticals have not yet gained wide acceptance, while the use of more convenient therapeutic isotopes (simple, straightforward chemistry, and high production capacities), such as ^{90}Y and ^{177}Lu, is steadily increasing. This is clearly visible when making a bibliographical search on these isotopes, combined with "clinical" research term (**Figure 1**), despite the expected considerably higher costs. There are nonetheless research groups actively working on ^{188}Re-labeled compounds all over the world, aiming at demonstrating the potential clinical usefulness of ^{188}Re-radiopharmaceuticals for the treatment of various benign and malignant conditions. ^{188}Re, under different forms, from small labeled molecules to large antibodies, or loaded into particles, from nanosized colloids to microspheres, has been investigated in various malignant diseases. Several clinical trials are currently going in progress, and some very promising new compounds are in advanced preclinical evaluation and deserve further investigation in patients.

^{188}RE PRODUCTION

The attractive performance properties of the alumina-based ^{188}W/^{188}Re generator system have been widely described (27–32). However, factors which will affect the hopeful broader use of ^{188}Re in routine clinical practice include the costs and required routine reactor production of sufficient activity levels of ^{188}W. These are key issues which have challenged the broader use and routine clinical introduction of ^{188}Re-labeled radiopharmaceuticals. One very attractive characteristic for routine clinical use of the ^{188}W/^{188}Re generator is the relatively rapid ^{188}Re daughter in-growth (∼60% in 24 h) following bolus elution, which means the generator can be used on a daily basis to optimize clinical use of ^{188}Re-labeled therapeutic agents (**Figure 2**). The many advantages for radiotherapy with ^{188}Re would be expected to maintain broad interest in the continued availability of the ^{188}W/^{188}Re generator system. Unfortunately, efficient generator utilization has generally not been the case at most institutions evaluating the early stage clinical trial-based evaluation of ^{188}Re therapeutic agents. The limited *ad hoc* use of the ^{188}W/^{188}Re at many institutions has been often particularly inefficient, because of relatively high generator costs, discussed below. To offset these high costs, one strategy for the most cost-effective generator use, is installation of the generator at a central radiopharmacy site located in a high-density patient population area, where unit ^{188}Re doses can be dispensed to surrounding clinics. Another strategy would be generator installation at specialized regional clinical centers where patients could be referred from the surrounding area. The cost-effective use of the ^{188}W/^{188}Re generator is particularly attractive for use in developing countries because of the low unit dose costs generator system is effectively used (33).

Reactor Production of ^{188}W

The reactor production of ^{188}W by double neutron capture of enriched ^{186}W targets by the [^{186}W(n,γ)^{187}W(n,γ)^{188}W] double neutron capture pathway has been demonstrated in some detail (34, 35). Naturally occurring stable tungsten isotopes are: ^{182}W (26.5%), ^{183}W (14.3%), ^{184}W (20.64%), and ^{186}W (28.43%). Since neutron capture will thus produce a variety of generally unwanted radioisotope products, isotopically enriched ^{186}W (∼ > 90%) is used for reactor production of ^{188}W. Facilities in the U.S. (ORNL) and in the Russian Federation had traditionally

TABLE 1 | Characteristics of important β^- emitters studied for radionuclide therapy.

Radionuclide	$t_{1/2}$ (days)	E_β (MeV) (%)	E_γ (keV) (%)	Tissue penetration range (mm)	Production method
^{32}P	14.3	1.71 (100)	/	8.7	Nuclear reactor
^{47}Sc	3.4	0.600 (32)	159.4 (68.3)	3	Nuclear reactor Cyclotron
^{67}Cu	2.6	0.575 (20)	184.6 (49.6) 93.3 (3) 91.3 (7.6)	2.2	Nuclear reactor Cyclotron
^{89}Sr	50.5	1.492 (100)	/	8	Nuclear reactor
^{90}Y	2.7	2.284 (100)	/	12	^{90}Sr/^{90}Y generator Nuclear reactor for microspheres labeling
^{131}I	8	0.81 (90)	0.364 (81)	2.4	Nuclear reactor
^{153}Sm	1.95	0.808 (21)	103 (28.3)	3	Nuclear reactor
^{161}Tb	6.9	0.593 (100)	74.6 (10.2)	3	Nuclear reactor
^{166}Ho	1.1	1.84 (50.5)	81 (6.4)	8.7	Nuclear reactor
^{177}Lu	6.7	0.497 (79)	208 (11) 113 (6.4)	2.2	Nuclear reactor
^{186}Re	3.8	1.07 (72)	137 (9)	4.5	Nuclear reactor
^{188}Re	**0.7**	**2.118 (72)**	**155 (15)**	**11**	**^{188}W/^{188}Re generator** **Nuclear reactor**

$t_{1/2}$ (days), radioisotope half-life in days; E_β (MeV) (%), maximum particle energy and respective decay abundance shown in parentheses; E_γ (KeV) (%), gamma ray energy useful for imaging and respective abundance in total energy emission shown in parentheses; Tissue penetration range (mm), maximum tissue penetration shown in millimeters. Bold values indicates 188Re.

enriched isotopes of high Z metallic elements such as ^{186}W, and significant inventories of ^{186}W are still available. However, the aging and expensive calutron enrichment facilities which had been operated at ORNL since the 1940's, were taken out of operation in 1998. Significant inventory levels of ^{186}W are still available at ORNL, and the good news is that the ORNL isotope enrichment capability is now being re-established. A comprehensive detailed overview on the issues associated with reactor production of ^{188}W was published by the International Atomic Energy Agency (IAEA) in 2010 (36). Although the availability and broad use of particle accelerators for the production of many medical radioisotopes would be expected to be considerably less expensive than reactor production, no methods have yet been described for the practical accelerator production of ^{188}W.

The neutron cross sections (σ, probability of nuclear neutron capture) for ^{188}W production from neutron irradiation of ^{186}W have been well studied (37). Since the thermal neutron cross section values are a function of the square of the thermal flux for such a double neutron capture process, the ^{188}W product yield, for instance, is essentially doubled by a two-fold increase in neutron flux. Thus, the thermal neutron flux is an important crucial issue for production of ^{188}W. For this reason, high flux nuclear reactors with thermal neutron flux values of at least 10^{14} thermal neutrons/cm^2 are generally felt to be required for effective ^{188}W production (i.e., sufficient specific activity for generator use). The ^{188}W yields at these thermal neutron flux values are about 5–10 mCi/mg ^{186}W target, but depend on a variety of factors regarding the reactor used.

Important factors for reactor production which are beyond the scope of this discussion include the reactor neutron flux spectrum, thermal flux values, reactor cycle, target volume capabilities, shutdown between reactor cycles, etc. The saturation of ^{188}W production and maximization of specific activity are important factors to optimize ^{188}W production and processing costs. At the ORNL HFIR, for instance, two successive reactor cycles are optimal and practical for ^{188}W saturation as a balance between specific activity increase and operation costs, since the down time between cycles is usually only 1 week. Another issue is the radioactive impurities which are produced as irradiation increase and which should be minimized. By many standards, these modest production activity yields and low specific activity may seem low, but in the case of the ^{188}W/^{188}Re generator, these factors are significantly and practically off-set by several attractive operational parameters (38). These factors include the long ^{188}W 60-day physical half-life, the high routine daily ^{188}Re generator elution yields of 60–80% and the very long useful ^{188}W/^{188}Re operational shelf-life of several months.

^{188}W Target Material, Irradiation, and Processing

Because reactor irradiation costs are usually based on the target volume, the early use of low density encapsulated ^{186}W targets was replaced at some institutions by use of high density pressed/sintered ^{186}W targets (39), which greatly increases the ^{186}W mass within the target capsule, thus significantly decreasing the costs per Ci of the ^{188}W produced. *Ergo*, more target mass allows production of higher product activity levels. For this reason, the ^{188}W has been usually produced at the following three institutions (33): High Flux Isotope Reactor in Oak Ridge, TN *($1.8x10^{15}$/neutrons/cm/sec)*, the SM3 Reactor in Dimitrovgrad, Russian Federation *($3x10^{15}$/neutrons/cm/sec)*, and the BR2 reactor in Mol, Belgium *($1x10^{15}$/neutrons/cm/sec)* (40). Traditional processing of reactor-irradiated enriched ^{186}W metal oxide powder targets involved caustic dissolution (41, 42). Processing of the preferred pressed ^{186}W metal targets, involves initial high temperature conversion of the irradiated

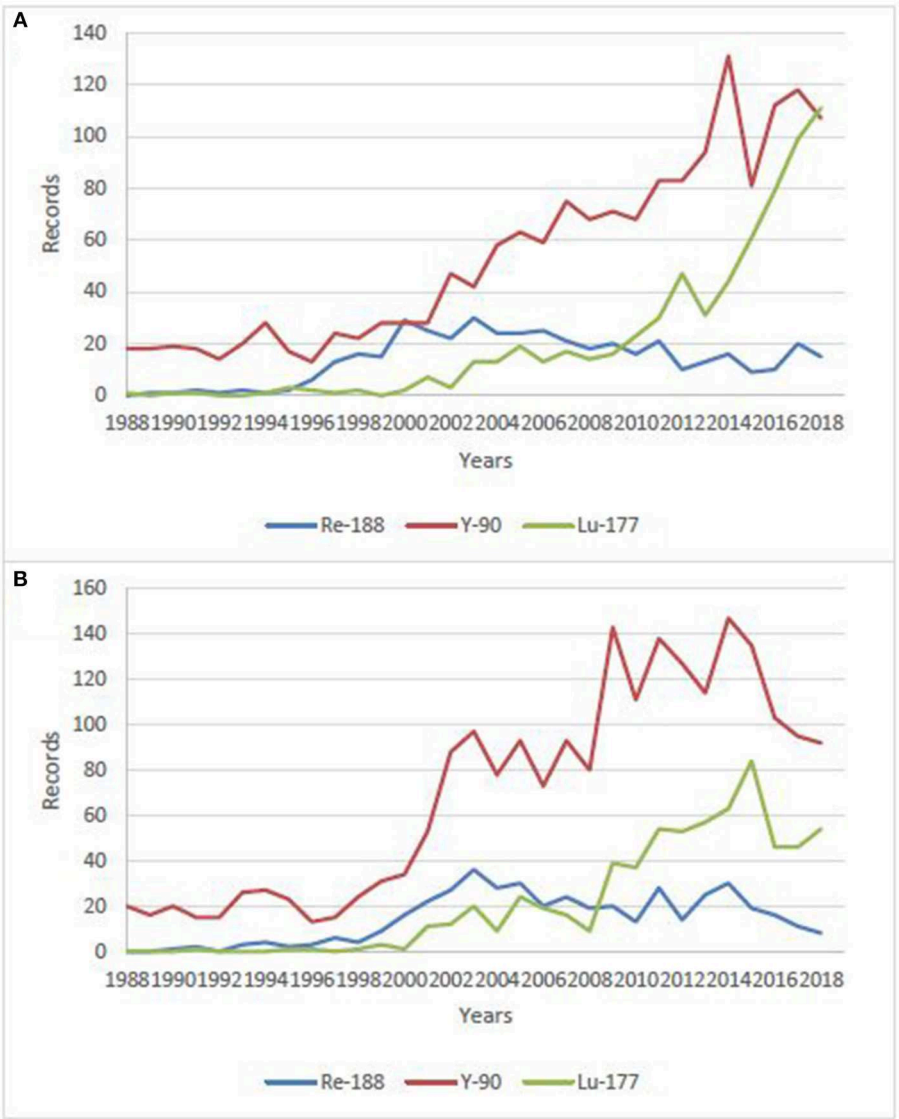

FIGURE 1 | Number of publications/year on clinical use of ^{188}Re, ^{177}Lu and, ^{90}Y over the last 30 years. **(A)** data from Sci-Finder, ©2019 American Chemical Society, **(B)** data from Web of Science, ©2019 Clarivate Analytics.

metallic ^{188}W/^{186}W (i.e., only low percent of ^{186}W atoms are activated) with the oxygen in atmospheric air using a quartz glass reaction apparatus (39). Subsequent dissolution of the [^{188}W]WO_2 product with caustic provides the ^{188}W-tungstate ([^{188}W]Na_2WO_4) stock solution which is then acidified to tungstic acid ([^{188}W]HWO_4) on an on-required basis for generator fabrication.

^{188}W Target Material Recovery

Because only a small fraction of the enriched ^{186}W target atoms are activated to ^{188}W during the reactor irradiation, once the activity levels of eluted ^{188}Re-perrhenate equilibrium from the generators reach activity levels which are too low and are impractical for radiopharmaceutical preparation, the non-activated ^{186}W remaining on the generator matrix can be removed by basic elution and then reprocessed for subsequent activation (43).

^{188}W/^{188}Re Generator Fabrication and Use

Generator Fabrication

Similar to fabrication of the ^{99}Mo/^{99m}Tc generator, activated alumina is currently the most widely used absorbent for fabrication of the ^{188}W/^{188}Re generator column (44, 45). Significant R&D has been devoted over the last three decades to the development of ^{188}W/^{188}Re generator prototypes, most notably in studies supported by the IAEA. A variety of other methods have been evaluated for separation of ^{188}Re from ^{188}W, although detailed discussion of these strategies is beyond

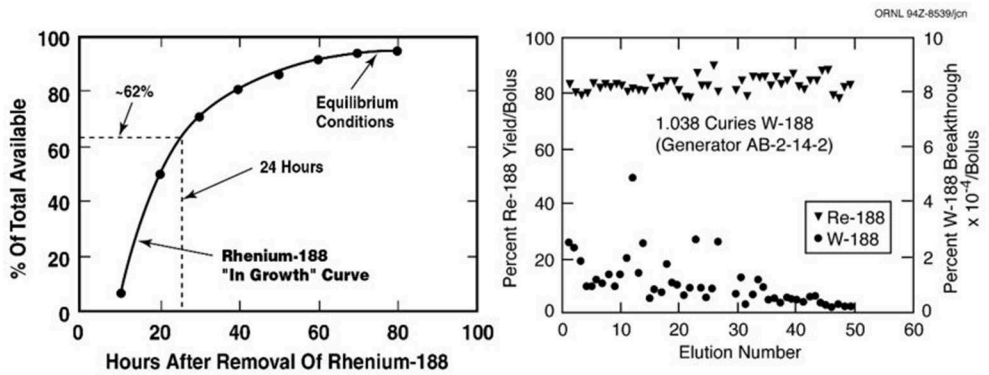

FIGURE 2 | The useful shelf-life of the ORNL alumina-based $^{188}W/^{188}Re$ generator shows consistently high ^{188}Re-perrhenate yields and low ^{188}W breakthrough over at least 2 months (Image property of ORNL, courtesy of Dr. Russ Knapp, Oak Ridge, TN).

the scope of this overview and has been reviewed elsewhere (32). As a brief summary, in addition to the use of alumina, other metal oxides, such as zirconium and titanium tungstates, nanocrystalline titania, polymeric titanium oxychloride sorbets and hydroxyapatite, have also been evaluated, and alternative methods which have been investigated for separation of ^{188}Re from ^{188}W include solvent extraction and electrochemistry. Evidently, these methods have not progressed further since the alumina-based $^{188}W/^{188}Re$ adsorbent has been extensively evaluated in the clinical setting with excellent performance.

For the alumina-based generator, the processed basic sodium tungstate stock solution ($[^{188}W]Na_2WO_4$) is then converted to tungstic acid by acidification with HCl to pH 2–3 and then slowly percolated through the saline-washed alumina column which is then washed thoroughly with additional saline solution.

$^{188}W/^{188}Re$ Generator Elution

The standard alumina-based generator is eluted with saline at a slow flow-rate of typically 1–2 mL/min., with the volume based on the size of the generator (i.e., "void volume") to insure complete removal of the ^{188}Re bolus. Some institutions have instituted the use of semi- or totally-automated elution systems (46–48). These methods have helped move use of the generator forward, and are important to insure reproducible results and reduce the user radiation burden. Microprocessor-controlled detector systems have also been often incorporated for selection of only the peak ^{188}Re activity volume, in order to optimize the bolus ^{188}Re volume. The potential importance for use of these methods is dependent on the particular clinical application and thus the total ^{188}Re activity and specific activity requirements.

^{188}Re Eluent Concentration

Because of the relatively low specific activity of reactor-produced ^{188}W (typically 5–10 Ci/g ^{186}W), the mass of alumina to bind the tungstic acid solution ($[^{188}W]HWO_4$) must be sufficient for irreversible ^{188}W-tungstic acid binding, typically 10 grams alumina/Ci of ^{188}W. In contrast, because of the very high specific activity of fission-produced ^{99}Mo, only very low amounts of alumina are required for the $^{99}Mo/^{99m}Tc$ generator system, resulting in very high specific volume of the saline bolus eluents (mCi/mL saline). Because of the much lower specific activity of ^{188}W, higher volumes of saline are thus required for elution of ^{188}Re eluents, resulting in relatively low specific volumes. With high activity (5–10 Ci) $^{188}W/^{188}Re$ generators, especially for initial use, bolus concentration is often unnecessary since the ^{188}Re specific volume is adequate. However, use of bolus concentration is very important to extend generator shelf-life almost indefinitely and for use of generators fabricated with lower specific activity ^{188}W.

Thus, a convenient and useful strategy for extending the $^{188}W/^{188}Re$ generator half-life involves post-elution concentration of the ^{188}Re bolus solution. Generally, all methods which have been evaluated are based on a similar strategy, focused on the separation of the eluent anions for subsequent specific trapping of the eluted ^{188}Re-perrhenate. The first and currently most widely used convenient method involves a simple two-column tandem flow-through system based on the specific separation of the macroscopic levels of the chloride anions (Cl^-) from the saline eluting solution from the microscopic levels of the eluted perrhenate anions ($[^{188}Re]ReO_4^-$) (49, 50). The system, which was first described by Blower for concentrating ^{99m}Tc generator eluates (51), is based on the specific trapping of the chloride anions on a silver-nitrate-based anion trapping column through which the perrhenate anions flow through and then are subsequently retained in a second anion trapping column. The perrhenate is then obtained by low volume elution of the second column, providing very high ^{188}Re specific volume solutions. The increase in ^{188}Re specific volume from elution of the initial of the generator column can be at least 8–10-fold. An effective similar system uses salts of weak acids such as ammonium acetate for generator elution with subsequent trapping of $[^{188}Re]$-perrhenate (52). Subsequently, a variety of potentially useful alternative methods have also been described (53–57).

Availability of GMP/Pharmaceutical-Grade Generators

Of course, for both early stage through routine clinical applications of ^{188}Re-labeled therapeutic radiopharmaceuticals,

GMP-manufactured generators are required, with subsequent GMP preparation of specific therapeutic agents. One previously widely used $^{188}W/^{188}Re$ generator had been available for several years form the Oak Ridge National Laboratory (ORNL) in the U.S., which were manufactured and distributed throughout the world as a non-sterile GMP-generator. Over about a 20-year period, several hundreds of these generators had been use in both pre-clinical and for a variety of clinical applications. The GMP generators are no longer available from ORNL. More recently, IRE in Fleurus, Belgium, has begun routine production and distribution of the "Rheni Eo" $^{188}W/^{188}Re$ generator system equipped with a GMP remote-controlled bolus concentration system. Because the reactor-production/processing/cGMP costs are not insignificant, the radiopharmacy use of the generator system and use of the eluted ^{188}Re must be optimized to amortize the initial generator investment costs. In many cases through the last decades, the radiopharmacy/clinical use of these generators had not been optimized, thus resulting in unacceptably high unit ^{188}Re costs.

^{188}RE-LABELED SMALL MOLECULES

[^{188}Re]-perrhenate, due to its structural analogy with iodide (near ionic radii, identical charge), has been tested in models of cancers expressing the sodium/iodide transporter (NIS). NIS is a plasma membrane protein that mediates active iodide transport into the thyroid gland and several extra-thyroidal tissues, and notably breast cancer, which naturally expresses NIS in more than 80% of cases. Beside, NIS can be used both as a reporter and as a therapeutic gene, making it possible to image and treat the tumor with radioiodide (^{131}I), just as in differentiated thyroid cancer (58, 59). Using ^{188}Re instead of ^{131}I seems to be a potential alternative (60), and has been investigated in NIS-expressing mammary tumors (61, 62), as well as prostate (63), liver (64) and cervical cancers (65), after NIS gene transfection with adenoviruses or lentiviruses. This use of a virally-directed radioisotope therapy, called radiovirotherapy, seems particularly attractive (66), but it needs to be demonstrated in patients.

Apart from this above example, to be able to deliver its therapeutic activity to the tumor cells, rhenium-188 needs to be attached to a tumor-seeking agent, either based on specific site affinity or a particular mechanism (67).

^{188}Re-DMSA for Medullary Carcinoma

DMSA (meso-2,3-dimercaptosuccinic acid) is a small molecule which exists in two forms labeled with technetium-99 m. Tc(III)-DMSA is a routinely used radiopharmaceutical useful for renal imaging, to evaluate renal structure and morphology, particularly in pediatric imaging for detection of scarring and pyelonephritis (68), while ^{99m}Tc(V)-DMSA is useful for imaging medullary carcinoma of thyroid, head and neck tumors and metastasis from breast carcinoma to liver, brain and skeleton (69). It was thus logical that ^{188}Re(V)-DMSA was envisaged to be useful for the treatment of the above cancers. Three isomers (syn-endo, syn-exo and anti) are formed (**Figure 3**). The isomeric composition may vary depending on the conditions of preparation. The complex is synthesized from the commercial kit for ^{99m}Tc. Bolzati et al. have proposed a new approach (70) for the synthesis of ^{188}Re(V)-DMSA, requiring less stringent conditions. The biological properties of ^{188}Re(V)-DMSA have been studied in animals and humans (71, 72). The results in patients showed a selective attachment to tumor tissues, particularly to metastatic bone cancer originating from prostatic carcinoma, similar to that of the technetium analog (73). The limiting factor for the use of ^{188}Re(V)-DMSA may be its high renal accumulation, higher than the ^{99m}Tc-counterpart (74), though, according to Blower et al. (73), this potential kidney irradiation should not be precluding a therapeutic or palliative use of ^{188}Re(V)-DMSA.

Bone Pain Palliation Agents

Skeletal metastases occur in ∼50% of women with breast cancer, the most common cancer in women, and in 80% of patients with prostate carcinoma, the second most common cancer in men, as well as some other tumors, such as myeloma or lung cancer (75). Medullary infiltration and matrix involvement are usually associated. Tumor infiltration is directly responsible for the pain phenomenon. Approximately half of the patients will continue to have substantial bone pain after the standard surgical and/or non-radiologic treatment options are exhausted. Metabolic radiotherapy offers a therapeutic alternative that is particularly noteworthy (76–78). All localizations are treated immediately by means of a single intravenous injection. Peptide receptor radionuclide therapy (PRRT) with somatostatin analogs (^{177}Lu-octreotate) and PSMA ligands has also demonstrated its potential clinical usefulness for bone metastases arising from neuroendocrine tumors and metastatic castration-resistant prostate cancers (mCRPC), respectively, (79, 80). The idea of using therapeutic radioisotopes to treat the pain of bone metastases dates back to the 1940s. The first tests were due to Lawrence (81) who used phosphorus-32 as an orthophosphate. However, the major disadvantage of ^{32}P is its high hematological toxicity related to the importance of the activity delivered to the bone marrow. For over 20 years, a wide variety of radiopharmaceuticals that can be used to deliver radiation to metastatic bone sites have been developed (82–87). Currently, four are commercially available: $^{89}SrCl_2$ (Metastron®), $^{223}RaCl_2$ (Xofigo®) ^{153}Sm-EDTMP (Quadramet®), and ^{186}Re-HEDP (^{186}Re-etidronate®). ^{89}Sr and ^{223}Ra are used as such because of their natural tropism for bone, mimicking the Ca^{2+} cation, whereas ^{153}Sm and ^{186}Re are used as phosphonates (EDTMP = ethylenediaminetetramethylene phosphonate and HEDP = hydroxyethylidene diphosphonate), which are molecules having a very strong affinity toward calcium present in the actively growing bone. To date, $^{223}RaCl_2$ is the only one with a proven benefit on overall survival (86, 88).

In a recent review on new radionuclides for bone pain palliation, ^{188}Re appears to be one of the most promising candidates (89). The first example of the use of ^{188}Re-HEDP to treat patients was reported by Maxon et al. (90). The cost and availability of ^{188}Re make it a radioisotope more interesting than ^{186}Re. In addition, it is expected that the maximum tolerated dose by the patient is more important for ^{188}Re than for ^{186}Re (91) and the shorter life of ^{188}Re allows to fractionate the injected doses (92–94). The comparison of the biodistribution

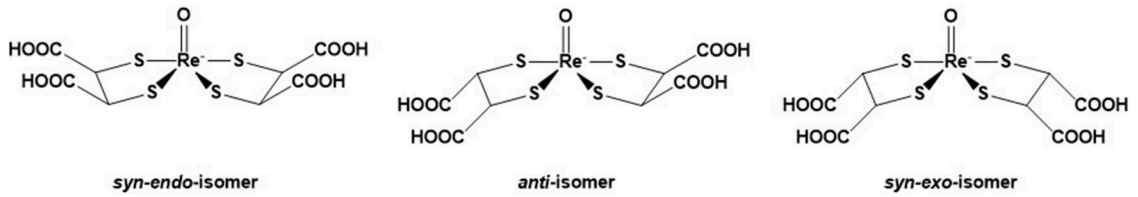

FIGURE 3 | ^{188}Re-DMSA isomers.

of ^{186}Re-HEDP and ^{188}Re-HEDP showed an identical behavior for the two molecules (95, 96). ^{188}Re-HEDP also demonstrated similar efficacy in comparative studies with ^{186}Re-HEDP, ^{153}Sm-EDTMP and $^{89}SrCl_2$ (97, 98). A Phase III trial has recently started to compare its efficacy to $^{223}RaCl_2$, in patients with castration-resistant prostate cancer metastatic to bone (RaRe trial, NCT03458559). The maximum tolerated dose (MTD) of ^{188}Re-HEDP was established to be 3.3 GBq in a dose escalation study by Palmedo et al. (91). Two other dosimetry-based studies demonstrated treatment was safe with an acceptable radiation-absorbed dose to the normal bone-marrow and no limiting hematological toxicity (92, 99). In a study with 15 patients suffering from breast or prostate cancer bone metastases (100), Liepe et al. reported pain relief in 80% of the patients, with 20% patients who were pain-free and could discontinue their analgesics. The same team later reported similar results in 27 prostate cancer patients (101). In a study on patients with lung cancer bone metastases (102), 46% of the patients were able to suspend their analgesics intake. As can be seen, tolerance and efficacy are highly dependent on the primary tumor site. In a study with 61 patients with skeletal metastases from lung, prostate, breast, renal, rhinopharingeal and bladder cancers, pain reliefs were achieved for, respectively, 77, 80, 83, 50, 50, and 100% of the patients (103), while in another study with 64 patients with prostate, breast, lung and liver cancer (104), pain relief was reported for 84.62, 78.57, 62.50, and 55.56%, respectively. In a very recent study by Shinto et al. (105), overall response rate was 89.5% in 48 patients with metastases from different types of cancers. Results were not detailed according to the primary tumor (**Figure 4**). Lange et al. specifically studied the impact on quality of life, proving the routine clinical benefit of ^{188}Re-HEDP therapy (106). A small study by Sabet et al. on 6 patients, failed to demonstrate the usefulness of salvage therapy with ^{188}Re-HEDP for patients with progressive bone metastases after ^{177}Lu-octreotate therapy (107). It has been demonstrated that combination with a radiosensitizer, like capecitabine or taxane, could prove useful and lead to increased efficacy (108, 109). There is also evidence that, compared to single injection, multiple injection could lead to improved overall survival (88, 93, 94). In their retrospective analysis, Biersack et al. reported overall survivals increasing with the number of injections (from 1 to 3), from 4.50 to 15.66 months. The ongoing RaRe trial should answer this question.

An important point in the preparation of ^{188}Re-HEDP is the necessity of decreasing the specific activity by adding "cold" rhenium (*aka* carrier) in order to have good bone fixation. Several studies have investigated the influence of the reaction conditions and kit composition on final product's stability and *in vivo* behavior (110–118). All of them pointed out that the addition of carrier was crucial. A GMP grade kit for the preparation of ^{188}Re-HEDP has recently been described (119) and a standard procedure following the ICH Q8 guideline, and investigating the critical step parameters, has been reported by the same team (118).

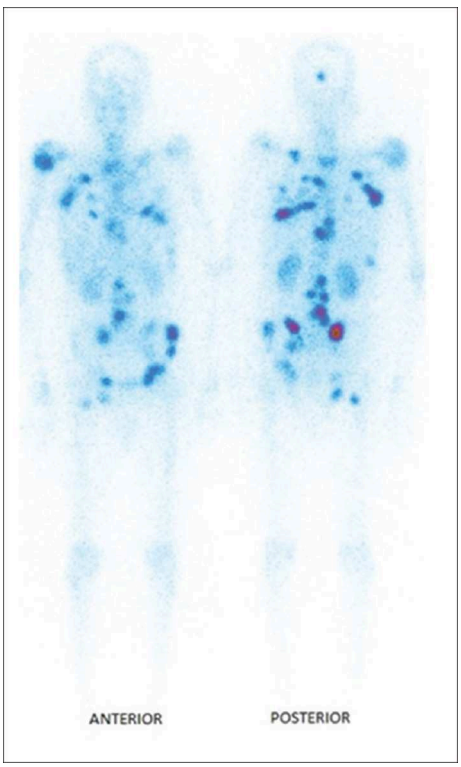

FIGURE 4 | Typical distribution of ^{188}Re-HEDP, 24 h post-injection [from Shinto et al. (105), available under the terms of the Creative Commons Attribution-NonCommercial-ShareAlike License (CC BY-NC-SA)].

Another bisphosphonate has recently been investigated in patients (120). In a Phase I/II trial including 63 patients, ^{188}Re-zoledronic acid was compared with $^{89}SrCl_2$, and demonstrated similar safety profile. In terms of survival, it seems treatment was more beneficial to breast cancer patients than prostate cancer

ones, although the difference was not significant. Several other bisphosphonates and aminophosphonates derivatives have been the subject of development, but have not reach the clinic yet (121). As noted above, ^{188}Re(V)-DMSA exhibited a high affinity for bone metastases from prostate cancer, but no further study was ever carried out following the one by Blower et al. (73).

^{188}RE-LABELED PEPTIDES AND ANTIBODIES FOR HEMATOLOGICAL AND SOLID TUMORS

Tumor cells overexpress a large range of cellular receptors not or poorly expressed by normal tissues. It is, in consequence, possible to selectively target these receptors through the use of targeting moieties with high affinity and selectivity for these receptors. For instance, antibodies targeting antigens expressed on the surface of the tumor or peptides acting as agonist or antagonist to those receptors. Radioimmunotherapy (RIT) and peptide receptor radionuclide therapy (PRRT) have demonstrated their clinical effectiveness, with some radiopharmaceuticals currently approved and a many more under clinical investigation (122–126). Best responses to RIT have been obtained with hematopoietic malignancies, in contrast to solid tumors, in spite of the delivery of somewhat low doses. This can be explained by a better vascularization, more homogenous tumor cell population and the contribution of apoptotic and immune mechanisms (127).

RIT With ^{188}Re-Labeled Antibodies

Antibodies have long circulating times, so ^{188}Re, with its short half-life, might not be the best suited radionuclide for antibody labeling, for which ^{186}Re, with its 3.8-day half-life, could be more appropriate (**Table 1**). Nonetheless, several antibodies or antibody fragments have been labeled with ^{188}Re, by direct or indirect methods (128), and investigated preclinically in a wide variety of tumors, like anti-CD52 and anti-CD66 in leukemia (129, 130), anti-CD20 (rituximab) in lymphoma (131), trastuzumab derivatives in breast, nasopharyngeal or prostate carcinomas (123–134), bevacizumab in non-small-cell lung cancer (135), cetuximab in lung cancer (136), anti-EGF-R antibody h-R3 (nimotuzumab) in glioma (137), anti-CEA MN-14 antibody in gastrointestinal cancers (138), C595 (anti-MUC1) in transitional cell bladder carcinoma (139), MEM238 (IGF2R-specific) in osteosarcoma (140), mAbCx-99 (anti-Ck19 antigen) and C1P5 (targeting E6 viral oncoprotein in human papillomavirus positive cervical cancers) in cervical cancers (141, 142), Listeria-binding antibodies in metastatic pancreatic cancer (143) or melanin-binding IgG or IgM in melanoma (144). Some of them have made their way to the clinics.

BW 250/183 [anti-CD66 (a, b, c, e) antibody], of murine origin and of IgG1 isotype, has a high affinity for the CD-66 antigen present on the cells of the granulocyte line. It is non-specifically directed against a surface glycoprotein, NCA-95, overexpressed on the membrane surface of human myelocytes and metamyelocytes. Radiolabeled with ^{188}Re, it has been tested as an adjunct in marrow transplant packaging in 12 patients with acute leukemia (145) and in 36 patients with acute myeloid leukemia or myelodysplastic syndrome (146). Initial results suggest delivery of a significant radiation dose to bone marrow and minimal toxicity, demonstrating its potential clinical interest prior to bone marrow transplantation. Indeed, injection of radiolabeled antibodies maximizes immunosuppresion in the marrow while avoiding extra-medullary adverse effects (147). A phase I/II study was of particular interest in patients over 55 years of age with a high risk of acute leukemia (148, 149). Nevertheless, one of the main complications is the appearance of transplantation-related toxicity (150) and particularly nephropathies (151). To minimize its adverse effects, the use of ACE inhibitors, angiotensin receptor blockers or forced diuresis is recommended (152). A Phase II study demonstrated that combination of ^{188}Re-radioimmunotherapy with reduced-intensity conditioning was feasible and effective (149), but that dose-reduction of alemtuzumab did not impact overall and disease-free survival (152). ^{188}Re-RIT has also been investigated in patients with non-Hodgkin's lymphoma, using ^{188}Re-rituximab (131). Preliminary dosimetric results indicate it could compare favorably with ^{131}I-rituximab.

A study by Juweid et al. investigated the use of ^{188}Re-labeled antibodies in solid tumors such as gastrointestinal or pancreatic cancer (138). They used an antibody of murine origin, MN 14, directed against the specific CEA epitope. Their results showed that the stability of the selected antibody was not the most suitable especially in patients with weak CEA expression and low tumor burden. The presence of a tumor that is too large and poorly vascularized decreases the therapeutic efficacy given the slow biodistribution of the antibodies. The authors proposed to develop more stable compounds *in vivo* using multi-step delivery system, to use bivalent antibodies or antibody fragments. However, the use of antibody fragments could increase the dose delivered to the kidneys. It would then be advisable to use cationic amino acid infusions to prevent these adverse effects. Another way to maximize the dose to the tumor while sparing healthy tissue is to administer radiolabeled antibodies locoregionally, or directly into the tumor cavity (153). This is the case of nimotuzumab radiolabeled with rhenium-188 in the management of high-grade gliomas in adults (154, 155). Indeed, some patients are not eligible for complete surgical resection or irradiation of lesions by conventional radiotherapy. Therefore, an uncontrolled, open-label, clinical phase I study was conducted to evaluate the safety and maximum tolerated dose of single intracavitary administration of radiolabeled nimotuzumab with ^{188}Re, in 3 patients with anaplastic astrocytoma and 8 with glioblastoma multiforme. It is a humanized monoclonal antibody of IgG1 isotype that recognizes an epitope located in the extracellular domain of EGF-R receptors. Administration of a maximum activity of 10 mCi in brain tissue showed a high tumoricidal dose with acceptable irradiation of the kidneys, liver and bladder.

In consecutive Phase Ia and Phase Ib studies (156), Klein et al. demonstrated that ^{188}Re-6D2, a radiolabeled IgM targeting melanin, was well tolerated, localized in melanoma metastases

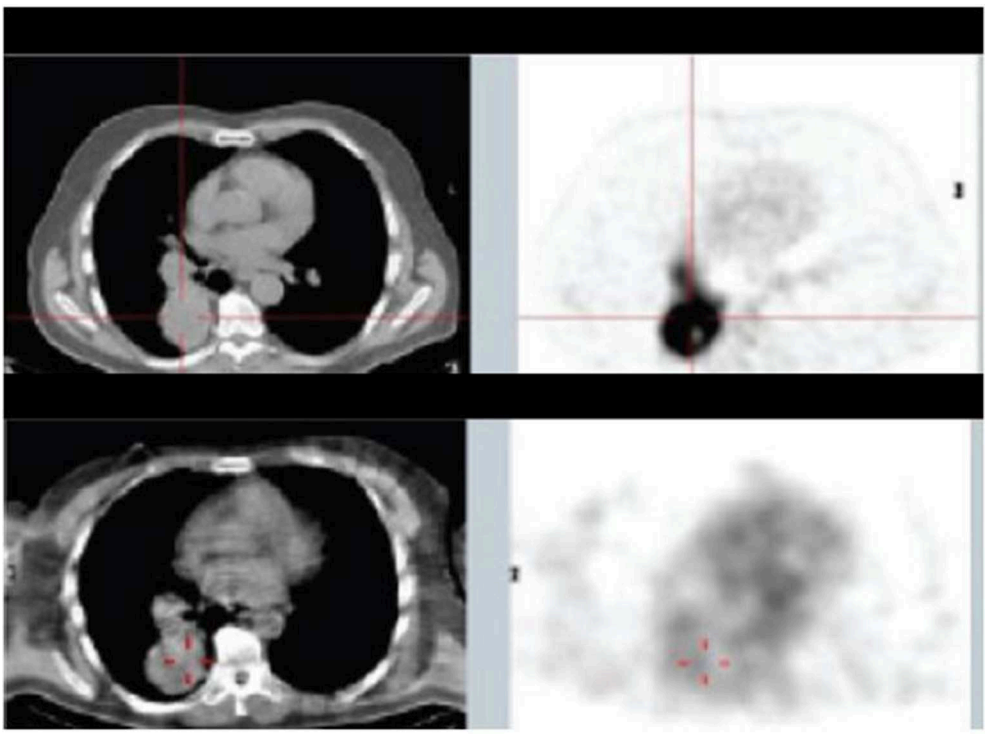

FIGURE 5 | Patient from Phase Ia study with mediastinal and lung metastases: top panel—^{18}FDG PET/CT 10 days before the study, lower panel—SPECT/CT of ^{188}Re-6D2 mAb at 2 h after injection [from Klein et al. (156), available under the terms of the Creative Commons Attribution (CC BY)].

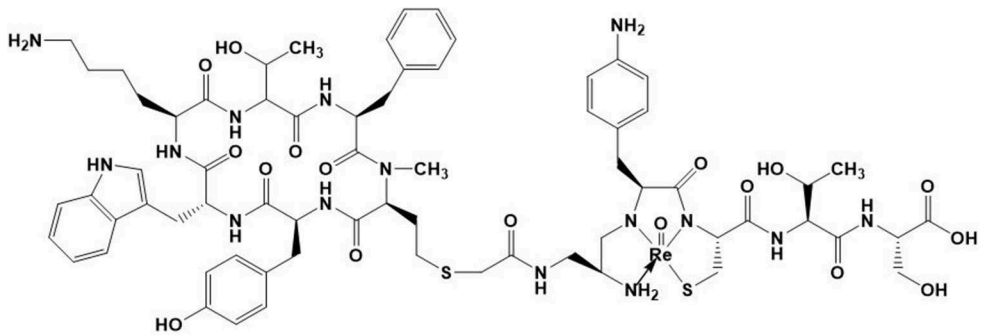

FIGURE 6 | Structure of ^{188}ReO-P2045.

(**Figure 5**), and had antitumor activity, with a median overall survival of 13 months and no dose-limiting toxicities. The advantage of targeting melanin instead of ordinary antigens is that, in rapidly growing melanoma tumors, cell necrosis releases melanin into the extracellular space where it can easily be targeted (157). Moreover, melanin is insoluble, resistant to degradation, and can be expected to accumulate in targeted tissues.

Some other really intriguing potential applications of ^{188}Re-labeled antibodies, but falling out of the scope of this review, have been proposed by Dadachova's team. They aim at treating infectious diseases, such as microbial or fungal infection (158, 159) or HIV (160).

PRRT With ^{188}Re

Peptides have several advantages over antibodies such as low immunogenicity, rapid penetration in the target tissue and clearance from plasma and non-target tissues. Moreover, due to the relatively short half-life of ^{188}Re and the long circulating time of antibodies, radiolabeling peptides might be more suitable. Research on the labeling of peptides with ^{188}Re has been very active, either on the search for the ideal chelating system (161) or on the quest for the analog having the highest affinity and stability (162, 163). A number of peptides have been radiolabeled with ^{188}Re, mainly somatostatin derivatives (164–168). Other considered targets include gastrin releasing peptide receptor

(GRPr) with bombesin (169) or GRPr-antagonist RM26 (170), $\alpha_V\beta_3$ integrin (169), NK1 receptors, with Substance P (171), HCC with SP94 peptide (172), VEGFR (173) or GRP78, a specific cancer cell-surface marker (174). Much work has also been done on targeting melanoma, either through melanin or melanocortin-1 receptor (MC1-R) (162, 175, 176).

There is, to date, however only one ^{188}Re-labeled peptide that has been clinically investigated. It is ^{188}Re-P2045 (**Figure 6**), an 11-amino acid peptide derived from ^{99m}Tc-P829 (depreotide) targeting SST receptors, which has been studied in patients with advanced pulmonary cancer (177). 5 of the 8 patients had stabilized disease for at least 8 weeks, and median overall survival was 11.5 months. Nevertheless, this study has shown a dose delivered to the kidneys that can cause irreversible damage, which prevented further escalation. This renal toxicity can occur in the long term without having early indicators of this failure. Future challenges for the development of radiolabeled antibodies and peptides will notably be to minimize these toxicities, in particular to minimize renal failure.

^{188}RE PARTICULATES

Radiolabeled Lipiodol and Microspheres for Liver Cancers

Primary and secondary liver tumors are a major cause of death, and their incidence is increasing. Among them, hepatocellular carcinoma (HCC), the major primary liver cancer, often appears on an underlying disease (fibrosis, cirrhosis) and is usually detected late, with a curative treatment which therefore can only be proposed to a small minority of patients. Taking advantage of the dual blood supply and rich vasculature of the liver, transarterial radioembolization (TARE) with radiolabeled Lipiodol or microspheres has demonstrated its interest for the management of HCCs at intermediate to advanced stages and intra-hepatic metastases (178–180). Notably, two ^{90}Y-microspheres devices (SIR-Sphere® and TheraSphere®) have been successfully used for ∼2 decades, and have been recently FDA-approved. Thanks to its on-site availability, and to its low-energy gamma-emission authorizing imaging, ^{188}Re represents a potential alternative to ^{90}Y.

Radiolabeled Lipiodol

There has been very active research on radiolabeling of Lipiodol with rhenium-188 (181). Three different ^{188}Re-chelates are currently evaluated for the preparation of clinical ^{188}Re-labeled Lipiodol, i.e., ^{188}Re-HDD (182), ^{188}ReN-DEDC (183) and ^{188}Re-SSS (184), most clinical studies being carried out with the first one (185–198). ^{188}Re-Lipiodol has been investigated in several early phase feasibility studies in non-operable HCC, with patients with advanced cirrhosis (189), or with extensive portal vein thrombosis (191), in second-line therapy to manage recurrences after a curative treatment (192, 193) and to stabilize patients on the liver transplant waiting list (190). To assess the maximum tolerated dose, several dose-escalation studies have been carried out (183, 186, 194, 199). The main at-risk organs are the lungs and healthy liver. In the frame of a Coordinated Research Project funded by the IAEA (200), Phase I (186) then Phase II (196) trials were undertaken in several countries. The overall results demonstrated favorable responses and potential usefulness of ^{188}Re-Lipiodol for the therapy of HCC, which is now almost routinely used in several centers in India. One limitation of these studies is that, except the IAEA-sponsored trials, all of them included a very small number of patients, making it difficult to be conclusive. More trials, including larger cohorts of patients,

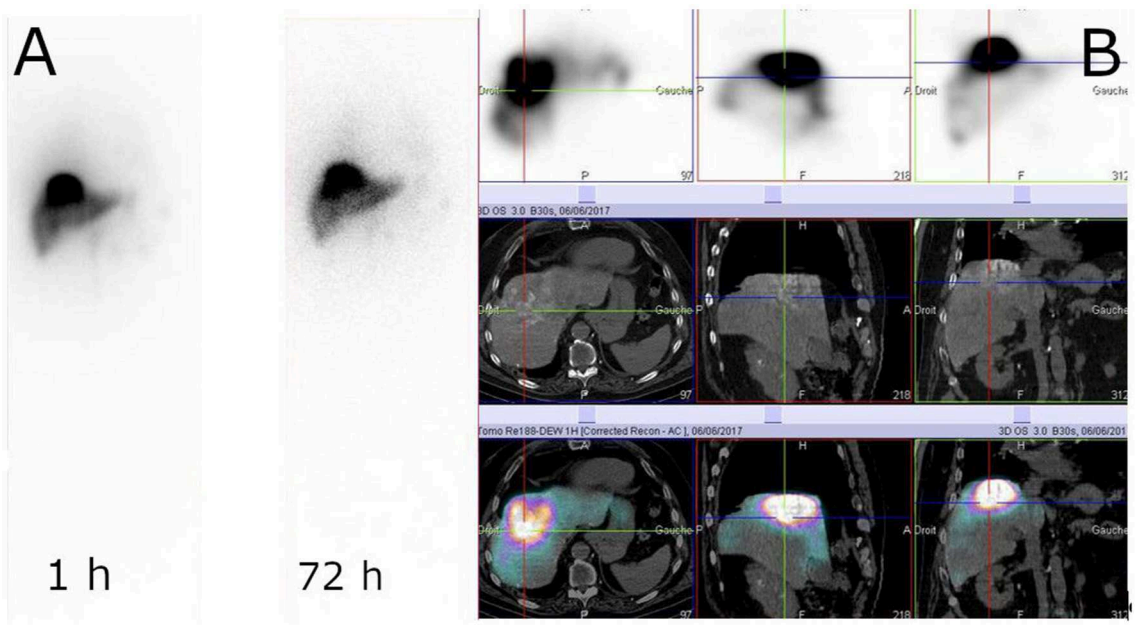

FIGURE 7 | Example of ^{188}Re-SSS biodistribution profile. Whole-body scintigraphy at 1 and 72 h **(A)** and SPECT/CT at 1 h **(B)** (Courtesy of Prof. Etienne Garin, Rennes, France).

are warranted. Another limitation, specifically with ^{188}Re-HDD, is the low labeling yields and high urinary excretion (more than 40% at 72 h) (198). The next generation compounds, such as ^{188}ReN-DEDC and ^{188}Re-SSS, demonstrated higher yields and higher *in vivo* stabilities (183, 199) (**Figure 7**). A newly developed HDD complex (201) is expected to solve the problems encountered with the previous HDD, but no clinical data are available yet.

Radiolabeled Microspheres

Different materials have been investigated for the preparation of ^{188}Re-microspheres (202–205), but, to date, only human serum albumin (HSA) microspheres have made their way to the clinic. One advantage of HSA is that it is an approved drug, with ^{99m}Tc-HSA routinely used in nuclear medicine centers. Two feasibility studies, with patients suffering from HCC or metastatic tumors from various origin, have been published (206, 207). Both studies demonstrated a high product stability, with a low urinary excretion (208), and good tolerance, with acceptable toxicity. In the first study, 2 patients out of 10 demonstrated a partial response (PR) at 3 months, while, in the second one, 5 out of 13 had a PR (**Figure 8**). These encouraging studies included a small number of patients, with heterogeneous tumors. Larger cohorts are mandatory to be able to conclude on the usefulness of this device.

Radiocolloids and Liposomes

An alternative route to target and deliver radioactivity into close contact with tumors that are spread out over the serous membrane of cavities and to tumor cells present in the malignant effusions, is to inject the radiopharmaceutical directly into these cavities, as exemplified above with RIT. Intracavitary radionuclide therapy can be applied to the pleural, pericardial and peritoneal cavities, intrathecally and also into cystic tumors.

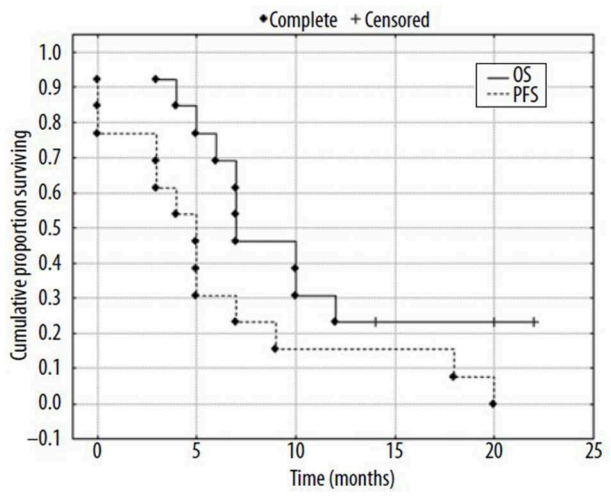

FIGURE 8 | Kaplan-Mayer surviving curves for patients ($N = 13$) after radioembolization of liver tumors with ^{188}Re-HSA microspheres [from Nowicki et al. (207), available under the terms of the Creative Commons Attribution Non Commercial-No Derivs 3.0 (CC BY-NC-ND 3.0)].

For this purpose, radiolabeled colloids have been proven safe and effective (209), but most of the research conducted with ^{188}Re has been preclinical. Melanoma-bearing mice have been treated with intra-peritoneal injection of ^{188}Re-colloids, leading to an increased survival of the treated animals compared to control group (210). ^{188}Re-microspheres embedded in a fibrin glue gel have been proposed as a potential adjuvant treatment to be applied in the tumor bed immediately after resection of glioblastomas (211). ^{188}Re-loaded lipid nanocapsules demonstrated outstanding efficacy in rat glioblastoma models, after convection-enhanced delivery into the tumor, with a significant increase in the survival and induction of an immune response (212–214) (**Figure 9**). A Phase I/II study is expected to start soon. A radiobiological study by Hrycushko et al. aimed at demonstrating the potential usefulness of ^{188}Re-loaded liposomes to prevent recurrence after surgical resection of breast tumors. Based on biodistribution results in rats, dose distributions were modeled and radiobiological indexes determined, following direct injection of ^{188}Re-liposomes into the lumpectomy cavity (215, 216). The same group also carried out a similar work with head and neck squamous cell carcinoma, following direct intratumoral infusion of ^{99m}Tc-labeled liposomes (217, 218). These theoretical results would need to be confirmed *in vivo*. There is currently a clinical trial running in Taiwan, on ^{188}Re-liposomes in patients with primary solid tumor in advanced or metastatic stage (NCT02271516). To date, only preliminary results have been published (219). One patient with advanced serous ovarian adenocarcinoma and one patient with endometrioid ovarian adenocarcinoma were treated twice with intraperitoneal injection of ^{188}Re-BMEDA-liposome, leading to a decrease of cancer antigen 125 in serum, used as a biomarker of treatment response, and a longer than expected survival. The completion of the trial is thus expected to confirm these results.

Another intracavitary application of ^{188}Re and other β-emitter-labeled radiocolloids is the radionuclide treatment of benign diseases by intra-articular injection in cases of persistent

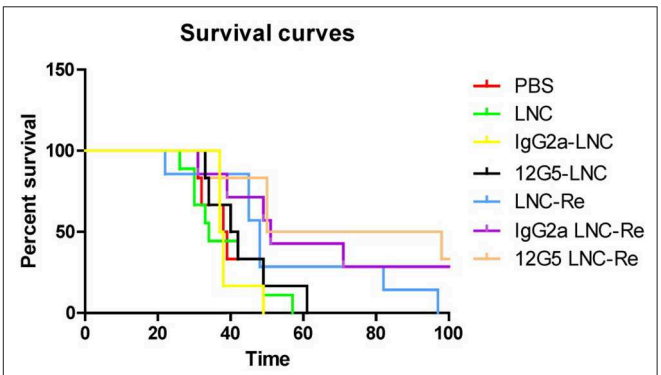

FIGURE 9 | Kaplan Meier curves of mice treated with saline solution (PBS), blank LNC, immuno-LNCs (12G5-LNCs and IgG2a-LNCs) and internal radiation therapies (LNC^{188}Re, IgG2a-LNC^{188}Re, and 12G5-LNC^{188}Re) after single infusion through convection-enhanced delivery into CXCR4-positive brain tumors [from Séhédic et al. (214), available under the terms of the Creative Commons Attribution Non Commercial 4.0 (CC BY-NC 4.0)].

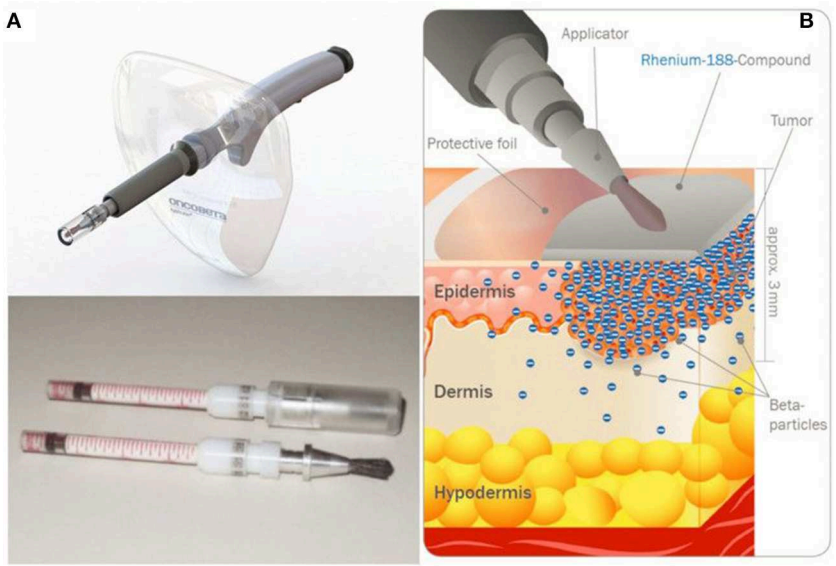

FIGURE 10 | Rhenium-SCT device developed by OncoBeta® GmbH (Garching, Germany). Applicator and dispensing carpoules filled with ^{188}Re-cream **(A)** and illustration of the principle **(B)** (Courtesy of Dr. Shannon Brown III, OncoBeta®).

synovial effusions due to rheumatoid arthritis and other inflammatory joint disease (220).

Brachytherapy of Skin Cancers

A particularly original and attractive treatment modality using ^{188}Re-particulates is the use of ^{188}Re-colloids within a brachytherapy device for skin cancer treatment. Radioactive patches made of nitrocellulose filter paper loaded with ^{188}Re-tin colloids were developed by Jeong et al. (221). This method was successfully used in patients with keloids, a benign dermal fibro proliferative tumor, and non-melanoma skin cancers (222, 223).

An alternative device embeds radiocolloids inside a mix of synthetic acrylic co-polymers inert matrix, and tensioactives, and has been investigated in patients with basal and squamous cell carcinomas (224). Fifty-three patients with histologically confirmed basal cell carcinoma (BCC) or squamous cell carcinoma (SCC) were treated. Three months later, complete healing was obtained in 100% of the treated patients; even after a single application in 82% of the cases. After a mean follow-up of 51 months, no clinical relapses were observed in the treated patients, and histological examination confirmed complete tumor regression. The inert matrix containing the ^{188}Re is able to adapt to every skin surface without contamination, imparting an accurate distribution of dose and sparing the healthy tissue. The technology was further improved, and, in a more recent study (225), 29 BCC and 14 SCC patients were treated. One patient was lost to follow-up before wound closing, but wound healing was complete for all other 42 patients (average 65 days), with no side effects to be reported. During the period of follow-up (average 288 days), no single recurrence occurred. This ^{188}Re-cream can be deposited through a CE-labeled applicator (**Figure 10**), now commercially available under tradename Rhenium-SCT® (Skin Cancer Therapy), from OncoBeta® GmbH (Garching, Germany) and this system is routinely used in Italy and South-Africa, where it is an approved therapy for the treatment of BCC and SCC, including Bowen's disease, in patients with comorbidities, when surgical intervention is not possible or conventional therapies cannot be expected to provide a satisfactory cosmetic result due to the anatomical location. This treatment modality is particularly interesting when surgery is not desirable, as in the case of SCC of the penis (226). In that study, 15 patients, ranging in age from 31 to 92 years, were treated with the Re-SCT® brachytherapy kit. After one to seven different previous treatments (for multifocal lesions), 12 patients were in complete remission, 2 did not respond, and one patient was lost to follow-up, with a mean follow-up of 51 months. Most importantly, this technique was painless and spared the anatomical integrity of the organ. In addition to BCC and SCC, this method was investigated in patients suffering from extramammary Paget's disease (EMPD) (227). Five patients with primary or secondary EMPD were successfully treated, in one or two sessions, with a mean follow-up of 34 months. All patients showed complete remission at the end of the treatments. Four patients later had relapse, either inside or at the periphery of the treated area.

CONCLUSION

Many clinical trials, from feasibility studies to Phase II studies, have been carried out with Rhenium-188-labeled radiopharmaceuticals and have demonstrated the feasibility and clinical usefulness of ^{188}Re-labeled radiopharmaceuticals for a wide range of pathologies, especially in oncology, but also for benign diseases. Despite the advent of more "user-friendly" radionuclides such as ^{90}Y and ^{177}Lu, ^{188}Re

still holds great promise with compounds like ^{188}Re-HEDP for bone pain palliation or ^{188}Re-Lipiodol for liver cancers. Large cohorts of patients are now needed for these agents to find their place within a very competitive environment, with therapies already in use. Brachytherapy of skin cancers also appears particularly attractive, with no direct concurrent for these pathologies. Besides, the development of new ^{188}Re radiotracers, with novel, more stable, cores like tricarbonyl, HYNIC, or nitrido, should lead to molecules with more favorable pharmacokinetic characteristics. More widespread use of ^{188}Re-radiopharmaceuticals will now rely on availability of fully pharmaceutical grade generators and wide clinical proofs of its interest in radionuclide therapy, particularly with the possibility of having a matched theranostic pair with ^{99m}Tc.

AUTHOR CONTRIBUTIONS

All authors listed have made a substantial, direct and intellectual contribution to the work, and approved it for publication.

FUNDING

This work has been supported in part by grants from the French National Agency for Research called Investissements d'Avenir Labex IRON (Grant no. ANR-11-LABX-0018).

ACKNOWLEDGMENTS

The authors thank Dr. Shannon Brown III for providing pictures and for his critical reading of the manuscript.

REFERENCES

1. Volkert WA, Hoffman TJ. Therapeutic radiopharmaceuticals. *Chem Rev*. (1999) 99:2269–92. doi: 10.1021/cr9804386
2. Chatal JF, Hoefnagel CA. Radionuclide therapy. *Lancet*. (1999) 354:931–5. doi: 10.1016/S0140-6736(99)06002-X
3. Srivastava S, Dadachova E. Recent advances in radionuclide therapy. *Semin Nucl Med*. (2001) 31:330–41. doi: 10.1053/snuc.2001.27043
4. Oyen WJ, Bodei L, Giammarile F, Maecke HR, Tennvall J, Luster M, et al. Targeted therapy in nuclear medicine–current status and future prospects. *Ann Oncol*. (2007) 18:1782–92. doi: 10.1093/annonc/mdm111
5. Elgqvist J, Frost S, Pouget JP, Albertsson P. The potential and hurdles of targeted alpha therapy - clinical trials and beyond. *Front Oncol*. (2014) 3:324. doi: 10.3389/fonc.2013.00324
6. Müller C, van der Meulen NP, Benešová M, Schibli R. Therapeutic radiometals beyond ^{177}Lu and ^{90}Y: production and application of promising α-Particle, β-Particle, and auger electron emitters. *J Nucl Med*. (2017) 58: 91S−6S. doi: 10.2967/jnumed.116.186825
7. Lacœuille F, Arlicot N, Faivre-Chauvet A. Targeted alpha and beta radiotherapy: an overview of radiopharmaceutical and clinical aspects. *Med Nucl*. (2018) 42:32–44. doi: 10.1016/j.mednuc.2017.12.002
8. Makvandi M, Dupis E, Engle JW, Nortier FM, Fassbender ME, Simon S, et al. Alpha-emitters and targeted alpha therapy in oncology: from basic science to clinical investigations. *Target Oncol*. (2018) 13:189–203. doi: 10.1007/s11523-018-0550-9
9. Arano Y. Recent advances in ^{99m}Tc radiopharmaceuticals. *Ann Nucl Med*. (2002) 16:79–93. doi: 10.1007/BF02993710
10. Zolle I. *Technetium-99m Pharmaceuticals*. Berlin: Springer-Verlag. (2007). 345 p. doi: 10.1007/978-3-540-33990-8
11. Bartholomä MD, Louie AS, Valliant JF, Zubieta J. Technetium and gallium derived radiopharmaceuticals: comparing and contrasting the chemistry of two important radiometals for the molecular imaging era. *Chem Rev*. (2010) 110:2903–20. doi: 10.1021/cr1000755
12. Vites JC, Lynam MM. Rhenium 1996. *Coord Chem Rev*. (1998) 172:357–88. doi: 10.1016/S0010-8545(98)00095-2
13. Alberto R, Schibli R, Waibel R, Abram U, Schubiger AP. Basic aqueous chemistry of $[M(OH_2)_3(CO)_3]^+$. (M = Re, Tc) directed towards radiopharmaceutical application. *Coord Chem Rev*. (1999) 190–2:901–19. doi: 10.1016/S0010-8545(99)00128-9
14. Bandoli G, Tisato F, Refosco F, Gerber TIA. Rhenium(V) Complexes: from pure hard donors to mixed soft/hard functionalized phosphine ligands. *Rev Inorg Chem*. (1999) 19:187–210. doi: 10.1515/REVIC.1999.19.3.187
15. Liu G, Hnatowich DJ. Labeling biomolecules with radiorhenium - a review of the bifunctional chelators. *Anticancer Agents Med Chem*. (2007) 7:367–77. doi: 10.2174/187152007780618144
16. Hahn EM, Casini A, Kühn FE. Re(VII) and Tc(VII) trioxo complexes stabilized by tridentate ligands and their potential use as radiopharmaceuticals. *Coord Chem Rev*. (2014) 276:97–111. doi: 10.1016/j.ccr.2014.05.021
17. Guertin A, Duchemin C, Haddad F, Michel N, Métivier V. Measurements of ^{186}Re production cross section induced by deuterons on ^{nat}W target at ARRONAX facility. *Nucl Med Biol*. (2014) 41:e16–8. doi: 10.1016/j.nucmedbio.2013.11.003
18. Moustapha ME, Ehrhardt GJ, Smith CJ, Szajek LP, Eckelman WC, Jurisson SS. Preparation of cyclotron-produced ^{186}Re and comparison with reactor-produced ^{186}Re and generator-produced ^{188}Re for the labeling of bombesin. *Nucl Med Biol*. (2006) 33:81–9. doi: 10.1016/j.nucmedbio.2005.09.006
19. Dilworth JR, Parrott SJ. The biomedical chemistry of technetium and rhenium. *Chem Soc Rev*. (1998) 27:43–55. doi: 10.1039/a827043z
20. Mévellec F, Lepareur N, Roucoux A, Noiret N, Patin H, Bandoli G, et al. Chelated hydrazido(3-)rhenium(V) complexes: on the way to the nitrido-M(V) core (M = Tc, Re). *Inorg Chem*. (2002) 41:1591–7. doi: 10.1021/ic0110979
21. Wang JH, Eychenne R, Wolff M, Mallet-Ladeira S, Lepareur N, Benoist E. Design, synthesis, and reactivity of multidentate ligands with Rhenium(I) and Rhenium(V) Cores. *Eur J Inorg Chem*. (2017) 3908–18. doi: 10.1002/ejic.201700632
22. Deutsch E, Libson K, Vanderheyden JL, Ketring AR, Maxon HR. The chemistry of rhenium and technetium as related to the use of isotopes of these elements in therapeutic and diagnostic nuclear medicine. *Nucl Med Biol*. (1986) 13:465–77. doi: 10.1016/0883-2897(86)90027-9
23. De Rosales RTM, Blower P. Role of ^{99m}Tc in the development of rhenium radiopharmaceuticals. In: *Technetium-99m Radiopharmaeuticals: Status and Trends*. Vienna: IAEA Radioisotopes and Radiopharmaceuticals Series 1 (2010). Available online at: https://www-pub.iaea.org/MTCD/Publications/PDF/Pub1405_web.pdf
24. Helm L. Ligand exchange and complex formation kinetics studied by NMR exemplified on fac-$[(CO)_3M(H_2O)]^+$. (M = Mn, Tc, Re). *Coord Chem Rev*. (2008) 252:2346–61. doi: 10.1016/j.ccr.2008.01.009
25. Donnelly PS. The role of coordination chemistry in the development of copper and rhenium radiopharmaceuticals. *Dalton Trans*. (2011) 40:999–1010. doi: 10.1039/c0dt01075h
26. Blower PJ. Rhenium-188 radiochemistry: challenges and prospects. *Int J Nucl Med Res*. (2017) 39–53. doi: 10.15379/2408-9788.2017.04
27. Knapp FF (Russ) Jr. Rhenium-188 - a generator-derived radioisotope for cancer therapy cancer. *Cancer Biother Radiopharm*. (1998) 13:337–49. doi: 10.1089/cbr.1998.13.337
28. Pillai MRA, Dash A, Knapp FF Jr. Rhenium-188: availability from the ^{188}W/^{188}Re generator and status of current applications. *Curr Radiopharm*. (2012) 5:228–3. doi: 10.2174/1874471011205030228
29. Knapp FF (Russ), Kropp J, Liepe K. (2012) Rhenium-188 generator-based radiopharmaceuticals for therapy. In: Baum R, ed. *Therapeutic Nuclear Medicine. Medical Radiology*. Berlin; Heidelberg: Springer. doi: 10.1007/174_2012_669

30. Argyrou M, Valassi A, Andreou M, Lyra M. Rhenium-188 production in hospitals, by w-188/re-188 generator, for easy use in radionuclide therapy. *Int J Mol Imaging*. (2013) 3:290750. doi: 10.1155/2013/290750
31. Dash A, Knapp FF (Russ) Jr. An overview of radioisotope separation technologies for development of ^{188}W/^{188}Re radionuclide generators providing ^{188}Re to meet future research and clinical demands. *RSC Adv*. (2015) 5:39012–36. doi: 10.1039/C5RA03890A
32. Knapp FF (Russ). Continued availability of the tungsten-188/rhenium-188 generator to enhance therapeutic utility of ^{188}Re *Int J Nucl Med Res*. (2017) 3–15. doi: 10.15379/2408-9788.2017.02
33. Shinto A, Pillai AMR. Rhenium-188 as a therapeutic radionuclide in low-income and middle-income countries. *Nucl Med Commun*. (2018) 39:1–2. doi: 10.1097/MNM.0000000000000755
34. Knapp FF (Russ) Jr., Mirzadeh S, Beets AL. Reactor production and processing of therapeutic radioisotopes for applications in nuclear medicine. *J Radioanal Nucl Chem*. (1996) 205:93–100. doi: 10.1007/BF02040554
35. Knapp FF (Russ) Jr., Mirzadeh S, Beets AL, Du M. Production of therapeutic radioisotopes in the ORNL High Flux Isotope Reactor. (HFIR) for applications in nuclear medicine, oncology and interventional cardiology *J Radioanal Nucl Chem*. (2005) 263:503–9. doi: 10.1007/s10967-005-0083-4
36. Knapp FF (Russ) Jr., Mirzadeh S, Garland M, Kuznetsov R. Reactor Production and Processing of ^{188}W. In: *Production of Long Lived Parent Radionuclides for Generators: ^{68}Ge, ^{82}Sr, ^{90}Sr and ^{188}W*. International Atomic Energy Agency. Vienna: (IAEA) Radioisotopes and Radiopharmaceutical Series No. 2, IAEA (2010)
37. Mirzadeh S, Knapp FF (Russ) Jr., Lambrecht RM. Burn-up Cross Section of ^{188}W. *Radiochim Acta*. (1997) 77:99–102. doi: 10.1524/ract.1997.77.12.99
38. Knapp FF (Russ) Jr., Turner JH, Jeong JM, Padhy AK. Issues associated with the use of the Tungsten-188/Rhenium188 generator and concentrator system and preparation of Re-188 HDD: A report. *World J Nucl Med*. (2004) 3:137–143.
39. Mirzadeh S, Du M, Beets AL, Knapp FF (Russ) Jr. Thermoseparation of neutron-irradiated tungsten from Re and Os. *Indust Engineer Chem Res*. (2000) 39:3169–72. doi: 10.1021/ie990582x
40. Ponsard B, Hiltunen J, Penttilla P, Vera-Ruiz H, Beets AL, Mirzadeh S, et al. The tungsten-188/rhenium-188 generator: effective coordination of tungsten-188 production between the HFIR and BR2 Reactors. *J Radioanal Nucl Chem*. (2003) 257:169–174. doi: 10.1023/A:1024730301381
41. Lewis RE, Eldridge, JS. Production of 70-day W-188 and development of a 17-hour Re-188 radioisotope generator *J Nucl Med*. (1966) 7:804–5.
42. Knapp FF (Russ) Jr., Callahan AP, Beets AL, Mirzadeh S, Hsieh. BT. Processing of reactor-produced tungsten-188 for fabrication of clinical scale alumina-based tungsten-188/Rhenium-188 generators *Appl Radiat Isot*. (1994) 45:1123–8. doi: 10.1016/0969-8043(94)90026-4
43. Mushtaq A. Recovery of enriched ^{186}W from spent ^{188}W/^{188}Re generators. *Appl Radiat Isot. (*1996) 47:727–9. doi: 10.1016/0969-8043(96)00032-2
44. Kamioki H, Mirzadeh S, Lambrecht RM, Knapp FF (Russ) Jr., Dadachova E. Tungsten-188/Rhenium-188 generator for biomedical applications *Radiochim Acta*. (1994) 65:39–46.
45. Lee JS, Lee JS, Park UJ, Son KJ, Han HS. Development of a high performance ^{188}W/^{188}Re generator using synthetic alumina. *Appl Radiat Isot*. (2009) 67:1162–6. doi: 10.1016/j.apradiso.2009.02.062
46. Jäckel B, Cripps R, Güntay S, Bruchertseifer H. Development of semi-automated system for preparation of ^{188}Re aqueous solutions of high and reproducible activity concentrations. *Appl Radiat Isot*. (2005) 63:299–304. doi: 10.1016/j.apradiso.2005.04.009
47. Luo TY, Lo AR, Hsieh BT, Lin WJ. A design for automatic preparation of highly concentrated ^{188}Re-perrhenate solutions. *Appl Radiat Isot*. (2007) 65:21–5. doi: 10.1016/j.apradiso.2006.03.016
48. Wunderlich G, Hartmann H, Andreef M, Kotzerke J. A semi-automated system for concentration of rhenium-188 for radiopharmaceutical applications. *Appl Radiat Isot*. (2008) 66:1876–80. doi: 10.1016/j.apradiso.2008.04.015
49. Singh J, Reghebi K, Lazarus CR, Clarke SEM, Callahan AP, Knapp FF Jr., et al. Studies on the preparation and isomeric composition of [^{186}Re]- and [^{188}Re]-pentavalent rhenium dimercaptosuccinic acid complex. *Nucl Med Commun*. (1993) 14:197–203. doi: 10.1097/00006231-199303000-00009
50. Knapp FF (Russ) Jr. Guhlke S, Weinberger J, Beets AL, Amols H, Palmedo H, et al. High specific volume rhenium-188 - clinical potential of a readily available therapeutic radioisotope *Nuklearmedizin*. (1997) 36:A38.
51. Blower PJ. Extending the life of a ^{99m}Tc generator: a simple and convenient method for concentrating generator eluate for clinical use. *Nucl Med Commun*. (1993) 14:995–7. doi: 10.1097/00006231-199311000-00010
52. Guhlke S, Beet al, Oetjen K, Mirzadeh S, Biersack HJ, Knapp FF (Russ) Jr. Simple new method for effective concentration of ^{188}Re solutions from alumina-based ^{188}W—^{188}Re Generator. *J Nucl Med*. (2000) 41:1271–1278.
53. Mushtaq A. Concentration of $^{99m}Tc0_4^-$/$^{188}Re0_4^-$ by a single, compact, anion exchange cartridge *Nucl Med Commun. (*2004) 25:957–62. doi: 10.1097/00006231-200409000-00014
54. Sarkar SK, Venkatesh M, Ramammorthy N. Evaluation of two methods for concentrating perrhenate. (^{188}Re) eluates obtained from ^{188}W-^{188}Re generator. *Appl Radiat Isot*. (2009) 67:234–9. doi: 10.1016/j.apradiso.2008.09.011
55. Chakravarty R, Dash A, Pillai MRA, Venkatesh M. Post-elution concentration of ^{188}Re by an electrochemical method. *Appl Radiat Isot*. (2010) 68:2302–5. doi: 10.1016/j.apradiso.2010.06.022
56. Le VS, Morcos N, Bogulski Z. Development of multiple-elution cartridge-based radioisotope concentrator device for increasing the ^{99m}Tc and ^{188}Re concentration and the effectiveness of ^{99m}Tc/^{99}Mo utilisation. *J Radioanal Nucl Chem*. (2015) 303:1173–8. doi: 10.1007/s10967-014-3439-9
57. Chhabra A, Rathore Y, Bhusari P, Vatsa R, Mittal BR, Shukla J. Concentration protocol of rhenium-188 perrhenate eluted from tungsten-188/rhenium-188 generator for the preparation of high-yield rhenium-188-labelled radiopharmaceuticals. *Nucl Med Commun*. (2018) 39:957–9. doi: 10.1097/MNM.0000000000000893
58. Dadachova E, Carrasco N. The Na/I symporter. (NIS): imaging and therapeutic applications. *Semin Nucl Med*. (2004) 34:23–31. doi: 10.1053/j.semnuclmed.2003.09.004
59. Riesco-Eizaguirre G, Santisteban P. A perspective view of sodium iodide symporter research and its clinical implications. *Eur J Endocrinol*. (2006) 155:495–512. doi: 10.1530/eje.1.02257
60. Zuckier LS, Dohan O, Li Y, Chang CJ, Carrasco N, Dadachova E. Kinetics of perrhenate uptake and comparative biodistribution of perrhenate, pertechnetate, and iodide by NaI symporter-expressing tissues *in vivo*. *J Nucl Med*. (2004) 45:500–7.
61. Dadachova E, Bouzahzah B, Zuckier LS, Pestell RG. Rhenium-188 as an alternative to Iodine-131 for treatment of breast tumors expressing the sodium/iodide symporter. (NIS). *Nucl Med Biol*. (2002) 29:13–8. doi: 10.1016/S0969-8051(01)00279-7
62. Dadachova E, Nguyen A, Lin EY, Gnatovskiy L, Lu P, Pollard JW. Treatment with rhenium-188-perrhenate and iodine-131 of NIS-expressing mammary cancer in a mouse model remarkably inhibited tumor growth. *Nucl Med Biol*. (2005) 32:695–700. doi: 10.1016/j.nucmedbio.2005.05.007
63. Willhauck MJ, Sharif Samani BR, Gildehaus FJ, Wolf I, Senekowitsch-Schmidtke R, Stark HJ, et al. Application of 188rhenium as an alternative radionuclide for treatment of prostate cancer after tumor-specific sodium iodide symporter gene expression. *J Clin Endocrinol Metab*. (2007) 92:4451–8. doi: 10.1210/jc.2007-0402
64. Klutz K, Willhauck MJ, Wunderlich N, Zach C, Anton M, Senekowitsch-Schmidtke R, et al. Sodium iodide symporter. (NIS)-mediated radionuclide. (^{131}I, ^{188}Re) therapy of liver cancer after transcriptionally targeted intratumoral *in vivo* NIS gene delivery. *Hum Gene Ther*. (2011) 22:1403–12. doi: 10.1089/hum.2010.158
65. Zhang M, Shi S, Guo R, Miao Y, Li B. Use of rhenium-188 for in vivo imaging and treatment of human cervical cancer cells transfected with lentivirus expressing sodium iodide symporter. *Oncol Rep*. (2016) 36:2289–97. doi: 10.3892/or.2016.5034
66. Touchefeu Y, Franken P, Harrington KJ. Radiovirotherapy: principles and prospects in oncology. *Curr Pharm Des*. (2012) 18:3313–20. doi: 10.2174/1381612811209023313
67. Jürgens S, Herrmann WA, Kühn FE. Rhenium and technetium based radiopharmaceuticals: Development and recent advances. *J Organomet Chem*. (2014) 751:83–9. doi: 10.1016/j.jorganchem.2013.07.042

68. Piepsz A, Colarinha P, Gordon I, Hahn K, Olivier P, Roca I, et al. Guidelines for ^{99m}Tc-DMSA scintigraphy in children. *Eur J Nucl Med*. (2001) 28: BP37–41.
69. Clarke SE, Lazarus CR, Wraight P, Sampson C, Maisey MN. Pentavalent [^{99m}Tc]DMSA, [^{131}I]MIBG, and [^{99m}Tc]MDP–an evaluation of three imaging techniques in patients with medullary carcinoma of the thyroid. *J Nucl Med*. (1988) 29:33–8.
70. Bolzati C, Boschi A, Uccelli L, Duatti A, Franceschini R, Piffanelli A. An alternative approach to the preparation of 188Re radiopharmaceuticals from generator-produced [$^{188}ReO_4]^-$: efficient synthesis of ^{188}Re(V)-meso-2,3-dimercaptosuccinic acid. *Nucl Med Biol*. (2000) 27:309–14. doi: 10.1016/S0969-8051(00)00079-2
71. Blower PJ, Lam AS, O'Doherty MJ, Kettle AG, Coakley AJ, Knapp FF Jr. Pentavalent rhenium-188 dimercaptosuccinic acid for targeted radiotherapy: synthesis and preliminary animal and human studies. *Eur J Nucl Med*. (1998) 25:613–21. doi: 10.1007/s002590050263
72. García-Salinas L, Ferro-Flores G, Arteaga-Murphy C, Pedraza-López M, Hernández-Gutiérrez S, Azorin-Nieto J. Uptake of the ^{188}Re(V)-DMSA complex by cervical carcinoma cells in nude mice: pharmacokinetics and dosimetry. *Appl Radiat Isot*. (2001) 54:413–8. doi: 10.1016/S0969-8043(00)00278-5
73. Blower PJ, Kettle AG, O'Doherty MJ, Coakley AJ, Knapp FF Jr. ^{99m}Tc(V)DMSA quantitatively predicts ^{188}Re(V)DMSA distribution in patients with prostate cancer metastatic to bone. *Eur J Nucl Med*. (2000) 27:1405–9. doi: 10.1007/s002590000307
74. Dadachova E, Chapman J. ^{188}Re(V)-DMSA revisited: preparation and biodistribution of a potential radiotherapeutic agent with low kidney uptake. *Nucl Med Commun*. (1998) 19:173–81. doi: 10.1097/00006231-199802000-00012
75. Gdowski AS, Ranjan A, Vishwanatha JK. Current concepts in bone metastasis, contemporary therapeutic strategies and ongoing clinical trials. *J Exp Clin Cancer Res*. (2017) 36:108. doi: 10.1186/s13046-017-0578-1
76. Damerla V, Packianathan S, Boerner PS, Jani AB, Vijayakumar S, Vijayakumar V. Recent developments in nuclear medicine in the management of bone metastases: a review and perspective. *Am J Clin Oncol*. (2005) 28:513–20. doi: 10.1097/01.coc.0000162425.55457.10
77. Liepe K, Kotzerke J. Internal radiotherapy of painful bone metastases. *Methods*. (2011) 55:258–70. doi: 10.1016/j.ymeth.2011.07.001
78. Rubini G, Nicoletti A, Rubini D, Asabella AN. Radiometabolic treatment of bone-metastasizing cancer: from ^{186}rhenium to ^{223}radium. *Cancer Biother Radiopharm*. (2014) 29:1–11. doi: 10.1089/cbr.2013.1549
79. Sabet A, Khalaf F, Haslerud T, Al-Zreiqat A, Sabet A, Simon B, et al. Bone metastases in GEP-NET: response and long-term outcome after PRRT from a follow-up analysis. *Am J Nucl Med Mol Imaging*. (2013) 3:437–45.
80. Heck MM, Retz M, D'Alessandria C, Rauscher I, Scheidhauer K, Maurer T, et al. Systemic Radioligand Therapy with ^{177}Lu labeled prostate specific membrane antigen ligand for imaging and therapy in patients with metastatic castration resistant prostate cancer. *J Urol*. (2016) 196:382–91. doi: 10.1016/j.juro.2016.02.2969
81. Lawrence JH, Tuttle LW, Scott KG, Connor CL. Studies on neoplasms with the aid of radioactive phosphorus. I. The total phosphorus metabolism of normal and leukemic mice. *J Clin Invest*. (1940) 19:267–71. doi: 10.1172/JCI101129
82. Mathieu L, Chevalier P, Galy G, Berger M. Preparation of rhenium-186 labelled EHDP and its possible use in the treatment of osseous neoplasms. *Int J Appl Radiat Isot*. (1979) 30:725–7. doi: 10.1016/0020-708X(79)90150-9
83. Hosain F, Spencer RP. Radiopharmaceuticals for palliation of metastatic osseous lesions: biologic and physical background. *Semin Nucl Med*. (1992) 22:11–6. doi: 10.1016/S0001-2998(05)80152-7
84. Bouchet LG, Bolch WE, Goddu SM, Howell RW, Rao DV. Considerations in the selection of radiopharmaceuticals for palliation of bone pain from metastatic osseous lesions. *J Nucl Med*. (2000) 41:682–7.
85. Pauwels EK, Stokkel MP. Radiopharmaceuticals for bone lesions. Imaging and therapy in clinical practice. *Q J Nucl Med*. (2001) 45:18–26.
86. Liepe K, Shinto A. From palliative therapy to prolongation of survival: $^{223}RaCl_2$ in the treatment of bone metastases. *Ther Adv Med Oncol*. (2016) 8:294–304. doi: 10.1177/1758834016640494
87. Das T, Banerjee S. Radiopharmaceuticals for metastatic bone pain palliation: available options in the clinical domain and their comparisons. *Clin Exp Metastasis*. (2017) 34:1–10. doi: 10.1007/s10585-016-9831-9
88. Bouman-Wammes EW, de Klerk JMH, Bloemendal HJ, Van Dodewaard-de Jong JM, Lange R, Ter Heine R, et al. Bone-targeting radiopharmaceuticals as monotherapy or combined with chemotherapy in patients with castration-resistant prostate cancer metastatic to bone. *Clin Genitourin Cancer*. (2018) 17:e281-92. doi: 10.1016/j.clgc.2018.11.014
89. Guerra-Liberal FDC, Tavares AAS, Tavares JMRS. Palliative treatment of metastatic bone pain with radiopharmaceuticals: a perspective beyond Strontium-89 and Samarium-153. *Appl Radiat Isot*. (2016) 110:87–99. doi: 10.1016/j.apradiso.2016.01.003
90. Maxon HR 3rd, Schroder LE, Washburn LC, Thomas SR, Samaratunga RC, Biniakiewicz D, et al. Rhenium-188(Sn)HEDP for treatment of osseous metastases. *J Nucl Med*. (1998) 39:659–63.
91. Palmedo H, Guhlke S, Bender H, Sartor J, Schoeneich G, Risse J, et al. Dose escalation study with rhenium-188 hydroxyethylidene diphosphonate in prostate cancer patients with osseous metastases. *Eur J Nucl Med*. (2000) 27:123–30. doi: 10.1007/s002590050017
92. Savio E, Gaudiano J, Robles AM, Balter H, Paolino A, López A, et al. Re-HEDP: pharmacokinetic characterization, clinical and dosimetric evaluation in osseous metastatic patients with two levels of radiopharmaceutical dose. *BMC Nucl Med*. (2001) 1: 2. doi: 10.1186/1471-2385-1-2
93. Palmedo H, Manka-Waluch A, Albers P, Schmidt-Wolf IG, Reinhardt M, Ezziddin S, et al. Repeated bone-targeted therapy for hormone-refractory prostate carcinoma: tandomized phase II trial with the new, high-energy radiopharmaceutical rhenium-188 hydroxyethylidenediphosphonate. *J Clin Oncol*. (2003) 21:2869–75. doi: 10.1200/JCO.2003.12.060
94. Biersack HJ, Palmedo H, Andris A, Rogenhofer S, Knapp FF (Russ), Guhlke S, et al. Palliation and survival after repeated ^{188}Re-HEDP therapy of hormone-refractory bone metastases of prostate cancer: a retrospective analysis. *J Nucl Med*. (2011) 52:1721–6. doi: 10.2967/jnumed.111.093674
95. Liepe K, Kropp J, Hliscs R, Franke WG. Significant reduction of the mass of bone metastasis 1 year after rhenium-186 HEDP pain palliation therapy. *Clin Nucl Med*. (2000) 25:901–4. doi: 10.1097/00003072-200011000-00009
96. Liepe K, Franke WG, Kropp J, Koch R, Runge R, Hliscs R. Comparison of Rhenium-188, Rhenium-186-HEDP and Strontium-89 in palliation of painful bone metastases. *Nuklearmedizin*. (2000) 39:146–51. doi: 10.1055/s-0038-1632262
97. Liepe K, Runge R, Kotzerke J. The benefit of bone-seeking radiopharmaceuticals in the treatment of metastatic bone pain. *J Cancer Res Clin Oncol*. (2005) 131:60–6. doi: 10.1007/s00432-004-0625-0
98. Liepe K, Kotzerke J. A comparative study of ^{188}Re-HEDP, ^{186}Re-HEDP, ^{153}Sm-EDTMP and ^{89}Sr in the treatment of painful skeletal metastases. *Nucl Med Commun*. (2007) 28:623–30. doi: 10.1097/MNM.0b013e32825a6adc
99. Liepe K, Hliscs R, Kropp J, Runge R, Knapp FF (Russ) Jr., Franke WG. Dosimetry of ^{188}Re-hydroxyethylidene diphosphonate in human prostate cancer skeletal metastases. *J Nucl Med*. (2003) 44:953–60.
100. Liepe K, Hliscs R, Kropp J, Grüning T, Runge R, Koch R, et al. Rhenium-188-HEDP in the palliative treatment of bone metastases. *Cancer Biother Radiopharm*. (2000) 15:261–5. doi: 10.1089/108497800414356
101. Liepe K, Kropp J, Runge R, Kotzerke J. Therapeutic efficiency of rhenium-188-HEDP in human prostate cancer skeletal metastases. *Br J Cancer*. (2003) 89:625–9. doi: 10.1038/sj.bjc.6601158
102. Zhang H, Tian M, Li S, Liu J, Tanada S, Endo K. Rhenium-188-HEDP therapy for the palliation of pain due to osseous metastases in lung cancer patients. *Cancer Biother Radiopharm*. (2003) 18:719–26. doi: 10.1089/108497803770418265
103. Li S, Liu J, Zhang H, Tian M, Wang J, Zheng X. Rhenium-188 HEDP to treat painful bone metastases. *Clin Nucl Med*. (2001) 26:919–22. doi: 10.1097/00003072-200111000-00006
104. Cheng A, Chen S, Zhang Y, Yin D, Dong M. The tolerance and therapeutic efficacy of rhenium-188 hydroxyethylidene diphosphonate in advanced cancer patients with painful osseous metastases. *Cancer Biother Radiopharm*. (2011) 26:237–44. doi: 10.1089/cbr.2010.0873

105. Shinto AS, Mallia MB, Kameswaran M, Kamaleshwaran KK, Joseph J, Radhakrishnan ER, et al. Clinical utility of ^{188}Rhenium-hydroxyethylidene-1,1-diphosphonate as a bone pain palliative in multiple malignancies. *World J Nucl Med*. (2018) 17:228–35. doi: 10.4103/wjnm.WJNM_68_17
106. Lange R, Overbeek F, de Klerk JM, Pasker-de Jong PC, van den Berk AM, Ter Heine R, et al. Treatment of painful bone metastases in prostate and breast cancer patients with the therapeutic radiopharmaceutical rhenium-188-HEDP. Clinical benefit in a real-world study. *Nuklearmedizin*. (2016) 55:188–95. doi: 10.3413/Nukmed-0828-16-05
107. Sabet A, Khalaf F, Mahjoob S, Al-Zreiqat A, Biersack HJ, Ezziddin S. May bone-targeted radionuclide therapy overcome PRRT-refractory osseous disease in NET? A pilot report on ^{188}Re-HEDP treatment in progressive bone metastases after ^{177}Lu-octreotate *Am J Nucl Med Mol Imaging*. (2014) 4:80–8.
108. Lam M, Bosma TB, van Rijk PP, Zonnenberg BA. ^{188}Re-HEDP combined with capecitabine in hormone-refractory prostate cancer patients with bone metastases: a phase I safety and toxicity study. *Eur J Nucl Med Mol Imaging*. (2009) 369:1425–33. doi: 10.1007/s00259-009-1119-8
109. Lange R, ter Heine R, van Wieringen WN, Tromp AM, Paap M, Bloemendal HJ, et al. Cytotoxic effects of the therapeutic radionuclide rhenium-188 combined with taxanes in human prostate carcinoma cell lines. *Cancer Biother Radiopharm*. (2017) 32:16–23. doi: 10.1089/cbr.2016.2129
110. Verdera ES, Gaudiano J, Leon A, Martinez G, Robles A, Savio E, et al. Rhenium-188-HEDP-kit formulation and quality control. *Radiochim Acta*. (1997) 2:113–7. doi: 10.1524/ract.1997.79.2.113
111. Hashimoto K. Synthesis of a ^{188}Re-HEDP complex using carrier-free ^{188}Re, and a study of its stability. *Appl Radiat Isot*. (1998) 49:351–6. doi: 10.1016/S0969-8043(97)00284-4
112. Hsieh BT, Hsieh JF, Tsai SC, Lin WY, Wang SJ, Ting G. Comparison of various rhenium-188-labeled diphosphonates for the treatment of bone metastases. *Nucl Med Biol*. (1999) 26:973–6. doi: 10.1016/S0969-8051(99)00075-X
113. Lin WY, Hsieh JF, Lin CP, Hsieh BT, Ting G, Wang SJ, et al. Effect of reaction conditions on preparations of rhenium-188 hydroxyethylidene diphosphonate complexes. *Nucl Med Biol*. (1999) 26:455–9. doi: 10.1016/S0969-8051(99)00007-4
114. Petriev VM. Influence of reactant concentrations and solution acidity on the complexation of ^{188}Re with 1-hydroxyethane-1,1-diphosphonic acid. *Radiochemistry*. (2008) 50:203–7. doi: 10.1134/S1066362208020227
115. Nassar MY, El-Kolaly MT, Mahran MRH. Synthesis of a ^{188}Re-HEDP complex using carrier-free ^{188}Re and a study of its stability and biological distribution. *Radiochemistry*. (2011) 53:352–6. doi: 10.1134/S1066362211040151
116. Shiryaeva VK, Petriev VM, Bryukhanova AA, Smoryzanova OA, Skvortsov VG, Shvert OE. Evaluation of the influence of preparation conditions on pharmacokinetics of bone-seeking radiopharmaceutical 188Re-labeled hydroxyethylidenediphosphonic acid monopotassium salt in rats. *Pharm Chem J*. (2012) 46:443–8. doi: 10.1007/s11094-012-0818-9
117. Lange R, de Klerk JMH, Bloemendal HJ, Ramakers RM, Beekman FJ, van der Westerlaken MML, et al. Drug composition matters: the influence of carrier concentration on the radiochemical purity, hydroxyapatite affinity and in-vivo bone accumulation of the therapeutic radiopharmaceutical ^{188}Rhenium-HEDP. *Nucl Med Biol*. (2015) 42:465–9. doi: 10.1016/j.nucmedbio.2015.01.007
118. Lange R, Ter Heine R, van der Gronde T, Selles S, de Klerk J, Bloemendal H, et al. Applying quality by design principles to the small-scale preparation of the bone-targeting therapeutic radiopharmaceutical rhenium-188-HEDP. *Eur J Pharm Sci*. (2016) 30: 90:96–101. doi: 10.1016/j.ejps.2016.01.008
119. ter Heine R, Lange R, Breukels OB, Bloemendal HJ, Rummenie RG, Wakker AM, et al. Bench to bedside development of GMP grade Rhenium-188-HEDP, a radiopharmaceutical for targeted treatment of painful bone metastases. *Int J Pharm*. (2014) 465:317–24. doi: 10.1016/j.ijpharm.2014.01.034
120. Kochetova T, Krylov V, Smolyarchuk M, Sokov D, Lunev A, Shiryaev S, et al. ^{188}Re zoledronic acid in the palliative treatment of painful bone metastases. *Int J Nucl Med Res*. (2017) 92–100. doi: 10.15379/2408-9788.2017.08
121. Lange R, Ter Heine R, Knapp FF (Russ), de Klerk JM, Bloemendal HJ, Hendrikse NH. Pharmaceutical and clinical development of phosphonate-based radiopharmaceuticals for the targeted treatment of bone metastases. *Bone*. (2016) 91:159–79. doi: 10.1016/j.bone.2016.08.002
122. Ansquer C, Kraeber-Bodéré F, Chatal JF. Current status and perspectives in peptide receptor radiation therapy. *Curr Pharm Des*. (2009) 15:2453–62. doi: 10.2174/138161209788682262
123. Lozza C, Navarro-Teulon I, Pèlegrin A, Pouget JP, Vivès E. Peptides in receptor-mediated radiotherapy: from design to the clinical application in cancers. *Front Oncol*. (2013) 3:247. doi: 10.3389/fonc.2013.00247
124. Dash A, Chakraborty S, Pillai MR, Knapp FF (Russ) Jr. Peptide receptor radionuclide therapy: an overview. *Cancer Biother Radiopharm*. (2015) 30:47–71. doi: 10.1089/cbr.2014.1741
125. Larson SM, Carrasquillo JA, Cheung NK, Press OW. Radioimmunotherapy of human tumours. *Nat Rev Cancer*. (2015) 15:347–60. doi: 10.1038/nrc3925
126. Kraeber-Bodéré F, Barbet J, Chatal JF. Radioimmunotherapy: from current clinical success to future industrial breakthrough? *J Nucl Med*. (2016) 57:329–31. doi: 10.2967/jnumed.115.167247
127. Goldenberg DM, Sharkey RM. Advances in cancer therapy with radiolabeled monoclonal antibodies. *Q J Nucl Med Mol Imaging*. (2006) 50:248–64.
128. Uccelli L, Martini P, Pasquali M, Boschi A. Monoclonal Antibodies Radiolabeling with Rhenium-188 for Radioimmunotherapy. *Biomed Res Int*. (2017) 2017:5923609. doi: 10.1155/2017/5923609
129. Bunjes D. ^{188}Re-labeled anti-CD66 monoclonal antibody in stem cell transplantation for patients with high-risk acute myeloid leukemia. *Leukemia Lymphoma*. (2002) 43:2125–31. doi: 10.1080/1042819021000033015
130. De Decker M, Bacher K, Thierens H, Slegers G, Dierckx RA, De Vos F. *In vitro* and *in vivo* evaluation of direct rhenium-188-labeled anti-CD52 monoclonal antibody alemtuzumab for radioimmunotherapy of B-cell chronic lymphocytic leukemia. *Nucl Med Biol*. (2008) 35:599–604. doi: 10.1016/j.nucmedbio.2008.03.001
131. Torres-García E, Ferro-Flores G, Arteaga de Murphy C, Correa-González L, Pichardo-Romero PA. Biokinetics and dosimetry of ^{188}Re-anti-CD20 in patients with non-Hodgkin's lymphoma: preliminary experience. *Arch Med Res*. (2008) 39:100–9. doi: 10.1016/j.arcmed.2007.06.023
132. Li G, Wang Y, Huang K, Zhang H, Peng W, Zhang C. The experimental study on the radioimmunotherapy of the nasopharyngeal carcinoma overexpressing HER2/neu in nude mice model with intratumoral injection of ^{188}Re-herceptin. *Nucl Med Biol*. (2005) 32:59–65. doi: 10.1016/j.nucmedbio.2004.09.003
133. Luo TY, Tang IC, Wu YL, Hsu KL, Liu SW, Kung HC, et al. Evaluating the potential of ^{188}Re-SOCTA-trastuzumab as a new radioimmunoagent for breast cancer treatment. *Nucl Med Biol*. (2009) 36:81–8. doi: 10.1016/j.nucmedbio.2008.10.014
134. Wang HY, Lin WY, Chen MC, Lin T, Chao CH, Hsu FN, et al. Inhibitory effects of Rhenium-188-labeled Herceptin on prostate cancer cell growth: a possible radioimmunotherapy to prostate carcinoma. *Int J Radiat Biol*. (2013) 89:346–55. doi: 10.3109/09553002.2013.762136
135. Xiao J, Xu X, Li X, Li Y, Liu G, Tan H, et al. Re-188 enhances the inhibitory effect of bevacizumab in non-small-cell lung cancer. *Molecules*. (2016) 21:E1308 doi: 10.3390/molecules21101308
136. Kuo WI, Cheng KH, Chang YJ, Wu TT, Hsu WC, Chen LC, et al. Radiolabeling, Characteristics and NanoSPECT/CT Imaging of ^{188}Re-cetuximab in NCI-H292 Human Lung Cancer Xenografts. *Anticancer Res*. (2019) 39:183–90. doi: 10.21873/anticanres.13096
137. González-Navarro BO, Casaco A, León M, Leyva R, León A, Santana E, et al. High dose of hR-3, an anti-epidermal growth factor receptor monoclonal antibody labeled with ^{188}rhenium following intravenous injection into rats. *J Appl Res*. (2006) 6:77–88.
138. Juweid M, Sharkey RM, Swayne LC, Griffiths GL, Dunn R, Goldenberg DM. Pharmacokinetics, dosimetry and toxicity of rhenium-188-labeled anti-carcinoembryonic antigen monoclonal antibody, MN-14, in gastrointestinal cancer. *J Nucl Med*. (1998) 39:34–42.
139. Murray A, Simms MS, Scholfield DP, Vincent RM, Denton G, Bishop MC, et al. Production and characterization of ^{188}Re-C595 antibody for radioimmunotherapy of transitional cell bladder cancer. *J Nucl Med*. (2001) 42:726–32.
140. Geller DS, Morris J, Revskaya E, Kahn M, Zhang W, Piperdi S, et al. Targeted therapy of osteosarcoma with radiolabeled monoclonal antibody

to an insulin-like growth factor-2 receptor (IGF2R). *Nucl Med Biol*. (2016) 43:812–7. doi: 10.1016/j.nucmedbio.2016.07.008

141. Chang CH, Tsai LC, Chen ST, Yuan CC, Hung MW, Hsieh BT, et al. Radioimmunotherapy and apoptotic induction on Ck19-overexpressing human cervical carcinoma cells with Re-188-mAbCx-99 *Anticancer Res*. (2005) 25:2719–28.
142. Phaeton R, Jiang Z, Revskaya E, Fisher DR, Goldberg GL, Dadachova E. Beta emitters rhenium-188 and lutetium-177 are equally effective in radioimmunotherapy of HPV-positive experimental cervical cancer. *Cancer Med*. (2016) 5:9–16. doi: 10.1002/cam4.562
143. Quispe-Tintaya W, Chandra D, Jahangir A, Harris M, Casadevall A, Dadachova E, et al. Nontoxic radioactive Listeria(at) is a highly effective therapy against metastatic pancreatic cancer. *Proc Natl Acad Sci USA*. (2013) 110:8668–73. doi: 10.1073/pnas.1211287110
144. Nosanchuk JD, Jeyakumar A, Ray A, Revskaya E, Jiang Z, Bryan RA, et al. Structure-function analysis and therapeutic efficacy of antibodies to fungal melanin for melanoma radioimmunotherapy. *Sci Rep*. (2018) 8:5466. doi: 10.1038/s41598-018-23889-z
145. Seitz U, Neumaier B, Glatting G, Kotzerke J, Bunjes D, Reske SN. Preparation and evaluation of the rhenium-188-labelled anti-NCA antigen monoclonal antibody BW 250/183 for radioimmunotherapy of leukaemia. *Eur J Nucl Med*. (1999) 26:1265–73. doi: 10.1007/s002590050582
146. Bunjes D, Buchmann I, Duncker C, Seitz U, Kotzerke J, Wiesneth M, et al. Rhenium 188-labeled anti-CD66. (a, b, c, e) monoclonal antibody to intensify the conditioning regimen prior to stem cell transplantation for patients with high-risk acute myeloid leukemia or myelodysplastic syndrome: results of a phase I-II study. *Blood*. (2001) 98:565–72. doi: 10.1182/blood.V98.3.565
147. Buchmann I, Bunjes D, Kotzerke J, Martin H, Glatting G, Seitz U, et al. Myeloablative radioimmunotherapy with Re-188-anti-CD66-antibody for conditioning of high-risk leukemia patients prior to stem cell transplantation: biodistribution, biokinetics and immediate toxicities. *Cancer Biother Radiopharm*. (2002) 17:151–63. doi: 10.1089/108497802753773775
148. Ringhoffer M, Blumstein N, Neumaier B, Glatting G, von Harsdorf S, Buchmann I, et al. ^{188}Re or ^{90}Y-labelled anti-CD66 antibody as part of a dose-reduced conditioning regimen for patients with acute leukaemia or myelodysplastic syndrome over the age of 55: results of a phase I-II study. *Br J Haematol*. (2005) 130:604–13. doi: 10.1111/j.1365-2141.2005.05663.x
149. Lauter A, Strumpf A, Platzbecker U, Schetelig J, Wermke M, Radke J, et al. ^{188}Re anti-CD66 radioimmunotherapy combined with reduced-intensity conditioning and *in-vivo* T cell depletion in elderly patients undergoing allogeneic haematopoietic cell transplantation. *Br J Haematol*. (2010) 148:910–7. doi: 10.1111/j.1365-2141.2009.08025.x
150. Klein SA, Hermann S, Dietrich JW, Hoelzer D, Martin H. Transplantation-related toxicity and acute intestinal graft-versus-host disease after conditioning regimens intensified with Rhenium 188-labeled anti-CD66 monoclonal antibodies. *Blood*. (2002) 99:2270–1. doi: 10.1182/blood.V99.6.2270
151. Zenz T, Schlenk RF, Glatting G, Neumaier B, Blumstein N, Buchmann I, et al. Bone marrow transplantation nephropathy after an intensified conditioning regimen with radioimmunotherapy and allogeneic stem cell transplantation. *J Nucl Med*. (2006) 47:278–86.
152. Schneider S, Strumpf A, Schetelig J, Wunderlich G, Ehninger G, Kotzerke J, et al. Reduced-intensity conditioning combined with ^{188}Rhenium radioimmunotherapy before allogeneic hematopoietic stem cell transplantation in elderly patients with acute myeloid leukemia: the role of *in vivo* t cell depletion. *Biol Blood Marrow Transplant*. (2015) 21:1754–60. doi: 10.1016/j.bbmt.2015.05.012
153. Zhi Y, Meiying Z, Baohe L, Changying Z, Yan H, Aping M, et al. ^{188}Re-labelled McAb 3H11 used as preventive for the peritoneal micro-metastasis of gastric cancer. *Nuclear Science and Techniques*. (1999) 10:203–6.
154. Torres LA, Coca MA, Batista JF, Casaco A, Lopez G, García I, et al. Biodistribution and internal dosimetry of the ^{188}Re-labelled humanized monoclonal antibody anti-epidermal growth factor receptor, nimotuzumab, in the locoregional treatment of malignant gliomas. *Nucl Med Commun*. (2008) 29:66–75. doi: 10.1097/MNM.0b013e3282f1bbce
155. Casacó A, López G, García I, Rodríguez JA, Fernández R, Figueredo J, et al. Phase I single-dose study of intracavitary-administered Nimotuzumab labeled with ^{188}Re in adult recurrent high-grade glioma. *Cancer Biol Ther*. (2008) 7:333–9. doi: 10.4161/cbt.7.3.5414
156. Klein M, Lotem M, Peretz T, Zwas ST, Mizrachi S, Liberman Y, et al. Safety and efficacy of 188-rhenium-labeled antibody to melanin in patients with metastatic melanoma. *J Skin Cancer*. (2013) 2013:828329. doi: 10.1155/2013/828329
157. Dadachova E, Nosanchuk JD, Shi L, Schweitzer AD, Frenkel A, Nosanchuk JS, et al. Dead cells in melanoma tumors provide abundant antigen for targeted delivery of ionizing radiation by a mAb to melanin. *Proc Natl Acad Sci USA*. (2004) 101:14865–70. doi: 10.1073/pnas.0406180101
158. Dadachova E, Nakouzi A, Bryan RA, Casadevall A. Ionizing radiation delivered by specific antibody is therapeutic against a fungal infection. *Proc Natl Acad Sci USA*. (2003) 100:10942–7. doi: 10.1073/pnas.1731272100
159. Rivera J, Nakouzi AS, Morgenstern A, Bruchertseifer F, Dadachova E, Casadevall A. Radiolabeled antibodies to Bacillus anthracis toxins are bactericidal and partially therapeutic in experimental murine anthrax. *Antimicrob Agents Chemother*. (2009) 53:4860–8. doi: 10.1128/AAC.01269-08
160. Dadachova E, Patel MC, Toussi S, Apostolidis C, Morgenstern A, Brechbiel MW, et al. Targeted killing of virally infected cells by radiolabeled antibodies to viral proteins. *PLoS Med*. (2006) 3:e427. doi: 10.1371/journal.pmed.0030427
161. Bolzati C, Carta D, Salvarese N, Refosco F. Chelating systems for ^{99m}Tc/^{188}Re in the development of radiolabeled peptide pharmaceuticals. *Anticancer Agents Med Chem*. (2012) 12:428–61. doi: 10.2174/187152012800617821
162. Howell RC, Revskaya E, Pazo V, Nosanchuk JD, Casadevall A, Dadachova E. Phage display library derived peptides that bind to human tumor melanin as potential vehicles for targeted radionuclide therapy of metastatic melanoma. *Bioconjug Chem*. (2007) 18:1739–48. doi: 10.1021/bc060330u
163. Li Y, Ma L, Gaddam V, Gallazzi F, Hennkens HM, Harmata M, et al. Synthesis, characterization, and in vitro evaluation of new ^{99m}Tc/Re(V)-cyclized octreotide analogues: an experimental and computational approach. *Inorg Chem*. (2016) 55:1124–33. doi: 10.1021/acs.inorgchem.5b02306
164. Zamora PO, Marek MJ, Knapp FF (Russ) Jr. Preparation of ^{188}Re-RC-160 somatostatin analog: a peptide for local/regional radiotherapy. *Appl Radiat Isot*. (1997) 48:305–9. doi: 10.1016/S0969-8043(96)00226-6
165. Arteaga de Murphy C, Pedraza-López M, Ferro-Flores G, Murphy-Stack E, Chávez-Mercado L, Ascencio JA, et al. Uptake of ^{188}Re-beta-naphthyl-peptide in cervical carcinoma tumours in athymic mice. *Nucl Med Biol*. (2001) 28:319–26. doi: 10.1016/S0969-8051(00)00174-8
166. Molina-Trinidad EM, de Murphy CA, Ferro-Flores G, Murphy-Stack E, Jung-Cook H. Radiopharmacokinetic and dosimetric parameters of ^{188}Re-lanreotide in athymic mice with induced human cancer tumors. *Int J Pharm*. (2006) 310:125–30. doi: 10.1016/j.ijpharm.2005.11.043
167. Cyr JE, Pearson DA, Wilson DM, Nelson CA, Guaraldi M, Azure MT, et al. Somatostatin receptor-binding peptides suitable for tumor radiotherapy with Re-188 or Re-186. Chemistry and initial biological studies. *J Med Chem*. (2007) 50:1354–64. doi: 10.1021/jm061290i
168. Yu F, Lv M, Cai H, Li D, Yuan X, Lv Z. Therapeutic effect of ^{188}Re-MAG$_3$-depreotide on non-small cell lung cancer *in vivo* and in vitro. *Int J Clin Exp Pathol*. (2013) 6:421–30.
169. Cui L, Liu Z, Jin X, Jia B, Li F, Wang F. Evaluation of ^{188}Re-MAG2-RGD-bombesin for potential prostate cancer therapy. *Nucl Med Biol*. (2013) 40:182–9. doi: 10.1016/j.nucmedbio.2012.11.002
170. Kan W, Zhou Z, Wei H, Zhong Z. Effective way to radiolabel the peptide of MAG$_3$-RM26 with ^{188}Re and the study on its coordination chemistry. *J Radioanal Nucl Chem*. (2017) 314:2087–90. doi: 10.1007/s10967-017-5580-8
171. Smilkov K, Janevik E, Guerrini R, Pasquali M, Boschi A, Uccelli L, et al. Preparation and first biological evaluation of novel Re-188/Tc-99m peptide conjugates with Substance-P. *Appl Radiat Isot*. (2014) 92:25–31. doi: 10.1016/j.apradiso.2014.06.003
172. Li Y, Hu Y, Xiao J, Liu G, Li X, Zhao Y, et al. Investigation of SP94 Peptide as a specific probe for hepatocellular carcinoma imaging and therapy. *Sci Rep*. (2016) 6:33511. doi: 10.1038/srep33511
173. Zhang X, Feng S, Liu J, Li Q, Zheng L, Xie L, et al. Novel small peptides derived from VEGF$_{125-136}$: potential drugs for radioactive diagnosis and therapy in A549 tumor-bearing nude mice. *Sci Rep*. (2017) 7:4278. doi: 10.1038/s41598-017-04513-y

174. Wang SH, Lee AC, Chen IJ, Chang NC, Wu HC, Yu HM, et al. Structure-based optimization of GRP78-binding peptides that enhances efficacy in cancer imaging and therapy. *Biomaterials*. (2016) 94:31–44. doi: 10.1016/j.biomaterials.2016.03.050
175. Miao Y, Quinn TP. Peptide-targeted radionuclide therapy for melanoma. *Crit Rev Oncol Hematol*. (2008) 67:213–28. doi: 10.1016/j.critrevonc.2008.02.006
176. Carta D, Salvarese N, Morellato N, Gao F, Sihver W, Pietzsch HJ, et al. Melanoma targeting with [^{99m}Tc(N)(PNP3)]-labeled α-melanocyte stimulating hormone peptide analogs: effects of cyclization on the radiopharmaceutical properties. *Nucl Med Biol*. (2016) 43:788–801. doi: 10.1016/j.nucmedbio.2016.08.014
177. Edelman MJ, Clamon G, Kahn D, Magram M, Lister-James J, Line BR. Targeted radiopharmaceutical therapy for advanced lung cancer: phase I trial of rhenium Re188 P2045, a somatostatin analog. *J Thorac Oncol*. (2009) 4:1550–4. doi: 10.1097/JTO.0b013e3181bf1070
178. Khajornjiraphan N, Thu NA, Chow PK. Yttrium-90 microspheres: a review of its emerging clinical indications. *Liver Cancer*. (2015) 4:6–15. doi: 10.1159/000343876
179. Bozkurt MF, Salanci BV, Ugur Ö. Intra-arterial radionuclide therapies for liver tumors. *Semin Nucl Med*. (2016) 46:324–39. doi: 10.1053/j.semnuclmed.2016.01.008
180. Bouvry C, Palard X, Edeline J, Ardisson V, Loyer P, Garin E, et al. Transarterial radioembolisation (TARE) agents beyond ^{90}Y-microspheres. *Biomed Res Int*. (2018) 2018:1435302. doi: 10.1155/2018/1435302
181. Lepareur N, Garin E. Transarterial radionuclide therapy with ^{188}Re-labelled lipiodol. *Int J Nucl Med Res*. (2017) 79–91. doi: 10.15379/2408-9788.2017.07
182. Paeng JC, Jeong JM, Yoon CJ, Lee YS, Suh YG, Chung JW, et al. Lipiodol solution of ^{188}Re-HDD as a new therapeutic agent for transhepatic arterial embolization in liver cancer: preclinical study in a rabbit liver cancer model. *J Nucl Med*. (2003) 44:2033–8.
183. Boschi A, Uccelli L, Duatti A, Colamussi P, Cittanti C, Filice A, et al. A kit formulation for the preparation of ^{188}Re-lipiodol: preclinical studies and preliminary therapeutic evaluation in patients with unresectable hepatocellular carcinoma. *Nucl Med Commun*. (2004) 25:691–9. doi: 10.1097/01.mnm.0000130241.22068.45
184. Lepareur N, Ardisson V, Noiret N, Garin E. ^{188}Re-SSS/Lipiodol: development of a potential treatment for HCC from bench to bedside. *Int J Mol Imaging*. (2012) 2012:278306. doi: 10.1155/2012/278306
185. Keng GH, Sundram FX, Yu SW, Somanesan S, Premaraj J, Oon CJ, et al. Preliminary experience in radionuclide therapy of hepatocellular carcinoma using hepatic intra-arterial radioconjugates. *Ann Acad Med Singapore*. (2002) 31:382–6.
186. Sundram F, Chau TCM, Onkhuudai P, Bernal P, Padhy AK. Preliminary results of transarterial rhenium-188 HDD Lipiodol in the treatment of inoperable primary hepatocellular carcinoma. *Eur J Nucl Med Mol Imaging*. (2004) 31:250–7. doi: 10.1007/s00259-003-1363-2
187. De Ruyck K, Lambert B, Bacher K, Gemmel F, De Vos F, Vral A, et al. Biologic dosimetry of ^{188}Re-HDD/Lipiodol versus ^{131}I-Lipiodol therapy in patients with hepatocellular carcinoma. *J Nucl Med*. (2004) 45:612–8.
188. Lambert B, Bacher K, Defreyne L, Gemmel F, Van Vlierberghe H, Jeong JM, et al. ^{188}Re-HDD/Lipiodol therapy for hepatocellular carcinoma: a phase I clinical trial. *J Nucl Med*. (2005) 46:60–6.
189. Lambert B, Bacher K, De Keukeleire K, Smeets P, Colle I, Jeong JM, et al. ^{188}Re-HDD/Lipiodol for treatment of hepatocellular carcinoma: a feasibility study in patients with advanced cirrhosis. *J Nucl Med*. (2005) 46:1326–32.
190. Lambert B, Praet M, Vanlangenhove P, Troisi R, de Hemptinne B, Gemmel F, et al. Radiolabeled Lipiodol therapy for hepatocellular carcinoma in patients awaiting liver transplantation: pathology of the explant livers and clinical outcome. *Cancer Biother Radiopharm*. (2005) 20:209–14. doi: 10.1089/cbr.2005.20.209
191. Kumar A, Bal C, Srivastava DN, Acharya SK, Thulkar SP, Sharma S, et al. Transarterial radionuclide therapy with Re-188-HDD-lipiodol in case of unresectable hepatocellular carcinoma with extensive portal vein thrombosis. *Eur J Radiology Extra*. (2005) 56:55–9. doi: 10.1016/j.ejrex.2005.07.016
192. Kumar A, Srivastava DN, Bal C. Management of postsurgical recurrence of hepatocellular carcinoma with Rhenium 188–HDD labeled iodized oil. *J Vasc Interv Radiol*. (2006) 17:157–161. doi: 10.1097/01.RVI.0000195321.20579.F2
193. Kumar A, Bal C, Srivastava DN, Thulkar SP, Sharma S, Acharya SK, et al. Management of multiple intrahepatic recurrences after radiofrequency ablation of hepatocellular carcinoma with rhenium-188–HDD-Lipiodol. *Eur J Gastroenterol Hepatol*. (2006) 18:219–3. doi: 10.1097/00042737-200602000-00016
194. Lambert B, Bacher K, Defreyne L, Van Vlierberghe H, Jeong JM, Wang RF, et al. ^{188}Re-HDD/lipiodol therapy for hepatocellular carcinoma: an activity escalation study. *Eur J Nucl Med Mol Imaging*. (2006) 33:344–52. doi: 10.1007/s00259-005-1954-1
195. Kumar A, Srivastava DN, Chau TTM, Long HD, Bal C, Chandra P, et al. Inoperable hepatocellular carcinoma: transarterial ^{188}Re HDD-labeled iodized oil for treatment prospective multicenter clinical trial. *Radiology*. (2007) 243:509–19. doi: 10.1148/radiol.2432051246
196. Bernal P, Raoul JL, Vidmar G, Sereegotov E, Sundram FX, Kumar A, et al. Intra-arterial Rhenium-188 Lipiodol in the treatment of inoperable hepatocellular carcinoma: results of an IAEA-sponsored multination study. *Int J Radiat Oncol Biol Phys*. (2007) 69:1448–55. doi: 10.1016/j.ijrobp.2007.05.009
197. Bernal P, Raoul JL, Stare J, Sereegotov E, Sundram FX, Kumar A, et al. International Atomic Energy Agency sponsored multination study of intra-arterial rhenium-188-labeled Lipiodol in the treatment of inoperable hepatocellular carcinoma: results with special emphasis on prognostic value of dosimetric study. *Sem Nucl Med*. (2008) 38:S40–5. doi: 10.1053/j.semnuclmed.2007.10.006
198. Esquinas PL, Shinto A, Kamaleshwaran KK, Joseph J, Celler A. Biodistribution, pharmacokinetics, and organ-level dosimetry for ^{188}Re-AHDDLipiodol radioembolization based on quantitative post-treatment SPECT/CT scans. *EJNMMI Physics*. (2018) 5:30. doi: 10.1186/s40658-018-0227-6
199. Delaunay K, Garin E, Rolland Y, Lepareur N, Laffont S, Ardisson V, et al. Biodistribution and dosimetry assessments for hepatocellular carcinoma treated with ^{188}Re-SSS Lipiodol: Preliminary results of the phase 1 trial Lip Re 1. *J Nucl Med*. (2018) 59:602. doi: 10.1007/s00259-019-04277-9
200. Padhy AK, Dondi M. A report on the implementation aspects of the International Atomic Energy Agency's first doctoral coordinated research project, "Management of liver cancer using radionuclide methods with special emphasis on trans-arterial radio-conjugate therapy and internal dosimetry". *Semin Nucl Med*. (2008) 38:S5–12. doi: 10.1053/j.semnuclmed.2007.10.002
201. Banka VK, Moon SH, Jeong JM, Seelam SR, Lee YS, Kim YJ, et al. Development of 4-hexadecyl-4,7-diaza-1,10-decanedithiol. (HDD) kit for the preparation of the liver cancer therapeutic agent Re-188-HDD/lipiodol. *Nucl Med Biol*. (2015) 42:317–322. doi: 10.1016/j.nucmedbio.2014.11.013
202. Conzone SD, Häfeli UO, Day DE, Ehrhardt GJ. Preparation and properties of radioactive rhenium glass microspheres intended for *in vivo* radioembolization therapy. *J Biomed Mater Res*. (1998) 42:617–25.
203. Wang SJ, Lin WY, Chen MN, Chi CS, Chen JT, Ho WL, et al. Intratumoral injection of rhenium-188 microspheres into an animal model of hepatoma. *J Nucl Med*. (1998) 39:1752–7.
204. Wunderlich G, Pinkert J, Stintz M, Kotzerke J. Labeling and biodistribution of different particle materials for radioembolization therapy with ^{188}Re. *Appl Radiat Isot*. (2005) 62:745–50. doi: 10.1016/j.apradiso.2004.11.003
205. Verger E, Drion P, Meffre G, Bernard C, Duwez L, Lepareur N, et al. ^{68}Ga and ^{188}Re starch-based microparticles as theranostic tool for the hepatocellular carcinoma: radiolabeling and preliminary *in vivo* rat studies. *PLoS ONE*. (2016) 11:e0164626. doi: 10.1371/journal.pone.0164626
206. Liepe K, Brogsitter C, Leonhard J, Wunderlich G, Hliscs R, Pinkert J, et al. Feasibility of high activity rhenium-188-microsphere in hepatic radioembolization. *Jpn J Clin Oncol*. (2007) 37:942–50. doi: 10.1093/jjco/hym137
207. Nowicki ML, Cwikla JB, Sankowski AJ, Shcherbinin S, Grimmes J, Celler A, et al. Initial study of radiological and clinical efficacy radioembolization using ^{188}Re-human serum albumin. (HSA) microspheres in patients with progressive, unresectable primary or secondary liver cancers. *Med Sci Monit*. (2014) 20:1353–62. doi: 10.12659/MSM.890480

208. Liepe K, Kotzerke J, Lambert B. Advantage of ^{188}Re-radiopharmaceuticals in hepatocellular cancer and liver metastases. *J Nucl Med*. (2005) 46:1407–8.
209. Hoefnagel CA. Radionuclide therapy revisited. *Eur J Nucl Med*. (1991) 18:408–31. doi: 10.1007/BF02258432
210. Chen FD, Hsieh BT, Wang HE, Ou YH, Yang WK, Whang-Peng J, et al. Efficacy of Re-188-labelled sulphur colloid on prolongation of survival time in melanoma-bearing animals. *Nucl Med Biol*. (2001) 28:835–44. doi: 10.1016/S0969-8051(01)00244-X
211. Häfeli UO, Pauer GJ, Unnithan J, Prayson RA. Fibrin glue system for adjuvant brachytherapy of brain tumors with ^{188}Re and ^{186}Re-labeled microspheres. *Eur J Pharm Biopharm*. (2007) 65:282–8. doi: 10.1016/j.ejpb.2006.10.016
212. Vanpouille-Box C, Lacoeuille F, Belloche C, Lepareur N, Lemaire L, LeJeune JJ, et al. Tumor eradication in rat glioma and bypass of immunosuppressive barriers using internal radiation with ^{188}Re-lipid nanocapsules. *Biomaterials*. (2011) 32:6781–90. doi: 10.1016/j.biomaterials.2011.05.067
213. Cikankowitz A, Clavreul A, Tétaud C, Lemaire L, Rousseau A, Lepareur N, et al. Characterization of the distribution, retention, and efficacy of internal radiation of ^{188}Re-lipid nanocapsules in an immunocompromised human glioblastoma model. *J Neurooncol*. (2017) 131:49–58. doi: 10.1007/s11060-016-2289-4
214. Séhédic D, Chourpa I, Tétaud C, Griveau A, Loussouarn C, Avril S, et al. Locoregional confinement and major clinical benefit of ^{188}Re-Loaded CXCR4-targeted nanocarriers in an orthotopic human to mouse model of glioblastoma. *Theranostics*. (2017) 7:4517–36. doi: 10.7150/thno.19403
215. Hrycushko BA, Gutierrez AN, Goins B, Yan W, Phillips WT, Otto PM, et al. Radiobiological characterization of post-lumpectomy focal brachytherapy with lipid nanoparticle-carried radionuclides. *Phys Med Biol*. (2011) 56:703–19. doi: 10.1088/0031-9155/56/3/011
216. Hrycushko BA, Li S, Shi C, Goins B, Liu Y, Phillips WT, et al. Postlumpectomy focal brachytherapy for simultaneous treatment of surgical cavity and draining lymph nodes. *Int J Radiat Oncol Biol Phys*. (2011) 79:948–55. doi: 10.1016/j.ijrobp.2010.05.062
217. Hrycushko BA, Li S, Goins B, Otto RA, Bao A. Direct intratumoral infusion of liposome encapsulated rhenium radionuclides for cancer therapy: effects of nonuniform intratumoral dose distribution. *Med Phys*. (2011) 38:1339–47. doi: 10.1118/1.3552923
218. Hrycushko BA, Ware S, Li S, Bao A. Improved tumour response prediction with equivalent uniform dose in pre-clinical study using direct intratumoural infusion of liposome-encapsulated ^{86}Re radionuclides. *Phys Med Biol*. (2011) 56:5721–34. doi: 10.1088/0031-9155/56/17/016
219. Chang CM, Lan KL, Huang WS, Lee YJ, Lee TW, Chang CH et al. ^{188}Re-liposome can induce mitochondrialautophagy and reverse drug resistance for ovarian cancer: from bench evidence to preliminary clinical proof-of-concept. *Int J Mol Sci*. (2017) 18:903. doi: 10.3390/ijms18050903
220. Liepe K, Zaknun JJ, Padhy A, Barrenechea E, Soroa V, Shrikant S, et al. Radiosynovectomy using yttrium-90, phosphorus-32 or rhenium-188 radiocolloids versus corticoid instillation for rheumatoid arthritis of the knee. *Ann Nucl Med*. (2011) 25:317–23. doi: 10.1007/s12149-011-0467-1
221. Jeong JM, Lee YJ, Kim EH, Chang YS, Kim YJ, Son M, et al. Preparation of ^{188}Re-labeled paper for treating skin cancer. *Appl Radiat Isot*. (2003) 58:551–5. doi: 10.1016/S0969-8043(03)00063-0
222. Bhusari P, Shukla J, Kumar M, Vatsa R, Chhabra A, Palarwar K, et al. Noninvasive treatment of keloid using customized Re-188 skin patch. *Dermatol Ther*. (2017) 30:e12515. doi: 10.1111/dth.12515
223. Shukla J, Mittal BR. ^{188}Re Tailor Made Skin Patch for the treatment of skin cancers and keloid: overview and technical considerations. *Int J Nucl Med Res*. (2017) 107–113. doi: 10.15379/2408-9788.2017.10
224. Sedda AF, Rossi G, Cipriani C, Carrozzo AM, Donati P. Dermatological high-dose-rate brachytherapy for the treatment of basal and squamous cell carcinoma. *Clin Exp Dermatol*. (2008) 33:745–9. doi: 10.1111/j.1365-2230.2008.02852.x
225. Cipriani C, Frisch B, Scheidhauer K, Desantis M. Personalized high-dose-rate brachytherapy with non-sealed rhenium-188 in non-melanoma skin cancer. *Int J Nucl Med Res*. (2017) 114–22. doi: 10.15379/2408-9788.2017.11
226. Carrozzo AM, Sedda AF, Muscardin L, Donati P, Cipriani C. Dermo beta brachytherapy with ^{188}Re in squamous cell carcinoma of the penis: a new therapy. *Eur J Dermatol*. (2013) 23:183–8. doi: 10.1684/ejd.2013.1927
227. Carrozzo AM, Cipriani C, Donati P, Muscardin L, Sedda AF. Dermo Beta Brachytherapy with ^{188}Re in extramammary Paget's disease. *G Ital Dermatol Venereol*. (2014) 149:115–21.

Conflict of Interest Statement: The authors declare that the research was conducted in the absence of any commercial or financial relationships that could be construed as a potential conflict of interest.

frontiers in Medicine

ORIGINAL RESEARCH
published: 24 October 2019
doi: 10.3389/fmed.2019.00228

Risk Management Through an "Activity Contradictions" Lens: Exposure to Low Doses of Radiation in Nuclear Medicine

Romain Lonceint[1], Françoise Bodéré[2,3,4] and Bénédicte Geffroy[1]*

[1] IMT Atlantique, Laboratoire d'Économie et de Management Nantes-Atlantique, Nantes, France, [2] CHU Nantes, Centre de Recherche en Cancérologie et Immunologie Nantes-Angers, Nantes, France, [3] Nuclear Medicine, University Hospital, Nantes, France, [4] CRCINA, INSERM, CNRS, Université d'Angers, Université de Nantes, Nantes, France

Risk management is a major concern for health organizations. In hospitals, it concerns both medical and occupational risks, particularly those related to exposure to ionizing radiation. Medical personnel represent 70% of workers exposed to ionizing radiation. The highest doses in the order of a few mSv are recorded in nuclear medicine departments. Nuclear medicine health professionals are thus exposed, in the context of their work activity to daily low doses—though their effects remain uncertain. In the face of this uncertainty, the precautionary approach prevails in the field of radiation protection. Thus, health professionals are called upon to treat the patient while protecting themselves from exposure to low doses of radioactivity. This research aims to understand the relationship of health professionals to the risks of exposure to low doses and how they combine the logic of patient care and cure with that of self-protection. It is based on a qualitative study of two embedded cases carried out in two units of a nuclear medicine department at a university hospital, combining two data collection methods: 23 interviews with various health professionals in the department and 10 weeks of observations of the work activity of these same professionals. The analysis of the data shows the coexistence of care/cure and radiation protection logics to be a source of contradictions for nuclear medicine professionals. Analysis of the results focuses on the identification and characterization of the different forms of contradictions inherent in working in the nuclear medicine department. The results show that the intensity of these contradictions varies in line with four factors: phases (preparation, administration, patient installation, and examination); type of medical act; patient behavior and characteristics, and type of professionals. Finally, the results set out the different types of responses provided by health professionals in order to regulate these contradictions. These risk regulation strategies differ according to occupational groups and their relationship to risk.

Keywords: risk management, activity contradictions, nuclear medicine, care, radiation protection

OPEN ACCESS

Edited by:
Anil Kumar Mishra, Institute of Nuclear Medicine & Allied Sciences (DRDO), India

Reviewed by:
Serge Goldman, Université libre de Bruxelles, Belgium
Baljinder Singh, Post Graduate Institute of Medical Education and Research (PGIMER), India

****Correspondence:***
Romain Lonceint
romain.lonceint@imt-atlantique.fr

Specialty section:
This article was submitted to Nuclear Medicine, a section of the journal Frontiers in Medicine

Received: *28 February 2019*
Accepted: *03 October 2019*
Published: *24 October 2019*

Citation:
Lonceint R, Bodéré F and Geffroy B (2019) Risk Management Through an "Activity Contradictions" Lens: Exposure to Low Doses of Radiation in Nuclear Medicine. Front. Med. 6:228. doi: 10.3389/fmed.2019.00228

INTRODUCTION

Risk management is a major concern for health organizations. In hospitals, it concerns both medical and occupational risks, in particular those related to exposure to radioactivity. While radiotherapy accidents such as the one that occurred at Épinal Hospital (where several patients were overexposed between 2001 and 2006) have contributed to higher-profile media visibility for this type of risk

to patients, the risk associated with exposure to radioactivity also concerns hospital staff. Indeed, health professionals represent 70% of workers exposed to radioactivity, making this occupational risk a subject of interest for health organizations. Occupational exposure to radioactivity in the medical sector generally falls within the domain of low doses, for which the risks are not known (1). This is therefore a situation of uncertainty in the sense that no "causal explanation system" (2) has been established between exposure to radioactivity for doses below 100 mSv and the appearance of pathologies. However, this lack of a causal link between exposure to low doses and the appearance of pathologies does not mean that the risk does not exist. Thus, applied to the field of low doses of radioactivity, radiation protection is based on a logic of prudence and precaution since it applies to hypothetical risks (3).

In addition to these uncertainties relating to radioactive risks, nuclear medicine professionals also find themselves confronted with medical uncertainties. A number of studies in the field of medical sociology (4, 5) have highlighted the finding that uncertainty is inherent in any medical practice. This research has shown that the knowledge and techniques of medicine and doctors are only ever less than perfect, and that the result of a treatment or examination can never be known *a priori*. The existence of these medical uncertainties means that, in the benefit/risk ratio in medicine, the result is always an expected benefit. Nuclear medicine does not escape the problem of medical uncertainties that directly affect the healthcare (and thus, the medical benefits) of imaging examinations and treatments.

In addition, the implementation of radiation protection measures may lead health organizations to believe that the issue of risks associated with radioactivity is controlled. The absence of personal protective equipment (or circumvention of radiation protection rules) is then interpreted as a failure to comply with recommendations. However, this ignores the fact that social science research has long shown, first, that there is a link between risk representations and professional practices (6) and second, that these practices (perceived as deviations from the rules) reveal that in the background lies a lack of consideration of the activity as it takes place, including all of its contradictions and requirements (7). Occupational risk management based on the application of radiation protection measures thus goes beyond the sole question of technical and scientific understanding of the risk, in that it is also marked by different professional logics and the situated nature of work practices. This is why we consider occupational risk in the context of the work activity, that is, the practical accomplishment of the activity (8).

The research focuses on occupational exposure to radioactivity in the nuclear medicine sector. This is a medical specialty that includes all applications of radiopharmaceuticals for diagnostic and therapeutic purposes. However, the use of radiopharmaceuticals in imaging examinations or therapeutic procedures is a source of daily occupational exposure to radioactivity. The challenges of exposure to low doses call for an interest in the management of a hypothetical occupational risk in nuclear medicine, as distinct from the nosocomial infections that are a proven risk faced by health professionals (9). The analysis of work activity in nuclear medicine reveals the coexistence of two potentially contradictory logics of action, namely the logic of patient care in the context of diagnostic or therapeutic medical procedures and the logic of self-protection against the possible risks associated with exposure to low doses of radioactivity. This leads us to analyze occupational risk management in nuclear medicine from the point of view of work contradictions. Thus, this research aims to answer a 2-fold question:

1) What are the forms of contradictions between patient care and radiation protection in nuclear medicine?
2) What methods of regulating these contradictions are implemented by health professionals?

In order to answer this question, the research is based on a qualitative survey conducted in two nuclear medicine units and combining semi-directive interviews with *in situ* observations (**Box 1**).

First, we show that activity in nuclear medicine gives rise to different contradictions as a result of the coexistence of the logics of patient care and of self-protection. In a second step, we describe the methods implemented by the various professional groups to regulate the contradictions that are inherent to the nuclear medicine activity. These are based on differentiated relationships to the risk associated with exposure to low doses of radioactivity. Occupational risk management is thus understood in the light of the contradictions inherent to working in nuclear medicine.

NUCLEAR MEDICINE ACTIVITY AT THE ROOT OF CONTRADICTIONS BETWEEN PATIENT CARE AND RADIATION PROTECTION

The Coexistence of Patient Care and Radiation Protection Logics

Occupational exposure to low doses of radioactivity in nuclear medicine requires the implementation of protection against the risks of contamination and radiation. The work of nuclear medicine health professionals is to provide care to the patient while protecting themselves from radioactivity. Health professionals are thus called upon to jointly manage both patient care and the application of radiation protection rules. In other words, the work activity in nuclear medicine consists of articulating and combining two heterogeneous logics of action, namely patient care and self-protection. Analysis of the activity reveals the coexistence of these two logics of action: *"You have to work fast as you can, and as best you can. So obviously, you have to keep in mind all the protective screening as well. You have to work with leaded shields and the shielded case - but then it's all about trying to be as efficient and as quick as you can"* (Technologist NM1).

On the one hand, the logic of patient care is characterized by the dual nature of the care activity: the cure activity (the provision of care to someone to cure a disease with the aim of eliminating it, to improve the patient's state of health), and the care activity, which is more oriented toward caring for someone

BOX 1 | Methodological framework and survey field.

Since the knowledge project focuses on perception of the risks of exposure to low doses and its management methods, we have opted for a qualitative research methodology that is characterized by a comprehensive approach. Indeed, as highlighted by Mays and Pope, "The goal of qualitative research is the development of concepts which help us to understand social phenomena in natural (rather than experimental) settings, giving due emphasis to the meanings, experiences, and views of all the participants" [(10), p. 43]. In opting for such a methodology, we seek to understand how actors think, speak and act in relation to a particular context (11).

We therefore opted for a case study to gain an in-depth understanding of this field of investigation (12). Since our objective was to understand the risk relationship of professionals to low-dose exposure through their radiation protection practices (13), we sought to collect data according to a number of aspects such as: locations, persons (actors) and activities (14).

The survey was conducted in two units of a nuclear medicine department of a university hospital. These two services, under the responsibility of a head of department, are located on two separate sites at the university hospital. One of the services (MN1) is specialized in nuclear medicine for therapeutic and diagnostic purposes in the field of rheumatology, endocrinology, pulmonology, and urology, and the other service (NM2) mainly specializes in diagnostic examinations in cardiology.

According to Yin (11), the objectivity of the case study is based on "multiple sources of evidence" (p. 10). There are traditionally six such sources: direct observations, interviews, archival records, documents, participant observation, and physical artifacts (e.g., computer downloads of employees' work). It is this heterogeneity of empirical sources in qualitative research that guarantees its objectivity, because it allows data to be triangulated. Also, we used a double data collection system, combining semi-directive interviews with observation. This system is also well-suited for analyzing the meaning that actors give to their practices and the events with which they are confronted, in particular their social representations, value systems and interpretations of conflict situations, as well as the reconstruction of action processes.

Similarly, unlike a quantitative approach that aims for representativeness and thus allows statistical inference, representativeness in qualitative research is based on the criteria for selecting individuals (which is the maximum diversity of profiles with regard to the problem studied) and on the principle of saturation (which refers to the fact that, as the interviews succeed one another and reveal their lessons, the contribution made by each additional interview will be minimal). Twenty three interviews were conducted with the various categories of professionals in the nuclear medicine department (see **Appendix 1**).

The content of the interview covered: the person's background; their role and place within the department's activity; the characteristics of their working environment; the perception of exposure to radioactivity in the context of nuclear medicine activity; consideration of radiation protection in working practices; any difficulties encountered in implementing the various radiation protection measures and the sources of risk (socio-organizational factors impacting exposure to ionizing radiation). Other interviews with actors outside the department were also conducted with: an INSERM radiobiologist; a nuclear doctor (member of the National Academy of Medicine); a nuclear doctor and epidemiologist at IRSN; an occupational doctor, and an ASN inspector. All interviews were recorded and transcribed. To study working practices, this data collection system was supplemented by field observation (15) in the context of exposure to low doses. Indeed, the relationship to an uncertain risk and its management methods could not all be identified solely in the light of the actors' discourse, because there may be a gap between what the actors say about compliance with radiation protection measures and what they actually do in terms of risk regulation. This may be explained by the fact that actors may be blind to their own practices (because these are totally internalized) or that some practices developed consciously by actors are difficult to verbalize. Observation allows the researcher to access representations of actors constructed from their own perceptions (16) and update the resources mobilized by actors in their practices. Thus, a total of 10 weeks of observation were carried out in the two nuclear medicine departments. The objective was to deepen understanding of work practices, particularly in the field of radiation protection, as actual work always exceeds the prescribed work. Observation makes it possible to go beyond normative discourses on the risk of exposure to low doses to grasp the meaning of the gap between doctrine and practice. Observation sequences focused on action in situations, making it possible to understand the situated nature of the practices by considering the multiple variables that constitute health professionals' environment. In practice, it was a matter of direct observation of both actions and activity, as well as the collection of elements of informal discourse gleaned here and there, as the researcher's presence in the field allowed. Collection of this data resulted in notes being taken in a notebook, named a "research journal" by Wacheux (17).

The data collected were then subjected to thematic content analysis (18) using N vivo to identify and analyze professional practices for regulating low-dose exposure risks (The main role of this data processing software is to help manage, format and give meaning to qualitative data).

Thus, we sought to characterize the data by mode of collection (interview or observation) and unit (MN1 or MN2). Each interview was analyzed according to the respondent's occupational group (nuclear doctor, cardiologist, manipulator, nurse, etc.) in order to characterize the different professional logics. Then we developed a number of categories and sub-categories of analysis (19) in order to be able to code the different management situations (20), their dimensions and variability. The coding method used is both bottom-up and top-down in the sense that it is based on a combination of "*a priori* coding" from the literature and "emerging coding" that refers to categories of analysis from the field (21). The data processing made it possible to trace facts back to the general proposals.

and seeking their well-being (22). Care, then, can be understood as the management of a patient as part of a medical procedure requiring both technical-scientific work (handling machines and administering treatments) and expressive-communicative work (informing and reassuring the patient) (23). In this respect, patient care appears to be relational work, with patients and their relatives as well as between health professionals (24). Moreover, as a medical specialty that has an essentially diagnostic focus, the logic of patient care in nuclear medicine is guided by the search for *"the perfect image*," that is, the production of a quality image, suitable for interpretation by the practitioner in order to establish a diagnosis.

On the other hand, the logic of self-protection or radiation protection seeks to limit the exposure of nuclear medicine health professionals to radioactivity. The logic of radiation protection is based on a number of rules, such as the use of dosimeters, but also on principles such as the ALARA (As Low As Reasonably Achievable) principle. This principle implies integrating into the work activity the triptych "distance, screen, time": distance refers to the distance from the radioactive source and the use of remote controls of the processes; screen refers to the use of leaded shields when the activity does not allow movement away from the radioactive source; time refers to the duration of exposure which must be reduced as much as possible. This demands rapid execution of gestures and movements (25). The following quotation reflects the logic of radiation protection in nuclear medicine: *"Let's say that working in nuclear medicine, you really have to be extremely vigilant. Vigilance must be constant,*

saying to yourself all the time: is being there good or bad? And always keep in mind that as soon as you can get away from the patient, away from the source, you must do so. But then, it happens that a child needs to be held. The distance that is our first protection, is the distance from the source, from the patient being injected. You can't necessarily work from behind leaded screens. So, there are the screens, but it's already the distance and then the time, since we're going to try to inject as quickly as possible and when we need to be with the patient to do something, whatever it may be, we're going to try to be as quick as possible, so as not to stay too long with the patient" (Technologist NM1).

The coexistence of patient care and radiation protection approaches in nuclear medicine leads to contradictions in the activities of health professionals. These contradictions result from a situation of competition over objectives, in which actors are confronted with multiple and divergent objectives. Indeed, health professionals are required to provide patient care from a diagnostic or therapeutic perspective while continuously applying radiation protection principles and rules so as to limit their exposure to radioactivity, related to both the radiopharmaceutical and the patient. Occupational risk thus arises not only from the handling of radiopharmaceuticals, but also from working in the presence of the patient once the radiopharmaceutical has been administered. The patient is therefore both the object of care and a potential source of risk, as one NM1 technologist points out: *"We're handling radioactivity here, it is both the product and the patients - because the patients are radioactive"*.

Moreover, the contradictions between patient care and radiation protection appear to be inseparable from the work activity in nuclear medicine, insofar as health professionals are confronted with a permanent risk of irradiation and contamination, which requires that radiation protection rules be considered throughout the care activity, as expressed by this radio pharmacist of NM2: *"We are all exposed, if we work with ionizing radiation. So as soon as we enter the nuclear medicine department, we are all exposed, we all have a dosimetry"*. The risk is described, then, as inherent to working in nuclear medicine, according to an NM1 technologist: *"Radioactivity is ambient, it's everywhere. Patients become sources, and that's why you can't stay too close to the patient"*.

The Forms of Contradiction Between Patient Care and Radiation Protection

In addition, contradictions between patient care and radiation protection take two forms, related to the various aspects of patient care. First, there are contradictions between cure activity and radiation protection, reflecting the existence of contradictions between the administration of patient care (including injection of the radiopharmaceutical or positioning the patient under the gamma camera) and the application of radiation protection rules. The following verbatim account allows us to take stock of this first form of contradiction: *"The lady we saw earlier, the one with no legs, we spent a lot of time with her, beside her. So in this case we are much more exposed. With a patient who is autonomous and everything, who is doing very well, we quickly put the tape around the chest, we put it in place, we move away. Well, on the other hand, the one with no legs, who we need to do everything for, to set everything up, we spend time with her. We're more exposed, that's for sure"* (Nurse NM2).

Second, contradictions are expressed between patient care activity and radiation protection, reflecting the existence of contradictions between patient reassurance and the application of radiation protection rules, as the following verbatim account shows: *"If they are a bit anxious, or a bit claustrophobic, you have to stay close, there are people who panic about the camera, about the examination. Sometimes it's the brain [patients undergoing brain scans], you stay next to them to reassure them, so they can see the examination through. To reassure them, to talk, so they can hear that there is someone right there, because it is not easy to go behind a screen, and they feel as though they are alone. So sometimes they are anxious about that, about being alone"* (Nurse NM2).

The analysis also suggests that these contradictions are divided into three forms, relating to the various aspects of radiation protection. First, spatial contradictions, insofar as care implies being with the patient to provide care and reassurance, whereas radiation protection, on the contrary, requires putting the patient at a distance to protect yourself from it. This is reflected in the following verbatim account: *"A child, even if they are strapped down, you still have to be a little more present. Sometimes we have to hold them, touch their cheeks, so that they stay still, to get a good image. When they are babies or children, we have to stay closer to them. We get more doses."* (Technologist NM1).

Second, there are physical contradictions, since the use of radiopharmaceuticals does not always allow the complete interposition of leaded screens between health professionals and radioactive products, as shown in the words of a radio pharmacist at NM2: *"In the hot lab, this is where we are likely to get the highest dose, because it's where we prepare the radiopharmaceuticals. It's at the extremities - the fingers – that we're vulnerable, because although the armored enclosure protects us at full body level, at the extremities we still have to put our hands in a lot actually, to make the preparations"*.

Third, there are temporal contradictions, because care requires taking the time to provide care and reassurance to the patient, whereas radiation protection requires working quickly to limit the duration of exposure to radioactivity. The following verbatim account allows us to grasp the issue of temporal contradictions: *"You have to reassure them, but it's the same thing, it's a little odd, because you haven't got three hours to spend reassuring them, because your capsule is there, you know, and so what worried me was that once they had been given the capsule there were some who asked questions at that time, and you at that time have a single desire: to get away from there"* (Nuclear Doctor NM2).

In short, we show that working in nuclear medicine is a source of contradictions that arise in multiple forms, related to the various aspects of patient care and to radiation protection. These contradictions, which appear consubstantial with the work activity of nuclear medicine health professionals, demand

implementation of the answers we are now endeavoring to present.

THE REGULATION OF CONTRADICTIONS BETWEEN PATIENT CARE AND RADIATION PROTECTION IN NUCLEAR MEDICINE

Disregarding Radiation Protection in Favor of Patient Care

Contradictions between the logics of patient care and self-protection can be managed by disregarding radiation protection in favor of care. This response to contradictions can be analyzed from the point of view of the division of labor, insofar as those who disregard radiation protection in favor of patient care are also those who are least exposed in their work activity. Indeed, patient management within nuclear medicine units is based on a division of labor between medical personnel (nuclear doctors and cardiologists) and paramedical personnel (technologists and nurses). Doctors carry out consultations and image analysis in order to establish medical diagnosis; however, they neither handle radiopharmaceuticals nor position patients under gamma cameras. Conversely, paramedical personnel proceed with injection of the radiopharmaceutical, positioning of the patient under the gamma camera and reconstruction of the images, prior to their analysis by doctors. Finally, doctors work mainly on the patient's imaged body, i.e., a representation of the body produced by the imaging technique, while paramedical professions work mainly on the patient's physical body (26). This division between work on the imaged body and work on the patient's physical body, which also refers to the separation between interpretative and productive work (27), has a direct impact on levels of exposure to radioactivity of the various professional groups in nuclear medicine. Thus, by working mainly on the patient's imaged body, exposure to radioactivity of nuclear doctors and cardiologists is relatively low, unlike paramedical personnel who work mainly on the patient's physical body. The distribution of work is therefore not only technical, but also concerns exposure to radioactivity. *"We are not exposed to very high doses in the department, at least not the way it is designed - that is, the technologists ultimately spend much more time with patients than we do. We tend to see them before they've been injected, perhaps again afterwards if they wish, but we are not exposed to very high doses"* (Nuclear Doctor NM1).

The division of labor within nuclear medicine units therefore helps clarify disregard of radiation protection in that it also corresponds to a vertical distribution of risk, in which the most irradiating activities are performed by paramedical personnel. In addition, disregard of radiation protection can also be assessed in terms of the risk profile of these actors. Indeed, both doctors and radio pharmacists are challenging the idea that any exposure to radioactivity is a potential source of risk. The existence of risks associated with exposure to low doses is thus put into perspective, as shown in the following verbatim account: *"Ultimately, we are subjected to the ionizing and deadly radiation of our products[laughs]. Ionizing yes, deadly no. Honestly, I don't have a lot of experience, I'm not going to be able to tell you stories like a seasoned pro, but what we were told at our first lecture, what I heard in the workshops, whether it was true of my leaders or even of the other interns, is that on the whole, low doses are not massively risky."* (Nuclear Doctor Intern NM2).

Occupational risk is considered, then, to be low or non-existent insofar as it has not been identified. According to these actors, the uncertainty associated with exposure to low doses of radioactivity reflects the existence of a negligible risk—or even the absence of risk. The question of evidence and causal relationship appears at the heart of these two interpretations of uncertainty: *"We do have a fairly scientific culture, yet we're still awaiting papers that demonstrate the risk of low doses – or at least, any excessive risk, high enough to be taken into account - because I am slightly inclined to think that risk is a part of life, but I think we have much less risk of dying as a consequence of low doses than from getting run down on the street, or in a car accident on holiday."* (Nuclear Doctor NM2).

Disregarding radiation protection thus results in prioritization of patient protection over self-protection. As the following verbatim account shows, these actors are more inclined to implement radiation protection principles to protect patients (such as optimization to limit exposure to radioactivity as much as possible), than to protect themselves from radioactivity in the course of their professional activity. Indeed, patient protection (unlike self-protection) is considered an integral part of patient care. More generally, the disregarding of radiation protection in favor of patient care results in the prioritization of the logic of patient care over the logic of self-protection. Indeed, unlike patient care, radiation protection does not appear to be a structuring dimension of these actors' work activity. The operational rules of radiation protection are thus poorly adhered to in work practices, and this is highlighted by the following verbatim account: *"I have no significant exposure in my opinion, so dosimetry is absolutely not a concern, and neither is radiation protection, as far as I am concerned. For me, this is not a concern at all"* (Nuclear Doctor NM1).

Lastly, disregarding radiation protection in favor of patient care allows these actors to manage the contradictions between the logics of patient care and of radiation protection in that it entails removing one of the two logics of action underlying the contradictions from working practice, as shown in the following verbatim account: *"I have never stopped myself from going to move the patient, or if I see that the technologist is struggling to get them on the table, I will go. At no point will I be reminding myself not to take too long. I'm not looking to spend more or less time in the hot lab or next to the syringe or next to the patient. Later on, when you're interpreting, you're always behind the protective glass, so it doesn't make any difference. But yes, if the patient needs moving, or if I see that the syringe has been placed just behind me, I'm not going to stand aside watching someone else make the effort"* (Nuclear Doctor Intern NM2).

Adapting Radiation Protection to Patient Care Work

Unlike doctors and radio pharmacists, paramedical actors (technologists, nurses and preparers) have to manage the

contradictions between the logics of care and of self-protection, by adapting radiation protection to patient care. This response aims to hold the two logics of action together, rather than disregarding radiation protection in favor of patient care. Indeed, paramedical actors seem to show a differentiated relationship to risk, considering that exposure to low doses is likely to have harmful effects, although these low doses are not necessarily harmful to the working group, as these words of an NM1 technologist reveal: *"I don't often admit it, but I am a little afraid of radiation"*.

The uncertainty associated with exposure to low doses is interpreted as a potential source of occupational risk, rather than as an absence of risk. In other words, these actors establish a possible causal link between their occupational exposure to radioactivity and the incidence of adverse effects. This interpretation of uncertainty is based in part on the experience of the actor and the professional group, as this excerpt from the interview shows: *"In the department, three of us had children and all three of us had major problems. It does make you ask questions, after a while. You tell yourself, unlucky, but there are three of us and we've had a lot of problems with our pregnancies, or a lot of pregnancies that didn't make it to full term. So, then we did ask ourselves: wasn't it because of our environment that we've had problems? So, we realized, even though we don't know for sure, maybe it can be a factor, and we should take care of ourselves. We are in charge of working practices that can affect our health*" (Technologist NM2).

Paramedics also point out that the potential risk is not so much from exposure to low doses of radioactivity as from the repeated nature of this exposure. Thus, according to a nurse from NM2: *"There are risks, because it accumulates over time"*. For health professionals, the risk therefore results more from the accumulation of long-term exposure doses, as evidenced by the following verbatim account: *"I think that by the end of a career, there can be concerns. That's why I think a whole career in nuclear medicine... then it's like smoking and lung cancer, you have some that won't, and some that will"* (Technologist NM2).

The relationship between paramedical actors and risk leads them to take radiation protection into account in their work activity, i.e., to act "as if" the risk associated with exposure to low doses of radioactivity were real, even though they know it is only hypothetical. Thus, as the following verbatim account highlights, radiation protection appears to be a structuring dimension of the activity of these actors, in that it should enable them to protect themselves from possible risks: *"There is no risk as long as these measures are respected, otherwise there may be consequences for our bodies. But if the instructions are followed properly, there is no reason to be afraid to work here*" (Technologist NM1).

Our analysis of the data allows us to underline the fact that these actors manage contradictions by adapting radiation protection to patient care in order to hold the two logics of action together at the very source of the contradictions. Insofar as these actors consider that occupational risk results from the accumulation of radiation exposure doses, the adaptation of radiation protection to patient care results in the development of practices for the division of patient care work that are aimed at collectively distributing radiation exposure doses. Adaptation is thus based on the rotation of workstations concerned with the management of routine procedures. To this end, paramedical staff in nuclear medicine units share responsibility for medical procedures. This distribution is based on the introduction of mechanisms for rotating workstations. Indeed, each work schedule is associated with certain predefined tasks in the various examination and therapy rooms. Rotations take place on a weekly basis, since the technologists and nurses change their working hours (and therefore their shifts) each week. These rotation systems allow a distribution of doses of exposure to radioactivity. According to one NM2 technologist, this represents *"dose rotation"*. Indeed, within each unit of the nuclear medicine department, there is a tacit agreement between paramedical staff to balance their levels of exposure to radioactivity. This work organization makes it possible to distribute exposure to radioactivity among technologists and nurses, insofar as the various workstations are more or less radiant, as shown in this verbatim account: *"We must all rotate our work across different rooms and if we do so, we are less irradiated too, since there are some examinations, there are days when, depending on your working hours, your schedule and your room, you get more or less radiation. So that's another benefit of rotation - you're not always irradiated in the same way"* (Technologist NM2).

In addition, this dose distribution is based on an organization of work established independently by the technologists and nurses of the nuclear medicine units. These actors use what room for maneuver they have to organize their patient care work internally and establish a balance in terms of exposure to radioactivity. Indeed, several technologists and nurses point out that this job rotation system is at their own initiative, since it was set up without the support of health executives or doctors. One NM1 technologist put it this way: *"We settled this between us"*. Ultimately, this workplace organization instigated by paramedical personnel in nuclear medicine units is based on the adoption of tacit rules and shared standards of behavior within the professional group. Job rotation appears to be a collective health preservation strategy (28), enabling stakeholders to carry out their healthcare missions while protecting themselves from radioactivity. By allowing the doses of exposure to radioactivity that are inherent to the care activity to be distributed, the adaptation allows nuclear medicine paramedics to provide care to the patient while limiting their exposure to low doses. In the end, this response can be analyzed as a reformulation of radiation protection rules, in forms adapted to the specificities of patient care.

Contextualized Prioritization Between Patient Care and Radiation Protection

However, the analysis reveals that adaptation alone does not provide a solution to every contradictory situation faced by paramedical actors. Situations still arise in which contradictions cannot be managed by adapting radiation protection to the treatment. Such situations lead paramedical staff in nuclear medicine to operate a contextualized hierarchy, i.e., an arbitration between the logics of patient care and of self-protection, depending on the situation in hand. From that point on,

contradictions are managed by the temporary abandonment of one action logic in favor of the other. Arbitration, then, is situation-dependent; it seems that some situations lead paramedical staff to favor patient care (to the detriment of their own protection), while others lead them to favor their own protection (to the detriment of patient care). The contextualized prioritization strategy appears to be based on a benefit-risk type assessment of the situation by paramedical actors. In the field of radiation protection, benefit-risk analysis refers to the principle of justification according to which any activity entailing exposure to radioactivity must be justified by the benefits it procures, in relation to the risks to which it exposes individuals. From this perspective, risk-taking cannot be justified unless there is a quid pro quo. Paramedical staff in nuclear medicine units weigh up the expected benefits of the examination for the patient and the anticipated risk for the conduct of the examination against the potential occupational risks associated with exposure to low doses. The trade-off between the logics of patient care and self-protection results from this assessment of the situation. Contextualized prioritization thus integrates the two action logics, prioritizing them according to the situation.

Our results also highlight the fact that this contextualized prioritization takes into account various situational parameters such as: patient state of health, type of medical procedure and occupational exposure to radioactivity. We must also point out that the benefit-risk analysis underpinning contextualized prioritization refers to temporal issues that render arbitration more complex. The hierarchy operated by paramedical staff balances a dual temporality that is linked to benefit-risk assessment. Indeed, the benefits and risks for the patient examination are of short-term temporality, whereas the possible occupational risks related to the accumulation of doses of exposure to radioactivity are of long-term temporality.

Ultimately, it seems that the contextualized prioritization implemented by nuclear medicine paramedical personnel gives rise to two types of situations.

- Type 1 situations: actors favor care over protection against the risks associated with low doses where they consider that either the benefit of the examination (or the immediate risk for the examination) to be greater than the long-term occupational risk.
- Type 2 situations: actors favor their protection over care where they consider that the long-term occupational risk associated with low doses to be higher than either the benefit of the examination or the immediate risk for the examination.

For paramedics to prioritize patient care over their own protection, the situation must present an immediate risk to the examination. Thus, where relatives' involvement in the care activity fails to guarantee the proper conduct of the examination, paramedical actors may have to take over from the relatives at the expense of their own protection, as shown in the observation sequence below. This prioritization allows actors to manage the cognitive dissonance they are confronted with by temporarily favoring the logic of patient care—to the detriment of the logic of radiation protection.

Observation NM1

A technologist positions an 18 month-old child under the ECAM gamma camera. The child, suffering from neuroblastoma, is on a drip. The mother is also present in the examination room. To prevent the child from moving during the scintigraphy, the technologist straps her to the gamma camera table at leg and chest. Once the child is positioned under the camera, the technologist adjusts the height of the detectors and then asks the mother to hold her child's head still during the examination. The technologist then returns to the control room, starts the examination, but says, a few minutes into the process: *"She moved her head"*. The technologist then returns to the examination room.

- Technologist (to the mother): *"Do you want me to hold her head?"*
- Mother: *"Yes, please."*

The technologist then places both hands on the child's face to prevent her from moving her head, while the mother sits on a stool next to her child, holding her hand.

Paramedical staff may also be led to favor the logic of patient care at the expense of their own protection when they consider that the patient's difficulties in carrying out the tasks requested of them risk jeopardizing the progress of the medical procedure. For example, anticipation of possible patient movements may lead paramedics to stay with the patient throughout the examination, as highlighted in the following observation sequence. Where the patient is unable to perform the tasks required of them, this may lead health professionals to engage in additional work. In the sequence presented below, prioritization is based on taking into account the situational parameters—in particular the patient's state of health.

Observation NM2

As part of a myocardial scintigraphy, a nurse has just positioned a patient for the CCAM gamma camera. As the nurse is about to return to the control room to start the examination, the patient, obviously worried, asks *"Will you be nearby?"*, to which the nurse replies: *"Yes, I'm next door"*. The nurse returns to the control room, starts the examination and then addresses one of the technologists in the room: *"This lady might move. She has memory problems, she may forget that I told her not to move"*. The nurse then returns to the examination room and stands next to the patient, at her head. The nurse remains with the patient until the end of the scintigraphic examination.

The existence of an immediate risk for the examination seems to be a necessary (though not stand-alone) condition for understanding the prioritization of patient care over self-protection in certain circumstances. Indeed, prioritization also results from a benefit-risk analysis in which the expected benefit of the examination is weighed against the occupational risk associated with exposure to low doses. As the following verbatim accounts highlight, the actors therefore momentarily favor the logic of patient care over their own protection, where they consider the benefits of the examination for the patient to outweigh the occupational risk: *"I have done brain scans on*

patients with dementia and almost had to lie down on them to keep them from moving. Because the exam really needed to be done, so right now the irradiation – never mind. Well, you try to put on a lead apron beforehand, but if you're spending 45 minutes with it, holding the patient like that, irradiation, okay, but the patient must have their examination and it must be interpretable. So, you try to do everything, even if it means taking a bit higher dose than usual" (Technologist NM2).

In addition, situations in which actors favor patient care over protection are also related to exposure to low doses in the long term. Indeed, since the occupational risk comes more from the accumulation of doses than from one-time exposure to radioactivity, these situations allow a hierarchy in favor of patient care precisely because they occur only sporadically in the work activity. As the following verbatim accounts illustrate, these are situations of contradictions related to the clinical and social characteristics of patients, or to certain particularly radiant medical procedures whose frequency of appearance is not daily. *"There have also been a few cases of brain scans, since these patients are a little disturbed anyway, we had to stay with them to talk to them, to keep them company. Since they must not move and it takes a long time, it has happened that we have to stay beside them, but it's still highly unusual"* (Technologist NM2).

However, paramedical personnel in nuclear medicine units do not *systematically* prioritize patient care over their own protection. Indeed, the weighing up of patient benefits against occupational risks can also lead actors to favor their own protection, to the detriment of patient care. This analysis of situations proves a deciding factor in terms of the nature of the hierarchy between the logics of patient care and self-protection, as the following verbatim account shows: *"You have no choice but to let them [the patient] wriggle, and then the images will not be interpretable and they'll never get their examination. If the doctor tells you that the stakes are high for the patient, you'll take the irradiation. However, if the doctor says: "Well, there's nothing else we can do, they move every time", well, you say to yourself, then I'm not going to… I'm going to let them move, and the exam will be a failure, and they won't get their exam."* (Technologist NM2).

Paramedical staff therefore prioritize their own protection at the expense of patient care when the occupational risk of the situation is greater than the benefit of the examination for the patient. Thus, insofar as it constitutes a potential source of risk, occupational exposure to radioactivity is not justified if the anticipated benefit of the examination is low or non-existent. The following verbatim account reflects this form of prioritization in the working practices of nuclear medicine paramedical actors: *"I don't know if we would stay to hold an adult, if we can't, we can't. In the end, we are right beside them for their safety, but if they move in all directions, the examination will not be possible. You can't hold a restless patient under the camera"* (Technologist NM2).

Beyond situations in which paramedics consider the risk associated with low doses to be higher than the expected benefit of the examination for the patient, it appears that these actors also favor their own protection over patient care when their analysis of the situation leads them to conclude that the occupational risk is higher than the immediate risk for the examination. Thus, as the following sequence of observations shows, this hierarchy allows nurses and technologists to manage the contradictions between the logics of patient care and of radiation protection by temporarily promoting their own protection, to the detriment of patient care.

Prioritization of the logic of self-protection must also be part of a long temporality that reaches beyond the immediate temporality of the situation. As the following sequence of observations shows, certain situations can lead nuclear medicine paramedics to protect themselves at the expense of patient care, where they anticipate an accumulation of low-dose exposure related to their patient care activity.

Observation NM2

In the SYMBIA examination room, a brain scan is underway. The patient keeps calling out to the technologist, who is behind the leaded screens. The technologist goes to the patient, but says that she cannot stay with them during the examination, adding *"You are not alone"*. The technologist then returns behind the leaded screens, explaining that she cannot expose herself too much for one patient, because she has to see several every day.

Finally, it seems that the question of the accumulation of exposure doses also allows paramedical personnel to manage the contradictions between the expressive-communication dimension of patient care, and self-protection. Indeed, as the following verbatim account illustrates, the actors justify their own protection to the patient by reference to the repeated nature of the exposure to radioactivity, distinguishing it from the occasional exposure with which patients are confronted in the context of nuclear medicine examinations and treatments: *"Sometimes we have patients who are claustrophobic, dreading the examination, and yet we cannot stay with them. We explain to them that we are continuously exposed to radiation, so we can't hold their hands, be with them for the duration of the imaging. That's why we can't stay too close to the patient, we explain to them that it's because we are exposed all year round. It is still important for us not to increase the dose"* (Technologist NM1).

CONCLUSION

The nuclear medicine sector is the subject of little social science research, particularly on the issue of managing the risks of exposure to low doses of radioactivity. This case is all the more interesting because it reflects a situation of uncertainty, in which the logic of precaution is imposed on health professionals. In this particular context, it was interesting to investigate both the relationship to this hypothetical risk and the articulation between risk representations and work practices.

In this respect, this research shows that radiation protection plays an important role in nuclear medicine practice, but that this prevailing precautionary logic is perceived differently. On the one hand, the identified occupational risk management practices reflect a differentiated relationship to the risk of exposure to low doses according to occupational group. On the other, unless we focus on the characteristics of the work

activity in nuclear medicine, which is marked by potentially-conflicting patient care and radiation protection requirements, it is difficult to understand why some professional groups react differently to certain situations, deviating from prescribed patient care and radiation protection standards. Risk management practices form part of the work of health professionals, which entails constantly building a compromise between contradictory requirements, and adjustments to both radiation protection rules, and specific situations.

This research makes it possible to identify conflicting logics of action between patient care and occupational radiation protection that challenge the practical intelligence of health professionals and solicit their creativity in managing these arbitration situations. The results highlight the fact that, beyond the prescribed rules, the work activity (which leaves a margin of autonomy) offers professionals (particularly nurses and technologists) the option of resolving these conflict situations that are consubstantial with the work activity in nuclear medicine. The risk management procedures implemented emphasize that the precautionary approach is integrated into the professional practices of the most exposed carers and is based on a temporal assessment of exposure in the short and medium term. The procedures rely on the adoption of tacit rules and shared standards of behavior within nuclear medicine units. Risk management is conducted via a joint distribution of risk among technologists and nurses, and via a vertical distribution of risk between paramedical staff and doctors.

From a methodological point of view, investigating work practices by observation makes it possible to show, beyond normative discourse, that the logic of action has its own dynamics; practice is not entirely regulated in advance by radiation protection measures. Work activity carried out in the context of exposure to low doses of radioactivity results from an adaptation of procedures to the singularity of concrete situations. Yet the activity plays out in the interaction between health professionals, the patient and family members, and this makes it possible to highlight both the collective and situated dimension of risk management.

Given the problem addressed and our choice of methodology (qualitative research), the results are not universal in scope; we remain bounded by contexts and situations. It is thus a matter of what Yin calls theoretical generalization: "analytic generalizations depend on using a study's theoretical framework to establish a logic that might be applicable to other situations" [(11), p. 18]. The aim is to understand what types of representations and mechanisms are at work in a nuclear medicine department, and report on actors' behavior in relation to an unproven risk.

Our results, particularly those highlighting a differentiated relationship to the risk of exposure to low doses between doctors and preparers, concur with those of Zonabend (29) on nuclear workers at La Hague, who shows that while the risk is relativized verbally, workers' practices reveal both a more complex relationship to risk and differentiated forms of collective management. This relationship to differentiated risk can be explained by cultural and identity determinants (30). By highlighting the role of social structures in the construction of risk representations, Douglas' theoretical approach puts the plurality of risk relationships into perspective. This helps explain the relationship between individuals and risks by linking their behavior to the culture of the group to which they belong: a culture characterized by values and beliefs that constitute an implicit frame of reference, mobilized by individuals in their interactions. This work shows the importance of the flexibility available to groups in collectively interpreting and managing risk. It helps explain the relationship between individuals and risks by linking their professional practices to the culture of the group to which they belong. Finally, it shows that although perception of risk is embedded in social structures and contingent contexts, its mobilization also constitutes an identity resource determined by the nature of socio-professional relations, as Zonabend (29) has also demonstrated.

DATA AVAILABILITY STATEMENT

The datasets generated for this study are available on request to the corresponding author.

ETHICS STATEMENT

This research was carried out within the framework of the IRON Labex (ANR-11-LABX-0018-01). Ethics approval was not required for this study as per applicable institutional and national guidelines and regulations. The informed consent of the participants was implied through survey completion.

AUTHOR CONTRIBUTIONS

RL: framing the research, qualitative study, and writing the paper. BG: framing the research and writing the paper. FB: framing the research.

REFERENCES

1. Boudia S. Les problèmes de santé publique de longue durée. Les effets des faibles doses de radioactivité. In: Gilbert C, Henry E, editors. *Comment se Construisent les Problèmes de Santé Publique,* Paris: La Découverte (2009). p. 35–53.
2. Callon M, Lascoumes P, Barthe Y. *Agir Dans un Monde Incertain. Essai sur la Démocratie Technique*. Paris: Le Seuil (2001).
3. Godard O, Lochard J. *L'histoire de la Radiation Protection, un Antécédent au Principe de Précaution*. Chaire Développement durable EDF - École Polytechnique (2005).
4. Davis F. Uncertainty in medical prognosis clinical and functional. *Am J Sociol.* (1960) 66:41–7. doi: 10.1086/222821
5. Fox R. *L'incertitude Médicale*. Paris: L'Harmattan (1988).
6. Duclos D. La construction sociale du risque: le cas des ouvriers de la chimie face aux dangers industriels. *Rev. Française Sociol.* (1987) 1:17–42. doi: 10.2307/3321444

7. Amiel C. On sait qu'il n'y a pas de vrais risques. Discours et pratiques de soignants autour des infections nosocomiales. *Sci Social Santé*. (2005) 3:37–58. doi: 10.3406/sosan.2005.1658
8. Bidet A. Le travail et sa sociologie au prisme de l'activité. In: A Bidet, editor. *Sociologie du Travail et Activité*. Toulouse: Octares (2006). p. 5–23.
9. Carricaburu D, Lhuilier D, Merle V. Quand soigner rend malade: des soignants face au risque infectieux à l'hôpital. *Santé Publique*. (2008) 20:57–67. doi: 10.3917/spub.080.0057
10. Mays N, Pope C. Qualitative research: reaching the parts other methods cannot reach: an introduction to qualitative methods in health and health services research. *BMJ*. (1995) 311:42–5. doi: 10.1136/bmj.311.6996.42
11. Yin RK. *Applications of Case Study Research*. Thousand Oaks, CA: Sage Publications (2012).
12. Hlady Rispal M. *La Méthode des cas. Application à la Recherche en Gestion*. Brussels: De Boeck (2002).
13. Orlikowski WJ. Knowing in practice: enacting a collective capability in distributed organizing. *Organ Sci*. (2002) 13:249–73. doi: 10.1287/orsc.13.3.249.2776
14. Spradley JP. *Participant Observation*. New York, NY: Holt (1980).
15. Orlikowski WJ. Practice in research: phenomenon, perspective and philosophy. In: Golsorkhi D, Rouleau L, Seidl D, Vaara E, editors. *Cambridge Handbook of Strategy as Practice*. Cambridge: Cambridge University Press (2010). p. 23–33.
16. Denzin NK, Lincoln YS. *Strategies of Qualitative Inquiry*. Thousand Oaks, CA: Sage (2008).
17. Wacheux F. *Méthodes Qualitatives et Recherche en Gestion*. Paris: Economica (1996).
18. Miles MB, Huberman AM. *Analyse des Données Qualitatives*. Bruxelles: De Boeck Supérieur (2003).
19. Paillé P, Mucchielli A. *L'analyse Qualitative en Sciences Humaines et Sociales*. Paris: Armand Colin (2003).
20. Girin J. L'analyse empirique des situations de gestion: éléments de théorie et de méthode. In: Martinet AC, editor. *Épistémologies et Sciences de Gestion*. Paris: Economica (1990). p. 141–82.
21. Huberman AM, Miles MB. Analyse des Données Qualitatives: Recueil de Nouvelles Méthodes. Brussels: De Boeck (1991).
22. Tronto J. *Un Monde Vulnérable. Pour une Politique du Care*. Paris: La Découverte (2009).
23. Saillant F. *Cancer et Culture. Produire le Sens de la Maladie*. Montréal, QC: Les éditions Saint-Martin (1988).
24. Rothier Bautzer E. Une approche sociologique du soin comme travail relationnel. *J Int Bioéthique*. (2016) 27:41–57. doi: 10.3917/jib.271.0041
25. Fournier P. *Travailler Dans le Nucléaire. Enquête au Cœur d'un Site à Risques*. Paris: Armand Colin (2012).
26. Estival C. *Corps, Imagerie Médicale et Relation Soignant-Soigné. Étude Anthropologique au Centre de Cancérologie*. Paris: Seli Arslan (2009).
27. Barley S. Technology as an occasion for structuring: evidence from observations from CT scanners and the social order of radiology departments. *Adm Sci Q*. (1986) 3:78–108. doi: 10.2307/2392767
28. Rocha R, Daniellou F, Nascimiento A. La rotation et les stratégies collectives de préservation de la santé développées par les opérateurs d'une usine de boissons. *Activités*. (2012) 9:1–21. doi: 10.4000/activites.304
29. Zonabend F. *La Presqu'île au Nucléaire*. Paris: Odile Jacob (1989).
30. Douglas M. *Risk and Blame, Essays in Cultural Theory*. Londres: Routledge (1992).

Conflict of Interest: The authors declare that the research was conducted in the absence of any commercial or financial relationships that could be construed as a potential conflict of interest.

APPENDIX 1

TABLE 1 | Interviews in nuclear medicine.

Occupational group	Number of interviews		Proportion	
	NM1	NM2	NM1	NM2
Nuclear doctor	3	2	75%	66%
Nuclear doctor intern	1	1	50%	100%
Cardiologist	–	2	–	50%
Radio pharmacist	1	1	100%	100%
Technologist	4	2	80%	50%
Nurse	-	2	–	100%
Healthcare manager	1	1	100%	100%
Auxiliary nurse	-	1	–	100%
Medical physicist	1		100%	
Total	**23**		**70%**	

frontiers in Medicine

REVIEW
published: 27 November 2019
doi: 10.3389/fmed.2019.00268

Innovative Molecular Imaging for Clinical Research, Therapeutic Stratification, and Nosography in Neuroscience

Marie Beaurain[1,2]*, *Anne-Sophie Salabert*[1,2], *Maria Joao Ribeiro*[3,4,5], *Nicolas Arlicot*[3,4,5], *Philippe Damier*[6], *Florence Le Jeune*[7], *Jean-François Demonet*[8] *and Pierre Payoux*[1,2]

[1] CHU de Toulouse, Toulouse, France, [2] ToNIC, Toulouse NeuroImaging Center, Inserm U1214, Toulouse, France, [3] UMR 1253, iBrain, Université de Tours, Inserm, Tours, France, [4] Inserm CIC 1415, University Hospital, Tours, France, [5] CHRU Tours, Tours, France, [6] Inserm U913, Neurology Department, University Hospital, Nantes, France, [7] Centre Eugène Marquis, Rennes, France, [8] Leenards Memory Centre, Department of Clinical Neuroscience, Centre Hospitalier Universitaire Vaudois, Lausanne, Switzerland

Over the past few decades, several radiotracers have been developed for neuroimaging applications, especially in PET. Because of their low steric hindrance, PET radionuclides can be used to label molecules that are small enough to cross the blood brain barrier, without modifying their biological properties. As the use of 11C is limited by its short physical half-life (20 min), there has been an increasing focus on developing tracers labeled with 18F for clinical use. The first such tracers allowed cerebral blood flow and glucose metabolism to be measured, and the development of molecular imaging has since enabled to focus more closely on specific targets such as receptors, neurotransmitter transporters, and other proteins. Hence, PET and SPECT biomarkers have become indispensable for innovative clinical research. Currently, the treatment options for a number of pathologies, notably neurodegenerative diseases, remain only supportive and symptomatic. Treatments that slow down or reverse disease progression are therefore the subject of numerous studies, in which molecular imaging is proving to be a powerful tool. PET and SPECT biomarkers already make it possible to diagnose several neurological diseases *in vivo* and at preclinical stages, yielding topographic, and quantitative data about the target. As a result, they can be used for assessing patients' eligibility for new treatments, or for treatment follow-up. The aim of the present review was to map major innovative radiotracers used in neuroscience, and explain their contribution to clinical research. We categorized them according to their target: dopaminergic, cholinergic or serotoninergic systems, β-amyloid plaques, tau protein, neuroinflammation, glutamate or GABA receptors, or α-synuclein. Most neurological disorders, and indeed mental disorders, involve the dysfunction of one or more of these targets. Combinations of molecular imaging biomarkers can afford us a better understanding of the mechanisms underlying disease development over time, and contribute to early detection/screening, diagnosis, therapy delivery/monitoring, and treatment follow-up in both research and clinical settings.

Keywords: molecular imaging, clinical research, neurology, psychiatry, PET, SPECT

OPEN ACCESS

Edited by:
Samer Ezziddin, Saarland University, Germany

Reviewed by:
Puja Panwar Hazari, Institute of Nuclear Medicine & Allied Sciences (DRDO), India
Anupama Datta, Defence Research and Development Organisation (DRDO), India

***Correspondence:**
Marie Beaurain
marie.beaurain@inserm.fr

Specialty section:
This article was submitted to Nuclear Medicine, a section of the journal Frontiers in Medicine

Received: *26 February 2019*
Accepted: *01 November 2019*
Published: *27 November 2019*

Citation:
Beaurain M, Salabert A-S, Ribeiro MJ, Arlicot N, Damier P, Le Jeune F, Demonet J-F and Payoux P (2019) Innovative Molecular Imaging for Clinical Research, Therapeutic Stratification, and Nosography in Neuroscience. Front. Med. 6:268. doi: 10.3389/fmed.2019.00268

INTRODUCTION

Molecular imaging is the visualization, characterization, and measurement of biological processes at the molecular and cellular levels in humans and other living systems (1). Over the past few years, rapid improvement in molecular imaging has led to gain in specificity and quantification helpful for early diagnosis and disease follow-up, particularly within the field of neurology. A key advantage of *in vivo* molecular imaging is its ability to identify pathological processes without the need for invasive biopsies or surgical procedures (2).

This imaging technique is currently performed with positron emission tomography (PET) and single-photon emission tomography (SPECT). Several PET and SPECT radiotracers have been developed for neuroimaging applications. The first ones, namely 123I-labeled amines, 99mTc-hexamethylpropyleneamine-oxime (99mTc-HMPAO), and 99mTc-ethyl cysteinate dimer (99mTc-ECD), were developed in the 1990s to measure regional cerebral blood flow in the presurgical evaluation of patients with refractory partial epilepsy (3). The 2000s saw the advent of PET with the use of fluorine-18 fluorodeoxyglucose ([18F]FDG) in clinical routine, for the assessment of cerebral glucose metabolism. As such, it has also been used in the preoperative evaluation of partial epilepsy, but its indications equally include the early diagnosis and differential diagnosis of dementing disorders, differential diagnosis of cerebral space-occupying lesions, detection of viable tumor tissue (recurrence), non-invasive grading, and differentiation between Parkinson's disease and atypical Parkinsonian syndromes (4).

During the past decade, advances in molecular imaging have enabled scientists to focus on specific brain targets, such as receptors, neurotransmitter transporters, or abnormal protein deposits. There are a growing number of radiotracers, which are regarded as valuable tools for many medical imaging applications, including early detection, diagnosis, and treatment follow-up (2). New imaging biomarkers (e.g., amyloid peptide) allow for the diagnosis of neurological diseases at an early stage, thus contributing to the emergence of the concept of preclinical disease (5, 6). Several PET and SPECT radiotracers are used for both routine clinical applications and research that aim to improve the prevention, diagnosis and treatment of brain diseases. For instance, molecular imaging biomarkers can be used for treatment follow-up, or for selecting patients to be included in clinical trials, or for exploring the neurobiological underpinnings of disease progression.

The aim of the present review was to map out the main innovative radiotracers used in neurology, and explain their role in clinical research. We did not explore 11C-labeled tracers in any depth, as they are not widely used for clinical purposes, owing to their short half-life (20 min). We classified the radiotracers according to their target.

DOPAMINERGIC SYSTEM

Today, the main class of radiotracers targeting neurotransmission is the one that enables the dopaminergic pathways to be explored (7). These molecules allow for the imaging of nigrostriatal neurons and dopamine receptors. They are used as PET or SPECT radiotracers and assist with the diagnosis of Parkinson's disease (PD), other Parkinsonian syndromes, and Lewy body dementia (LBD) (8).

The first radiotracer to be introduced for the non-invasive assessment of nigrostriatal terminals was [18F]-DOPA in 1983 (9). This radiotracer reflects the activity of aromatic amino acid decarboxylase (AADC), an enzyme that converts L-DOPA to dopamine, through its subsequent accumulation in the dopamine neurons (10). Striatal F-DOPA uptake has been found to be closely related to the nigral cell count (11), except at the beginning of the disease as a consequence of functional compensation (F-DOPA uptake is preserved while motor symptoms can be already presents) (12). This molecule has a history of more than 30 years in clinical research and for the diagnosis of PD. However, in the past decade, the clinical practice led to prefer instead tracers targeting the plasma membrane dopamine transporter (DAT). The latter is easier to use and has a high sensitivity for detecting presynaptic dopaminergic degeneration at early-stage of PD. F-DOPA has recently regained interest in the context of regenerative therapy for PD such as the implantation of dopamine cells or the infusion of drugs with regenerating effects into the striatum (13, 14). The purpose of this therapy is to regenerate the dopaminergic presynaptic function by converting L-DOPA to dopamine. In that cases, DAT tracers are considered to be less relevant for measuring therapeutic response than F-DOPA.

As mentioned above, the second presynaptic dopaminergic target is the DAT, located on dopamine nerve cell terminals. In contrast to the AADC, the DAT is only expressed within dopamine neurons. However, the ligands used for its imaging may also bind to related transporters, such as the serotonine reuptake transporter (SERT) or the norepinephrine reuptake transporter (10). In SPECT imaging, several radiotracers have been developed. The most commonly used are the two cocaine derivatives: [123I]-βCIT and [123I]-FPCIT (8). Compared with [123I]-βCIT, [123I]-FPCIT has better selectivity for DAT vs. SERT, and due to its lower DAT affinity, it has better kinetic properties, with a striatal peak time at 148 min after intravenous injection (15). Although direct comparison of FP-CIT SPECT and F-DOPA PET has shown that both FP-CIT SPECT scans and F-DOPA PET scans are able to distinguish patients with PD from healthy controls with high levels of sensitivity and specificity, the decrease in [123I]-βCIT binding more closely mirrors the reduction in dopaminergic neurons than the decrease in F-DOPA uptake does, suggesting that β-CIT binding is a better index of dopaminergic neuron loss (16). These different sensitivity of the two tracers to a reduction in dopamine transmission is linked to differing degrees of decrease in the striatal uptake of the two tracers, with less striatal FP-CIT uptake than F-DOPA uptake at the early phase of disease (17). [123I]-FPCIT was licensed as DaTSCAN (Amersham Health) in Europe in 2000, and is now a frequently used SPECT radioligand in clinical routine, particularly as an ancillary tool for diagnosing patients with movement disorders, but also in clinical research (15). In the latter context, [123I]-FPCIT has been used in numerous studies seeking to determine the sensitivity and specificity of this tracer

in the differentiation of several causes of dementia (18), as well as to study variations in DAT density after different treatments, such as antipsychotics in patients with schizophrenia (19), or psychotherapy in individuals with depression (20).

Tropane derivatives have also been labeled with 99mTc: TRODAT-1 has been compared with F-DOPA in patients with PD (21), and may represent a reliable alternative. 99mTc-labeled ligands are less expensive, and may therefore be more easily accessible, and more suitable for routine use (22–24).

Another tracer has been developed to image the DAT: PE2I. Like FP-CIT and β-CIT, this molecule is a cocaine derivative, which can be labeled with iodine-123 or−125, carbon-11, or tritium (25). This ligand has about a 30-fold higher affinity for DAT than for SERT, and its lower affinity for DAT makes [123I]-PE2I kinetics better than that of [123I]-FPCIT, with a striatal peak time of 30–60 min. However, despite its favorable properties, [123I]-PE2I is not currently licensed as a SPECT radioligand for clinical use (15).

The excellent properties of PE2I mentioned above recently were exploited to develop a new DAT tracer: LBT-999, exploited by Zionexa, which could be used in future PET explorations using fluorine-18 (26–28). Because of its higher resolution, PET imaging is more useful than SPECT for accurate *in vivo* quantification of DAT density. LBT-999 is a phenyltropane derivative that has demonstrated its suitability for *in vivo* quantification of DAT in non-human primates (29). An *in vivo* kinetic study in baboons confirmed that LBT-999 brain uptake is fast, high, and mainly located in the putamen and caudate, with peak uptake in these regions at 30 min postinjection.

A third way of investigating the function of dopamine terminals is to measure the density of vesicular monoamine transporter (VMAT2), which is responsible for taking up neurotransmitters into presynaptic secretory vesicles. Although a majority of VMAT2 are expressed in dopaminergic terminals, this transporter is also located in various monoaminergic neurons, and is involved in the vesicular trapping of a wide variety of neurotransmitters including dopamine, serotonin, norepinephrine, and epinephrine. This target can be investigated with [11C]-DTBZ, or more recently with fluorinated analog [18F]-AV-133, by PET (30). This presynaptic marker follows very typical patterns in several neurodegenerative diseases affecting dopaminergic function, such as PD, LBD, multiple system atrophy (MSA), progressive supranuclear palsy (PSP), and corticobasal syndrome (CBS). Their uptake/binding is altered in several brain areas, depending on the disease and its stage (31). In contrast to AADC activity or DAT binding, it has been suggested that VMAT2 activity is less inclined to changes induced by medication or compensatory mechanisms. However, VMAT2 activity can be impacted by the amount of vesicular dopamine, competing at the recognition site. Hence, the level of VMAT2 binding may decrease with levodopa administration (32). These tracers have a future in early detection/screening, diagnosis, and neuroprotective treatment follow-up of these neurodegenerative diseases, as well as in the monitoring of neural grafted cells after transplantation (8).

Dopaminergic neurotransmission can also be explored by visualizing postsynaptic D2 receptors. The binding potential of these receptors can be assessed using SPECT with the ligands [123I-IBZM and 123I]-IBF, as well as PET with [11C]-raclopride and [18F]-fallypride as radiotracers (**Figure 1**) (8, 31). The concomitant study of DAT and D2 receptors may improve the diagnostic value of molecular imaging in differentiating between PD and other parkinsonian syndromes (33, 34). Nowadays, however, the measurement of cardiac [123I]-MIBG uptake remains the most frequently used technique to differentiate PD and MSA (35). Molecular imaging of dopamine D2 receptors has also been used to study dopamine's role in drug abuse and addiction (36), and to evaluate several neuropsychiatric disorders (37).

Key features of all these tracers are summarized in **Figure 2** and **Table 1**.

AMYLOID IMAGING

β-amyloid (Aβ) plaques in the brain are one of the key histopathologic lesions of Alzheimer's disease (AD) (80). Advances in the understanding of the physiopathology of AD suggest that progressive amyloid accumulation begins during the presymptomatic phase, followed by synaptic dysfunction, tau-mediated neuronal injury, a reduction in brain volume, and finally the emergence of cognitive symptoms, followed by a clinical syndrome of overt dementia (81). This suggest that Aβ imaging is a critical step for the early diagnosis of AD.

These deposits were first imaged in PET in 2002, using a thioflavin-T derivative: 11C-Pittsburgh compound B ([11C]-PIB) (82). Although this is the best known compound, its use is restricted to the research field, owing to the short half-life of 11C. Numerous studies have showed that [11C]-PIB binds to Aβ plaques in several cortical regions in patients with AD (82–84). [11C]-PIB binding is correlated with a reduction in cerebrospinal fluid Aβ42 (85), cerebral atrophy (86), and episodic memory impairment in apparently healthy elderly individuals and those with mild cognitive impairment (MCI) (87). These studies have paved the way for the development of several Aβ plaque PET tracers labeled with 18F. To date, three radiopharmaceuticals with equivalent diagnostic performances have been authorized by the European Medicines Agency and the US Food and

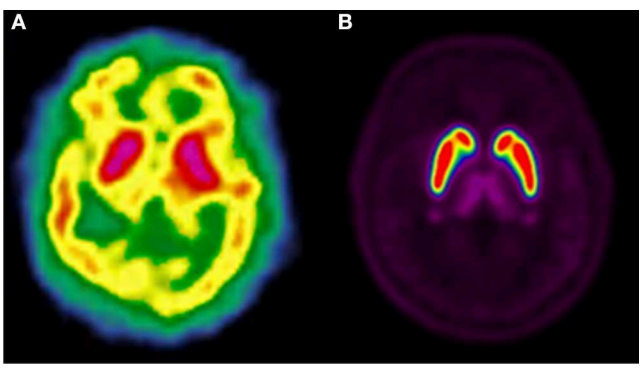

FIGURE 1 | Comparison of [123I]-IBZM image **(A)** and [18F]-fallypride image **(B)** within the same individual.

TABLE 1 | Main SPECT and PET dopaminergic tracers, molecular strucures, pharmacological properties, and examples of clinical studies.

Compounds	Imaging modality	Target/ measure	Affinity (nM)	Clinical studies	Compounds	Imaging modality	Target/ measure	Affinity (nM)	Clinical studies
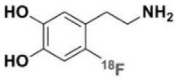 [^{18}F]-DOPA	PET	AADC activity	Uptake	PD (10, 13, 14) LBD (38, 39) MSA (40) PSP (41)	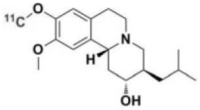 [^{11}C]-DTBZ	PET	VMAT2 density	K_i = 2 (42)	PD (43, 44) LBD (44, 45) MSA (46, 47)
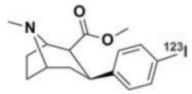 [^{123}I]-βCIT	SPECT	DAT density	K_i = 27±2 (DAT) K_i = 3±0.2 (SERT) K_i = 80±28 (NET) (48)	PD (49–52) LBD (53) MSA (34)	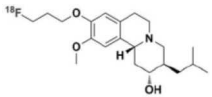 [^{18}F]-AV133	PET	VMAT2 density	K_d = 0.19 (striatum) K_d = 0.25 (hypothalamus)(54)	PD (55) LBD (56)
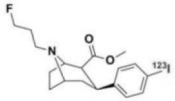 [^{123}I]-FPCIT	SPECT	DAT density	K_i = 3.5 (DAT) K_i = 9.7 (SERT) (48)	PD (57–59) LBD (60) MSA (61) PSP (58)	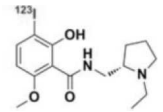 [^{123}I]-IBZM	SPECT	D2 receptors density	K_d = 3.1±0.62 K_i = 0.32 (D2) K_i = 4143 (D1) (62)	MSA (63, 64) PSP (63, 65)
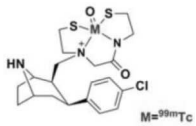 [^{99m}Tc]-TRODAT-1	SPECT	DAT density	K_i = 14.1±2.1 (DAT) K_i = 360±44 (SERT) (23)	PD (21, 66)	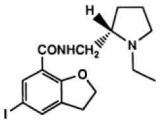 [^{123}I]-IBF	SPECT	D2 receptors density	K_d = 0.106±0.015 K_i = 0.015±0.002 (D2) K_i = 820±164 (D1) (67)	MSA (68) PSP (68, 69)
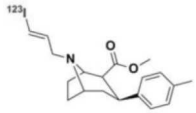 [^{123}I]-PE2I	SPECT	DAT density	K_i = 17±7 (DAT) K_i = 500±30 (SERT) K_i >1000 (NET) (25)	PD (70, 71) LBD (72) PSP (73)	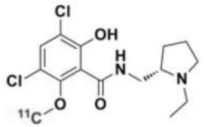 [^{11}C]-raclopride	PET	D2 receptors density	K_i = 7.5 (74)	MSA (75, 76)
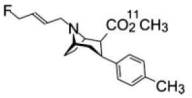 [^{18}F]-LBT-999	PET	DAT density	Kd = 9.15±2.8 (DAT) IC_{50} >1000 (SERT and NET) (26)	PD (77)*	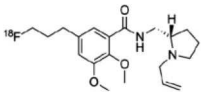 [^{18}F]-fallypride	PET	D2 receptors density	IC_{50} = 0.6 (78)	Epilepsy (79)

*Kd, dissociation constant; Ki, inhibition constant; IC50, half maximal inhibitory concentration. *Preclinical study.*

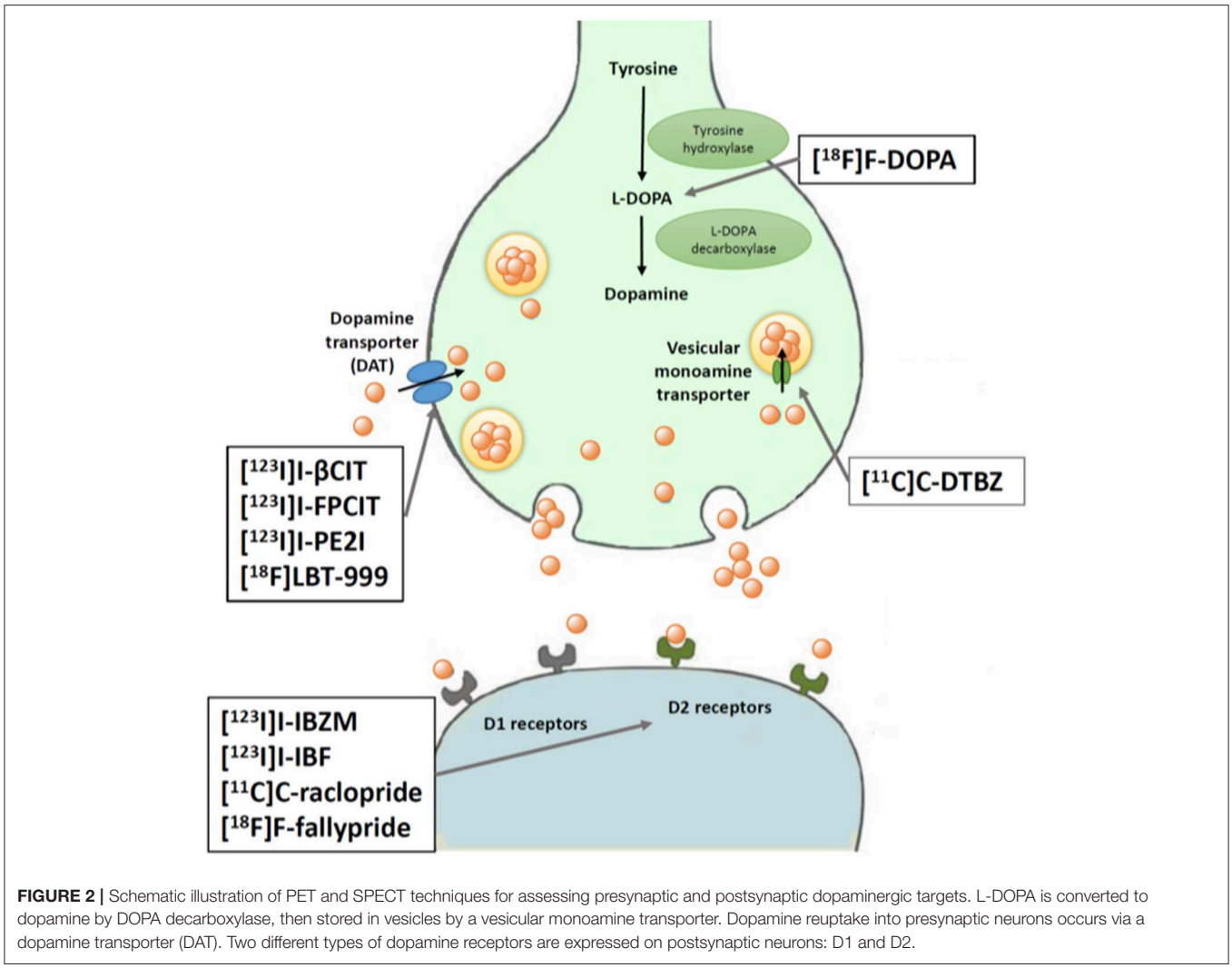

FIGURE 2 | Schematic illustration of PET and SPECT techniques for assessing presynaptic and postsynaptic dopaminergic targets. L-DOPA is converted to dopamine by DOPA decarboxylase, then stored in vesicles by a vesicular monoamine transporter. Dopamine reuptake into presynaptic neurons occurs via a dopamine transporter (DAT). Two different types of dopamine receptors are expressed on postsynaptic neurons: D1 and D2.

Drug Administration: 18F-florbetapir, 18F-florbetaben, and 18F-flutemetamol (88) (**Table 2**).

The clinical criteria that are currently used for AD diagnosis have variable specificity and sensitivity, with pooled averages of 70 and 81% (100). A recent review assessing studies published from January 1980 to March 2014 on the diagnostic utility of these three radiotracers demonstrated a pooled weighted sensitivity and specificity of 89.6% and 87.2% for florbetapir, and 89.3 and 87.6% for florbetaben in differentiating patients with AD from age-matched normal controls (101). These results suggest that 18F-labeled tracers have better sensitivity and specificity than clinical diagnosis and other biomarkers commonly used in practice (89), and are comparable to 11C-PiB. They have also been shown to have good patient tolerability (96). However, the extent and distribution of Aβ plaques and amyloid PET tracer binding in patients are only moderately correlated with patterns of neurodegeneration and cognitive deficits (102–104). This suggests that Aβ deposition, which is a prerequisite for diagnosing AD, is just the starting-point of a cascade of other neuropathological events, rather than the actual driver of neurodegeneration and clinical disease progression (105).

In this respect, these tracers are chiefly useful for their good negative predictive value. A negative scan (i.e., amyloid burden undetectable or extremely low) is considered to be incompatible with a diagnosis of AD. Although a moderate-to-high amyloid plaque density may point to AD, a positive test is not sufficient to diagnose this disorder, especially in elderly participants. It was in this context that the Society of Nuclear Medicine and Molecular Imaging and the Alzheimer's Association delineated "appropriate use criteria" in 2013, identifying three clinical circumstances in which amyloid PET imaging is recommended to clarify the diagnosis: "Patients with persistent or progressive unexplained mild cognitive impairment", "Patients satisfying core clinical criteria for possible (as opposed to probable) Alzheimer's disease (i.e., atypical clinical course or etiologically mixed presentation)", and "Patients with atypically young-onset dementia" (106).

In spite of its excellent diagnostic capacity, the use of amyloid PET imaging in clinical practice is still limited. However, this technique has proved extremely useful in clinical

TABLE 2 | Main amyloid PET tracer, molecular structures, pharmacological properties, and examples of clinical trials in AD.

Compounds	Target/ measure	Affinity (nM)(88)	Clinical studies in AD
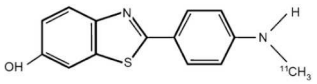 [^{11}C]-PIB	Aβ plaques (fibrillar oligomer)	$K_i = 0.9$	(82–84)
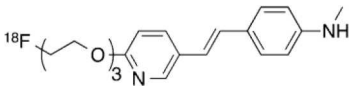 [^{18}F]-florbetapir	Aβ plaques (aggregated form)	$K_i = 2.2$	(89–92)
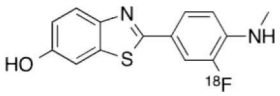 [^{18}F]-flutemetamol	Aβ plaques (soluble form)	$K_i = 0.7$	(93–95)
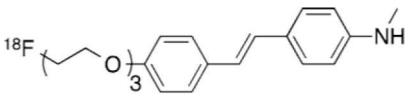 [^{18}F]-florbetaben	Aβ plaques (aggregated form)	$K_i = 2.4$	(96–99)

trials. Currently, the treatment options for AD are limited to symptomatic drugs, with no attenuation of the ultimate prognosis (107). Numerous studies are being conducted to find new treatments, as well as to better understand the physiopathology of AD. One of the research approaches to develop new treatments involves targeting the two pathological features associated with AD, namely senile plaques (Aβ) and neurofibrillary tangles (NFTs) composed of aggregates of hyperphosphorylated tau protein in paired helicoid filaments (PHF). According to the amyloid cascade hypothesis, toxic plaques are the earliest manifestation of the disease, a notion supported by evidence of Aβ up to 20 years prior to the onset of symptoms (107). Two main classes of medication are under development as a result: monoclonal anti-amyloid antibodies, and inhibitors of pathogenic cleavage of the amyloid precursor protein (APP). PET amyloid radiotracers in clinical trials evaluating the therapeutic potential of these medications are used for selecting and including patients with significant Aβ, or monitoring disease progression under treatment (108). For example, in an amyloid-based immunotherapy study, PET imaging used for treatment follow-up suggested that anti-amyloid antibodies were more effective in the early stages of amyloid accumulation (108). Soon after this discovery, another study was therefore conducted to study the effect of this class of medication in patients with few or no symptoms (MMSE 20–26) but positive amyloid PET imaging (109). This study failed to show a significant difference in cognitive outcomes between the study group and asymptomatic controls; however other drug studies with similar design using amyloid tracer PET imaging in asymptomatic patients with AD are ongoing.

TAU IMAGING

As previously indicated, several studies have reported that Aβ burden is only moderately correlated with glucose hypometabolism, disease severity, progression, and clinical presentation. Furthermore, clinical trials assessing monoclonal anti-amyloid antibodies have mostly failed to show a clinical benefit in AD. The other main histopathological figure of AD, abnormal tau protein aggregates, has therefore be considered with much interest. Several PET radiopharmaceuticals have therefore been developed to accurately target abnormal tau protein conformations. NFTs composed of aggregated hyperphosphorylated tau in paired helicoid filaments are one of the two key neuropathological substrates of AD, along with Aβ plaques (110). Whereas, Aβ levels stabilize at an early stage, the presence and extent of NFTs and neuronal injury increase in parallel with disease duration and severity of symptoms (111). Moreover, tau has been found to be more closely related to memory decline in post mortem studies of AD than amyloid pathology (112). Abnormal aggregation of tau protein has also been observed in the pathophysiology of other neurodegenerative diseases, including frontotemporal dementia (FTD), CBS, PSP and, to a smaller extent, LBD; the abnormal conformation of tau in these diseases are distinct from that observed in AD which involves paired helicoid filaments (PHF). These pathologies are collectively known as tauopathies. These tauopathies differ by the isomeric form and ultrastructural morphology of aggregated tau, affected brain regions, and spatial patterns of tau accumulation (110).

Over the past few years, six promising tau imaging agents have been developed: [11C]-PBB3, [18F]-AV-1451 (or flortaucipir, previously known as T807), [18F]-T808, and the THK family [18F]-THK523, [18F]-THK5105, and [18F]-THK5351. These radiotracers have been synthesized, using structure–activity relationship software, from N-benzylidene-benzohydrazide compounds used for the detection of tau-paired helical filament (PHF) (88).

One of the first radiotracers developed for tau imaging was [18F]-FDDNP. This tracer is rapidly metabolized in hydrophilic

compounds that cross the blood brain barrier (BBB), resulting in non-specific binding and therefore significant background noise. Furthermore, this tracer is not specific to NFTs, but also has an affinity for Aβ plaques, meaning that it is not the best choice for tau assessment (88, 113, 114).

The first tau-selective radioligand, [18F]-THK523 was synthesized by Okamura et al. (115), and its selectivity for phosphorylated tau was confirmed in post mortem studies, as well as in several *in vitro*, *ex vivo*, and *in vivo* experiments (116). However, this tracer is not able to bind to tau aggregates in non-AD tauopathies such as PSP and CBD, and is characterized by high retention in white matter (117, 118). New THK compounds have since been developed: [18F]-THK5105, [18F]-THK5117, and [18F]-THK5351. The latter has better kinetics, less white matter binding, and a higher affinity for tau than [18F]-THK523 (119). However, it also binds to MAO-B sites, and has a lower binding level in AD than AV-1451 does (110).

[11C]-PBB3 is another tau radiotracer with a high affinity for NFTs, a low level of white matter binding, good BBB penetration and rapid washout. The peculiarity of [11C]-PBB3 is its affinity for the tau isoforms of several non-AD tauopathies. However, it metabolizes to a radiolabeled compound that can cross the BBB, thus limiting its quantification (110).

[18F]-T807 ([18F]-AV1451 developed by Lilly Research Laboratories) and [18F]-T808 belong to the benzimidazole pyrimidine family. They have a nanomolar affinity for the tau PHF found in AD, and are 25 times more selective for tau PHF than for Aβ (120, 121). Today, [18F]-AV-1451 is the most widely used tau radioligand. Like [11C]-PBB3, it has low retention in white matter. Several clinical studies have shown a close correlation between [18F]-AV1451 binding and the neuropathological stages of tau (122), cognitive decline and tau levels in cerebrospinal fluid (123, 124). However, a recent autoradiographic evaluation of AV1451 reported a lower level of binding in non-AD tauopathies, as well as off-target binding in the basal ganglia and substantia nigra in the absence of tau pathology (125).

Recently, another radioligand ([18F]MK-6240, developed by Merck laboratories) was administered to patients with AD with promising results. This tracer showed a high specificity and selectivity for NFTs, good pharmacokinetic properties, and no apparent off-target binding, in contrast to [18F]-AV-1451 (110, 126–128).

As a link has been demonstrated between NFTs and AD symptoms, tau PET tracers are increasingly being used in AD clinical trials, especially those investigating drugs to reduce the tau or Aβ burden (129), such as Aβ monoclonal antibodies. The indirect effect of reducing Aβ on the rate of PHF deposition downstream further supports the amyloid hypothesis, and tau PET imaging may highlight the presumptive disease-modifying impact of these drugs. Furthermore, as tau monoclonal antibodies are designed and investigated, tau PET imaging will be helpful in demonstrating and quantifying the engagement of the molecular target. Many trials currently use cerebrospinal fluid (CSF) biomarkers of tau and phosphorylated tau to detect target engagement, but there are few data on how CSF biomarkers and tau PET imaging correlate. Tau PET imaging may also help to confirm that changes in tau deposition are correlated with clinical disease progression (130). Several tau vaccines have shown efficacity and safety in animal models (131). In a recent study, an anti-tau drug exhibited a good safety profile and even stimulated a positive immune response in human patients (132). Several other early-phase trials of drugs that target tau protein are currently underway, although the results are yet to be published (133).

In this context, like amyloid tracers, tau radioligands (summarized in **Table 3**) have an important role to play in clinical studies assessing new treatments and measuring disease progression.

NEUROINFLAMMATION

Neuroinflammation is an inflammatory and adaptive response within the central nervous system, and depends on several processes mediated by neuronal cells such as astrocytes, as well as by non-neuronal cells such as the brain's resident macrophages and microglia.

Although initiation of an inflammatory response may be beneficial in response to injury of the nervous system, chronic or maladaptive neuroinflammation can have harmful outcomes in many neurological diseases. During inflammatory processes, cytokines, chemokines and reactive oxygen species (ROS) are produced by glial cells, and all these molecules can be targeted by molecular imaging (146).

The main target for imaging neuroinflammation is currently translocator protein (TSPO) overexpression in activated microglia. TSPO is a highly hydrophobic protein that is mainly situated in the outer mitochondrial membrane. Classically not present in healthy brain parenchyma, TSPO has been widely identified in microglial cells in dementia neuropathology, which involves neuroinflammatory processes and microglial activation. The most widely used TSPO PET radiopharmaceutical tracer used to be [11C]-(R)-PK11195. A new generation of fluorinated tracers has been developed in the past decade (147, 148), with different compound families such as phenoxyarylacetamides derivatives ([18F]-FEDAA1106, [18F]-FEPPA, [18F]-PBR06), imidazopyridine derivatives ([18F]-PBR111), and pyrazolopyrimidine derivatives ([18F]-DPA-714) (**Figure 3**). However, while these fluorinated compounds have turned out to be more sensitive and specific, with a clear improvement in the signal-to-noise ratio, a major additional problem has been identified, in the shape of a polymorphism in the TSPO gene (rs6971) that affects TSPO binding, with a significant impact on its visualization and its quantification. To circumvent this drawback, a new generation of rs6971-insensitive TSPO radioligands have been developed, such as flutriciclamide ([18F]-GE180) (149), and this latest generation of tracers is currently under evaluation (150).

Other PET tracers of gliosis have been tested, such as [11C]-DED, which binds to MAO-B, and some results in transgenic animals (151) seem to indicate that gliosis occurs early in AD and precedes the deposition of Aβ senile plaque. Cyclooxygenase was also investigated by Shukuri et al. (152), who showed that

TABLE 3 | Main tau PET tracers, molecular structures, pharmacological properties, and examples of clinical studies.

Compounds	Target/measure	Affinity (nM)	Comments	Clinical studies
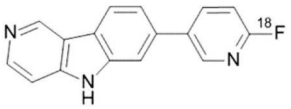 [^{18}F]-flortaucipir (AV1451, T807)	PHF-tau	K_d = 14.6 (88)	25 time more selective for tau PHF than for Aβ. Low retention in white matter. Off-target binding has been reported in the basal ganglia and substantia nigra in the absence of tau pathology.	AD (134–137)
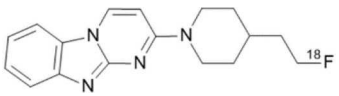 [^{18}F]-T808	PHF-tau	K_d = 22 (138)	Slow metabolic defluorination (139)	AD (120)
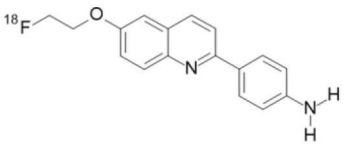 [^{18}F]-THK523	PHF-tau	K_d = 86 (88)	12-fold selectivity for tau over Aβ. High retention in white matter.	AD (118)
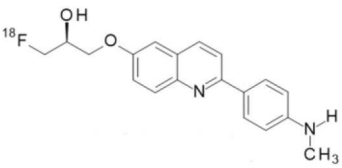 [^{18}F]-THK5117	PHF-tau	K_d = 5.19 (88)	High binding selectivity to tau over Aβ. Substantial white matter binding.	AD (140)
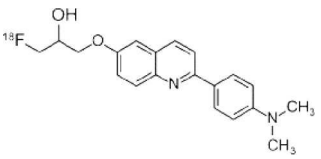 [^{18}F]-THK5105	PHF-tau	K_d = 2,63 (88)	Higher binding affinity to tau fibrils than to Aβ1–42 fibrils (K_d = 35.9 nM) (141) Substantial white matter binding.	AD (115, 142)
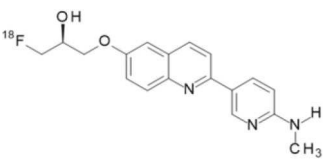 [^{18}F]-THK5351	PHF-tau	K_d = 2.9 (88)	Low binding affinity for white matter, and rapid pharmacokinetics. It also bind to MAO-B sites (110)	AD (119)
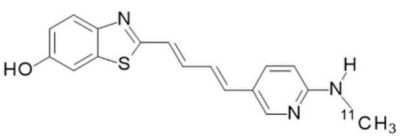 [^{11}C]-PBB3	PHF and non-PHF tau	K_d = 100 (88)	40–50 fold higher affinityfor NFTs than for Aβ, rapid washout, minimal white matter binding, but it metabolizes to a radiolabeled compound that cross the BBB (110)	AD (143), PSP (144), Amyotrophic lateral sclerosis/parkinsonism dementia complex [ALS/PDC (145)]
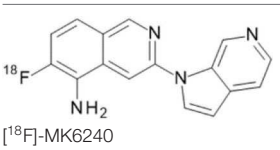 [^{18}F]-MK6240	PHF-tau	K_i = 0.36±0.8 (88)	Poor affinity for Aβ plaques (K_i = 10 μM) (127) No apparent off-target binding.	AD (128)

[11C]-ketoprofen methyl ester, a specific tracer of COX1, is useful for imaging cerebral inflammation in injured rats, with very different kinetics from TSPO tracers. However, a study in humans with this ketoprofen derivative in 2016 (153) failed to yield positive results, suggesting that COX1 expression is more specific for acute inflammation than for chronic inflammation.

Recently, researchers have shown increasing interest in the ROS system. In cardiology, [18F]-DHMT makes it possible

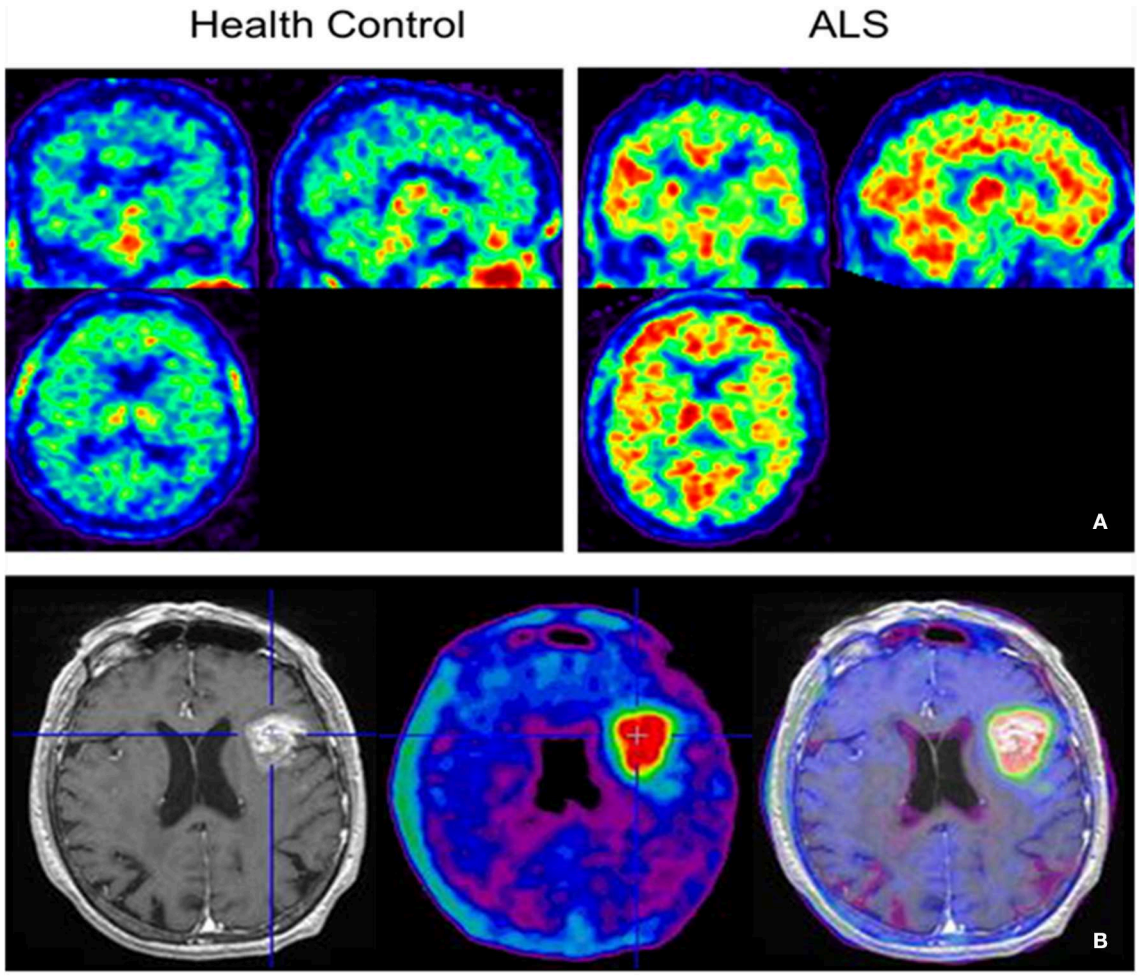

FIGURE 3 | [18F]-DPA-714 images obtained from two clinical studies: **(A)** Comparison between Amyotrophic Lateral Sclerosis (ALS) patients and healthy individuals, and **(B)** stroke patient.

to visualize early ROS activation prior to ventricular function deterioration induced by doxorubicin toxicity (154). In neurology, [18F]-ROStrace, a tracer trapped in the brain when it is metabolized by ROS is currently being assessed in models of AD, PD and other neurodegenerative diseases (155).

These tracers are summarized in **Table 4**.

GLUTAMATE RECEPTORS

Glutamate is the most abundant excitatory neurotransmitter, and glutamate receptors (GluRs) are implicated in plenty of neurological functions within the central nervous system (CNS). GluRs are classified into two groups: ionotropic receptors (iGluRs) and metabotropic receptors (mGluRs). iGluRs form ligand-gated ion channels and are divided into three subtypes based on their pharmacological properties: NMDA (N-methyl-D-aspartate receptors, NMDARs), AMPA (α-amino-3-hydroxy-5-methylisoxazole-4-proprionic acid) receptors, and kainate receptors. mGluRs are G-protein coupled receptors and include eight receptor subtypes, classified into three groups according to their sequence homology, signal transduction, and pharmacological profiles. Group I is comprised of mGluR1 and mGluR5, group II includes mGluR2 and mGluR3, and group III contains mGluR4, mGluR6, mGluR7, and mGluR8 (171). A dysfunction of these receptors may be involved in the pathophysiology of numerous brain disorders. Several PET and SPECT probes have been developed for GluRs imaging (**Table 5**).

NMDARs

Linked to ligand- and voltage-gated ion channels, NMDARs play an important role in many biological functions, including neurotransmission, neuroprotection, neurodegeneration, long-term potentiation, memory, and neurogenesis (188). These receptors are heteromeric multimers composed of one GluN1 (NR1 subunit) and combinations of GluN2 (NR2 subunits) (189) and GluN3 (NR3 subunits) (190). NR2 subunits come in four subtypes (A D) that determine the type of receptor, with A and B being the most widespread. NR2B subunits, preferentially

TABLE 4 | Main PET tracers for neuroinflammation imaging, molecular structures, pharmacological properties, and examples of clinical studies.

Compounds	Target/measure	Affinity (nM)	Clinical studies	Compounds	Target/ measure	Affinity (nM)	Clinical studies
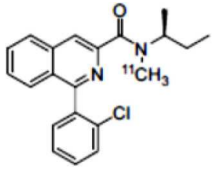 [^{11}C]-(R)-PK11195	TSPO density	K_i = 9.3 in rat (156)	AD (157, 158), PSP (157), multiple sclerosis (MS), PD, ALS, HI, Rasmussen's encepha-litis, Herpes encephalitis, Schizophrenia (156)	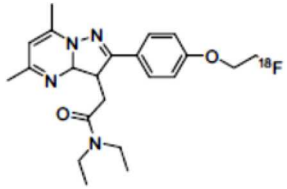 [^{18}F]-DPA714	TSPO density	K_i = 7.0 in rat (156)	AD (159, 160)
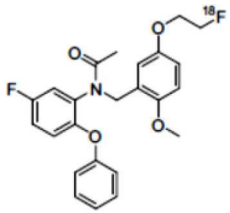 [^{18}F]-FEDAA1106	TSPO density	K_i = 0.078 in rat (156)	AD (161) MS (162)	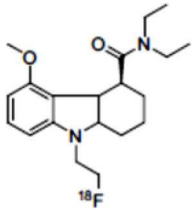 [^{18}F]-GE180	TSPO density	K_d = 0.87 in rats (163)	MS (164)
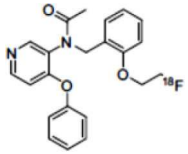 [^{18}F]-FEPPA	TSPO density	K_i = 0.07 in rat (156)	AD (165)	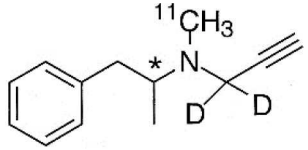 [^{11}C]-DED	MAO-B activity	NA	AD (166)
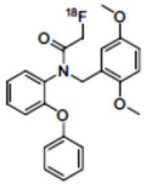 [^{18}F]-PBR06	TSPO density	K_i = 0.30 in monkey (156)	MS (167)	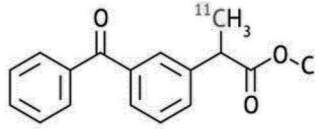 [^{11}C]-ketoprofen methyl ester	COX-1	IC_{50} = 47 (COX-1) IC_{50} = 2.9μM (COX-2) (152)	AD (153)
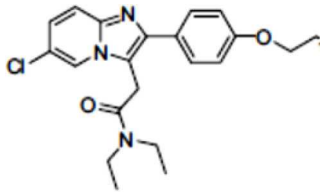 [^{18}F]-PBR111	TSPO density	K_i = 3.70 in rat (156)	MS (168) Schizophrenia (169) Epilepsy (170)	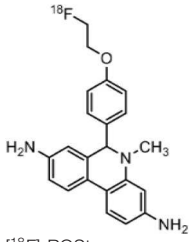 [^{18}F]-ROStrace	ROS activity	NA	Preclinical studies

TABLE 5 | Main SPECT and PET glutamatergic tracers, molecular structures, pharmacological properties, and examples of clinical studies.

Compounds	Imaging modality	Target/ measure	Affinity (nM)	Clinical studies	Compounds	Imaging modality	Target/ measure	Affinity (nM)	Clinical studies
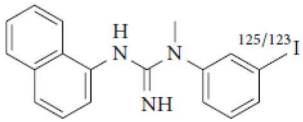 [$^{123/125}$I]-CNS-1261	SPECT	NMDARs density	K_i = 4.2 (171)	Schizophrenia (172, 173)	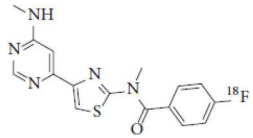 [^{18}F]-FIMX	PET	mGlu1Rs density	IC_{50} = 1.8 (171)	(174)
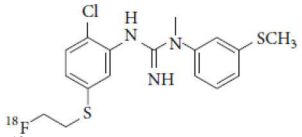 [^{18}F]-GE-179	PET	NMDARs density	K_i = 2.4 (171)	-	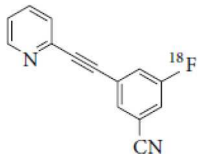 [^{18}F]-FPEB	PET	mGlu5Rs density	K_i = 0.2 (171)	PD (175), alcohol dependence (176), depression (177), autism (178)
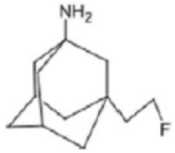 [^{18}F]-FNM	PET	NMDARs density	K_i = 3500 (179)	Tourette's syndrome (GlutaTour project, ToNIC TMBI)	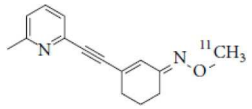 (E)-[^{11}C-]ABP688	PET	mGlu5Rs density	K_d = 5.7 (171)	Cocaine addiction (180), depression (181), FTD (182), alcohol dependence (183)
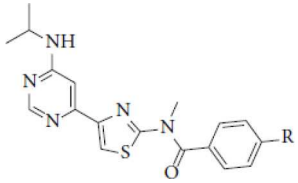 [^{11}C]-ITMM: R = O^{11}CH3 [^{11}C]-ITDM: R = ^{11}CH3	PET	mGlu1Rs density	K_i = 12.6 ([^{11}C]-ITMM) (171)	(184)	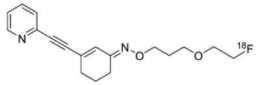 [^{18}F]-PSS232	PET	mGlu5Rs density	K_i = 1 (E-isomer) (185)	(186)
			K_i = 13.6 ([^{11}C]-ITDM) (171)	Preclinical studies	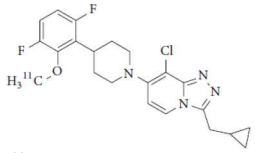 [^{11}C]-JNJ42491293	PET	mGlu2Rs density	IC_{50} = 9.2 (171)	(187)

expressed on primary afferent fibers (PAFs), play a particular role in the transmission of pain messages (191). NMDARs activation requires several types of agonists interacting in cooperation and the simultaneous presence of strong membrane depolarization. Furthermore, NMDARs activation is modulated by extracellular Mg2+, which exerts a voltage-dependent blockade of the open ion channel (192). First, two co-agonists, glutamate and glycine, have to simultaneously bind to their respective sites. Membrane depolarization then causes the release of Mg^{2+} from the channel to allow for the intraneuronal entry of calcium, the starting point for the synthesis of second and third messengers [e.g., prostaglandins and nitric oxide (NO)] (193). Under physiological conditions of synaptic transmission, NMDARs are activated for only brief periods of time. However, in pathological circumstances, their overactivation causes excessive Ca^{2+} influx into nerve cells, and can lead to cell death (194). This abnormal mechanism mediates excitotoxic neuronal injury after acute brain damage (195) and is thought to contribute to disorders of neuronal hyperexcitability (e.g., epilepsy) and chronic neurodegenerative (e.g., AD, Huntington's) (196) and psychotic (197) disorders. Several tracers have been synthesized in order to better understand the physiopathology of these diseases. Most of them are phencyclidine site ligands (PCP) that selectively bind to ion channels in the open and active state. These tracers thus make it possible to visualize only activated NMDARs. Several 123I-, 125I-, 11C-, or 18F-labeled SPECT/PET radiotracers have been developed, based on phencyclidine (PCP), thienylcyclohexyl piperidine (TCP) (198, 199), ketamine (200), memantine (201, 202) or MK-801 (203, 204), as these ligands are known to inhibit the intrachannel PCP sites of NMDARs. Although most of these radiotracers have been found to cross the BBB, none of them have detectable specific binding *in vivo*, owing to high non-specific binding, poor brain retention, or insufficient affinity for the small number of specific binding sites (205, 206). To our knowledge, only few NMDARs radiotracers have been used in human studies. The diarylguanidine analog, [123I]-CNS-1261 exhibited limited success in a clinical study of patients with schizophrenia (207). In PET imaging, despite encouraging results (208), a recent preclinical study using [18F]GE-179 was unable to demonstrate displaceable *in vivo* binding that would have been evidence of an *in vivo* activity-dependent NMDA signal in rats and primates (209–211). Recently, a new [18F]-labeled derivative of memantine, [18F]-fluoroethylnormemantine ([18F]-FNM), was synthesized. *In vivo* evaluation of this novel PET tracer has yielded encouraging results (179, 212), and it had been injected for the first time into humans, in a pilot study to explore the glutamatergic system in patients with Tourette syndrome (GlutaTour project, ToNIC TMBI) (**Figure 4**).

Other NMDAR binding sites, such as the glycine and NR2B sites located on the receptor's extracellular domain, have been the subject of various studies aimed at developing new tracers. However, radiotracer development for these targets has so far been unsuccessful, owing to the ligands' suboptimum physiochemical and pharmacological characteristics, such as affinity, lipophilicity, stability, BBB penetration and pharmacokinetics (171, 205, 206, 213–215).

mGluR

Group I

Group I mGluRs, predominantly expressed postsynaptically, are involved in modulation of synaptic plasticity, and their activation leads to increased neuronal excitability. They are implicated in the physiopathology of several neurological and psychiatric disorder, such as PD, motor dysfunction, multiple sclerosis, epilepsy and stroke, and are the target of recently developed PET probes (171).

mGluR1

mGluR1 are found extensively throughout the brain, but are highly expressed in the cerebellar cortex, hippocampus and thalamus. mGluR1 antagonists have shown promising anxiolytic and antidepressant effects, whereas positive modulators of mGluR1 have been reported to be useful for the treatment of schizophrenia (171). Among all developed molecules to image them, only two radioligands have been injected into humans. The first is [11C]-ITMM. *In vitro* and preclinical studies found that this ligand had high affinity and selectivity for mGluR1,

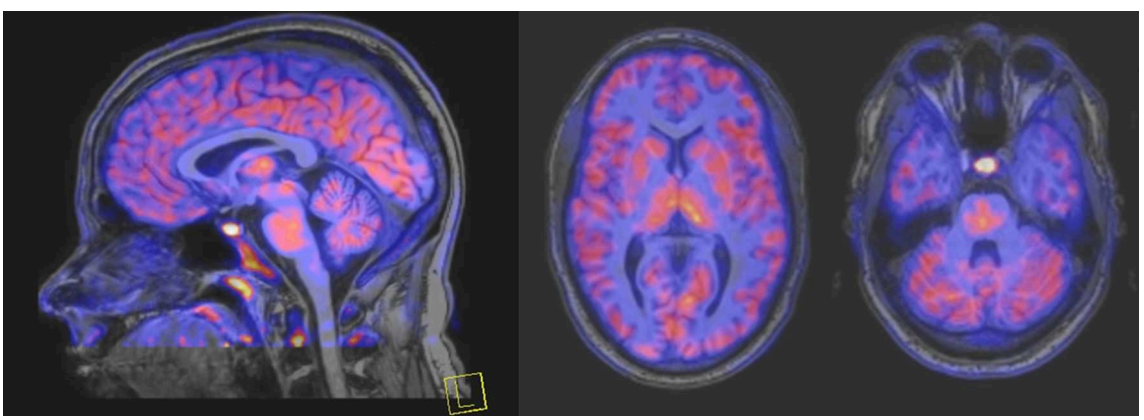

FIGURE 4 | Images from first-in-man injection of [18F]-FNM in a Tourette's syndrome patient (GlutaTour project).

and displayed high brain uptake, with highest uptake in the cerebellum (richest mGluR1 area). This cerebellar uptake has also been observed in human PET studies, however, [11C]-ITMM showed relatively low uptake in the brain regions with modest expression of mGluR1, such as thalamus, hippocampus, and cerebral cortex, making it difficult to examine target density in these regions (184). Nevertheless, [11C]-ITMM could be used to evaluate alterations in cerebellar mGluR1 under pathological conditions, and further clinical studies may be needed to assess the usefulness of this radioligand as a PET probe for mGluR1 quantification. [11C]-ITDM, an analog of ITMM, was considered superior to [11C]-ITMM after *in vivo* studies in monkeys because of its higher regional distribution volume in the mGluR1-rich region (216). To our knowledge, clinical PET studies with this radiotracer have not been published.

Finally, [18F]-FIMX, is the second high affinity mGluR1 radioligand injected into humans. The rank order of this tracer uptake correlated well with mGluR1 expression levels in the human brain, with a highest uptake in the cerebellum (174).

mGluR5

mGluR5 are found in the cerebral cortex, hippocampus, accessory olfactory bulbs, and nucleus accumbens (171). In physiological conditions, mGluR5 activates an intracellular cascade by second messenger processes and modulates functions as diverse as memory, anxiety, or learning. It has been demonstrated that the disruption of brain homeostasis in pathological conditions causes hyperactivation of mGluR5, which then contributes to excitotoxicity. mGluR5 dysregulation is therefore implicated in a broad variety of neuropsychiatric disorders and mGluR5 is recognized as a relevant molecular biomarker of glutamate pathology in these diseases. PET imaging of mGluR5 has expanded in recent years and has contributed to go deeper in the pathophysiology of brain diseases and to better evaluate new treatment strategies. Several PET radioligands targeting mGluR5 have been synthetized (205, 217) and the most promising candidates are currently being investigated in several preclinical and clinical studies.

[18F]-FPEB has been developed by Merck Research Laboratories and, regarding its high specificity and selectivity for mGluR5, together with a suitable brain kinetics (218, 219), has been extensively used to investigate mGluR5 density in neurological disorders. In neurology, [18F]-FPEB has shown mGluR5 upregulation in Parkinson's Disease (220), but recent main contributions of [18F]-FPEB imaging are about psychiatry and addictions. Thus, Leurquin-Sterk et al. studied the effects of acute alcohol intake on the glutamatergic system (221), and demonstrated that mGluR5 availability was lower in limbic regions of alcohol-dependent subjects than in healthy controls, suggesting that limbic mGluR5 was involved in a compensatory mechanism helping to reduce craving during abstinence (176). The alteration of mGluR5 availability was also demonstrated in posttraumatic stress disorder, with a higher cortical [18F]-FPEB *in vivo* binding that was positively correlated with avoidance symptoms (222). Besides, [18F]-FPEB PET imaging did not find any mGluR5 contribution in Major Depressive Disorder (177), whereas, considering neurodevelopmental diseases, an increased [18F]-FPEB binding was observed in postcentral gyrus and cerebellum of male individuals with autism Specter disorder (178).

[11C]ABP688 is a selective, high-affinity mGluR5 antagonist widely used in mGluR5 clinical PET imaging (223, 224). Recently, [11C]ABP688 revealed *in vivo* evidence of reduced availability of mGluR5 in behavioral variant frontotemporal dementia (182) and in focal cortical dysplasia, in tissue resected from epilepsy patients (225). Whereas, Akkus et al. reported no significance difference in [11C]ABP688 binding in individuals with schizophrenia compared with healthy controls (226), a multi-modal imaging approach, combining mGluR5 PET imaging with [11C]ABP688 together with fMRI reported a lower mGluR5 availability and related functional connectivity alterations in drug-naïve young adults with major depression (227). Esterlis et al. confirmed this hypothesis and objectified an antidepressant response of ketamine through a change in [11C]ABP688 binding that was associated with a significant reduction in depressive symptoms following ketamine administration (228). In alcohol consumption abuse, [11C]ABP688 evidenced altered mGluR5 signaling in the amygdala, that was correlated with the temptation to drink (183).

Regarding the limitations in clinical availability of [11C]ABP688, due to the short physical half-life of carbon-11, fluorinated ABP688 derivatives have been proposed, including the promising radioligand [18F]PSS232. After a preclinical validation evidencing specific and selective *in vitro* and *in vivo* properties (185), Warnock et al. reported recently the first-in-human evaluation of this tracer, highlighting in healthy volunteers a favorable brain uptake pattern and kinetics of [18F]PSS232 (186).

These clinical studies, with sometimes ambiguous or even discordant results, must be put in perspective with regard to the influence of the intrasynaptic concentration in endogenous glutamate on the binding of radioligands. For that purpose, pharmacological challenges have been performed in both preclinical and clinical settings, using several glutamate modulators, including ceftriaxone, a potent GLT-1 activator that decreases extracellular levels of glutamate, N-acetylcysteine (NAC), a promoter of the cysteine–glutamate antiporter that increases extrasynaptic glutamate release, and ketamine, an NMDA glutamate receptor antagonist, that increases glutamate release when administered at subanesthetic doses. To date, these pharmacological explorations remain equivocal according to: 1- the pharmacological compound used; 2- the tested radioligand; 3- the studied species (rodents, non-human primates, or human subjects). Thus, whereas ketamine administration decreases [11C]ABP688 binding *in vivo* in human subjects (229), this result has not been confirmed in rats (230). On the other hand, [18F]PSS232 binding appears to be not impacted to neither acute glutamate shifts after stimulation with N-acetylcysteine (NAC) in human (231) nor ketamine and ceftriaxone infusions in the rat brain (232). This parameter has to be considered carefully to accurately quantify mGluR5 expression *in vivo* using PET.

Group II and III

Group II and III mGluRs are mostly located within presynaptic regions and involved in the inhibition of neurotransmitter release. Of all the subtypes, only an mGluR2 tracer has been the subject of a human PET study. [11C]JNJ42491293 is a selective, high-affinity radioligand for the positive allosteric modulator (PAM) site of mGluR2. This site is a potential target for treating anxiety, schizophrenia or addiction. In the first human study, its *in vivo* distribution was consistent with known mGluR2 expression patterns (highest uptake in the striatum and cerebellum) (187). Unfortunately, recent experiments showed an off-target binding *in vivo* and [11C]JNJ42491293 was considered unsuitable for *in vivo* imaging of mGluR2 (233).

CHOLINERGIC SYSTEM

The cholinergic system is well known to be involved in cognitive function, and cholinergic dysfunction has been shown to play a key role in the physiopathology of dementia. Targets have been identified by post mortem studies, which have highlighted alterations in functional components of the cholinergic system (234). These include both presynaptic dysfunction [e.g., in acetylcholinesterase (AChE) or vesicular acetylcholine transporters (VAChTs)] and postsynaptic dysfunction [e.g., in nicotinic acetylcholine receptors (nAChR) or muscarinic acetylcholine receptors (mAChR)] (235, 236). Several radiotracers (summarized in **Figure 2**) have been developed for each of these targets.

There are two PET tracer substrates for AChE: [11C]-PMP and [11C]-MP4A. These have been used in several clinical studies over the past two decades to highlight modifications in AChE activity in patients with AD, PD, PSP or LBD (237–242). [11C]MP4A has a high specificity for AChE, but also a high rate of hydrolysis by this enzyme, and radioligand uptake in regions with high AChE activity is therefore strongly dependent on the rate of transport into the brain (243). By contrast, [11C]PMP exhibits a hydrolysis rate that is three to four times slower than that of [11C]MP4A, allowing for more precise estimates of AChE activity in regions of moderate-to-high AChE concentration (244). Presynaptic cholinergic terminal density can also be assessed with selective radioligands for presynaptic VAChTs. This has been done in clinical studies with [123I]-IBVM (237, 245) and, more recently, in PET imaging with [18F]FEOBV (246). [18F]FEOBV exhibits lower binding in the mesopontine junction and medulla than [123I]IBVM, providing a robust index of VAChT binding (247).

Postsynaptic cholinergic dysfunction has been assessed in patients with AD, using (S)-[11C]nicotine (248–250). However, these [11C]nicotine studies were hindered by high levels of non-specific binding, rapid metabolism, and washout from the brain, as well as a strong dependence on cerebral blood flow (234). New PET and SPECT radioligands have recently been developed to target α4β2 nAChR, which is the most severely affected receptor subtype in AD, with reductions of up to 50% in the neocortex, entorhinal cortex and hippocampus (251). Some clinical studies using either the SPECT tracer [123I]-5IA, or the PET tracer [18F]-2FA, in patients with AD have highlighted significant reductions in α4β2 nAChR in several brain areas, correlated with cognitive impairment (252, 253). Furthermore, another study found a negative correlation between α4β2 nAChR availability and Aβ load (measured by [11C]-PIB), suggesting that Aβ deposition induces the degeneration of cholinergic neurons (254). It was suggested 10 years ago that the α7 nAChR subtype plays a neuroprotective role, by modulating the neurotrophic system that is needed to maintain cholinergic neuron integrity, and by stimulating signal transduction pathways that support neuron survival. In AD, α7 nAChR is implicated in Aβ toxicity and tau phosphorylation (255). Moreover, deletion of the α7 nAChR gene has been shown to reduce cognitive impairment in animal models of AD (256). Further PET studies using radioligands specific to the α7 nAChR, such as [18F]ASEM, are needed to determine the relationship between α7 nAChR and AD pathology (234).

In PD, LBD or PSP, mAChR has also been imaged with [123I]QNB and [11C]NMPB (257, 258), which are high-affinity mAChR antagonists with similar chemical structures and regional brain distributions. These radiotracers are able to penetrate the BBB efficiently, but non-specifically in relation to the mAChR subtype (234).

All these cholinergic tracers are resumed in **Figure 5** and **Table 6**.

$GABA_A$ RECEPTORS

γ-Amino butyric acid (GABA), is the predominant inhibitory neurotransmitter in the central nervous system. This neurotransmitter is able to bind to two types of receptor: ionotropic GABAA/C and metabotropic GABAB. GABAA receptors, also known as the central benzodiazepine receptor, are found on most neurons in the brain, and are part of a superfamily of ligand-gated ion channels. They have a primary binding site for GABA, as well as multiple allosteric modulatory sites. When benzodiazepines, or other allosteric modulators such as barbiturates, bind to GABAA receptors, conformational changes increase the permeability of the central pore to chloride ions, resulting in a chloride flux that hyperpolarizes the neuron (271). GABAA receptors can be composed of several subunit isoforms (272), but only pentamers containing α1, α2, α3, α4, or α5 subunits are benzodiazepine sensitive. These various subunits have a region-specific distribution in the brain, and are believed to subserve different functional and physiological roles and mediate a variety of pharmacological effects. Impairment of GABAA receptor function is increasingly recognized to play a major role in the pathophysiology of several neuropsychiatric diseases such as AD, epilepsy, panic disorders, major depression, cortical brain damage following an acute stroke, anxiety disorders, and chronic alcohol dependency (273). Radiotracers that bind to benzodiazepine sites on GABAA receptors (GABAA-BZ sites) have been shown to be useful for investigating these

disorders (274). The first molecules developed for GABAA receptor imaging was carbon-11 labeled benzodiazepines such as [11C]flunitrazepam, [11C]diazepam, or [11C]fludiazepam, but the lack of specificity and *in vivo* affinity of these ligands (Kd $\geq$ 10 nM) did not allow accurate determination of GABAA receptor density (275). The triazolobenzodiazepine [11C]alprazolam have also been investigated. Despite an increased affinity (Kd = 3.4 nM), PET studies in six healthy volunteers showed a low extraction into brain (<1% of injected dose), and a substantial depot effect probably into the lungs (276). Finally, the imidazobenzodiazepine flumazenil (Ro 15-1788 or N-methyl-11C]flumazenil), became the most commonly used radioligand for GABAA receptor imagingand is still extensively used to quantify benzodiazepine binding in the human brain (277–279). It was used to measure changes in GABA levels (280), as well as to quantify BZ receptors density in the epileptic foci of patients with partial epilepsy (281–283), in schizophrenic patients (284), neuronal loss in stroke (285), and more recently as a tool in clinical research to evaluate GABAA receptor occupancy using molecules with potential anxiolytic properties (286). [123I]iomazenil, a iodo-analog of flumazenil with very similar binding profile, has also been widely used in clinical studies (287–289).

[11C]Ro15-4513 is a partial inverse agonist at the GABAA-BZ site, preferentially targeting α5 subunits (290, 291). Like the previous ones, this tracer has also been used in clinical studies to understand the precise involvement of GABAA receptors in different neuropsychiatric diseases and the relationship between GABAA receptor density and clinical symptoms (292, 293).

Several attempts of fluorine-18 labeling of flumazenil were performed. Thus, [18F]-FEF, [18F]-FFMZ, and [18F]-flumazenil have been tested. Studies have demonstrated the superiority of [18F]-flumazenil because of a higher affinity and lower levels of radiometabolites in brain (275, 294). Because of the longer half-life of the isotope, this tracer could become the "gold standard" in benzodiazepine PET studies.

The development of GABAA radioligands (summarized in **Table 7**) need several improvements. Several improvements are needed. First, is to develop receptor subtype specific radioligands such as [11C]Ro15-4513. Radioligands specific for all the GABAA receptor subtypes would be of great importance to PET imaging. The second important enhancement is to develop and apply

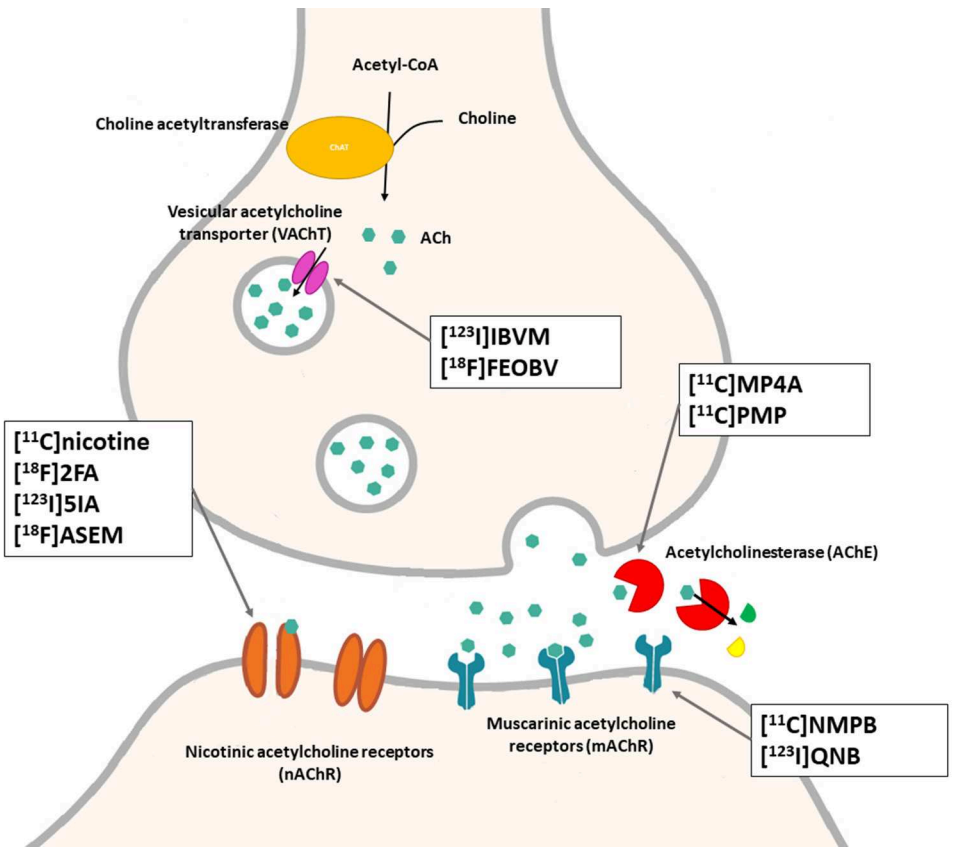

FIGURE 5 | Schematic illustration of the main cholinergic PET and SPECT radioligands, and their presynaptic or postsynaptic targets. Acetylcholine (ACh) is synthesized by choline acetyltransferase from choline and acetylCoA. ACh is released into the synaptic cleft, where it can bind to two types of receptors expressed on postsynaptic neurons: nicotinic receptors (nAChR) and muscarinic receptors (mAChR). ACh is degraded to choline and acetate by acetylcholinesterase (AChE). The reuptake of choline into presynaptic neurons occurs via a choline transporter. Choline is recycled within presynaptic neurons to form ACh, and stored in vesicles by a presynaptic vesicular ACh transporter (VAChT).

TABLE 6 | Main SPECT and PET cholinergic tracers, molecular structures, pharmacological properties, and examples of clinical studies.

Compounds	Imaging modality	Target/ measure	Affinity (nM)	Clinical studies	Compounds	Imaging modality	Target/ measure	Affinity (nM)	Clinical studies
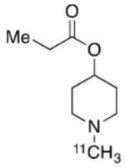 [^{11}C]-PMP	TEP	AChE activity	NA	AD (237, 239, 240, 259), PD (239)	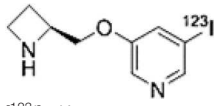 [^{123}I]-5IA	SPECT	α4β2 nAChR density	K_d = 0.011 in rats (260)	AD (252)
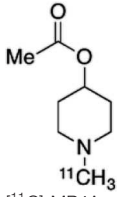 [^{11}C]-MP4A	TEP	AChE activity	NA	AD (242), PD (238, 241), LBD (261), PSP (238)	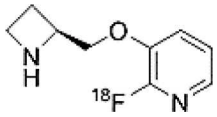 [^{18}F]-2FA	TEP	α4β2 nAChR density	K_i = 0.046 in rats (262)	AD (253)
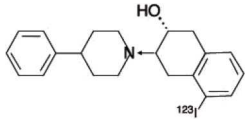 [^{123}I]-IBVM	SPECT	VAChT density	IC_{50} = 2.5±0.2 in rats (263)	MSA (245)	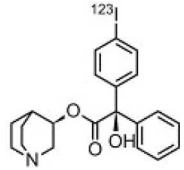 [^{123}I]-QNB	SPECT	mAChR density	IC_{50} = 0.8 in mouse (264)	AD (265), PD, LBD (258)
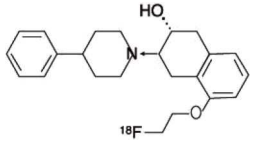 [^{18}F]-FEOBV	TEP	VAChT density		AD (266), LBD (246)	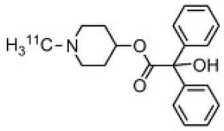 [^{11}C]-NMPB	TEP	mAChR density	IC_{50} = 1.8 in mouse (264)	AD (267), PD, PSP (257)
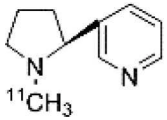 [^{11}C]-nicotine	TEP	α4β2 nAChR density	K_d = 2.4 in rats (268)	AD (248–250)	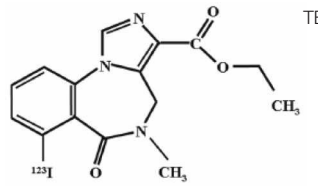 [^{18}F]-ASEM	TEP	α7 nAChR density	K_i = 0.3 in HEK293 cells stably transfected with rat α7 nAChR (269)	Schizophrenia (270)

TABLE 7 | Main radioligands for GABAA receptors imaging, molecular structures, pharmacological properties, and examples of clinical studies.

Compounds	Imaging modality	Target/ measure	Affinity (nM)	Clinical trials
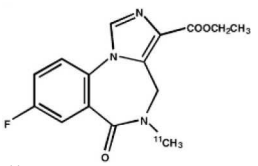 [^{11}C]-FMZ	PET	$GABA_A$-BZ sites (α1, α2, α3, and α5 subunits)	$K_i \approx 1.3$ (BZRs containing α1, α2, α3, or α5 subunits) $K_i \approx 150$ (BZRs containing α4, or α6 subunits) (295)	Epilepsy (281–283) Stroke (285) Schizophrenia (284)
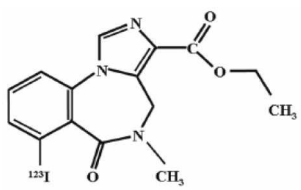 [^{123}I]-IMZ	SPECT	$GABA_A$-BZ sites	$K_i = 0.47$ (in primates) (296)	Stroke (287) Epilepsy (288) Anorexia nervosa (289)
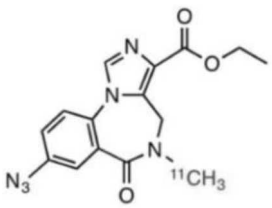 [^{11}C]Ro15-4513	PET	$GABA_A$-BZ sites α5 subtype	$K_i = 0.3$ (BZRs containing α5 subunits) (290)	Alcohol dependence (292) Schizophrenia (293) Autism (297)
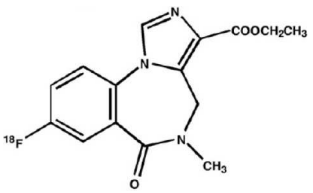 [^{18}F]-flumazenil	PET	$GABA_A$-BZ sites	–	Epilepsy (298, 299)

full agonist radioligands sensitive to changes in endogenous neurotransmitter levels. Finally, development of radiotracers specific to other sites than the BZ binding site will be important in order to further investigate GABAA pharmacology as well as to investigate the role of GABAA receptors in various disease staFinally, development of radiotracers specific to other sites than the BZ binding site will be important in order to further investigate GABAA pharmacology as well as to investigate the role of GABAA receptors in various disease states (275).

SEROTONINERGIC SYSTEM

The serotonergic system plays an important modulatory role in many central nervous system functions. It is the target of many drugs commonly used to treat brain disorders, either through reuptake blockade or via interactions with serotonin (5-HT) receptors. Serotonergic dysfunction has been involved in the etiology of many psychiatric disorders, including depression, anxiety and schizophrenia, as well as neurological diseases such as AD and epilepsy. Currently available radiotracers for *in vivo* brain imaging of the 5-HT system in humans include radioligands for the 5-HT1A, 5-HT1B, 5-HT2A and 5-HT4 receptors, and for the 5-HT transporter (SERT) (300).

The 5-HT1A receptor is one of the most extensively studied receptors in the serotonergic family. Like most 5-HT receptors, it is a G protein-coupled receptor (GPCR) with seven membrane-spanning domains. It serves as an inhibitory autoreceptor in the raphe nuclei, and is targeted by serotonin reuptake inhibitors. It also plays a role with 5-HT4 and 5-HT6 receptors in learning and memory (301, 302). Several radioligands have been synthesized up to now, but only three are in frequent use in clinical studies. The two most widely used are [carbonyl-11C]WAY-100635 and [18F]MPPF (300). These two radioligands are selective and high-affinity 5-HT1A receptor antagonists with a high target-to-background ratio. These tracers have been used in numerous studies of patients with psychiatric disorders such as panic disorder (303), bipolar depression (218) and anorexia nervosa (304), as well as in neurological disorders such as epilepsy, cognitive impairment, AD and migraine (305–311). The third 5-HT1A antagonist radioligand used in clinical studies is [18F]-FCWAY (312), a fluorinated analog of WAY-100635, which also has high 5-HT1A affinity and a high hippocampal-to-cerebellar binding ratio (313–317). However, this compound undergoes

high defluorination *in vivo*, leading to high bone radioactivity uptake. Although this radiodefluorination has been prevented in humans by preadministering disulfiram, this drawback may explain why its use has not been expanded beyond a single PET center (300). A novel and promising 18F-labeled radiotracer, [18F]MefWAY, that is thought to be resistant to defluorination *in vivo* was recently administered to healthy humans, but no clinical study has yet been published (318). There has been recent interest in the use of 5-HT1A agonists to study variations in endogenous 5-HT levels. [11C]CUMI-101 shows high affinity, but its sensitivity to endogenous 5-HT variations *in vivo* has not yet been reported (319).

Because they are involved in the etiology and treatment of many psychiatric disorders, 5-HT2A receptors have also been imaged. Five specific radioligands of this receptor have successfully been used in clinical studies: [123I]-R91150, and the PET radioligands [18F]setoperone, [18F]altanserin, [18F]deuteroaltanserin, and [11C]MDL 100, 907. Despite its low signal-to-noise ratio, [123I]-R91150 has often been used in drug occupancy studies, on account of the widespread availability of SPECT (320, 321). It has also been used to study changes in 5-HT2A receptor density that are implicated in various diseases, including cognitive decline (322), suicidal behavior (323), and anorexia nervosa (324). [18F]altanserin is the most frequently used PET tracer. Although it is metabolized to lipophilic radiometabolites, which contribute to non-specific binding, like the previous one, this tracer has been used to determine 5-HT2A receptor density in relation to several psychiatric diseases, such as depression (325), cognitive decline (326), Tourette's syndrome (327), schizophrenia (328) and other neuropsychiatric disorders (329, 330).

Another target allowing for serotoninergic system imaging is the SERT. Interest in SERT imaging has been stimulated by the success of serotonin reuptake inhibitors. The three most widely used belong to the diarylsulfide family: [11C]-DASB, [11C]-MADAM, [123I]-ADAM (300). These radiotracers have been successfully used to estimate SERT occupancy by selective serotonin reuptake inhibitors (331–337), in order to demonstrate changes in SERT density in several neuropsychiatric disorders and throughout their treatment (338–344), as well as in healthy individuals to investigate physiological variations such as personality traits (345) or seasonal changes (346). Other specific radiotracers for this target are still being developed: 4-[18F]ADAM has yielded promising results (347, 348).

All these serotoninergic tracers are summarized in **Table 8**.

α-SYNUCLEIN

α-synuclein (α-Syn) is a phosphoprotein found in Lewy bodies (LBs), pathological inclusions that are the hallmark of PD and LBD, as well as in the glial cytoplasmic inclusions (GCIs) that are typical of MSA. All these diseases fall now under the heading of synucleinopathies (363). α-Syn aggregates might induce mitochondrial and proteasomal dysfunction, and interfere with vesicular trafficking within dopamine neurons, leading to their degeneration (364). These protein aggregates have been shown to spread from cell to cell via the extracellular space, and the presence of α-Syn has been demonstrated in extracellular matrices such as plasma, conditioned cell media, and cerebrospinal fluid (365, 366). It is thought that occult α-Syn deposition may occur years before the onset of motor symptoms. Hence, accurate and early detection of premotor synucleinopathies may benefit more from α-Syn imaging, rather than from evidence of dopaminergic changes (367, 368). Although several molecules are able to bind to aggregated α-Syn, a selective imaging biomarker has not been found yet. A sensitive and specific α-Syn radiotracer would have to fulfill several criteria. First, α-Syn exist in different forms, including soluble and insoluble oligomers. An imbalance between these two species led to the formation of pathologic aggregates (369, 370), which have to be recognized by the tracer. Secondly, α-Syn aggregates have distinct cellular localization patterns according to the synucleinopathy, with intraneuronal aggregates (e.g., LBs) in PD, and oligodendrocytic aggregates (e.g., GCIs) in MSA. The ideal α-Syn radiotracer would be able to detect and differentiate these different locations, thereby providing a potential tool for differential diagnosis. Third, colocalization between α-Syn aggregates and other aggregating proteins, such as tau and Aβ (371), has frequently been reported. The optimum tracer would have to be able to specifically detect α-Syn with regard to other deposits, despite their small size and low density. Finally, α-Syn undergoes various posttranslational modifications, such as oxidative modification (372), phosphorylation (373, 374), and N-terminal acetylation, all of which the tracer should be able to detect (363).

As explained above, several molecules are able to cross the BBB and bind to aggregated α-Syn. Unfortunately, these molecules also tend to bind to other aggregated proteins, including Aβ plaques. In this context, diverse Aβ-binding compounds have been investigated for potential affinity for α-Syn, such as [11C]-PIB (375), and more especially [18F]-BF227. *In vitro* binding studies indicate that [18F]-BF227 binds with high affinity to two binding sites on Aβ1–42 fibrils, and to one class of binding site on α-Syn fibrils. [18F]-BF227 has been found to bind to Aβ-containing AD brain, but failed to bind to Aβ-free LBD or age-matched control homogenates. Furthermore, [18F]-BF227 labeled both Aβ plaques and LBs in an immunohistochemical/fluorescence analysis of human AD and PD brain sections (376). [18F]-BF227 has also been reported to stain GCIs in post mortem tissues, and [11C]-BF227 PET was used to measure the aggregated α-Syn load in eight cases of probable MSA (377). This study demonstrated high signals in GCI-rich brain regions, including subcortical white matter and the putamen, globus pallidus, primary motor cortex, and anterior and posterior cingulate cortex. However, a very recent autoradiography study failed to support binding of [18F]BF-227 to CGI at concentrations typically achieved in PET experiments (378). The lack of specificity and affinity of [18F]-BF227 means that it cannot be used to diagnose synucleinopathies, although it could, theoretically, still be used to monitor changes in α-Syn aggregate load after interventions such as immunotherapy. Levels of other aggregated proteins, such as Aβ, would first have to be independently determined (368).

TABLE 8 | Main serotoninergic radioligands, molecular structures, pharmacological properties, and examples of clinical studies.

Compounds	Imaging modality	Target/ measure	Affinity (nM)	Clinical studies	Compounds	Imaging modality	Target/ measure	Affinity (nM)	Clinical studies
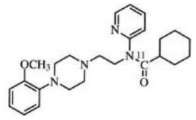 [^{11}C]-WAY-100635	PET	5-HT$_{1A}$ density (antagonist)	K_d = 0.2–0.4 (300)	PD (306), depression (349), panic disorder (303), social anxiety disorder (302), anorexia nervosa (304)	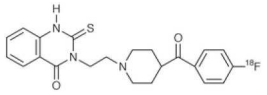 [^{18}F]altanserin	PET	5-HT$_{2A}$ density	K_i = 0.13 (300)	AD (326), depression (325), schizophrenia (328), Tourette's syndrome (327), anorexia nervosa (329), obsessive compulsive disorder (330)
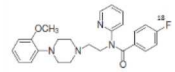 [^{18}F]MPPF	PET	5-HT$_{1A}$ density (antagonist)	K_d = 0.3 (300)	AD (308), epilepsy (282, 307, 311), migraine (309, 310)	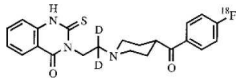 [^{18}F]deuteroaltanserin	PET	5-HT$_{2A}$ density	–	AD (350)
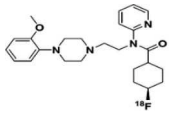 [^{18}F]FCWAY	PET	5-HT$_{1A}$ density (antagonist)	K_i = 0.25 (300)	Epilepsy (313–315), panic disorder (316)	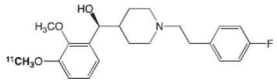 [^{11}C]MDL-100,907	PET	5-HT$_{2A}$ density	K_d = 0.14–0.19 (300)	Depression (351), obsessive compulsive disorder (352)
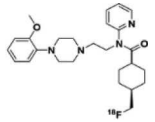 [^{18}F]MefWAY	PET	5-HT$_{1A}$ density (antagonist)	IC_{50} = 26 in rats (353)	–	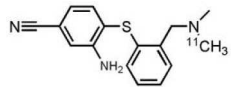 [^{11}C]DASB	PET	SERT density	Ki = 0.97±0.07(354)	Depression (340), schizophrenia (341), alcohol dependence (343), obsessive compulsive disorder (342), bipolar disorder (344)
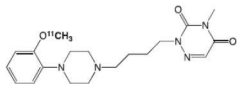 [^{11}C]CUMI-101	PET	5-HT$_{1A}$ density (partial agonist)	K_i = 0.15 (300)	Measure of endogenous changes in serotonergic neurotransmission (355)	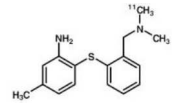 [^{11}C]MADAM	PET	SERT density	Kd = 0.02 (356)*	–
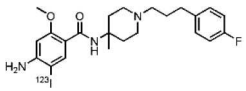 [^{123}I]R91150	SPECT	5-HT$_{2A}$ density	K_d = 0.11 (300)	AD (322), anorexia nervosa (324), suicidal behavior (323)	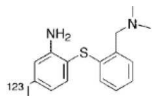 [^{123}I]ADAM	SPECT	SERT density	Kd = 0.03 (356)	Depression (338), migraine (339)
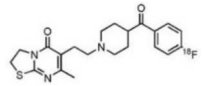 [^{18}F]setoperone	PET	5-HT$_{2A}$ density	K_d = 0.7 in rats (357)	AD (358), migraine (359), stroke (360), depression (361)	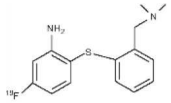 4-[^{18}F]ADAM	PET	SERT density	K_i = 0.081 (362)	Depression (348)

**Determined for [3H]MADAM.*

TABLE 9 | Main PET and SPECT radiotracers relevant to α-Syn imaging, molecular structures, pharmacological properties, and examples of clinical trials. *determined for [3H]-PIB.

Compounds	Imaging modality	Affinity for α-Syn fibrils (nM)	Affinity for Aβ fibrils (nM)	Clinical trials
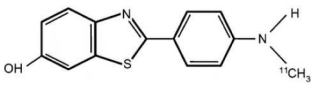 [11C]-PIB	PET	K_d = 4.16* (381)	K_{d1} = 0.71* K_{d2} = 19.80* ($Aβ_{1-42}$ fibrils) (382)	Not used in clinical trials for α-Syn imaging
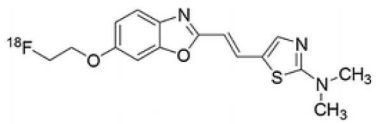 [18F]-BF227	PET	K_d = 14.03 ± 43.52 (380)	K_{d1} = 0.82±1.08 K_{d2} = 125.2±29.05 ($Aβ_{42}$ fibrils) (380)	MSA (377)
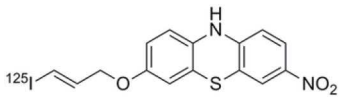 [125I]-SIL23	SPECT	K_d = 148 (379)	K_d = 635 (379)	–

The last reported α-Syn radioligand is [125I]-SIL23 (379). This tracer has been found to bind to α-Syn fibrils in post mortem brain tissue from patients with PD, as well as to α-Syn in a transgenic mouse model for PD. However, the affinity of SIL23 for α-Syn vs. Aβ and tau fibrils is not optimum for imaging fibrillar α-Syn *in vivo*. Moreover, high non-specific binding, including non-specific binding in white matter liable to be secondary to lipophilic interactions, also appeared to limit autoradiography with SIL23 in preliminary experiments.

To conclude, the development of an α-Syn PET radiotracer is particularly challenging, and although several studies have tried to develop suitable PET α-Syn radiotracers (380), the ideal candidate remains elusive. These three radiotracers and their main properties are resumed in **Table 9**.

DISCUSSION

Molecular imaging agents have evolved from non-specific agents to ligands with very high selectivity for specific brain targets such as receptors, neurotransmitter transporters, or abnormal protein deposits over the last decades. Through the nine targets mentioned above, we have seen that the specificity of the ligands for their target is of paramount importance. Indeed, cross binding affinities of several radioligands could reduce the specificity of the results and may interfere with diagnosis.

More and more the diagnosis of dopaminergic disorders is sustained by molecular imaging combined with clinical examination and have been included in guidelines (383, 384). Thus, molecular imaging is used as an ancillary tool when clinical symptoms are insufficient to confirm a diagnosis. Dopaminergic imaging rests on F-DOPA, but mostly on DAT imaging (especially [123I]-FPCIT), which is considered more relevant to evaluate dopaminergic neuron loss. Thus, LBT-999 could be of great interest in the future because of its better sensitivity, and the higher resolution of PET imaging. In parallel, the increase in attempted to graft dopaminergic neurons may drive up F-DOPA imaging to monitor cell survival. An interesting target remain particularly challenging: indeed, to date, α-Syn cannot be specifically detected with existing radiotracers. This target constituting the hallmark of PD, LBD and MSA, its early visualization could be considerably helpful for diagnosis.

In regards to AD imaging, the first investigations was the assessment of cerebral perfusion. Then, [18F]FDG has allowed to assess cerebral glucose metabolism, and remains a widely prescribed exam at present. Within the last decades, amyloid imaging became the most specific examination because of its excellent negative predictive value, and allow therapeutic stratification in clinical trials. In 2007 (later updated in 2010), Dubois and al. published revised criteria for AD that for the first time included AD biomarkers (amyloid PET and CSF Aβ42) as a supportive criteria. However, Aβ plaques are not correlated with cognitive decline, therefore, clinical research is increasingly turning to tau and neuroinflammation imaging to assess new treatments and follow-up disease progression. Further radiotracers targeting other mechanisms, such as [18F]FNM or [18F]-2FA, could be used in AD studies to improve understanding of the cascades of events leading to neurodegeneration.

Psychiatric diseases diagnosis does not call for molecular imaging in clinical routine. However, in psychiatry, physiopathological modifications behind the symptoms remain not well known and understood. Hence, PET and SPECT radioligands such as, serotonergic, GABAergic or glutamatergic tracers, are a powerful tool to improve psychiatric nosography. Nowadays, it is possible to quantify receptors and transporters imbalances in numerous psychiatric diseases including depression, anxiety and schizophrenia, and explore different treatments options. Moreover, several hypothesis suggest a potential link between excitotoxicity and psychiatrics disorders especially schizophrenia. The hypothesis suggest that progressive excitotoxic neural cell death in hippocampal and cortical areas occurs via "disinhibition" of glutamatergic projection to these areas. Disinhibited glutamatergic activity could result from

inhibition of glutamate-mediated neurotransmission and a consequent failure to stimulate inhibitory GABAergic neurons, and/or degeneration of inhibitory GABAergic interneurons (385). Unfortunately, too few studies have been performed yet to highlight this hypothesis. Today, more tracers are be needed to explore glutamatergic and GABAergic systems.

CONCLUSION

After several decades of research, some radiotracers targeting a hallmark of a disease are valuable diagnostic tools in clinical routine and research, and are used on a large scale. Recently, numerous radiotracers have been developed in order to detect primary changes in brain tissue, and improve our understanding of physiopathological mechanisms of neuropsychiatric diseases. These radioligands provide quantitative and topographical information on the evolution of their target during the course of the disease. More than diagnostic tools, they are one of the only ways to better understand the functioning of the brain in the healthy man and in pathological conditions. Their future usefulness is more focused on therapy monitoring than on the diagnosis itself. As in oncology, molecular neuroimaging is now becoming a therapeutic assistance tool, for screening patient's eligibility for drugs and monitoring the proper functioning of therapy. These new companion drugs are a new challenge for molecular imaging, and quantitative and kinetic analyzes seem to be increasingly relevant for image interpretation. Further development in understanding radiotracer metabolization, binding characteristics, BBB crossing, and clinicopathologic correlations of all these imaging probes will assert their clinical utility, and will lead to the development of more neuroimaging probes in the future.

AUTHOR CONTRIBUTIONS

This review was written by MB, A-SS and NA. Correction was made by MR, PD, FL, J-FD, and PP. PP was also involved in the plan development.

FUNDING

This work was supported by Labex IRON (ANR-11-LABX-18-01).

REFERENCES

1. Mankoff DA. A definition of molecular imaging. *J Nucl Med Off Publ Soc Nucl Med.* (2007) 48:18N, 21N.
2. Pysz MA, Gambhir SS, Willmann JK. Molecular imaging: current status and emerging strategies. *Clin Radiol.* (2010) 65:500–16. doi: 10.1016/j.crad.2010.03.011
3. O'Brien TJ, So EL, Mullan BP, Hauser MF, Brinkmann BH, Bohnen NI, et al. Subtraction ictal SPECT co-registered to MRI improves clinical usefulness of SPECT in localizing the surgical seizure focus. *Neurology.* (1998) 50:445–54. doi: 10.1212/WNL.50.2.445
4. Varrone A, Asenbaum S, Vander Borght T, Booij J, Nobili F, Någren K, et al. EANM procedure guidelines for PET brain imaging using [18F]FDG, version 2. *Eur J Nucl Med Mol Imaging.* (2009) 36:2103–10. doi: 10.1007/s00259-009-1264-0
5. Goldman JG, Holden SK, Litvan I, McKeith I, Stebbins GT, Taylor J-P. Evolution of diagnostic criteria and assessments for Parkinson's disease mild cognitive impairment. *Mov Disord Off J Mov Disord Soc.* (2018) 33:503–10. doi: 10.1002/mds.27323
6. Dubois B, Hampel H, Feldman HH, Scheltens P, Aisen P, Andrieu S, et al. Preclinical Alzheimer's disease: definition, natural history, and diagnostic criteria. *Alzheimers Dement.* (2016) 12:292–323. doi: 10.1016/j.jalz.2016.02.002
7. Finnema SJ, Scheinin M, Shahid M, Lehto J, Borroni E, Bang-Andersen B, et al. Application of cross-species PET imaging to assess neurotransmitter release in brain. *Psychopharmacology.* (2015) 232:4129–57. doi: 10.1007/s00213-015-3938-6
8. Baulieu J-L, Le-Pogam A, Leborgne A, Guilloteau D, Prunier-Aesch C. Imagerie moléculaire de la maladie de Parkinson : données actuelles. *Médecine Nucl.* (2008) 32:236–41. doi: 10.1016/j.mednuc.2008.02.001
9. Garnett ES, Firnau G, Nahmias C. Dopamine visualized in the basal ganglia of living man. *Nature.* (1983) 305:137–8. doi: 10.1038/305137a0
10. Becker G, Müller A, Braune S, Büttner T, Benecke R, Greulich W, et al. Early diagnosis of Parkinson's disease. *J Neurol.* (2002) 249:iii40–8. doi: 10.1007/s00415-002-1309-9
11. Snow BJ, Tooyama I, McGeer EG, Yamada T, Calne DB, Takahashi H, et al. Human positron emission tomographic [18F]fluorodopa studies correlate with dopamine cell counts and levels. *Ann Neurol.* (1993) 34:324–30. doi: 10.1002/ana.410340304
12. Ribeiro MJ, Remy P, Bendriem B, Almeida P, Brulon V, Samson Y, et al. Comparison of clinical data sets acquired on different tomographs using 6-18F-L-dopa. *Eur J Nucl Med.* (2000) 27:707–12. doi: 10.1007/s002590050566
13. Ma Y, Tang C, Chaly T, Greene P, Breeze R, Fahn S, et al. Dopamine cell implantation in Parkinson's disease: long-term clinical and (18)F-FDOPA PET outcomes. *J Nucl Med Off Publ Soc Nucl Med.* (2010) 51:7–15. doi: 10.2967/jnumed.109.066811
14. Akamatsu G, Ohnishi A, Aita K, Nishida H, Ikari Y, Sasaki M, et al. A revisit to quantitative PET with 18F-FDOPA of high specific activity using a high-resolution condition in view of application to regenerative therapy. *Ann Nucl Med.* (2017) 31:163–71. doi: 10.1007/s12149-016-1143-2
15. Ziebell M, Holm-Hansen S, Thomsen G, Wagner A, Jensen P, Pinborg LH, et al. Serotonin transporters in dopamine transporter imaging: a head-to-head comparison of dopamine transporter SPECT radioligands 123I-FP-CIT and 123I-PE2I. *J Nucl Med Off Publ Soc Nucl Med.* (2010) 51:1885–91. doi: 10.2967/jnumed.110.078337
16. Ito Y, Fujita M, Shimada S, Watanabe Y, Okada T, Kusuoka H, et al. Comparison between the decrease of dopamine transporter and that of L-DOPA uptake for detection of early to advanced stage of Parkinson's disease in animal models. *Synap N Y N.* (1999) 31:178–85. doi: 10.1002/(SICI)1098-2396(19990301)31:3<178::AID-SYN2>3.0.CO;2-M
17. Eshuis SA, Maguire RP, Leenders KL, Jonkman S, Jager PL. Comparison of FP-CIT SPECT with F-DOPA PET in patients with *de novo* and advanced Parkinson's disease. *Eur J Nucl Med Mol Imaging.* (2006) 33:200–9. doi: 10.1007/s00259-005-1904-y
18. McKeith I, O'Brien J, Walker Z, Tatsch K, Booij J, Darcourt J, et al. Sensitivity and specificity of dopamine transporter imaging with 123I-FP-CIT SPECT in dementia with Lewy bodies: a phase III, multicentre study. *Lancet Neurol.* (2007) 6:305–13. doi: 10.1016/S1474-4422(07)70057-1
19. Mateos JJ, Lomeña F, Parellada E, Mireia F, Fernandez-Egea E, Pavia J, et al. Lower striatal dopamine transporter binding in neuroleptic-naive schizophrenic patients is not related to antipsychotic treatment but it suggests an illness trait. *Psychopharmacology.* (2007) 191:805–11. doi: 10.1007/s00213-006-0570-5
20. Lehto SM, Tolmunen T, Joensuu M, Saarinen PI, Valkonen-Korhonen M, Vanninen R, et al. Changes in midbrain serotonin

transporter availability in atypically depressed subjects after one year of psychotherapy. *Prog Neuropsychopharmacol Biol Psychiatry*. (2008) 32:229–37. doi: 10.1016/j.pnpbp.2007.08.013
21. Huang W-S, Chiang Y-H, Lin J-C, Chou Y-H, Cheng C-Y, Liu R-S. Crossover study of (99m)Tc-TRODAT-1 SPECT and (18)F-FDOPA PET in Parkinson's disease patients. *J Nucl Med Off Publ Soc Nucl Med*. (2003) 44:999–1005.
22. Mozley PD, Schneider JS, Acton PD, Plössl K, Stern MB, Siderowf A, et al. Binding of [99mTc]TRODAT-1 to dopamine transporters in patients with Parkinson's disease and in healthy volunteers. *J Nucl Med Off Publ Soc Nucl Med*. (2000) 41:584–9.
23. Kung MP, Stevenson DA, Plössl K, Meegalla SK, Beckwith A, Essman WD, et al. [99mTc]TRODAT-1: a novel technetium-99m complex as a dopamine transporter imaging agent. *Eur J Nucl Med*. (1997) 24:372–80. doi: 10.1007/BF00881808
24. Huang WS, Lin SZ, Lin JC, Wey SP, Ting G, Liu RS. Evaluation of early-stage Parkinson's disease with 99mTc-TRODAT-1 imaging. *J Nucl Med Off Publ Soc Nucl Med*. (2001) 42:1303–8.
25. Emond P, Guilloteau D, Chalon S. PE2I: a radiopharmaceutical for *in vivo* exploration of the dopamine transporter. *CNS Neurosci Ther*. (2008) 14:47–64. doi: 10.1111/j.1755-5949.2007.00033.x
26. Chalon S, Hall H, Saba W, Garreau L, Dollé F, Halldin C, et al. Pharmacological characterization of (E)-N-(4-fluorobut-2-enyl)-2beta-carbomethoxy-3beta-(4'-tolyl)nortropane (LBT-999) as a highly promising fluorinated ligand for the dopamine transporter. *J Pharmacol Exp Ther*. (2006) 317:147–52. doi: 10.1124/jpet.105.096792
27. Dollé F, Emond P, Mavel S, Demphel S, Hinnen F, Mincheva Z, et al. Synthesis, radiosynthesis and *in vivo* preliminary evaluation of [11C]LBT-999, a selective radioligand for the visualisation of the dopamine transporter with PET. *Bioorg Med Chem*. (2006) 14:1115–25. doi: 10.1016/j.bmc.2005.09.035
28. Saba W, Valette H, Schöllhorn-Peyronneau M-A, Coulon C, Ottaviani M, Chalon S, et al. [11C]LBT-999: a suitable radioligand for investigation of extra-striatal dopamine transporter with PET. *Synap N Y N*. (2007) 61:17–23. doi: 10.1002/syn.20337
29. Varrone A, Stepanov V, Nakao R, Tóth M, Gulyás B, Emond P, et al. Imaging of the striatal and extrastriatal dopamine transporter with (18)F-LBT-999: quantification, biodistribution, and radiation dosimetry in nonhuman primates. *J Nucl Med Off Publ Soc Nucl Med*. (2011) 52:1313–21. doi: 10.2967/jnumed.111.089953
30. Brooks DJ. Technology insight: imaging neurodegeneration in Parkinson's disease. *Nat Clin Pract Neurol*. (2008) 4:267–77. doi: 10.1038/ncpneuro0773
31. Ghadery C, Strafella AP. New imaging markers for movement disorders. *Curr Neurol Neurosci Rep*. (2018) 18:22. doi: 10.1007/s11910-018-0830-x
32. Fuente-Fernández R de la, Sossi V, McCormick S, Schulzer M, Ruth TJ, Stoessl AJ. Visualizing vesicular dopamine dynamics in Parkinson's disease. *Synapse*. (2009) 63:713–6. doi: 10.1002/syn.20653
33. Plotkin M, Amthauer H, Klaffke S, Kühn A, Lüdemann L, Arnold G, et al. Combined 123I-FP-CIT and 123I-IBZM SPECT for the diagnosis of parkinsonian syndromes: study on 72 patients. *J Neural Transm*. (2005) 112:677–92. doi: 10.1007/s00702-004-0208-x
34. Knudsen GM, Karlsborg M, Thomsen G, Krabbe K, Regeur L, Nygaard T, et al. Imaging of dopamine transporters and D2 receptors in patients with Parkinson's disease and multiple system atrophy. *Eur J Nucl Med Mol Imaging*. (2004) 31:1631–8. doi: 10.1007/s00259-004-1578-x
35. Orimo S, Suzuki M, Inaba A, Mizusawa H. 123I-MIBG myocardial scintigraphy for differentiating Parkinson's disease from other neurodegenerative parkinsonism: a systematic review and meta-analysis. *Parkinsonism Relat Disord*. (2012) 18:494–500. doi: 10.1016/j.parkreldis.2012.01.009
36. Volkow ND, Fowler JS, Wang GJ, Baler R, Telang F. Imaging dopamine's role in drug abuse and addiction. *Neuropharmacology*. (2009) 56(Suppl. 1):3–8. doi: 10.1016/j.neuropharm.2008.05.022
37. Shen L-H, Liao M-H, Tseng Y-C. Recent advances in imaging of dopaminergic neurons for evaluation of neuropsychiatric disorders. *J Biomed Biotechnol*. (2012) 2012:259349. doi: 10.1155/2012/259349
38. Klein JC, Eggers C, Kalbe E, Weisenbach S, Hohmann C, Vollmar S, et al. Neurotransmitter changes in dementia with Lewy bodies and Parkinson disease dementia *in vivo*. *Neurology*. (2010) 74:885–92. doi: 10.1212/WNL.0b013e3181d55f61
39. Hu XS, Okamura N, Arai H, Higuchi M, Matsui T, Tashiro M, et al. 18F-fluorodopa PET study of striatal dopamine uptake in the diagnosis of dementia with Lewy bodies. *Neurology*. (2000) 55:1575–7. doi: 10.1212/WNL.55.10.1575
40. Lewis SJ, Pavese N, Rivero-Bosch M, Eggert K, Oertel W, Mathias CJ, et al. Brain monoamine systems in multiple system atrophy: a positron emission tomography study. *Neurobiol Dis*. (2012) 46:130–6. doi: 10.1016/j.nbd.2011.12.053
41. Tai YF, Ahsan RL, de Yébenes JG, Pavese N, Brooks DJ, Piccini P. Characterization of dopaminergic dysfunction in familial progressive supranuclear palsy: an 18F-dopa PET study. *J Neural Transm*. (2007) 114:337–40. doi: 10.1007/s00702-006-0536-0
42. Kilbourn MR. *In vivo* radiotracers for vesicular neurotransmitter transporters. *Nucl Med Biol*. (1997) 24:615–9. doi: 10.1016/S0969-8051(97)00101-7
43. Martin WRW, Wieler M, Stoessl AJ, Schulzer M. Dihydrotetrabenazine positron emission tomography imaging in early, untreated Parkinson's disease. *Ann Neurol*. (2008) 63:388–94. doi: 10.1002/ana.21320
44. Koeppe RA, Gilman S, Junck L, Wernette K, Frey KA. Differentiating Alzheimer's disease from dementia with Lewy bodies and Parkinson's disease with (+)-[11C]dihydrotetrabenazine positron emission tomography. *Alzheimers Dement J Alzheimers Assoc*. (2008) 4(1 Suppl. 1):S67–76. doi: 10.1016/j.jalz.2007.11.016
45. Gilman S, Koeppe RA, Little R, An H, Junck L, Giordani B, et al. Striatal monoamine terminals in Lewy body dementia and Alzheimer's disease. *Ann Neurol*. (2004) 55:774–80. doi: 10.1002/ana.20088
46. Gilman S, Chervin RD, Koeppe RA, Consens FB, Little R, An H, et al. Obstructive sleep apnea is related to a thalamic cholinergic deficit in MSA. *Neurology*. (2003) 61:35–9. doi: 10.1212/01.WNL.0000073624.13436.32
47. Gilman S, Koeppe RA, Chervin RD, Consens FB, Little R, An H, et al. REM sleep behavior disorder is related to striatal monoaminergic deficit in MSA. *Neurology*. (2003) 61:29–34. doi: 10.1212/01.WNL.0000073745.68744.94
48. Emond P, Garreau L, Chalon S, Boazi M, Caillet M, Bricard J, et al. Synthesis and ligand binding of nortropane derivatives: N-substituted 2beta-carbomethoxy-3beta-(4'-iodophenyl)nortropane and N-(3-iodoprop-(2E)-enyl)-2beta-carbomethoxy-3beta-(3',4'-disubstituted phenyl)nortropane. New high-affinity and selective compounds for the dopamine transporter. *J Med Chem*. (1997) 40:1366–72. doi: 10.1021/jm960795d
49. Jennings D, Siderowf A, Stern M, Seibyl J, Eberly S, Oakes D, et al. Imaging prodromal Parkinson disease: the Parkinson Associated Risk Syndrome Study. *Neurology*. (2014) 83:1739–46. doi: 10.1212/WNL.0000000000000960
50. Olanow CW, Jenner P, Brooks D. Dopamine agonists and neuroprotection in Parkinson's disease. *Ann Neurol*. (1998) 44(3 Suppl. 1):S167–174. doi: 10.1002/ana.410440725
51. Parkinson Study Group. Dopamine transporter brain imaging to assess the effects of pramipexole vs levodopa on Parkinson disease progression. *JAMA*. (2002) 287:1653–61. doi: 10.1001/jama.287.13.1653
52. Fahn S, Oakes D, Shoulson I, Kieburtz K, Rudolph A, Lang A, et al. Levodopa and the progression of Parkinson's disease. *N Engl J Med*. (2004) 351:2498–508. doi: 10.1056/NEJMoa033447
53. Lim SM, Katsifis A, Villemagne VL, Best R, Jones G, Saling M, et al. The 18F-FDG PET cingulate island sign and comparison to 123I-beta-CIT SPECT for diagnosis of dementia with Lewy bodies. *J Nucl Med Off Publ Soc Nucl Med*. (2009) 50:1638–45. doi: 10.2967/jnumed.109.065870
54. Tsao H-H, Lin K-J, Juang J-H, Skovronsky DM, Yen T-C, Wey S-P, et al. Binding characteristics of 9-fluoropropyl-(+)-dihydrotetrabenzazine (AV-133) to the vesicular monoamine transporter type 2 in rats. *Nucl Med Biol*. (2010) 37:413–9. doi: 10.1016/j.nucmedbio.2010.01.002
55. Hsiao I-T, Weng Y-H, Hsieh C-J, Lin W-Y, Wey S-P, Kung M-P, et al. Correlation of Parkinson disease severity and 18F-DTBZ positron emission tomography. *JAMA Neurol*. (2014) 71:758–66. doi: 10.1001/jamaneurol.2014.290
56. Villemagne VL, Okamura N, Pejoska S, Drago J, Mulligan RS, Chételat G, et al. *In vivo* assessment of vesicular monoamine transporter type 2 in dementia with lewy bodies and Alzheimer disease. *Arch Neurol*. (2011) 68:905–12. doi: 10.1001/archneurol.2011.142

57. Moccia M, Erro R, Picillo M, Santangelo G, Spina E, Allocca R, et al. A four-year longitudinal study on restless legs syndrome in Parkinson Disease. *Sleep*. (2016) 39:405–12. doi: 10.5665/sleep.5452
58. Filippi L, Manni C, Pierantozzi M, Brusa L, Danieli R, Stanzione P, et al. 123I-FP-CIT in progressive supranuclear palsy and in Parkinson's disease: a SPECT semiquantitative study. *Nucl Med Commun*. (2006) 27:381–6. doi: 10.1097/01.mnm.0000202858.45522.df
59. Booij J, Tissingh G, Boer GJ, Speelman JD, Stoof JC, Janssen AG, et al. [123I]FP-CIT SPECT shows a pronounced decline of striatal dopamine transporter labelling in early and advanced Parkinson's disease. *J Neurol Neurosurg Psychiatry*. (1997) 62:133–40. doi: 10.1136/jnnp.62.2.133
60. Walker Z, Moreno E, Thomas A, Inglis F, Tabet N, Rainer M, et al. Clinical usefulness of dopamine transporter SPECT imaging with 123I-FP-CIT in patients with possible dementia with Lewy bodies: randomised study. *Br J Psychiatry J Ment Sci*. (2015) 206:145–52. doi: 10.1192/bjp.bp.114.148643
61. El Fakhri G, Habert M-O, Maksud P, Kas A, Malek Z, Kijewski MF, et al. Quantitative simultaneous (99m)Tc-ECD/123I-FP-CIT SPECT in Parkinson's disease and multiple system atrophy. *Eur J Nucl Med Mol Imaging*. (2006) 33:87–92. doi: 10.1007/s00259-005-1920-y
62. Brücke T, Yuan Feen Tsai, McLellan C, Singhanyom W, Kung HF, Cohen RM, et al. *In vitro* binding properties and autoradiographic imaging of 3-iodobenzamide ([125I]-IBZM): A potential imaging ligand for D-2 dopamine receptors in spect. *Life Sci*. (1988) 42:2097–104. doi: 10.1016/0024-3205(88)90123-3
63. van Royen E, Verhoeff NF, Speelman JD, Wolters EC, Kuiper MA, Janssen AG. Multiple system atrophy and progressive supranuclear palsy. Diminished striatal D2 dopamine receptor activity demonstrated by 123I-IBZM single photon emission computed tomography. *Arch Neurol*. (1993) 50:513–6. doi: 10.1001/archneur.1993.00540050063017
64. Seppi K, Schocke MFH, Donnemiller E, Esterhammer R, Kremser C, Scherfler C, et al. Comparison of diffusion-weighted imaging and [123I]IBZM-SPECT for the differentiation of patients with the Parkinson variant of multiple system atrophy from those with Parkinson's disease. *Mov Disord Off J Mov Disord Soc*. (2004) 19:1438–45. doi: 10.1002/mds.20229
65. Arnold G, Tatsch K, Oertel WH, Vogl T, Schwarz J, Kraft E, et al. Clinical progressive supranuclear palsy: differential diagnosis by IBZM-SPECT and MRI. *J Neural Transm Suppl*. (1994) 42:111–8. doi: 10.1007/978-3-7091-6641-3_9
66. Van Laere K, De Ceuninck L, Dom R, Van den Eynden J, Vanbilloen H, Cleynhens J, et al. Dopamine transporter SPECT using fast kinetic ligands: 123I-FP-beta-CIT versus 99mTc-TRODAT-1. *Eur J Nucl Med Mol Imaging*. (2004) 31:1119–27. doi: 10.1007/s00259-004-1480-6
67. Kung MP, Kung HF, Billings J, Yang Y, Murphy RA, Alavi A. The characterization of IBF as a new selective dopamine D-2 receptor imaging agent. *J Nucl Med Off Publ Soc Nucl Med*. (1990) 31:648–54.
68. Kim YJ, Ichise M, Ballinger JR, Vines D, Erami SS, Tatschida T, et al. Combination of dopamine transporter and D2 receptor SPECT in the diagnostic evaluation of PD, MSA, and PSP. *Mov Disord Off J Mov Disord Soc*. (2002) 17:303–12. doi: 10.1002/mds.10042
69. Oyanagi C, Katsumi Y, Hanakawa T, Hayashi T, Thuy D ha D, Hashikawa K, et al. Comparison of striatal dopamine D2 receptors in Parkinson's disease and progressive supranuclear palsy patients using [123I] iodobenzofuran single-photon emission computed tomography. *J Neuroimaging Off J Am Soc Neuroimaging*. (2002) 12:316–24. doi: 10.1111/j.1552-6569.2002.tb00139.x
70. Sonni I, Fazio P, Schain M, Halldin C, Svenningsson P, Farde L, et al. Optimal acquisition time window and simplified quantification of dopamine transporter availability using 18F-FE-PE2I in healthy controls and Parkinson disease patients. *J Nucl Med Off Publ Soc Nucl Med*. (2016) 57:1529–34. doi: 10.2967/jnumed.115.171231
71. Prunier C, Payoux P, Guilloteau D, Chalon S, Giraudeau B, Majorel C, et al. Quantification of dopamine transporter by 123I-PE2I SPECT and the noninvasive Logan graphical method in Parkinson's disease. *J Nucl Med Off Publ Soc Nucl Med*. (2003) 44:663–70.
72. Ziebell M, Andersen BB, Pinborg LH, Knudsen GM, Stokholm J, Thomsen G, et al. Striatal dopamine transporter binding does not correlate with clinical severity in dementia with Lewy bodies. *J Nucl Med Off Publ Soc Nucl Med*. (2013) 54:1072–6. doi: 10.2967/jnumed.112.114025
73. Warren NM, Piggott MA, Greally E, Lake M, Lees AJ, Burn DJ. Basal ganglia cholinergic and dopaminergic function in progressive supranuclear palsy. *Mov Disord Off J Mov Disord Soc*. (2007) 22:1594–600. doi: 10.1002/mds.21573
74. Hall H, Ogren SO, Köhler C, Magnusson O. Animal pharmacology of raclopride, a selective dopamine D2 antagonist. *Psychopharmacol Ser*. (1989) 7:123–30. doi: 10.1007/978-3-642-74430-3_13
75. Antonini A, Leenders KL, Vontobel P, Maguire RP, Missimer J, Psylla M, et al. Complementary PET studies of striatal neuronal function in the differential diagnosis between multiple system atrophy and Parkinson's disease. *Brain J Neurol*. (1997) 120 (Pt 12):2187–95. doi: 10.1093/brain/120.12.2187
76. Van Laere K, Clerinx K, D'Hondt E, de Groot T, Vandenberghe W. Combined striatal binding and cerebral influx analysis of dynamic 11C-raclopride PET improves early differentiation between multiple-system atrophy and Parkinson disease. *J Nucl Med Off Publ Soc Nucl Med*. (2010) 51:588–95. doi: 10.2967/jnumed.109.070144
77. Sérrière S, Tauber C, Vercouillie J, Guilloteau D, Deloye J-B, Garreau L, et al. *In vivo* PET quantification of the dopamine transporter in rat brain with [^{18}F]LBT-999. *Nucl Med Biol*. (2014) 41:106–13. doi: 10.1016/j.nucmedbio.2013.09.007
78. Mukherjee J, Yang Z-Y, Brown T, Roemer J, Cooper M. 18F-desmethoxyfallypride: A fluorine-18 labeled radiotracer with properties similar to carbon-11 raclopride for pet imaging studies of dopamine D2 receptors. *Life Sci*. (1996) 59:669–78. doi: 10.1016/0024-3205(96)00348-7
79. Werhahn KJ, Landvogt C, Klimpe S, Buchholz H-G, Yakushev I, Siessmeier T, et al. Decreased dopamine D2/D3-receptor binding in temporal lobe epilepsy: an [18F]fallypride PET study. *Epilepsia*. (2006) 47:1392–6. doi: 10.1111/j.1528-1167.2006.00561.x
80. Mathis CA, Mason NS, Lopresti BJ, Klunk WE. Development of positron emission tomography β-amyloid plaque imaging agents. *Semin Nucl Med*. (2012) 42:423–32. doi: 10.1053/j.semnuclmed.2012.07.001
81. Jack CR, Knopman DS, Jagust WJ, Shaw LM, Aisen PS, Weiner MW, et al. Hypothetical model of dynamic biomarkers of the Alzheimer's pathological cascade. *Lancet Neurol*. (2010) 9:119–28. doi: 10.1016/S1474-4422(09)70299-6
82. Klunk WE, Engler H, Nordberg A, Wang Y, Blomqvist G, Holt DP, et al. Imaging brain amyloid in Alzheimer's disease with Pittsburgh Compound-B. *Ann Neurol*. (2004) 55:306–19. doi: 10.1002/ana.20009
83. Bacskai BJ, Frosch MP, Freeman SH, Raymond SB, Augustinack JC, Johnson KA, et al. Molecular imaging with Pittsburgh Compound B confirmed at autopsy: a case report. *Arch Neurol*. (2007) 64:431–4. doi: 10.1001/archneur.64.3.431
84. Hatashita S, Yamasaki H. Clinically different stages of Alzheimer's disease associated by amyloid deposition with [11C]-PIB PET imaging. *J Alzheimers Dis JAD*. (2010) 21:995–1003. doi: 10.3233/JAD-2010-100222
85. Fagan AM, Mintun MA, Mach RH, Lee S-Y, Dence CS, Shah AR, et al. Inverse relation between *in vivo* amyloid imaging load and cerebrospinal fluid Abeta42 in humans. *Ann Neurol*. (2006) 59:512–9. doi: 10.1002/ana.20730
86. Chételat G, Villemagne VL, Bourgeat P, Pike KE, Jones G, Ames D, et al. Relationship between atrophy and beta-amyloid deposition in Alzheimer disease. *Ann Neurol*. (2010) 67:317–24. doi: 10.1002/ana.21955
87. Pike KE, Savage G, Villemagne VL, Ng S, Moss SA, Maruff P, et al. Beta-amyloid imaging and memory in non-demented individuals: evidence for preclinical Alzheimer's disease. *Brain J Neurol*. (2007) 130(Pt 11):2837–44. doi: 10.1093/brain/awm238
88. Payoux P, Salabert AS. New PET markers for the diagnosis of dementia. *Curr Opin Neurol*. (2017) 30:608–16. doi: 10.1097/WCO.0000000000000489
89. Newberg AB, Arnold SE, Wintering N, Rovner BW, Alavi A. Initial clinical comparison of 18F-florbetapir and 18F-FDG PET in patients with Alzheimer disease and controls. *J Nucl Med Off Publ Soc Nucl Med*. (2012) 53:902–7. doi: 10.2967/jnumed.111.099606
90. Del Campo N, Payoux P, Djilali A, Delrieu J, Hoogendijk EO, Rolland Y, et al. Relationship of regional brain β-amyloid to gait speed. *Neurology*. (2016) 86:36–43. doi: 10.1212/WNL.0000000000002235
91. Bailly M, Ribeiro MJS, Vercouillie J, Hommet C, Gissot V, Camus V, et al. 18F-FDG and 18F-florbetapir PET in clinical practice: regional analysis in mild cognitive impairment and Alzheimer disease. *Clin Nucl Med*. (2015) 40:e111–6. doi: 10.1097/RLU.0000000000000666

92. Kobylecki C, Langheinrich T, Hinz R, Vardy ERLC, Brown G, Martino M-E, et al. 18F-florbetapir PET in patients with frontotemporal dementia and Alzheimer disease. *J Nucl Med Off Publ Soc Nucl Med*. (2015) 56:386–91. doi: 10.2967/jnumed.114.147454
93. de Lartigue J. Flutemetamol (18F): a β-amyloid positron emission tomography tracer for Alzheimer's and dementia diagnosis. *Drugs Today*. (2014) 50:219–29. doi: 10.1358/dot.2014.050.03.2116672
94. Duara R, Loewenstein DA, Shen Q, Barker W, Potter E, Varon D, et al. Amyloid positron emission tomography with (18)F-flutemetamol and structural magnetic resonance imaging in the classification of mild cognitive impairment and Alzheimer's disease. *Alzheimers Dement J Alzheimers Assoc*. (2013) 9:295–301. doi: 10.1016/j.jalz.2012.01.006
95. Morris E, Chalkidou A, Hammers A, Peacock J, Summers J, Keevil S. Diagnostic accuracy of (18)F amyloid PET tracers for the diagnosis of Alzheimer's disease: a systematic review and meta-analysis. *Eur J Nucl Med Mol Imaging*. (2016) 43:374–85. doi: 10.1007/s00259-015-3228-x
96. Barthel H, Luthardt J, Becker G, Patt M, Hammerstein E, Hartwig K, et al. Individualized quantification of brain β-amyloid burden: results of a proof of mechanism phase 0 florbetaben PET trial in patients with Alzheimer's disease and healthy controls. *Eur J Nucl Med Mol Imaging*. (2011) 38:1702–14. doi: 10.1007/s00259-011-1821-1
97. Chiaravalloti A, Danieli R, Lacanfora A, Palumbo B, Caltagirone C, Schillaci O. Usefulness of 18F florbetaben in diagnosis of Alzheimer's disease and other types of dementia. *Curr Alzheimer Res*. (2017) 14:154–60. doi: 10.2174/1567205013666160620114309
98. Sabri O, Sabbagh MN, Seibyl J, Barthel H, Akatsu H, Ouchi Y, et al. Florbetaben PET imaging to detect amyloid beta plaques in Alzheimer's disease: phase 3 study. *Alzheimers Dement J Alzheimers Assoc*. (2015) 11:964–74. doi: 10.1016/j.jalz.2015.02.004
99. Ong KT, Villemagne VL, Bahar-Fuchs A, Lamb F, Langdon N, Catafau AM, et al. Aβ imaging with 18F-florbetaben in prodromal Alzheimer's disease: a prospective outcome study. *J Neurol Neurosurg Psychiatry*. (2015) 86:431–6. doi: 10.1136/jnnp-2014-308094
100. Knopman DS, DeKosky ST, Cummings JL, Chui H, Corey-Bloom J, Relkin N, et al. Practice parameter: diagnosis of dementia (an evidence-based review). Report of the Quality Standards Subcommittee of the American Academy of Neurology. *Neurology*. (2001) 56:1143–53. doi: 10.1212/WNL.56.9.1143
101. Yeo JM, Waddell B, Khan Z, Pal S. A systematic review and meta-analysis of (18)F-labeled amyloid imaging in Alzheimer's disease. *Alzheimers Dement Amst Neth*. (2015) 1:5–13. doi: 10.1016/j.dadm.2014.11.004
102. Rabinovici GD, Furst AJ, Alkalay A, Racine CA, O'Neil JP, Janabi M, et al. Increased metabolic vulnerability in early-onset Alzheimer's disease is not related to amyloid burden. *Brain J Neurol*. (2010) 133(Pt 2):512–28. doi: 10.1093/brain/awp326
103. Lehmann M, Ghosh PM, Madison C, Laforce R, Corbetta-Rastelli C, Weiner MW, et al. Diverging patterns of amyloid deposition and hypometabolism in clinical variants of probable Alzheimer's disease. *Brain J Neurol*. (2013) 136(Pt 3):844–58. doi: 10.1093/brain/aws327
104. Jung Y, Whitwell JL, Duffy JR, Strand EA, Machulda MM, Senjem ML, et al. Regional β-amyloid burden does not correlate with cognitive or language deficits in Alzheimer's disease presenting as aphasia. *Eur J Neurol*. (2016) 23:313–9. doi: 10.1111/ene.12761
105. Laforce R, Soucy J-P, Sellami L, Dallaire-Théroux C, Brunet F, Bergeron D, et al. Molecular imaging in dementia: Past, present, and future. *Alzheimers Dement*. (2018) 14:1522–52. doi: 10.1016/j.jalz.2018.06.2855
106. Johnson KA, Minoshima S, Bohnen NI, Donohoe KJ, Foster NL, Herscovitch P, et al. Appropriate use criteria for amyloid PET: a report of the Amyloid Imaging Task Force, the Society of Nuclear Medicine and Molecular Imaging, and the Alzheimer's Association. *Alzheimers Dement*. (2013) 9:e-1-16. doi: 10.1016/j.jalz.2013.01.002
107. Weller J, Budson A. Current understanding of Alzheimer's disease diagnosis and treatment. *F1000Res*. (2018) 7:F1000 Faculty Rev-1161. doi: 10.12688/f1000research.14506.1
108. Delrieu J, Ousset PJ, Voisin T, Vellas B. Amyloid beta peptide immunotherapy in Alzheimer disease. *Rev Neurol*. (2014) 170:739–48. doi: 10.1016/j.neurol.2014.10.003
109. Honig LS, Vellas B, Woodward M, Boada M, Bullock R, Borrie M, et al. Trial of solanezumab for mild dementia due to Alzheimer's disease. *N Engl J Med*. (2018) 378:321–30. doi: 10.1056/NEJMoa1705971
110. Hall B, Mak E, Cervenka S, Aigbirhio FI, Rowe JB, O'Brien JT. *In vivo* tau PET imaging in dementia: pathophysiology, radiotracer quantification, and a systematic review of clinical findings. *Ageing Res Rev*. (2017) 36:50–63. doi: 10.1016/j.arr.2017.03.002
111. Gómez-Isla T, Hollister R, West H, Mui S, Growdon JH, Petersen RC, et al. Neuronal loss correlates with but exceeds neurofibrillary tangles in Alzheimer's disease. *Ann Neurol*. (1997) 41:17–24. doi: 10.1002/ana.410410106
112. van Rossum IA, Visser PJ, Knol DL, van der Flier WM, Teunissen CE, Barkhof F, et al. Injury markers but not amyloid markers are associated with rapid progression from mild cognitive impairment to dementia in Alzheimer's disease. *J Alzheimers Dis JAD*. (2012) 29:319–27. doi: 10.3233/JAD-2011-111694
113. Agdeppa ED, Kepe V, Liu J, Flores-Torres S, Satyamurthy N, Petric A, et al. Binding characteristics of radiofluorinated 6-dialkylamino-2-naphthylethylidene derivatives as positron emission tomography imaging probes for beta-amyloid plaques in Alzheimer's disease. *J Neurosci Off J Soc Neurosci*. (2001) 21:RC189. doi: 10.1523/JNEUROSCI.21-24-j0004.2001
114. Luurtsema G, Schuit RC, Takkenkamp K, Lubberink M, Hendrikse NH, Windhorst AD, et al. Peripheral metabolism of [(18)F]FDDNP and cerebral uptake of its labelled metabolites. *Nucl Med Biol*. (2008) 35:869–74. doi: 10.1016/j.nucmedbio.2008.09.002
115. Okamura N, Suemoto T, Furumoto S, Suzuki M, Shimadzu H, Akatsu H, et al. Quinoline and benzimidazole derivatives: candidate probes for *in vivo* imaging of tau pathology in Alzheimer's disease. *J Neurosci Off J Soc Neurosci*. (2005) 25:10857–62. doi: 10.1523/JNEUROSCI.1738-05.2005
116. Fodero-Tavoletti MT, Okamura N, Furumoto S, Mulligan RS, Connor AR, McLean CA, et al. 18F-THK523: a novel *in vivo* tau imaging ligand for Alzheimer's disease. *Brain J Neurol*. (2011) 134(Pt 4):1089–100. doi: 10.1093/brain/awr038
117. Fodero-Tavoletti MT, Furumoto S, Taylor L, McLean CA, Mulligan RS, Birchall I, et al. Assessing THK523 selectivity for tau deposits in Alzheimer's disease and non-Alzheimer's disease tauopathies. *Alzheimers Res Ther*. (2014) 6:11. doi: 10.1186/alzrt240
118. Villemagne VL, Furumoto S, Fodero-Tavoletti MT, Mulligan RS, Hodges J, Harada R, et al. *In vivo* evaluation of a novel tau imaging tracer for Alzheimer's disease. *Eur J Nucl Med Mol Imaging*. (2014) 41:816–26. doi: 10.1007/s00259-013-2681-7
119. Harada R, Okamura N, Furumoto S, Furukawa K, Ishiki A, Tomita N, et al. 18F-THK5351: a novel PET radiotracer for imaging neurofibrillary pathology in Alzheimer disease. *J Nucl Med Off Publ Soc Nucl Med*. (2016) 57:208–14. doi: 10.2967/jnumed.115.164848
120. Chien DT, Bahri S, Szardenings AK, Walsh JC, Mu F, Su M-Y, et al. Early clinical PET imaging results with the novel PHF-tau radioligand [F-18]-T807. *J Alzheimers Dis JAD*. (2013) 34:457–68. doi: 10.3233/JAD-122059
121. Chien DT, Szardenings AK, Bahri S, Walsh JC, Mu F, Xia C, et al. Early clinical PET imaging results with the novel PHF-tau radioligand [F18]-T808. *J Alzheimers Dis JAD*. (2014) 38:171–84. doi: 10.3233/JAD-130098
122. Johnson KA, Schultz A, Betensky RA, Becker JA, Sepulcre J, Rentz D, et al. Tau positron emission tomographic imaging in aging and early Alzheimer disease. *Ann Neurol*. (2016) 79:110–9. doi: 10.1002/ana.24546
123. Brier MR, Gordon B, Friedrichsen K, McCarthy J, Stern A, Christensen J, et al. Tau and Aβ imaging, CSF measures, and cognition in Alzheimer's disease. *Sci Transl Med*. (2016) 8:338ra66. doi: 10.1126/scitranslmed.aaf2362
124. Chhatwal JP, Schultz AP, Marshall GA, Boot B, Gomez-Isla T, Dumurgier J, et al. Temporal T807 binding correlates with CSF tau and phospho-tau in normal elderly. *Neurology*. (2016) 87:920–6. doi: 10.1212/WNL.0000000000003050
125. Lowe VJ, Curran G, Fang P, Liesinger AM, Josephs KA, Parisi JE, et al. An autoradiographic evaluation of AV-1451 Tau PET in dementia. *Acta Neuropathol Commun*. (2016) 4:58. doi: 10.1186/s40478-016-0315-6
126. Walji AM, Hostetler ED, Selnick H, Zeng Z, Miller P, Bennacef I, et al. Discovery of 6-(Fluoro-(18)F)-3-(1H-pyrrolo[2,3-c]pyridin-1-yl)isoquinolin-5-amine ([(18)F]-MK-6240): a Positron

Emission Tomography (PET) Imaging Agent for Quantification of Neurofibrillary Tangles (NFTs). *J Med Chem*. (2016) 59:4778–89. doi: 10.1021/acs.jmedchem.6b00166
127. Hostetler ED, Walji AM, Zeng Z, Miller P, Bennacef I, Salinas C, et al. Preclinical characterization of 18F-MK-6240, a promising PET tracer for *in vivo* quantification of human neurofibrillary tangles. *J Nucl Med Off Publ Soc Nucl Med*. (2016) 57:1599–606. doi: 10.2967/jnumed.115.171678
128. Lohith TG, Bennacef I, Vandenberghe R, Vandenbulcke M, Salinas-Valenzuela C, Declercq R, et al. First-in-human brain imaging of Alzheimer dementia patients and elderly controls with 18F-MK-6240, a PET tracer targeting neurofibrillary tangle pathology. *J Nucl Med Off Publ Soc Nucl Med*. (2019) 60:107–14. doi: 10.2967/jnumed.118.208215
129. Pedersen SF, Sandholt BV, Keller SH, Hansen AE, Clemmensen AE, Sillesen H, et al. 64Cu-DOTATATE PET/MRI for detection of activated macrophages in carotid atherosclerotic plaques. *Arterioscler Thromb Vasc Biol*. (2015) 35:1696–703. doi: 10.1161/ATVBAHA.114.305067
130. Brosch JR, Farlow MR, Risacher SL, Apostolova LG. Tau imaging in alzheimer's disease diagnosis and clinical trials. *Neurotherapeutics*. (2017) 14:62–8. doi: 10.1007/s13311-016-0490-y
131. Rosenmann H. Immunotherapy for targeting tau pathology in Alzheimer's disease and tauopathies. *Curr Alzheimer Res*. (2013) 10:217–28. doi: 10.2174/1567205011310030001
132. Novak P, Schmidt R, Kontsekova E, Zilka N, Kovacech B, Skrabana R, et al. Safety and immunogenicity of the tau vaccine AADvac1 in patients with Alzheimer's disease: a randomised, double-blind, placebo-controlled, phase 1 trial. *Lancet Neurol*. (2017) 16:123–34. doi: 10.1016/S1474-4422(16)30331-3
133. Panza F, Solfrizzi V, Seripa D, Imbimbo BP, Lozupone M, Santamato A, et al. Tau-based therapeutics for Alzheimer's disease: active and passive immunotherapy. *Immunotherapy*. (2016) 8:1119–34. doi: 10.2217/imt-2016-0019
134. Barret O, Alagille D, Sanabria S, Comley RA, Weimer RM, Borroni E, et al. Kinetic modeling of the Tau PET tracer 18F-AV-1451 in human healthy volunteers and Alzheimer disease subjects. *J Nucl Med Off Publ Soc Nucl Med*. (2017) 58:1124–31. doi: 10.2967/jnumed.116.182881
135. Maass A, Landau S, Baker SL, Horng A, Lockhart SN, La Joie R, et al. Comparison of multiple tau-PET measures as biomarkers in aging and Alzheimer's disease. *NeuroImage*. (2017) 157:448–63. doi: 10.1016/j.neuroimage.2017.05.058
136. Bejanin A, Schonhaut DR, La Joie R, Kramer JH, Baker SL, Sosa N, et al. Tau pathology and neurodegeneration contribute to cognitive impairment in Alzheimer's disease. *Brain J Neurol*. (2017) 140:3286–300. doi: 10.1093/brain/awx243
137. Ossenkoppele R, Rabinovici GD, Smith R, Cho H, Schöll M, Strandberg O, et al. Discriminative accuracy of [18F]flortaucipir positron emission tomography for alzheimer disease vs other neurodegenerative disorders. *JAMA*. (2018) 320:1151–62. doi: 10.1001/jama.2018.12917
138. Zhang W, Arteaga J, Cashion DK, Chen G, Gangadharmath U, Gomez LF, et al. A highly selective and specific PET tracer for imaging of tau pathologies. *J Alzheimers Dis JAD*. (2012) 31:601–12. doi: 10.3233/JAD-2012-120712
139. Choe YS, Lee K-H. PET radioligands for imaging of tau pathology: current status. *Nucl Med Mol Imaging*. (2015) 49:251–7. doi: 10.1007/s13139-015-0374-9
140. Harada R, Okamura N, Furumoto S, Furukawa K, Ishiki A, Tomita N, et al. [(18)F]THK-5117 PET for assessing neurofibrillary pathology in Alzheimer's disease. *Eur J Nucl Med Mol Imaging*. (2015) 42:1052–61. doi: 10.1007/s00259-015-3035-4
141. Okamura N, Furumoto S, Harada R, Tago T, Yoshikawa T, Fodero-Tavoletti M, et al. Novel 18F-labeled arylquinoline derivatives for noninvasive imaging of tau pathology in Alzheimer disease. *J Nucl Med Off Publ Soc Nucl Med*. (2013) 54:1420–7. doi: 10.2967/jnumed.112.117341
142. Okamura N, Furumoto S, Fodero-Tavoletti MT, Mulligan RS, Harada R, Yates P, et al. Non-invasive assessment of Alzheimer's disease neurofibrillary pathology using 18F-THK5105 PET. *Brain J Neurol*. (2014) 137(Pt 6):1762–71. doi: 10.1093/brain/awu064
143. Shimada H, Kitamura S, Shinotoh H, Endo H, Niwa F, Hirano S, et al. Association between Aβ and tau accumulations and their influence on clinical features in aging and Alzheimer's disease spectrum brains: A [11C]PBB3-PET study. *Alzheimers Dement Amst Neth*. (2017) 6:11–20. doi: 10.1016/j.jalz.2016.06.998
144. Perez-Soriano A, Arena JE, Dinelle K, Miao Q, McKenzie J, Neilson N, et al. PBB3 imaging in Parkinsonian disorders: evidence for binding to tau and other proteins. *Mov Disord Off J Mov Disord Soc*. (2017) 32:1016–24. doi: 10.1002/mds.27029
145. Shinotoh H, Shimada H, Kokubo Y, Tagai K, Niwa F, Kitamura S, et al. Tau imaging detects distinctive distribution of tau pathology in ALS/PDC on the Kii Peninsula. *Neurology*. (2019) 92:e136–47. doi: 10.1212/WNL.0000000000006736
146. Narayanaswami V, Dahl K, Bernard-Gauthier V, Josephson L, Cumming P, Vasdev N. Emerging PET radiotracers and targets for imaging of neuroinflammation in neurodegenerative diseases: outlook beyond TSPO. *Mol Imaging*. (2018) 17:1536012118792317. doi: 10.1177/1536012118792317
147. Vivash L, O'Brien TJ. Imaging microglial activation with TSPO PET: lighting up neurologic diseases? *J Nucl Med Off Publ Soc Nucl Med*. (2016) 57:165–8. doi: 10.2967/jnumed.114.141713
148. Dupont A-C, Largeau B, Santiago Ribeiro MJ, Guilloteau D, Tronel C, Arlicot N. Translocator Protein-18 kDa (TSPO) Positron Emission Tomography (PET) imaging and its clinical impact in neurodegenerative diseases. *Int J Mol Sci*. (2017) 18:E785. doi: 10.3390/ijms18040785
149. Fan Z, Calsolaro V, Atkinson RA, Femminella GD, Waldman A, Buckley C, et al. Flutriciclamide (18F-GE180) PET: first-in-human PET study of novel third-generation *in vivo* marker of human translocator protein. *J Nucl Med Off Publ Soc Nucl Med*. (2016) 57:1753–9. doi: 10.2967/jnumed.115.169078
150. Ikawa M, Lohith TG, Shrestha S, Telu S, Zoghbi SS, Castellano S, et al. 11C-ER176, a radioligand for 18-kDa translocator protein, has adequate sensitivity to robustly image all three affinity genotypes in human brain. *J Nucl Med Off Publ Soc Nucl Med*. (2017) 58:320–5. doi: 10.2967/jnumed.116.178996
151. Rodriguez-Vieitez E, Ni R, Gulyás B, Tóth M, Häggkvist J, Halldin C, et al. Astrocytosis precedes amyloid plaque deposition in Alzheimer APPswe transgenic mouse brain: a correlative positron emission tomography and *in vitro* imaging study. *Eur J Nucl Med Mol Imaging*. (2015) 42:1119–32. doi: 10.1007/s00259-015-3047-0
152. Shukuri M, Takashima-Hirano M, Tokuda K, Takashima T, Matsumura K, Inoue O, et al. *In vivo* expression of cyclooxygenase-1 in activated microglia and macrophages during neuroinflammation visualized by PET with 11C-ketoprofen methyl ester. *J Nucl Med Off Publ Soc Nucl Med*. (2011) 52:1094–101. doi: 10.2967/jnumed.110.084046
153. Ohnishi A, Senda M, Yamane T, Mikami T, Nishida H, Nishio T, et al. Exploratory human PET study of the effectiveness of (11)C-ketoprofen methyl ester, a potential biomarker of neuroinflammatory processes in Alzheimer's disease. *Nucl Med Biol*. (2016) 43:438–44. doi: 10.1016/j.nucmedbio.2016.04.005
154. Boutagy NE, Wu J, Cai Z, Zhang W, Booth CJ, Kyriakides TC, et al. *In vivo* reactive oxygen species detection with a novel positron emission tomography tracer, 18F-DHMT, allows for early detection of anthracycline-induced cardiotoxicity in rodents. *JACC Basic Transl Sci*. (2018) 3:378–90. doi: 10.1016/j.jacbts.2018.02.003
155. Hou C, Hsieh C-J, Li S, Lee H, Graham TJ, Xu K, et al. Development of a positron emission tomography radiotracer for imaging elevated levels of superoxide in neuroinflammation. *ACS Chem Neurosci*. (2018) 9:578–86. doi: 10.1021/acschemneuro.7b00385
156. Alam MM, Lee J, Lee S-Y. Recent progress in the development of TSPO PET ligands for neuroinflammation imaging in neurological diseases. *Nucl Med Mol Imaging*. (2017) 51:283–96. doi: 10.1007/s13139-017-0475-8
157. Passamonti L, Rodríguez PV, Hong YT, Allinson KSJ, Bevan-Jones WR, Williamson D, et al. [11C]PK11195 binding in Alzheimer disease and progressive supranuclear palsy. *Neurology*. (2018) 90:e1989–96. doi: 10.1212/WNL.0000000000005610
158. Edison P, Archer HA, Gerhard A, Hinz R, Pavese N, Turkheimer FE, et al. Microglia, amyloid, and cognition in Alzheimer's disease: An [11C](R)PK11195-PET and [11C]PIB-PET study. *Neurobiol Dis*. (2008) 32:412–9. doi: 10.1016/j.nbd.2008.08.001
159. Hamelin L, Lagarde J, Dorothée G, Leroy C, Labit M, Comley RA, et al. Early and protective microglial activation in Alzheimer's disease: a prospective

study using 18F-DPA-714 PET imaging. *Brain J Neurol.* (2016) 139(Pt 4):1252–64. doi: 10.1093/brain/aww017
160. Golla SSV, Boellaard R, Oikonen V, Hoffmann A, van Berckel BNM, Windhorst AD, et al. Quantification of [18F]DPA-714 binding in the human brain: initial studies in healthy controls and Alzheimer's disease patients. *J Cereb Blood Flow Metab Off J Int Soc Cereb Blood Flow Metab.* (2015) 35:766–72. doi: 10.1038/jcbfm.2014.261
161. Varrone A, Mattsson P, Forsberg A, Takano A, Nag S, Gulyás B, et al. *In vivo* imaging of the 18-kDa translocator protein (TSPO) with [18F]FEDAA1106 and PET does not show increased binding in Alzheimer's disease patients. *Eur J Nucl Med Mol Imaging.* (2013) 40:921–31. doi: 10.1007/s00259-013-2359-1
162. Takano A, Piehl F, Hillert J, Varrone A, Nag S, Gulyás B, et al. *In vivo* TSPO imaging in patients with multiple sclerosis: a brain PET study with [18F]FEDAA1106. *EJNMMI Res.* (2013) 3:30. doi: 10.1186/2191-219X-3-30
163. Wadsworth H, Jones PA, Chau W-F, Durrant C, Fouladi N, Passmore J, et al. [^{18}F]GE-180: a novel fluorine-18 labelled PET tracer for imaging Translocator protein 18 kDa (TSPO). *Bioorg Med Chem Lett.* (2012) 22:1308–13. doi: 10.1016/j.bmcl.2011.12.084
164. Vomacka L, Albert NL, Lindner S, Unterrainer M, Mahler C, Brendel M, et al. TSPO imaging using the novel PET ligand [18F]GE-180: quantification approaches in patients with multiple sclerosis. *EJNMMI Res.* (2017) 7:89. doi: 10.1186/s13550-017-0340-x
165. Suridjan I, Pollock BG, Verhoeff NPLG, Voineskos AN, Chow T, Rusjan PM, et al. *In-vivo* imaging of grey and white matter neuroinflammation in Alzheimer's disease: a positron emission tomography study with a novel radioligand, [18F]-FEPPA. *Mol Psychiatry.* (2015) 20:1579–87. doi: 10.1038/mp.2015.1
166. Rodriguez-Vieitez E, Saint-Aubert L, Carter SF, Almkvist O, Farid K, Schöll M, et al. Diverging longitudinal changes in astrocytosis and amyloid PET in autosomal dominant Alzheimer's disease. *Brain J Neurol.* (2016) 139(Pt 3):922–36. doi: 10.1093/brain/awv404
167. Singhal T, O'Connor K, Dubey S, Belanger AP, Hurwitz S, Chu R, et al. 18F-PBR06 versus 11C-PBR28 PET for assessing white matter translocator protein binding in multiple sclerosis. *Clin Nucl Med.* (2018) 43:e289–95. doi: 10.1097/RLU.0000000000002179
168. Colasanti A, Guo Q, Muhlert N, Giannetti P, Onega M, Newbould RD, et al. *In vivo* assessment of brain white matter inflammation in multiple sclerosis with (18)F-PBR111 PET. *J Nucl Med Off Publ Soc Nucl Med.* (2014) 55:1112–8. doi: 10.2967/jnumed.113.135129
169. Ottoy J, De Picker L, Verhaeghe J, Deleye S, Wyffels L, Kosten L, et al. 18F-PBR111 PET imaging in healthy controls and schizophrenia: test-retest reproducibility and quantification of neuroinflammation. *J Nucl Med Off Publ Soc Nucl Med.* (2018) 59:1267–74. doi: 10.2967/jnumed.117.203315
170. Amhaoul H, Hamaide J, Bertoglio D, Reichel SN, Verhaeghe J, Geerts E, et al. Brain inflammation in a chronic epilepsy model: Evolving pattern of the translocator protein during epileptogenesis. *Neurobiol Dis.* (2015) 82:526–39. doi: 10.1016/j.nbd.2015.09.004
171. Fuchigami T, Nakayama M, Yoshida S. Development of PET and SPECT probes for glutamate receptors. *ScientificWorldJournal.* (2015) 2015:716514. doi: 10.1155/2015/716514
172. Bressan RA, Erlandsson K, Mulligan RS, Gunn RN, Cunningham VJ, Owens J, et al. Evaluation of NMDA receptors *in vivo* in schizophrenic patients with [123I]CNS 1261 and SPET: preliminary findings. *Ann N Y Acad Sci.* (2003) 1003:364–7. doi: 10.1196/annals.1300.027
173. Bressan RA, Erlandsson K, Stone JM, Mulligan RS, Krystal JH, Ell PJ, et al. Impact of schizophrenia and chronic antipsychotic treatment on [123I]CNS-1261 binding to N-methyl-D-aspartate receptors *in vivo*. *Biol Psychiatry.* (2005) 58:41–6. doi: 10.1016/j.biopsych.2005.03.016
174. Zanotti-Fregonara P, Xu R, Zoghbi SS, Liow J-S, Fujita M, Veronese M, et al. The PET radioligand 18F-FIMX images and quantifies metabotropic glutamate receptor 1 in proportion to the regional density of its gene transcript in human brain. *J Nucl Med Off Publ Soc Nucl Med.* (2016) 57:242–7. doi: 10.2967/jnumed.115.162461
175. Barret O, Tamagnan G, Batis J, Jennings D, Zubal G, Russell D, et al. Quantitation of glutamate mGluR5 receptor with 18F-FPEB PET in humans. *J Nucl Med.* (2010) 51(Suppl. 2):215. doi: 10.1016/j.neuroimage.2010.04.164
176. Leurquin-Sterk G, Ceccarini J, Crunelle CL, de Laat B, Verbeek J, Deman S, et al. Lower limbic metabotropic glutamate receptor 5 availability in alcohol dependence. *J Nucl Med Off Publ Soc Nucl Med.* (2018) 59:682–90. doi: 10.2967/jnumed.117.199422
177. Abdallah CG, Hannestad J, Mason GF, Holmes SE, DellaGioia N, Sanacora G, et al. Metabotropic glutamate receptor 5 and glutamate involvement in major depressive disorder: a multimodal imaging study. *Biol Psychiatry Cogn Neurosci Neuroimaging.* (2017) 2:449–56. doi: 10.1016/j.bpsc.2017.03.019
178. Fatemi SH, Wong DF, Brašić JR, Kuwabara H, Mathur A, Folsom TD, et al. Metabotropic glutamate receptor 5 tracer [18F]-FPEB displays increased binding potential in postcentral gyrus and cerebellum of male individuals with autism: a pilot PET study. *Cerebellum Ataxias.* (2018) 5:3. doi: 10.1186/s40673-018-0082-1
179. Salabert A-S, Fonta C, Fontan C, Adel D, Alonso M, Pestourie C, et al. Radiolabeling of [18F]-fluoroethylnormemantine and initial *in vivo* evaluation of this innovative PET tracer for imaging the PCP sites of NMDA receptors. *Nucl Med Biol.* (2015) 42:643–53. doi: 10.1016/j.nucmedbio.2015.04.001
180. Martinez D, Slifstein M, Nabulsi N, Grassetti A, Urban NBL, Perez A, et al. Imaging glutamate homeostasis in cocaine addiction with the metabotropic glutamate receptor 5 positron emission tomography radiotracer [(11)C]ABP688 and magnetic resonance spectroscopy. *Biol Psychiatry.* (2014) 75:165–71. doi: 10.1016/j.biopsych.2013.06.026
181. Deschwanden A, Karolewicz B, Feyissa AM, Treyer V, Ametamey SM, Johayem A, et al. Reduced metabotropic glutamate receptor 5 density in major depression determined by [(11)C]ABP688 PET and postmortem study. *Am J Psychiatry.* (2011) 168:727–34. doi: 10.1176/appi.ajp.2011.09111607
182. Leuzy A, Zimmer ER, Dubois J, Pruessner J, Cooperman C, Soucy J-P, et al. *In vivo* characterization of metabotropic glutamate receptor type 5 abnormalities in behavioral variant FTD. *Brain Struct Funct.* (2016) 221:1387–402. doi: 10.1007/s00429-014-0978-3
183. Akkus F, Mihov Y, Treyer V, Ametamey SM, Johayem A, Senn S, et al. Metabotropic glutamate receptor 5 binding in male patients with alcohol use disorder. *Transl Psychiatry.* (2018) 8:17. doi: 10.1038/s41398-017-0066-6
184. Toyohara J, Sakata M, Oda K, Ishii K, Ito K, Hiura M, et al. Initial human PET studies of metabotropic glutamate receptor type 1 ligand 11C-ITMM. *J Nucl Med Off Publ Soc Nucl Med.* (2013) 54:1302–7. doi: 10.2967/jnumed.113.119891
185. Sephton SM, Herde AM, Mu L, Keller C, Rüdisühli S, Auberson Y, et al. Preclinical evaluation and test-retest studies of [(18)F]PSS232, a novel radioligand for targeting metabotropic glutamate receptor 5 (mGlu5). *Eur J Nucl Med Mol Imaging.* (2015) 42:128–37. doi: 10.1007/s00259-014-2883-7
186. Warnock G, Sommerauer M, Mu L, Pla Gonzalez G, Geistlich S, Treyer V, et al. A first-in-man PET study of [18F]PSS232, a fluorinated ABP688 derivative for imaging metabotropic glutamate receptor subtype 5. *Eur J Nucl Med Mol Imaging.* (2018) 45:1041–51. doi: 10.1007/s00259-017-3879-x
187. Laere KV, Koole M, Hoon J de, Hecken AV, Langlois X, Andres JI, et al. Biodistribution, dosimetry and kinetic modeling of [11C]JNJ-42491293, a PET tracer for the mGluR2 receptor in the human brain. *J Nucl Med.* (2012) 53(Suppl. 1):355.
188. Sahai S. Glutamate in the mammalian CNS. *Eur Arch Psychiatry Clin Neurosci.* (1990) 240:121–33. doi: 10.1007/BF02189982
189. Villmann C, Strutz N, Morth T, Hollmann M. Investigation by ion channel domain transplantation of rat glutamate receptor subunits, orphan receptors and a putative NMDA receptor subunit. *Eur J Neurosci.* (1999) 11:1765–78. doi: 10.1046/j.1460-9568.1999.00594.x
190. Paarmann I, Frermann D, Keller BU, Villmann C, Breitinger HG, Hollmann M. Kinetics and subunit composition of NMDA receptors in respiratory-related neurons. *J Neurochem.* (2005) 93:812–24. doi: 10.1111/j.1471-4159.2005.03027.x
191. Petrenko AB, Yamakura T, Baba H, Shimoji K. The role of N-methyl-D-aspartate (NMDA) receptors in pain: a review. *Anesth Analg.* (2003) 97:1108–16. doi: 10.1213/01.ANE.0000081061.12235.55
192. Dingledine R, Borges K, Bowie D, Traynelis SF. The glutamate receptor ion channels. *Pharmacol Rev.* (1999) 51:7–61.

193. Song XJ, Zhao ZQ. Cooperative interaction among the various regulatory sites within the NMDA receptor-channel complex in modulating the evoked responses to noxious thermal stimuli of spinal dorsal horn neurons in the cat. *Exp Brain Res*. (1998) 120:257–62. doi: 10.1007/s002210050399
194. Sattler R, Xiong Z, Lu WY, Hafner M, MacDonald JF, Tymianski M. Specific coupling of NMDA receptor activation to nitric oxide neurotoxicity by PSD-95 protein. *Science*. (1999) 284:1845–8. doi: 10.1126/science.284.5421.1845
195. Leker RR, Shohami E. Cerebral ischemia and trauma-different etiologies yet similar mechanisms: neuroprotective opportunities. *Brain Res Brain Res Rev*. (2002) 39:55–73. doi: 10.1016/S0165-0173(02)00157-1
196. Kalia LV, Kalia SK, Salter MW. NMDA receptors in clinical neurology: excitatory times ahead. *Lancet Neurol.* (2008) 7:742–55. doi: 10.1016/S1474-4422(08)70165-0
197. Lau CG, Zukin RS. NMDA receptor trafficking in synaptic plasticity and neuropsychiatric disorders. *Nat Rev Neurosci.* (2007) 8:413–26. doi: 10.1038/nrn2153
198. Ponchant M, Kamenkaj M, Crouzel C. Synthesis of 3-[18F]-fluoromethyl-TCP1, A potential tool for pet study of the nmda receptor channel complex. *J Label Compd Radiopharm.* (1992) 31:955–60. doi: 10.1002/jlcr.2580311115
199. Ponchant M, Crouzel C, Kamenka JM, Pappata S. Synthesis of a new analog of PCP Fluorine-18 3-fluoromethyl-TCP, a potent ligand for the NMDA glutamatergic receptor. *J Label Compd Radiopharm.* (1993) 32:352–3.
200. Shiue C-Y, Vallabhahosula S, Wolf AP, Dewey SL, Fowler JS, Schlyer DJ, et al. Carbon-11 labelled ketamine—Synthesis, distribution in mice and PET studies in baboons. *Nucl Med Biol.* (1997) 24:145–50. doi: 10.1016/S0969-8051(96)00186-2
201. Ametamey SM, Bruehlmeier M, Kneifel S, Kokic M, Honer M, Arigoni M, et al. PET studies of 18F-memantine in healthy volunteers. *Nucl Med Biol.* (2002) 29:227–31. doi: 10.1016/S0969-8051(01)00293-1
202. Ametamey SM, Samnick S, Leenders KL, Vontobel P, Quack G, Parsons CG, et al. Fluorine-18 radiolabelling, biodistribution studies and preliminary pet evaluation of a new memantine derivative for imaging the NMDA receptor. *J Recept Signal Transduct.* (1999) 19:129–41. doi: 10.3109/10799899909036640
203. Kiesewetter DO, Finn RD, Rice KC, Monn JA. Synthesis of 11C-labeled (±)-5-methyl-10, 11-dihydro-5H-dibenzo[a,d]cyclohepten-5, 10-imine [(±)-[11C]MK801]. *Int J Rad Appl Instrum.* (1990) 41:139–42. doi: 10.1016/0883-2889(90)90098-2
204. Brown DR, Wyper DJ, Owens J, Patterson J, Kelly RC, Hunter R, et al. 123Iodo-MK-801: a spect agent for imaging the pattern and extent of glutamate (NMDA) receptor activation in Alzheimer's disease. *J Psychiatr Res*. (1997) 31:605–19. doi: 10.1016/S0022-3956(97)00031-9
205. Majo VJ, Prabhakaran J, Mann JJ, Kumar JSD. PET and SPECT tracers for glutamate receptors. *Drug Discov Today*. (2013) 18:173–84. doi: 10.1016/j.drudis.2012.10.004
206. Sobrio F, Gilbert G, Perrio C, Barré L, Debruyne D. PET and SPECT imaging of the NMDA receptor system: an overview of radiotracer development. *Mini Rev Med Chem.* (2010) 10:870–86. doi: 10.2174/138955710791608299
207. Stone JM. Imaging the glutamate system in humans: relevance to drug discovery for schizophrenia. *Curr Pharm Des.* (2009) 15:2594–602. doi: 10.2174/138161209788957438
208. McGinnity CJ, Hammers A, Riaño Barros DA, Luthra SK, Jones PA, Trigg W, et al. Initial evaluation of 18F-GE-179, a putative PET Tracer for activated N-methyl D-aspartate receptors. *J Nucl Med Off Publ Soc Nucl Med*. (2014) 55:423–30. doi: 10.2967/jnumed.113.130641
209. López-Picón F, Snellman A, Shatillo O, Lehtiniemi P, Grönroos TJ, Marjamäki P, et al. *Ex vivo* tracing of NMDA and GABA-A receptors in rat brain after traumatic brain injury using 18F-GE-179 and 18F-GE-194 autoradiography. *J Nucl Med Off Publ Soc Nucl Med*. (2016) 57:1442–7. doi: 10.2967/jnumed.115.167403
210. Zhou W, Bao W, Jiang D, Kong Y, Hua F, Lu X, et al. [18F]-GE-179 positron emission tomography (PET) tracer for N-methyl-d-aspartate receptors: One-pot synthesis and preliminary micro-PET study in a rat model of MCAO. *Nucl Med Biol.* (2018) 61:45–55. doi: 10.1016/j.nucmedbio.2018.04.002
211. Schoenberger M, Schroeder FA, Placzek MS, Carter RL, Rosen BR, Hooker JM, et al. *In vivo* [18F]GE-179 brain signal does not show NMDA-specific modulation with drug challenges in rodents and nonhuman primates. *ACS Chem Neurosci.* (2018) 9:298–305. doi: 10.1021/acschemneuro.7b00327
212. Salabert A-S, Mora-Ramirez E, Beaurain M, Alonso M, Fontan C, Tahar HB, et al. Evaluation of [18F]FNM biodistribution and dosimetry based on whole-body PET imaging of rats. *Nucl Med Biol.* (2018) 59:1–8. doi: 10.1016/j.nucmedbio.2017.12.003
213. van der Aart J, Golla SSV, van der Pluijm M, Schwarte LA, Schuit RC, Klein PJ, et al. First in human evaluation of [18F]PK-209, a PET ligand for the ion channel binding site of NMDA receptors. *EJNMMI Res.* (2018) 8:69. doi: 10.1186/s13550-018-0424-2
214. Roger G, Dollé F, De Bruin B, Liu X, Besret L, Bramoullé Y, et al. Radiosynthesis and pharmacological evaluation of [11C]EMD-95885: a high affinity ligand for NR2B-containing NMDA receptors. *Bioorg Med Chem*. (2004) 12:3229–37. doi: 10.1016/j.bmc.2004.03.065
215. Labas R, Gilbert G, Nicole O, Dhilly M, Abbas A, Tirel O, et al. Synthesis, evaluation and metabolic studies of radiotracers containing a 4-(4-[18F]-fluorobenzyl)piperidin-1-yl moiety for the PET imaging of NR2B NMDA receptors. Eur *J Med Chem.* (2011) 46:2295–309. doi: 10.1016/j.ejmech.2011.03.013
216. Yamasaki T, Maeda J, Fujinaga M, Nagai Y, Hatori A, Yui J, et al. PET brain kinetics studies of (11)C-ITMM and (11)C-ITDM,radioprobes for metabotropic glutamate receptor type 1, in a nonhuman primate. *Am J Nucl Med Mol Imaging*. (2014) 4:260–9.
217. Pillai RLI, Tipre DN. Metabotropic glutamate receptor 5 – a promising target in drug development and neuroimaging. *Eur J Nucl Med Mol Imaging*. (2016) 43:1151–70. doi: 10.1007/s00259-015-3301-5
218. Sullivan EV, Adalsteinsson E, Sood R, Mayer D, Bell R, McBride W, et al. Longitudinal brain magnetic resonance imaging study of the alcohol-preferring rat. Part I: adult brain growth. *Alcohol Clin Exp Res*. (2006) 30:1234–47. doi: 10.1111/j.1530-0277.2006.00145.x
219. Sullivan JM, Lim K, Labaree D, Lin S, McCarthy TJ, Seibyl JP, et al. Kinetic analysis of the metabotropic glutamate subtype 5 tracer [18F]FPEB in bolus and bolus-plus-constant-infusion studies in humans. *J Cereb Blood Flow Metab*. (2013) 33:532. doi: 10.1038/jcbfm.2012.195
220. Kang Y, Henchcliffe C, Verma A, Vallabhajosula S, He B, Kothari PJ, et al. 18F-FPEB PET/CT shows mGluR5 upregulation in Parkinson's disease. *J Neuroimaging Off J Am Soc Neuroimaging*. (2019) 29:97–103. doi: 10.1111/jon.12563
221. de Laat B, Weerasekera A, Leurquin-Sterk G, Gsell W, Bormans G, Himmelreich U, et al. Effects of alcohol exposure on the glutamatergic system: a combined longitudinal 18 F-FPEB and 1 H-MRS study in rats. *Addict Biol*. (2018) 24:696–706. doi: 10.1111/adb.12635
222. Holmes SE, Girgenti MJ, Davis MT, Pietrzak RH, DellaGioia N, Nabulsi N, et al. Altered metabotropic glutamate receptor 5 markers in PTSD: *in vivo* and postmortem evidence. *Proc Natl Acad Sci USA*. (2017) 114:8390–5. doi: 10.1073/pnas.1701749114
223. Ametamey SM, Treyer V, Streffer J, Wyss MT, Schmidt M, Blagoev M, et al. Human PET studies of metabotropic glutamate receptor subtype 5 with 11C-ABP688. *J Nucl Med Off Publ Soc Nucl Med*. (2007) 48:247–52.
224. Burger C, Deschwanden A, Ametamey S, Johayem A, Mancosu B, Wyss M, et al. Evaluation of a bolus/infusion protocol for 11C-ABP688, a PET tracer for mGluR5. *Nucl Med Biol.* (2010) 37:845–51. doi: 10.1016/j.nucmedbio.2010.04.107
225. DuBois JM, Rousset OG, Guiot M-C, Hall JA, Reader AJ, Soucy J-P, et al. Metabotropic Glutamate Receptor Type 5 (mGluR5) cortical abnormalities in focal cortical dysplasia identified *in vivo* with [11C]ABP688 Positron-Emission Tomography (PET) imaging. *Cereb Cortex N Y N*. (2016) 26:4170–9. doi: 10.1093/cercor/bhw249
226. Akkus F, Treyer V, Ametamey SM, Johayem A, Buck A, Hasler G. Metabotropic glutamate receptor 5 neuroimaging in schizophrenia. *Schizophr Res*. (2017) 183:95–101. doi: 10.1016/j.schres.2016.11.008
227. Kim J-H, Joo Y-H, Son Y-D, Kim J-H, Kim Y-K, Kim H-K, et al. *In vivo* metabotropic glutamate receptor 5 availability-associated functional connectivity alterations in drug-naïve young adults with major depression. *Eur Neuropsychopharmacol.* (2018) 29:278–90. doi: 10.1016/j.euroneuro.2018.12.001
228. Esterlis I, DellaGioia N, Pietrzak RH, Matuskey D, Nabulsi N, Abdallah CG, et al. Ketamine-induced reduction in mGluR5 availability is associated with an antidepressant response: an [11C]ABP688 and PET imaging study in depression. *Mol Psychiatry*. (2018) 23:824–32. doi: 10.1038/mp.2017.58

229. DeLorenzo C, DellaGioia N, Bloch M, Sanacora G, Nabulsi N, Abdallah C, et al. *In vivo* ketamine-induced changes in [^{11}C]ABP688 binding to metabotropic glutamate receptor subtype 5. *Biol Psychiatry.* (2015) 77:266–75. doi: 10.1016/j.biopsych.2014.06.024
230. Kosten L, Verhaeghe J, Wyffels L, Stroobants S, Staelens S. Acute ketamine infusion in rat does not affect *in vivo* [11C]ABP688 binding to metabotropic glutamate receptor subtype 5. *Mol Imaging.* (2018) 17:1536012118788636. doi: 10.1177/1536012118788636
231. O'Gorman Tuura R, Warnock G, Ametamey S, Treyer V, Noeske R, Buck A, et al. Imaging glutamate redistribution after acute N-acetylcysteine administration: a simultaneous PET/MR study. *NeuroImage*. (2019) 184:826–33. doi: 10.1016/j.neuroimage.2018.10.017
232. Müller Herde A, Boss SD, He Y, Schibli R, Mu L, Ametamey SM. Ketamine and ceftriaxone-induced alterations in glutamate levels do not impact the specific binding of metabotropic glutamate receptor subtype 5 radioligand [18F]PSS232 in the rat brain. *Pharm Basel Switz*. (2018) 11:E83. doi: 10.3390/ph11030083
233. Leurquin-Sterk G, Celen S, Laere KV, Koole M, Bormans G, Langlois X, et al. What we observe *in vivo* is not always what we see *in vitro*: development and validation of 11C-JNJ-42491293, a novel radioligand for mGluR2. *J Nucl Med.* (2017) 58:110–6. doi: 10.2967/jnumed.116.176628
234. Roy R, Niccolini F, Pagano G, Politis M. Cholinergic imaging in dementia spectrum disorders. *Eur J Nucl Med Mol Imaging.* (2016) 43:1376–86. doi: 10.1007/s00259-016-3349-x
235. Perry EK, Gibson PH, Blessed G, Perry RH, Tomlinson BE. Neurotransmitter enzyme abnormalities in senile dementia: choline acetyltransferase and glutamic acid decarboxylase activities in necropsy brain tissue. *J Neurol Sci*. (1977) 34:247–65. doi: 10.1016/0022-510X(77)90073-9
236. Davis KL, Mohs RC, Marin D, Purohit DP, Perl DP, Lantz M, et al. Cholinergic markers in elderly patients with early signs of Alzheimer disease. *JAMA*. (1999) 281:1401–6. doi: 10.1001/jama.281.15.1401
237. Kuhl DE, Koeppe RA, Minoshima S, Snyder SE, Ficaro EP, Foster NL, et al. *In vivo* mapping of cerebral acetylcholinesterase activity in aging and Alzheimer's disease. *Neurology.* (1999) 52:691–9. doi: 10.1212/WNL.52.4.691
238. Shinotoh H, Namba H, Yamaguchi M, Fukushi K, Nagatsuka S, Iyo M, et al. Positron emission tomographic measurement of acetylcholinesterase activity reveals differential loss of ascending cholinergic systems in Parkinson's disease and progressive supranuclear palsy. *Ann Neurol.* (1999) 46:62–9.
239. Bohnen NI, Kaufer DI, Ivanco LS, Lopresti B, Koeppe RA, Davis JG, et al. Cortical cholinergic function is more severely affected in parkinsonian dementia than in Alzheimer disease: an *in vivo* positron emission tomographic study. *Arch Neurol.* (2003) 60:1745–8. doi: 10.1001/archneur.60.12.1745
240. Bohnen NI, Kaufer DI, Hendrickson R, Ivanco LS, Lopresti B, Davis JG, et al. Cognitive correlates of alterations in acetylcholinesterase in Alzheimer's disease. *Neurosci Lett*. (2005) 380:127–32. doi: 10.1016/j.neulet.2005.01.031
241. Hilker R, Thomas AV, Klein JC, Weisenbach S, Kalbe E, Burghaus L, et al. Dementia in Parkinson disease: functional imaging of cholinergic and dopaminergic pathways. *Neurology.* (2005) 65:1716–22. doi: 10.1212/01.wnl.0000191154.78131.f6
242. Eggers C, Herholz K, Kalbe E, Heiss W-D. Cortical acetylcholine esterase activity and ApoE4-genotype in Alzheimer disease. *Neurosci Lett*. (2006) 408:46–50. doi: 10.1016/j.neulet.2006.08.061
243. Irie T, Fukushi K, Akimoto Y, Tamagami H, Nozaki T. Design and evaluation of radioactive acetylcholine analogs for mapping brain acetylcholinesterase (AchE) *in vivo*. *Nucl Med Biol.* (1994) 21:801–8. doi: 10.1016/0969-8051(94)90159-7
244. Koeppe RA, Frey KA, Snyder SE, Meyer P, Kilbourn MR, Kuhl DE. Kinetic modeling of N-[11C]Methylpiperidin-4-yl propionate: alternatives for analysis of an irreversible positron emission tomography tracer for measurement of acetylcholinesterase activity in human brain. *J Cereb Blood Flow Metab*. (1999) 19:1150–63. doi: 10.1097/00004647-199910000-00012
245. Mazere J, Meissner WG, Sibon I, Lamare F, Tison F, Allard M, et al. [(123)I]-IBVM SPECT imaging of cholinergic systems in multiple system atrophy: a specific alteration of the ponto-thalamic cholinergic pathways (Ch5-Ch6). *NeuroImage Clin*. (2013) 3:212–7. doi: 10.1016/j.nicl.2013.07.012
246. Nejad-Davarani S, Koeppe RA, Albin RL, Frey KA, Müller MLTM, Bohnen NI. Quantification of brain cholinergic denervation in dementia with Lewy bodies using PET imaging with [18F]-FEOBV. *Mol Psychiatry*. (2018) 24:322–7. doi: 10.1038/s41380-018-0130-5
247. Petrou M, Frey KA, Kilbourn MR, Scott PJH, Raffel DM, Bohnen NI, et al. *In vivo* imaging of human cholinergic nerve terminals with (-)-5-(18)F-fluoroethoxybenzovesamicol: biodistribution, dosimetry, and tracer kinetic analyses. *J Nucl Med Off Publ Soc Nucl Med*. (2014) 55:396–404. doi: 10.2967/jnumed.113.124792
248. Nordberg A, Hartvig P, Lilja A, Viitanen M, Amberla K, Lundqvist H, et al. Decreased uptake and binding of 11C-nicotine in brain of Alzheimer patients as visualized by positron emission tomography. *J Neural Transm Park Dis Dement Sect*. (1990) 2:215–24. doi: 10.1007/BF02257652
249. Nordberg A, Lundqvist H, Hartvig P, Lilja A, Långström B. Kinetic analysis of regional (S)(-)11C-nicotine binding in normal and Alzheimer brains–*in vivo* assessment using positron emission tomography. *Alzheimer Dis Assoc Disord*. (1995) 9:21–7. doi: 10.1097/00002093-199505000-00006
250. Kadir A, Almkvist O, Wall A, Långström B, Nordberg A. PET imaging of cortical 11C-nicotine binding correlates with the cognitive function of attention in Alzheimer's disease. *Psychopharmacology*. (2006) 188:509–20. doi: 10.1007/s00213-006-0447-7
251. Sabbagh MN, Shah F, Reid RT, Sue L, Connor DJ, Peterson LKN, et al. Pathologic and nicotinic receptor binding differences between mild cognitive impairment, Alzheimer disease, and normal aging. *Arch Neurol.* (2006) 63:1771–6. doi: 10.1001/archneur.63.12.1771
252. O'Brien JT, Colloby SJ, Pakrasi S, Perry EK, Pimlott SL, Wyper DJ, et al. Alpha4beta2 nicotinic receptor status in Alzheimer's disease using 123I-5IA-85380 single-photon-emission computed tomography. *J Neurol Neurosurg Psychiatry.* (2007) 78:356–62. doi: 10.1136/jnnp.2006.108209
253. Sabri O, Kendziorra K, Wolf H, Gertz H-J, Brust P. Acetylcholine receptors in dementia and mild cognitive impairment. *Eur J Nucl Med Mol Imaging*. (2008) 35 (Suppl. 1):S30–45. doi: 10.1007/s00259-007-0701-1
254. Okada H, Ouchi Y, Ogawa M, Futatsubashi M, Saito Y, Yoshikawa E, et al. Alterations in α4β2 nicotinic receptors in cognitive decline in Alzheimer's aetiopathology. *Brain J Neurol.* (2013) 136(Pt 10):3004–17. doi: 10.1093/brain/awt195
255. Hu M, Waring JF, Gopalakrishnan M, Li J. Role of GSK-3beta activation and alpha7 nAChRs in Abeta(1-42)-induced tau phosphorylation in PC12 cells. *J Neurochem.* (2008) 106:1371–7. doi: 10.1111/j.1471-4159.2008.05483.x
256. Dziewczapolski G, Glogowski CM, Masliah E, Heinemann SF. Deletion of the alpha 7 nicotinic acetylcholine receptor gene improves cognitive deficits and synaptic pathology in a mouse model of Alzheimer's disease. *J Neurosci Off J Soc Neurosci*. (2009) 29:8805–15. doi: 10.1523/JNEUROSCI.6159-08.2009
257. Asahina M, Suhara T, Shinotoh H, Inoue O, Suzuki K, Hattori T. Brain muscarinic receptors in progressive supranuclear palsy and Parkinson's disease: a positron emission tomographic study. *J Neurol Neurosurg Psychiatry.* (1998) 65:155–63. doi: 10.1136/jnnp.65.2.155
258. Colloby SJ, Pakrasi S, Firbank MJ, Perry EK, Piggott MA, Owens J, et al. *In vivo* SPECT imaging of muscarinic acetylcholine receptors using (R,R) 123I-QNB in dementia with Lewy bodies and Parkinson's disease dementia. *NeuroImage*. (2006) 33:423–9. doi: 10.1016/j.neuroimage.2006.07.026
259. Kadir A, Darreh-Shori T, Almkvist O, Wall A, Grut M, Strandberg B, et al. PET imaging of the *in vivo* brain acetylcholinesterase activity and nicotine binding in galantamine-treated patients with AD. *Neurobiol Aging.* (2008) 29:1204–17. doi: 10.1016/j.neurobiolaging.2007.02.020
260. Otto CA, Mulholland GK, Perry SE, Combs R, Sherman PS, Fisher SJ. *In vitro* and *ex vivo* evaluation of cyclic aminoalkyl benzilates as potential emission tomography ligands for the muscarinic receptor. *Int J Rad Appl Instrum B*. (1989) 16:51–5. doi: 10.1016/0883-2897(89)90215-8
261. Horti AG, Koren AO, Lee KS, Mukhin AG, Vaupel DB, Kimes AS, et al. Radiosynthesis and preliminary evaluation of 5-[123/125I]iodo-3-(2(S)-azetidinylmethoxy)pyridine: a radioligand for nicotinic acetylcholine receptors. *Nucl Med Biol.* (1999) 26:175–82. doi: 10.1016/S0969-8051(98)00086-9
262. Pakrasi S, Colloby SJ, Firbank MJ, Perry EK, Wyper DJ, Owens J, et al. Muscarinic acetylcholine receptor status in Alzheimer's disease assessed using (R, R) 123I-QNB SPECT. *J Neurol.* (2007) 254:907–13. doi: 10.1007/s00415-006-0473-8
263. Shimada H, Hirano S, Shinotoh H, Aotsuka A, Sato K, Tanaka N, et al. Mapping of brain acetylcholinesterase alterations in Lewy body

disease by PET. *Neurology*. (2009) 73:273–8. doi: 10.1212/WNL.0b013e3181ab2b58
264. Aghourian M, Legault-Denis C, Soucy J-P, Rosa-Neto P, Gauthier S, Kostikov A, et al. Quantification of brain cholinergic denervation in Alzheimer's disease using PET imaging with [18F]-FEOBV. *Mol Psychiatry*. (2017) 22:1531–8. doi: 10.1038/mp.2017.183
265. Yoshida T, Kuwabara Y, Ichiya Y, Sasaki M, Fukumura T, Ichimiya A, et al. Cerebral muscarinic acetylcholinergic receptor measurement in Alzheimer's disease patients on 11C-N-methyl-4-piperidyl benzilate–comparison with cerebral blood flow and cerebral glucose metabolism. *Ann Nucl Med*. (1998) 12:35–42. doi: 10.1007/BF03165414
266. Koren AO, Horti AG, Mukhin AG, Gündisch D, Kimes AS, Dannals RF, et al. 2-, 5-, and 6-Halo-3-(2(S)-azetidinylmethoxy)pyridines: synthesis, affinity for nicotinic acetylcholine receptors, and molecular modeling. *J Med Chem*. (1998) 41:3690–8. doi: 10.1021/jm980170a
267. Sihver W, Fasth KJ, Ogren M, Bivehed H, Bergström M, Nordberg A, et al. *In vitro* evaluation of 11C-labeled (S)-nicotine, (S)-3-methyl-5-(1-methyl-2-pyrrolidinyl)isoxazole, and (R,S)-1-methyl-2-(3-pyridyl)azetidine as nicotinic receptor ligands for positron emission tomography studies. *J Neurochem*. (1998) 71:1750–60. doi: 10.1046/j.1471-4159.1998.71041750.x
268. Jung YW, Frey KA, Mulholland GK, del Rosario R, Sherman PS, Raffel DM, et al. Vesamicol receptor mapping of brain cholinergic neurons with radioiodine-labeled positional isomers of benzovesamicol. *J Med Chem*. (1996) 39:3331–42. doi: 10.1021/jm9507486
269. Horti AG, Gao Y, Kuwabara H, Wang Y, Abazyan S, Yasuda RP, et al. 18F-ASEM, a radiolabeled antagonist for imaging the α7-nicotinic acetylcholine receptor with PET. *J Nucl Med*. (2014) 55:672–7. doi: 10.2967/jnumed.113.132068
270. Wong DF, Kuwabara H, Horti AG, Roberts JM, Nandi A, Cascella N, et al. Brain PET imaging of α7-nAChR with [18F]ASEM: reproducibility, occupancy, receptor density, and changes in schizophrenia. *Int J Neuropsychopharmacol*. (2018) 21:656–67. doi: 10.1101/245118
271. Lin S-F, Bois F, Holden D, Nabulsi N, Pracitto R, Gao H, et al. The search for a subtype-selective PET imaging agent for the GABAA receptor complex: evaluation of the radiotracer [11C]ADO in nonhuman primates. *Mol Imaging*. (2017) 16:1536012117731258. doi: 10.1177/1536012117731258
272. Stephens DN, King SL, Lambert JJ, Belelli D, Duka T. GABAA receptor subtype involvement in addictive behaviour. *Genes Brain Behav*. (2017) 16:149–84. doi: 10.1111/gbb.12321
273. Rodnick ME, Hockley BG, Sherman P, Quesada C, Battle MR, Jackson A, et al. Novel fluorine-18 PET radiotracers based on flumazenil for GABAA imaging in the brain. *Nucl Med Biol*. (2013) 40:901–5. doi: 10.1016/j.nucmedbio.2013.06.004
274. Baldwin RM, Horti AG, Bremner JD, Stratton MD, Dannals RF, Ravert HT, et al. Synthesis and PET imaging of the benzodiazepine receptor tracer [N-methyl-11C]iomazenil. *Nucl Med Biol*. (1995) 22:659–65. doi: 10.1016/0969-8051(94)00139-B
275. Andersson JD, Halldin C. PET radioligands targeting the brain GABAA /benzodiazepine receptor complex. *J Label Compd Radiopharm*. (2013) 56:196–206. doi: 10.1002/jlcr.3008
276. Dobbs FR, Banks W, Fleishaker JC, Valentine AD, Kinsey BM, Franceschini MP, et al. Studies with [11C]alprazolam: an agonist for the benzodiazepine receptor. *Nucl Med Biol*. (1995) 22:459–66. doi: 10.1016/0969-8051(94)00131-3
277. Persson A, Ehrin E, Eriksson L, Farde L, Hedström CG, Litton JE, et al. Imaging of [11C]-labelled Ro 15-1788 binding to benzodiazepine receptors in the human brain by positron emission tomography. *J Psychiatr Res*. (1985) 19:609–22. doi: 10.1016/0022-3956(85)90080-9
278. Pike VW, Halldin C, Crouzel C, Barré L, Nutt DJ, Osman S, et al. Radioligands for PET studies of central benzodiazepine receptors and PK (peripheral benzodiazepine) binding sites–current status. *Nucl Med Biol*. (1993) 20:503–25. doi: 10.1016/0969-8051(93)90082-6
279. Abadie P, Rioux P, Scatton B, Zarifian E, Barré L, Patat A, et al. Central benzodiazepine receptor occupancy by zolpidem in the human brain as assessed by positron emission tomography. *Eur J Pharmacol*. (1996) 295:35–44. doi: 10.1016/0014-2999(95)00633-8
280. Frankle WG, Cho RY, Narendran R, Mason NS, Vora S, Litschge M, et al. Tiagabine increases [^{11}C]flumazenil binding in cortical brain regions in healthy control subjects. *Neuropsychopharmacology*. (2009) 34:624–33. doi: 10.1038/npp.2008.104
281. Savic I, Pauli S, Thorell JO, Blomqvist G. *In vivo* demonstration of altered benzodiazepine receptor density in patients with generalised epilepsy. *J Neurol Neurosurg Psychiatry*. (1994) 57:797–804. doi: 10.1136/jnnp.57.7.797
282. la Fougère C, Rominger A, Förster S, Geisler J, Bartenstein P. PET and SPECT in epilepsy: a critical review. *Epilepsy Behav*. (2009) 15:50–5. doi: 10.1016/j.yebeh.2009.02.025
283. Savic I, Roland P, Sedvall G, Persson A, Pauli S, Widen L. *In-vivo* demonstration of reduced benzodiazepine receptor binding in human epileptic FOCI. *Lancet*. (1988) 332:863–6. doi: 10.1016/S0140-6736(88)92468-3
284. Egerton A, Modinos G, Ferrera D, McGuire P. Neuroimaging studies of GABA in schizophrenia: a systematic review with meta-analysis. *Transl Psychiatry*. (2017) 7:e1147. doi: 10.1038/tp.2017.124
285. Heiss WD, Sobesky J, Smekal UV, Kracht LW, Lehnhardt FG, Thiel A, et al. Probability of cortical infarction predicted by flumazenil binding and diffusion-weighted imaging signal intensity. *Stroke*. (2004) 35:1892–8. doi: 10.1161/01.STR.0000134746.93535.9b
286. Jucaite A, Cselényi Z, Lappalainen J, McCarthy DJ, Lee C-M, Nyberg S, et al. GABAA receptor occupancy by subtype selective GABAAα2,3 modulators: PET studies in humans. *Psychopharmacology*. (2017) 234:707–16. doi: 10.1007/s00213-016-4506-4
287. Taguchi Y, Takashima S, Noguchi K, Tanaka K. Findings of 123I-iomazenil SPECT during and after stroke-like episodes in a patient with MELAS. *Clin Nucl Med*. (2014) 39:e334–5. doi: 10.1097/RLU.0b013e318299610f
288. Fujitani S, Matsuda K, Nakamura F, Baba K, Usui N, Tottori T, et al. Statistical parametric mapping of interictal 123I-iomazenil SPECT in temporal lobe epilepsy surgery. *Epilepsy Res*. (2013) 106:173–80. doi: 10.1016/j.eplepsyres.2013.03.008
289. Nagamitsu S, Sakurai R, Matsuoka M, Chiba H, Ozono S, Tanigawa H, et al. Altered SPECT (123)I-iomazenil binding in the cingulate cortex of children with anorexia nervosa. *Front Psychiatry*. (2016) 7:16. doi: 10.3389/fpsyt.2016.00016
290. Lingford-Hughes A, Hume SP, Feeney A, Hirani E, Osman S, Cunningham VJ, et al. Imaging the GABA-benzodiazepine receptor subtype containing the alpha5-subunit *in vivo* with [11C]Ro15 4513 positron emission tomography. *J Cereb Blood Flow Metab Off J Int Soc Cereb Blood Flow Metab*. (2002) 22:878–89. doi: 10.1097/00004647-200207000-00013
291. Maeda J, Suhara T, Kawabe K, Okauchi T, Obayashi S, Hojo J, et al. Visualization of alpha5 subunit of GABAA/benzodiazepine receptor by 11C Ro15-4513 using positron emission tomography. *Synap N Y N*. (2003) 47:200–8. doi: 10.1002/syn.10169
292. Lingford-Hughes A, Reid AG, Myers J, Feeney A, Hammers A, Taylor LG, et al. A [11C]Ro15 4513 PET study suggests that alcohol dependence in man is associated with reduced α5 benzodiazepine receptors in limbic regions. *J Psychopharmacol Oxf Engl*. (2012) 26:273–81. doi: 10.1177/0269881110379509
293. Asai Y, Takano A, Ito H, Okubo Y, Matsuura M, Otsuka A, et al. GABAA/Benzodiazepine receptor binding in patients with schizophrenia using [11C]Ro15-4513, a radioligand with relatively high affinity for alpha5 subunit. *Schizophr Res*. (2008) 99:333–40. doi: 10.1016/j.schres.2007.10.014
294. Dedeurwaerdere S, Gregoire M-C, Vivash L, Roselt P, Binns D, Fookes C, et al. *In-vivo* imaging characteristics of two fluorinated flumazenil radiotracers in the rat. *Eur J Nucl Med Mol Imaging*. (2009) 36:958–65. doi: 10.1007/s00259-009-1066-4
295. Sieghart W. Structure and pharmacology of gamma-aminobutyric acidA receptor subtypes. *Pharmacol Rev*. (1995) 47:181–234.
296. Laruelle M, Abi-Dargham A, al-Tikriti MS, Baldwin RM, Zea-Ponce Y, Zoghbi SS, et al. SPECT quantification of [123I]iomazenil binding to benzodiazepine receptors in nonhuman primates: II. Equilibrium analysis of constant infusion experiments and correlation with *in vitro* parameters. *J Cereb Blood Flow Metab Off J Int Soc Cereb Blood Flow Metab*. (1994) 14:453–65. doi: 10.1038/jcbfm.1994.56
297. Mendez MA, Horder J, Myers J, Coghlan S, Stokes P, Erritzoe D, et al. The brain GABA-benzodiazepine receptor alpha-5 subtype in autism spectrum disorder: a pilot [11C]Ro15-4513

positron emission tomography study. *Neuropharmacology*. (2013) 68:195–201. doi: 10.1016/j.neuropharm.2012.04.008
298. Vivash L, Gregoire M-C, Lau EW, Ware RE, Binns D, Roselt P, et al. 18F-flumazenil: a γ-aminobutyric acid A-specific PET radiotracer for the localization of drug-resistant temporal lobe epilepsy. *J Nucl Med Off Publ Soc Nucl Med*. (2013) 54:1270–7. doi: 10.2967/jnumed.112.107359
299. Hodolic M, Topakian R, Pichler R. (18)F-fluorodeoxyglucose and (18)F-flumazenil positron emission tomography in patients with refractory epilepsy. *Radiol Oncol*. (2016) 50:247–53. doi: 10.1515/raon-2016-0032
300. Paterson LM, Kornum BR, Nutt DJ, Pike VW, Knudsen GM. 5-HT radioligands for human brain imaging with PET and SPECT. *Med Res Rev*. (2013) 33:54–111. doi: 10.1002/med.20245
301. King MV, Marsden CA, Fone KCF. A role for the 5-HT(1A), 5-HT4 and 5-HT6 receptors in learning and memory. *Trends Pharmacol Sci*. (2008) 29:482–92. doi: 10.1016/j.tips.2008.07.001
302. Akimova E, Lanzenberger R, Kasper S. The serotonin-1A receptor in anxiety disorders. *Biol Psychiatry*. (2009) 66:627–35. doi: 10.1016/j.biopsych.2009.03.012
303. Nash JR, Sargent PA, Rabiner EA, Hood SD, Argyropoulos SV, Potokar JP, et al. Serotonin 5-HT1A receptor binding in people with panic disorder: positron emission tomography study. *Br J Psychiatry J Ment Sci*. (2008) 193:229–34. doi: 10.1192/bjp.bp.107.041186
304. Bailer UF, Frank GK, Henry SE, Price JC, Meltzer CC, Mathis CA, et al. Exaggerated 5-HT1A but normal 5-HT2A receptor activity in individuals ill with anorexia nervosa. *Biol Psychiatry*. (2007) 61:1090–9. doi: 10.1016/j.biopsych.2006.07.018
305. Kumar JSD, Mann JJ. PET tracers for 5-HT(1A) receptors and uses thereof. *Drug Discov Today*. (2007) 12:748–56. doi: 10.1016/j.drudis.2007.07.008
306. Doder M, Rabiner EA, Turjanski N, Lees AJ, Brooks DJ, 11C-WAY 100635 PET study. Tremor in Parkinson's disease and serotonergic dysfunction: an 11C-WAY 100635 PET study. *Neurology*. (2003) 60:601–5. doi: 10.1212/01.WNL.0000031424.51127.2B
307. Merlet I, Ostrowsky K, Costes N, Ryvlin P, Isnard J, Faillenot I, et al. 5-HT1A receptor binding and intracerebral activity in temporal lobe epilepsy: an [18F]MPPF-PET study. *Brain J Neurol*. (2004) 127(Pt 4):900–13. doi: 10.1093/brain/awh109
308. Truchot L, Costes SN, Zimmer L, Laurent B, Le Bars D, Thomas-Antérion C, et al. Up-regulation of hippocampal serotonin metabolism in mild cognitive impairment. *Neurology*. (2007) 69:1012–7. doi: 10.1212/01.wnl.0000271377.52421.4a
309. Lothe A, Merlet I, Demarquay G, Costes N, Ryvlin P, Mauguière F. Interictal Brain 5-HT1A receptors binding in migraine without Aura: a 18F-MPPF-PET study. *Cephalalgia*. (2008) 28:1282–91. doi: 10.1111/j.1468-2982.2008.01677.x
310. Demarquay G, Lothe A, Royet J, Costes N, Mick G, Mauguière F, et al. Brainstem changes in 5-HT1A receptor availability during migraine attack. *Cephalalgia*. (2011) 31:84–94. doi: 10.1177/0333102410385581
311. Lothe A, Didelot A, Hammers A, Costes N, Saoud M, Gilliam F, et al. Comorbidity between temporal lobe epilepsy and depression: a [18F]MPPF PET study. *Brain J Neurol*. (2008) 131(Pt 10):2765–82. doi: 10.1093/brain/awn194
312. Carson RE, Lang L, Watabe H, Der MG, Adams HR, Jagoda E, et al. PET evaluation of [(18)F]FCWAY, an analog of the 5-HT(1A) receptor antagonist, WAY-100635. *Nucl Med Biol*. (2000) 27:493–7. doi: 10.1016/S0969-8051(00)00118-9
313. Toczek MT, Carson RE, Lang L, Ma Y, Spanaki MV, Der MG, et al. PET imaging of 5-HT1A receptor binding in patients with temporal lobe epilepsy. *Neurology*. (2003) 60:749–56. doi: 10.1212/01.WNL.0000049930.93113.20
314. Giovacchini G, Toczek MT, Bonwetsch R, Bagic A, Lang L, Fraser C, et al. 5-HT 1A receptors are reduced in temporal lobe epilepsy after partial-volume correction. *J Nucl Med Off Publ Soc Nucl Med*. (2005) 46:1128–35.
315. Hasler G, Bonwetsch R, Giovacchini G, Toczek MT, Bagic A, Luckenbaugh DA, et al. 5-HT1A receptor binding in temporal lobe epilepsy patients with and without major depression. *Biol Psychiatry*. (2007) 62:1258–64. doi: 10.1016/j.biopsych.2007.02.015
316. Neumeister A, Bain E, Nugent AC, Carson RE, Bonne O, Luckenbaugh DA, et al. Reduced serotonin type 1A receptor binding in panic disorder. *J Neurosci Off J Soc Neurosci*. (2004) 24:589–91. doi: 10.1523/JNEUROSCI.4921-03.2004
317. Bonne O, Bain E, Neumeister A, Nugent AC, Vythilingam M, Carson RE, et al. No change in serotonin type 1A receptor binding in patients with posttraumatic stress disorder. *Am J Psychiatry*. (2005) 162:383–5. doi: 10.1176/appi.ajp.162.2.383
318. Choi JY, Lyoo CH, Kim JS, Kim KM, Kang JH, Choi S-H, et al. 18F-Mefway PET imaging of serotonin 1A receptors in humans: a comparison with 18F-FCWAY. *PLoS ONE*. (2015) 10:e0121342. doi: 10.1371/journal.pone.0121342
319. Milak MS, DeLorenzo C, Zanderigo F, Prabhakaran J, Kumar JSD, Majo VJ, et al. *In vivo* quantification of human serotonin 1A receptor using 11C-CUMI-101, an agonist PET radiotracer. *J Nucl Med Off Publ Soc Nucl Med*. (2010) 51:1892–900. doi: 10.2967/jnumed.110.076257
320. Travis MJ, Busatto GF, Pilowsky LS, Mulligan R, Acton PD, Gacinovic S, et al. 5-HT2A receptor blockade in patients with schizophrenia treated with risperidone or clozapine. A SPET study using the novel 5-HT2A ligand 123I-5-I-R-91150. *Br J Psychiatry J Ment Sci*. (1998) 173:236–41. doi: 10.1192/bjp.173.3.236
321. Jones HM, Travis MJ, Mulligan R, Bressan RA, Visvikis D, Gacinovic S, et al. *In vivo* 5-HT2A receptor blockade by quetiapine: an R91150 single photon emission tomography study. *Psychopharmacology*. (2001) 157:60–6. doi: 10.1007/s002130100761
322. Versijpt J, Van Laere KJ, Dumont F, Decoo D, Vandecapelle M, Santens P, et al. Imaging of the 5-HT2A system: age-, gender-, and Alzheimer's disease-related findings. *Neurobiol Aging*. (2003) 24:553–61. doi: 10.1016/S0197-4580(02)00137-9
323. van Heeringen C, Audenaert K, Van Laere K, Dumont F, Slegers G, Mertens J, et al. Prefrontal 5-HT2a receptor binding index, hopelessness and personality characteristics in attempted suicide. *J Affect Disord*. (2003) 74:149–58. doi: 10.1016/S0165-0327(01)00482-7
324. Goethals I, Vervaet M, Audenaert K, Jacobs F, Ham H, Van de Wiele C, et al. Differences of cortical 5-HT2A receptor binding index with SPECT in subtypes of anorexia nervosa: relationship with personality traits? *J Psychiatr Res*. (2007) 41:455–8. doi: 10.1016/j.jpsychires.2005.04.002
325. Sheline YI, Mintun MA, Barch DM, Wilkins C, Snyder AZ, Moerlein SM. Decreased hippocampal 5-HT(2A) receptor binding in older depressed patients using [18F]altanserin positron emission tomography. *Neuropsychopharmacol Off Publ Am Coll Neuropsychopharmacol*. (2004) 29:2235–41. doi: 10.1038/sj.npp.1300555
326. Meltzer CC, Price JC, Mathis CA, Greer PJ, Cantwell MN, Houck PR, et al. PET imaging of serotonin type 2A receptors in late-life neuropsychiatric disorders. *Am J Psychiatry*. (1999) 156:1871–8.
327. Haugbøl S, Pinborg LH, Regeur L, Hansen ES, Bolwig TG, Nielsen FA, et al. Cerebral 5-HT2A receptor binding is increased in patients with Tourette's syndrome. *Int J Neuropsychopharmacol*. (2007) 10:245–52. doi: 10.1017/S1461145706006559
328. Erritzoe D, Rasmussen H, Kristiansen KT, Frokjaer VG, Haugbol S, Pinborg L, et al. Cortical and subcortical 5-HT2A receptor binding in neuroleptic-naive first-episode schizophrenic patients. *Neuropsychopharmacol Off Publ Am Coll Neuropsychopharmacol*. (2008) 33:2435–41. doi: 10.1038/sj.npp.1301656
329. Frank GK, Kaye WH, Meltzer CC, Price JC, Greer P, McConaha C, et al. Reduced 5-HT2A receptor binding after recovery from anorexia nervosa. *Biol Psychiatry*. (2002) 52:896–906. doi: 10.1016/S0006-3223(02)01378-1
330. Adams KH, Hansen ES, Pinborg LH, Hasselbalch SG, Svarer C, Holm S, et al. Patients with obsessive-compulsive disorder have increased 5-HT2A receptor binding in the caudate nuclei. *Int J Neuropsychopharmacol*. (2005) 8:391–401. doi: 10.1017/S1461145705005055
331. Erlandsson K, Sivananthan T, Lui D, Spezzi A, Townsend CE, Mu S, et al. Measuring SSRI occupancy of SERT using the novel tracer [123I]ADAM: a SPECT validation study. *Eur J Nucl Med Mol Imaging*. (2005) 32:1329–36. doi: 10.1007/s00259-005-1912-y
332. Klein N, Sacher J, Geiss-Granadia T, Attarbaschi T, Mossaheb N, Lanzenberger R, et al. *In vivo* imaging of serotonin transporter occupancy by means of SPECT and [123I]ADAM in healthy subjects administered

different doses of escitalopram or citalopram. *Psychopharmacology*. (2006) 188:263–72. doi: 10.1007/s00213-006-0486-0
333. Herold N, Uebelhack K, Franke L, Amthauer H, Luedemann L, Bruhn H, et al. Imaging of serotonin transporters and its blockade by citalopram in patients with major depression using a novel SPECT ligand [123I]-ADAM. *J Neural Transm*. (2006) 113:659–70. doi: 10.1007/s00702-005-0429-7
334. Meyer JH, Wilson AA, Ginovart N, Goulding V, Hussey D, Hood K, et al. Occupancy of serotonin transporters by paroxetine and citalopram during treatment of depression: a [(11)C]DASB PET imaging study. *Am J Psychiatry*. (2001) 158:1843–9. doi: 10.1176/appi.ajp.158.11.1843
335. Parsey RV, Kent JM, Oquendo MA, Richards MC, Pratap M, Cooper TB, et al. Acute occupancy of brain serotonin transporter by sertraline as measured by [11C]DASB and positron emission tomography. *Biol Psychiatry*. (2006) 59:821–8. doi: 10.1016/j.biopsych.2005.08.010
336. Voineskos AN, Wilson AA, Boovariwala A, Sagrati S, Houle S, Rusjan P, et al. Serotonin transporter occupancy of high-dose selective serotonin reuptake inhibitors during major depressive disorder measured with [11C]DASB positron emission tomography. *Psychopharmacology*. (2007) 193:539–45. doi: 10.1007/s00213-007-0806-z
337. Lundberg J, Christophersen JS, Petersen KB, Loft H, Halldin C, Farde L. PET measurement of serotonin transporter occupancy: a comparison of escitalopram and citalopram. *Int J Neuropsychopharmacol*. (2007) 10:777–85. doi: 10.1017/S1461145706007486
338. Newberg AB, Amsterdam JD, Wintering N, Ploessl K, Swanson RL, Shults J, et al. 123I-ADAM binding to serotonin transporters in patients with major depression and healthy controls: a preliminary study. *J Nucl Med Off Publ Soc Nucl Med*. (2005) 46:973–7.
339. Schuh-Hofer S, Richter M, Geworski L, Villringer A, Israel H, Wenzel R, et al. Increased serotonin transporter availability in the brainstem of migraineurs. *J Neurol*. (2007) 254:789–96. doi: 10.1007/s00415-006-0444-0
340. Bhagwagar Z, Murthy N, Selvaraj S, Hinz R, Taylor M, Fancy S, et al. 5-HTT binding in recovered depressed patients and healthy volunteers: a positron emission tomography study with [11C]DASB. *Am J Psychiatry*. (2007) 164:1858–65. doi: 10.1176/appi.ajp.2007.06111933
341. Frankle WG, Narendran R, Huang Y, Hwang D-R, Lombardo I, Cangiano C, et al. Serotonin transporter availability in patients with schizophrenia: a positron emission tomography imaging study with [11C]DASB. *Biol Psychiatry*. (2005) 57:1510–6. doi: 10.1016/j.biopsych.2005.02.028
342. Reimold M, Smolka MN, Zimmer A, Batra A, Knobel A, Solbach C, et al. Reduced availability of serotonin transporters in obsessive-compulsive disorder correlates with symptom severity – a [11C]DASB PET study. *J Neural Transm*. (2007) 114:1603–9. doi: 10.1007/s00702-007-0785-6
343. Brown AK, George DT, Fujita M, Liow J-S, Ichise M, Hibbeln J, et al. PET [11C]DASB imaging of serotonin transporters in patients with alcoholism. *Alcohol Clin Exp Res*. (2007) 31:28–32. doi: 10.1111/j.1530-0277.2006.00261.x
344. Cannon DM, Ichise M, Fromm SJ, Nugent AC, Rollis D, Gandhi SK, et al. Serotonin transporter binding in bipolar disorder assessed using [11C]DASB and positron emission tomography. *Biol Psychiatry*. (2006) 60:207–17. doi: 10.1016/j.biopsych.2006.05.005
345. Kalbitzer J, Frokjaer VG, Erritzoe D, Svarer C, Cumming P, Nielsen FÅ, et al. The personality trait openness is related to cerebral 5-HTT levels. *NeuroImage*. (2009) 45:280–5. doi: 10.1016/j.neuroimage.2008.12.001
346. Kalbitzer J, Erritzoe D, Holst KK, Nielsen FA, Marner L, Lehel S, et al. Seasonal changes in brain serotonin transporter binding in short serotonin transporter linked polymorphic region-allele carriers but not in long-allele homozygotes. *Biol Psychiatry*. (2010) 67:1033–9. doi: 10.1016/j.biopsych.2009.11.027
347. Huang Y-Y, Huang W-S, Ma K-H, Chou T-K, Kuo Y-Y, Cheng C-Y, et al. Synthesis and comparison of 4-[18F]F-ADAM, 2-[18F]F-ADAM, N-Desmethyl-4-[18F]F-ADAM and [18F]F-AFM as serotonin transporter imaging agents. *Appl Radiat Isot*. (2012) 70:2298–307. doi: 10.1016/j.apradiso.2012.06.005
348. Yeh Y-W, Ho P-S, Kuo S-C, Chen C-Y, Liang C-S, Yen C-H, et al. Disproportionate reduction of serotonin transporter may predict the response and adherence to antidepressants in patients with major depressive disorder: a positron emission tomography study with 4-[18F]-ADAM. *Int J Neuropsychopharmacol*. (2015) 18:pyu120. doi: 10.1093/ijnp/pyu120
349. Sullivan GM, Oquendo MA, Simpson N, Van Heertum RL, Mann JJ, Parsey RV. Brain serotonin1A receptor binding in major depression is related to psychic and somatic anxiety. *Biol Psychiatry*. (2005) 58:947–54. doi: 10.1016/j.biopsych.2005.05.006
350. Santhosh L, Estok KM, Vogel RS, Tamagnan GD, Baldwin RM, Mitsis EM, et al. Regional distribution and behavioral correlates of 5-HT2A receptors in Alzheimer's disease with [18F]deuteroaltanserin and PET. *Psychiatry Res Neuroimaging*. (2009) 173:212–7. doi: 10.1016/j.pscychresns.2009.03.007
351. Bhagwagar Z, Hinz R, Taylor M, Fancy S, Cowen P, Grasby P. Increased 5-HT(2A) receptor binding in euthymic, medication-free patients recovered from depression: a positron emission study with [(11)C]MDL 100,907. *Am J Psychiatry*. (2006) 163:1580–7. doi: 10.1176/ajp.2006.163.9.1580
352. Perani D, Garibotto V, Gorini A, Moresco RM, Henin M, Panzacchi A, et al. *In vivo* PET study of 5HT(2A) serotonin and D(2) dopamine dysfunction in drug-naive obsessive-compulsive disorder. *NeuroImage*. (2008) 42:306–14. doi: 10.1016/j.neuroimage.2008.04.233
353. Saigal N, Pichika R, Easwaramoorthy B, Collins D, Christian BT, Shi B, et al. Synthesis and biologic evaluation of a novel serotonin 5-HT1A receptor radioligand, 18F-labeled mefway, in rodents and imaging by PET in a nonhuman primate. *J Nucl Med Off Publ Soc Nucl Med*. (2006) 47:1697–706.
354. Wilson AA, Ginovart N, Hussey D, Meyer J, Houle S. *In vitro* and *in vivo* characterisation of [11C]-DASB: a probe for *in vivo* measurements of the serotonin transporter by positron emission tomography. *Nucl Med Biol*. (2002) 29:509–15. doi: 10.1016/S0969-8051(02)00316-5
355. Selvaraj S, Turkheimer F, Rosso L, Faulkner P, Mouchlianitis E, Roiser JP, et al. Measuring endogenous changes in serotonergic neurotransmission in humans: a [^{11}C]CUMI-101 PET challenge study. *Mol Psychiatry*. (2012) 17:1254–60. doi: 10.1038/mp.2012.78
356. Elfving B, Madsen J, Knudsen GM. Neuroimaging of the serotonin reuptake site requires high-affinity ligands. *Synapse*. (2007) 61:882–8. doi: 10.1002/syn.20443
357. Maziere B, Crouzel C, Venet M, Stulzaft O, Sanz G, Ottaviani M, et al. Synthesis, affinity and specificity of 18F-setoperone, a potential ligand for *in-vivo* imaging of cortical serotonin receptors. *Int J Rad Appl Instrum B*. (1988) 15:463–8. doi: 10.1016/0883-2897(88)90018-9
358. Blin J, Baron JC, Dubois B, Crouzel C, Fiorelli M, Attar-Lévy D, et al. Loss of brain 5-HT2 receptors in Alzheimer's disease. *In vivo* assessment with positron emission tomography and [18F]setoperone. *Brain J Neurol*. (1993) 116 (Pt 3):497–510. doi: 10.1093/brain/116.3.497
359. Chabriat H, Tehindrazanarivelo A, Vera P, Samson Y, Pappata S, Boullais N, et al. 5HT2 receptors in cerebral cortex of migraineurs studied using PET and 18F-fluorosetoperone. *Cephalalgia Int J Headache*. (1995) 15:104–8; discussion 77. doi: 10.1046/j.1468-2982.1995.015002104.x
360. Véra P, Zilbovicius M, Chabriat H, Amarenco P, Kerdraon J, Ménard JF, et al. Post-stroke changes in cortical 5-HT2 serotonergic receptors. *J Nucl Med Off Publ Soc Nucl Med*. (1996) 37:1976–81.
361. Massou JM, Trichard C, Attar-Levy D, Feline A, Corruble E, Beaufils B, et al. Frontal 5-HT2A receptors studied in depressive patients during chronic treatment by selective serotonin reuptake inhibitors. *Psychopharmacology*. (1997) 133:99–101. doi: 10.1007/s002130050377
362. Shiue GG, Choi S-R, Fang P, Hou C, Acton PD, Cardi C, et al. N,N-Dimethyl-2-(2-Amino-4-18F-Fluorophenylthio)-Benzylamine (4-18F-ADAM): an improved PET radioligand for serotonin transporters. *J Nucl Med*. (2003) 44:1890–7.
363. Shah M, Seibyl J, Cartier A, Bhatt R, Catafau AM. Molecular imaging insights into neurodegeneration: focus on α-synuclein radiotracers. *J Nucl Med Off Publ Soc Nucl Med*. (2014) 55:1397–400. doi: 10.2967/jnumed.113.136515
364. Burré J, Sharma M, Tsetsenis T, Buchman V, Etherton MR, Südhof TC. Alpha-synuclein promotes SNARE-complex assembly *in vivo* and *in vitro*. *Science*. (2010) 329:1663–7. doi: 10.1126/science.1195227
365. El-Agnaf OMA, Salem SA, Paleologou KE, Cooper LJ, Fullwood NJ, Gibson MJ, et al. Alpha-synuclein implicated in Parkinson's disease is present in extracellular biological fluids, including human plasma. *FASEB J Off Publ Fed Am Soc Exp Biol*. (2003) 17:1945–7. doi: 10.1096/fj.03-0098fje
366. Lee H-J, Patel S, Lee S-J. Intravesicular localization and exocytosis of alpha-synuclein and its aggregates. *J Neurosci Off J Soc Neurosci*. (2005) 25:6016–24. doi: 10.1523/JNEUROSCI.0692-05.2005

367. Dickson DW, Braak H, Duda JE, Duyckaerts C, Gasser T, Halliday GM, et al. Neuropathological assessment of Parkinson's disease: refining the diagnostic criteria. *Lancet Neurol.* (2009) 8:1150–7. doi: 10.1016/S1474-4422(09)70238-8
368. Brooks DJ, Tambasco N. Imaging synucleinopathies. *Mov Disord Off J Mov Disord Soc*. (2016) 31:814–29. doi: 10.1002/mds.26547
369. Paleologou KE, Kragh CL, Mann DMA, Salem SA, Al-Shami R, Allsop D, et al. Detection of elevated levels of soluble alpha-synuclein oligomers in post-mortem brain extracts from patients with dementia with Lewy bodies. *Brain J Neurol.* (2009) 132(Pt 4):1093–101. doi: 10.1093/brain/awn349
370. Choi JH, Stubblefield B, Cookson MR, Goldin E, Velayati A, Tayebi N, et al. Aggregation of α-synuclein in brain samples from subjects with glucocerebrosidase mutations. *Mol Genet Metab.* (2011) 104:185–8. doi: 10.1016/j.ymgme.2011.06.008
371. Kotzbauer PT, Cairns NJ, Campbell MC, Willis AW, Racette BA, Tabbal SD, et al. Pathologic accumulation of α-synuclein and Aβ in parkinson disease patients with dementia. *Arch Neurol.* (2012) 69:1326–31. doi: 10.1001/archneurol.2012.1608
372. Schildknecht S, Gerding HR, Karreman C, Drescher M, Lashuel HA, Outeiro TF, et al. Oxidative and nitrative alpha-synuclein modifications and proteostatic stress: implications for disease mechanisms and interventions in synucleinopathies. *J Neurochem*. (2013) 125:491–511. doi: 10.1111/jnc.12226
373. Uchihara T, Nakamura A, Mochizuki Y, Hayashi M, Orimo S, Isozaki E, et al. Silver stainings distinguish Lewy bodies and glial cytoplasmic inclusions: comparison between Gallyas-Braak and Campbell-Switzer methods. *Acta Neuropathol*. (2005) 110:255–60. doi: 10.1007/s00401-005-1044-2
374. Anderson JP, Walker DE, Goldstein JM, de Laat R, Banducci K, Caccavello RJ, et al. Phosphorylation of Ser-129 is the dominant pathological modification of alpha-synuclein in familial and sporadic Lewy body disease. *J Biol Chem.* (2006) 281:29739–52. doi: 10.1074/jbc.M600933200
375. Maetzler W, Reimold M, Liepelt I, Solbach C, Leyhe T, Schweitzer K, et al. [11C]PIB binding in Parkinson's disease dementia. *NeuroImage*. (2008) 39:1027–33. doi: 10.1016/j.neuroimage.2007.09.072
376. Fodero-Tavoletti MT, Mulligan RS, Okamura N, Furumoto S, Rowe CC, Kudo Y, et al. *In vitro* characterisation of BF227 binding to alpha-synuclein/Lewy bodies. *Eur J Pharmacol*. (2009) 617:54–8. doi: 10.1016/j.ejphar.2009.06.042
377. Kikuchi A, Takeda A, Okamura N, Tashiro M, Hasegawa T, Furumoto S, et al. *In vivo* visualization of alpha-synuclein deposition by carbon-11-labelled 2-[2-(2-dimethylaminothiazol-5-yl)ethenyl]-6-[2-(fluoro)ethoxy]benzoxazole positron emission tomography in multiple system atrophy. *Brain J Neurol.* (2010) 133(Pt 6):1772–8. doi: 10.1093/brain/awq091
378. Verdurand M, Levigoureux E, Lancelot S, Zeinyeh W, Billard T, Quadrio I, et al. Amyloid-beta radiotracer [18F]BF-227 does not bind to cytoplasmic glial inclusions of postmortem multiple system atrophy brain tissue. *Contrast Media Mol Imaging.* (2018) 2018:9165458. doi: 10.1155/2018/9165458
379. Bagchi DP, Yu L, Perlmutter JS, Xu J, Mach RH, Tu Z, et al. Binding of the radioligand SIL23 to α-synuclein fibrils in Parkinson disease brain tissue establishes feasibility and screening approaches for developing a Parkinson disease imaging agent. *PLoS ONE*. (2013) 8:e55031. doi: 10.1371/journal.pone.0055031
380. Verdurand M, Levigoureux E, Zeinyeh W, Berthier L, Mendjel-Herda M, Cadarossanesaib F, et al. *In silico*, *in vitro*, and *in vivo* evaluation of new candidates for α-synuclein PET imaging. *Mol Pharm*. (2018) 15:3153–66. doi: 10.1021/acs.molpharmaceut.8b00229
381. Ye L, Velasco A, Fraser G, Beach TG, Sue L, Osredkar T, et al. *In vitro* high affinity alpha-synuclein binding sites for the amyloid imaging agent PIB are not matched by binding to Lewy bodies in postmortem human brain. *J Neurochem.* (2008) 105:1428–37. doi: 10.1111/j.1471-4159.2008.05245.x
382. Fodero-Tavoletti MT, Smith DP, McLean CA, Adlard PA, Barnham KJ, Foster LE, et al. *In vitro* characterization of pittsburgh compound-B binding to lewy bodies. *J Neurosci.* (2007) 27:10365–71. doi: 10.1523/JNEUROSCI.0630-07.2007
383. McKeith IG. Consensus guidelines for the clinical and pathologic diagnosis of dementia with Lewy bodies (DLB): report of the Consortium on DLB International Workshop. *J Alzheimers Dis JAD*. (2006) 9(Suppl. 3):417–23. doi: 10.3233/JAD-2006-9S347
384. Gilman S, Low PA, Quinn N, Albanese A, Ben-Shlomo Y, Fowler CJ, et al. Consensus statement on the diagnosis of multiple system atrophy. *J Neurol Sci.* (1999) 163:94–8. doi: 10.1016/S0022-510X(98)00304-9
385. Deutsch SI, Rosse RB, Schwartz BL, Mastropaolo J. A revised excitotoxic hypothesis of schizophrenia: therapeutic implications. *Clin Neuropharmacol*. (2001) 24:43. doi: 10.1097/00002826-200101000-00008

Conflict of Interest: The authors declare that the research was conducted in the absence of any commercial or financial relationships that could be construed as a potential conflict of interest.

frontiers in Medicine

REVIEW
published: 14 February 2020
doi: 10.3389/fmed.2020.00034

Cell Tracking in Cancer Immunotherapy

*Justine Perrin[1†], Marisa Capitao[1†], Marie Mougin-Degraef[1,2], François Guérard[1], Alain Faivre-Chauvet[1,2], Latifa Rbah-Vidal[1], Joëlle Gaschet[1], Yannick Guilloux[1], Françoise Kraeber-Bodéré[1,2,3], Michel Chérel[1,3] and Jacques Barbet[4]**

[1] CRCINA, INSERM, CNRS, Université d'Angers, Université de Nantes, Nantes, France, [2] Nuclear Medicine, University Hospital, Nantes, France, [3] Nuclear Medicine, ICO Cancer Center, Saint-Herblain, France, [4] GIP Arronax, Saint-Herblain, France

OPEN ACCESS

Edited by:
Anil Kumar Mishra, Institute of Nuclear Medicine & Allied Sciences (DRDO), India

Reviewed by:
Baljinder Singh, Post Graduate Institute of Medical Education and Research (PGIMER), India
Puja Panwar Hazari, Institute of Nuclear Medicine & Allied Sciences (DRDO), India

***Correspondence:**
Jacques Barbet
barbet@arronax-nantes.fr

[†]These authors have contributed equally to this work

Specialty section:
This article was submitted to Nuclear Medicine, a section of the journal Frontiers in Medicine

Received: *04 March 2019*
Accepted: *23 January 2020*
Published: *14 February 2020*

Citation:
Perrin J, Capitao M, Mougin-Degraef M, Guérard F, Faivre-Chauvet A, Rbah-Vidal L, Gaschet J, Guilloux Y, Kraeber-Bodéré F, Chérel M and Barbet J (2020) Cell Tracking in Cancer Immunotherapy. Front. Med. 7:34. doi: 10.3389/fmed.2020.00034

The impressive development of cancer immunotherapy in the last few years originates from a more precise understanding of control mechanisms in the immune system leading to the discovery of new targets and new therapeutic tools. Since different stages of disease progression elicit different local and systemic inflammatory responses, the ability to longitudinally interrogate the migration and expansion of immune cells throughout the whole body will greatly facilitate disease characterization and guide selection of appropriate treatment regiments. While using radiolabeled white blood cells to detect inflammatory lesions has been a classical nuclear medicine technique for years, new non-invasive methods for monitoring the distribution and migration of biologically active cells in living organisms have emerged. They are designed to improve detection sensitivity and allow for a better preservation of cell activity and integrity. These methods include the monitoring of therapeutic cells but also of all cells related to a specific disease or therapeutic approach. Labeling of therapeutic cells for imaging may be performed *in vitro*, with some limitations on sensitivity and duration of observation. Alternatively, *in vivo* cell tracking may be performed by genetically engineering cells or mice so that may be revealed through imaging. In addition, SPECT or PET imaging based on monoclonal antibodies has been used to detect tumors in the human body for years. They may be used to detect and quantify the presence of specific cells within cancer lesions. These methods have been the object of several recent reviews that have concentrated on technical aspects, stressing the differences between direct and indirect labeling. They are briefly described here by distinguishing *ex vivo* (labeling cells with paramagnetic, radioactive, or fluorescent tracers) and *in vivo* (*in vivo* capture of injected radioactive, fluorescent or luminescent tracers, or by using labeled antibodies, ligands, or pre-targeted clickable substrates) imaging methods. This review focuses on cell tracking in specific therapeutic applications, namely cell therapy, and particularly CAR (Chimeric Antigen Receptor) T-cell therapy, which is a fast-growing research field with various therapeutic indications. The potential impact of imaging on the progress of these new therapeutic modalities is discussed.

Keywords: cell tracking, immunotherapy, PET, SPECT, MRI, adoptive transfer, tumor microenvironment, cancer

INTRODUCTION

The origins of immunotherapy go back to early centuries of history as illustrated by the fight against smallpox. Realization that survivors were immune to the disease eventually led to the practice of inoculation or variolation, that spread throughout Europe in the early eighteenth century. The discovery of cowpox vaccination by Edward Jenner in 1796 ultimately resulted, after a global vaccination campaign, in the eradication of the disease announced by the World Health Organization in 1977. Fighting infectious diseases with vaccines proved successful, but eradication of other diseases remains elusive. While Jonas Salk developed the first poliomyelitis vaccine in the 1950, the disease is not yet considered as eradicated and remains endemic in several African countries (1). In the meantime, the role of immunity in other pathologies has been explored and the immune system is now identified as a general defense system that distinguishes self from non-self or altered self. Its ability to recognize normal cells from infected or tumor cells has implications in cancer immune surveillance, graft rejection, and many other pathologies but can also result in autoimmune, and inflammatory diseases. It was also realized that the immune system uses an incredibly complex network of connected cellular and molecular agents, not yet fully known and understood.

The focus of this review is on anti-cancer immunotherapy as it is making impressive progress. However, the concepts can also be paralleled in other immune-mediated disorders and for conditions requiring immunotherapeutic intervention. Therapeutic antibodies and cell-based therapies, such as adoptive immunotherapy and stem-cell therapy, have been developed years ago, but, in the last few years, a more precise understanding of control mechanisms of the immune system triggered an impressive development of immunotherapy (2). Novel therapeutic approaches have recently emerged that reached clinical practice with remarkable success in a variety of cancers (3, 4). The different types of tissue injuries and the different stages of disease progression are more precisely identified, as well as the different local and systemic inflammatory responses. Monitoring the depletion, migration, and expansion of immune cells throughout the whole body should help characterizing the diseases and guiding selection of appropriate treatment regiments (5). Such methods have an important role in basic cancer research, where they serve to elucidate novel biological mechanisms. The development of effective therapeutic strategies, targeting tumor cells as well as their micro-environment, also requires the ability to determine *in vivo* the location, distribution, and long-term viability of the cell populations as well as their biological fate with respect to cell activation and differentiation.

This process is referred to as cell tracking and is not limited to therapeutic cells but includes all cells related to a specific disease or therapeutic approach, like tumor cells, immune cells or microenvironment. It involves non-invasive methods for monitoring the distribution and migration of biologically active cells in living organisms. In conjunction with various non-invasive imaging modalities, cell-labeling methods, such as exogenous labeling or transfection with a reporter gene, allow visualization of labeled cells *in vivo* in real time, as well as monitoring and quantifying cell accumulation and function by a variety of imaging approaches. In this Review, we briefly describe the basic principles of cell-tracking methods and explain various approaches to cell tracking. Then we highlight recent examples of application of new technologies in animals, focusing on immune checkpoint inhibitor antibodies and cell-based therapies that use natural or genetically engineered T cells, dendritic cells, macrophages or stem cells, and when documented, the clinical potential of these methods.

CELL TRACKING METHODS: LOOKING FOR CELLS IN ANIMAL OR HUMAN BODIES

Most earlier reviews on this topic have classified imaging techniques as direct or indirect labeling methods. The distinction between direct and indirect labeling is not entirely clear and here we will discuss *ex vivo* vs. *in vivo* labeling: *ex vivo* labeling include labeling cells with paramagnetic, radioactive or fluorescent tracers before injection, while *in vivo* labeling relates to *in situ* imaging cells by injecting radioactive, fluorescent, or luminescent tracers, or antibodies.

SPECT and PET imaging with labeled monoclonal antibodies has been used for years to detect cancer cells. With the development of immuno-PET, they are now used to detect, quantify and longitudinally monitor *in vivo* a variety of cells in the context of immunotherapy of cancer and other diseases (6). Using radiolabeled tracers for *in vivo* imaging will thus be discussed in this review as one of the possible methods of cell tracking.

The various labeling techniques discussed in this review are presented schematically in **Figure 1**.

Ex vivo Cell Labeling

While the administration of radiolabeled white blood cells has been a classical nuclear medicine technique for years to detect inflammatory lesions (7), new non-invasive methods for monitoring the distribution and migration of biologically active cells in living organisms have emerged. They aim at improving the detection sensitivity and allowing for a better preservation of cell activity and integrity. These methods have been the subject of many reviews (8). Labeling therapeutic cells for imaging may now be performed *in vitro* with little impact on cell function nor migration ability, with some limitations on sensitivity and duration of observation (7, 9, 10). Methods based on radioactive imaging or MRI have the highest potential for clinical imaging. They are briefly presented here in this order, highlighting recent progress.

Radioactive (SPECT, PET)

Labeling cells with long-lived radionuclides before re-injection has been used for years in nuclear medicine routine, as mentioned above, but concerns about cell viability and maintenance of cell functions arose. Typically, ^{111}In-oxine is used to label leukocytes (11). Cell labeling yield is good, but a significant efflux rate was reported, and image

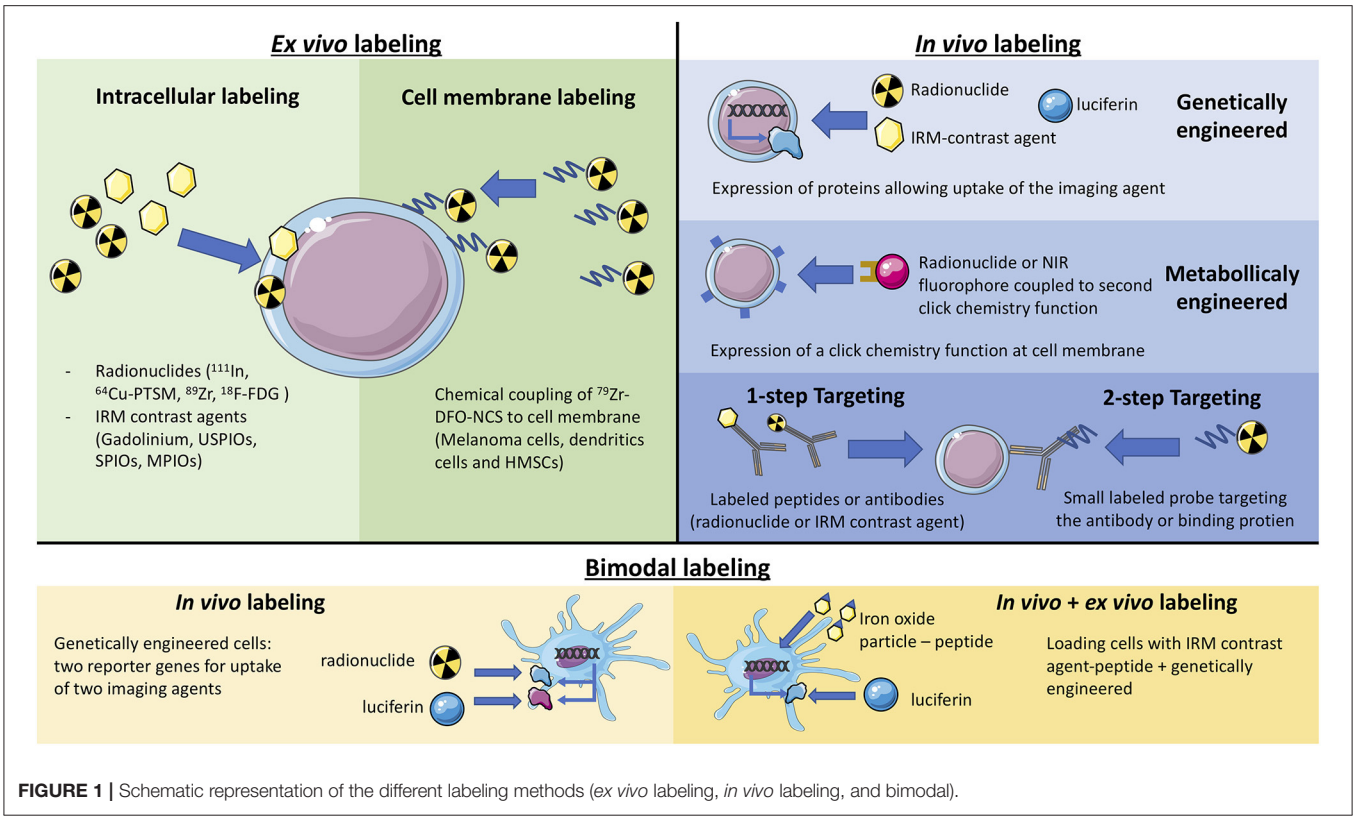

FIGURE 1 | Schematic representation of the different labeling methods (*ex vivo* labeling, *in vivo* labeling, and bimodal).

quality is considered suboptimal with this high energy single photon emitter.

Most recent developments relate to cell labeling using positron emitters because, in human, PET imaging offers better resolution and more precise quantification compared to SPECT. Copper-64 is an interesting candidate, with good imaging properties and a relatively long half-life of 12.7 h. ^{64}Cu-pyruvaldehyde-bis(N4-methylthiosemicarbazone (^{64}Cu-PTSM) was thus used to label C6 glioma cells, as the lipophilic complex is readily taken up in cells. A good cell labeling yield, but a significant efflux rate from cells was observed (12). Zirconium-89 has a half-life of 78.4 h, which is quite convenient to monitor cell trafficking over a few days after administration. Myeloma cells were labeled with ^{89}Zr-oxine using a technique similar to that used for In-111 cell labeling (9). Cell labeling yield was reasonable but contrasting results for efflux rate and cell viability were reported. Sato et al. (10) reported that ^{89}Zr-oxine complex readily labeled dendritic cells (DC) with an efficiency range of 13.0–43.9 and 83.5% ± 1.8 retention 5 days after labeling. In this study, it was considered that labeling did not affect the viability of mouse DCs and Cytotoxic T Lymphocytes (CTLs), nor did it affect functionality. More recently ^{89}Zr-labeled CAR (Chimeric Antigen Receptor) T cells were shown to retain more than 60% of the ^{89}Zr over 6 days while their capacity of *in vitro* cytokine production, migration, and tumor cytotoxicity, as well as their *in vivo* antitumor activity (13) were preserved. To further reduce efflux rate and improve viability and cell functions, labeling mixed lymphocyte cell populations with Zr-89 radiolabeled nanoparticles was explored (14, 15).

An alternative approach to loading the radionuclide inside the cells has been proposed. It uses Zr-89-desferrioxamine-NCS, which chemically couples to the membrane of cells. Mouse melanoma cells, dendritic cells and human mesenchymal stem cells were labeled by this method, which was shown to afford stable labeling for 7 days, with little effect of on cell viability and proliferation and to allow for serial PET scans in mouse models (16).

With its fast and efficient uptake and good retention, ^{18}F-labeled fluoro-2-deoxy-2-D-glucose (^{18}F-FDG) may be used to label cells *in vitro* to monitor cell traffic *in vivo*. For instance, cardiac stem cells were labeled and their biodistribution and retention was quantified in a pig model of chronic myocardial infarction (17). A potential drawback of ^{18}F-FDG for assessing cell therapies following implantation is the local retention of radiotracer released from the cells. Thus, 3′-deoxy-3′-L-[^{18}F]-fluorothymidine (^{18}F-FLT) has been proposed to label cells instead of ^{18}F-FDG. Human Umbilical Endothelial Vein Cells (HUVECs) incubated with ^{18}F-FLT and injected in mice with hind-limb ischemia were shown to provide a better estimation of HUVECs retention than cells labeled with ^{18}F-FDG (18).

Magnetic Resonance Imaging (MRI)

Gadolinium(III) chelates, such as gadopentetate dimeglumine, are effective paramagnetic contrast agents owing to their unpaired electrons. These electrons confer a magnetic moment

that increases the relaxivity of water protons, shortens the longitudinal relaxation rate (T1) and, therefore, increases the signal by creating a positive contrast in T1-weighted MRI images (19). The amount of gadolinium that may be loaded into cells obviously limits the sensitivity. As an example, rat mesenchymal stem cells (MSC) were loaded *in vitro* with Gd-DTPA using the lipidic transfection agent Effectene. Electron microscopy detected the presence of Gd-DTPA particles in the MSCs and no difference was observed in cell viability or proliferation between the labeled and unlabeled MSCs. T1-weighted MRI was then used to detect the labeled cells *in vitro* and in the rat brain (20).

Superparamagnetic iron-oxide particles have an inherently larger effect on MRI relaxivity than soluble paramagnetic agents. Their core may contain several thousand iron atoms, which increases the local iron concentration and sensitivity. These particles may be coated with dextran, siloxan, citrate, or polymers to improve biodistribution. The superparamagnetic agent results in negative contrast in T2-weighted sequences by causing inhomogeneities in the local magnetic field and spin–spin dephasing, which shortens transverse relaxation times (21). Ultra-small superparamagnetic iron oxide (USPIO) of 10–50 nm, superparamagnetic iron oxide (SPIO) of 50–100 nm and micrometer-sized iron oxide (MPIOs) up to $>1\,\mu m$ particles have been used (8). Again, cell viability limits the intracellular particle concentrations and thus cell detection sensitivity. Phagocytic cells, such as dendritic cells or pancreatic islet cells, can accumulate large amounts of nanoparticles to allow for their detection in animals and patients (22). Macrophages were easily and efficiently labeled with micrometer-sized particles of iron-oxide (MPIO) *in situ* and analyzed via *ex vivo* magnetic resonance microscopy (MRM) and *in vivo* monitoring by magnetic resonance imaging (MRI). The results were confirmed by fluorescence with an anti-macrophage phenotype marker F4/80 antibody (23). Technological improvements in the sensitivity of MRI equipment afforded promising results in detecting smaller numbers of cells that are difficult to label, including T lymphocytes (24).

Chemical exchange saturation transfer has been proposed as a new mechanism for contrast enhancement in MRI (25) in diamagnetic CEST or paramagnetic CEST (PARACEST), exchangeable protons resonate at a chemical shift different from that of water. Radiofrequency applied at their frequency saturates exchangeable protons, which transfer into water and reduce MRI signal in their vicinity. Although the sensitivity is rather low, the possibility of switching the signal "on" and "off" has attracted much interest (26).

Magnetic resonance also allows for high sensitivity detection of non-radioactive fluorine (^{19}F). Human NK cells were cultured for 24 or 48 h with a commercially available emulsified PFPE perfluorocarbon (CS-ATM-1000) under conditions where labeling had no measurable effect on cell viability and cytotoxicity against K562 leukemia cells. ^{19}F-labeled NK cells could then be detected at the site of injection and shown to migrate (27).

In vivo Labeling

Even if *in vitro* cell labeling looks rather easy and if progress has been made, direct labeling of cells prior to injection does not allow for long term *in vivo* imaging. Sensitivity is limited, especially for MRI, when cell viability and functionality is preserved. One drawback has been repeatedly mentioned: macrophages can take up cells or cell debris at the site of injection and migrate. The dilution of the imaging probe during cell division and its release from the cell eventually lead to the disappearance of the signal. Thus, finding alternative routes for tracking cells of interest *in vivo* has been the subject of many technical developments. One such alternative is the *in vitro* cell transfection with genes coding for transporters or enzymes as well as metabolic engineering that allow *in vivo* cell detection using various molecular imaging techniques after injection of a specific tracer.

Genetically Engineered Cells for Radioactive, MRI, or Bioluminescence Imaging

To achieve long term labeling, cells can be genetically engineered to express reporter genes. This reporter gene will allow the targeting of the cells by administering an imaging probe. A stable expression of this reporter allows for a virtually unlimited number of imaging sessions, without any impact of cell division.

Radioactive imaging

Iodine is taken up by the thyroid and by a few other tissues through the sodium-iodine symporter (NIS). Thus, cells were transfected with the NIS gene, most often the human gene (hNIS), injected and imaged by SPECT using a variety of radioactive tracers including iodine-123 (sodium iodide) and technetium-99m (sodium pertechnetate) in a variety of animal models (28). NIS may also be used for PET with iodine-124 or ^{18}F-tetrafluoroborate (29, 30). This approach was used recently to label tumor cells *in vivo* (31) and to monitor dendritic cell traffic from the skin to lymph nodes (32). This approach has some limitations, though. First, as mentioned above, NIS is expressed by a variety of normal cells, particularly in thyroid, salivary glands and stomach. Thus, imaging cells in these organs is excluded due to background signal. Second, sensitivity for the detection and quantification of transfected cells expressing NIS *in vivo* is limited because, in the transfected cells, the radioactive tracer does not become linked to tyrosine as iodine is in the thyroid.

Another reporter gene that has attracted much interest is the herpes simplex virus type 1 thymidine kinase (HSV1-tk). With this kind of genes that code for intracellular proteins, the risk of immune reactions is reduced. HSV1-tk allows for PET and SPECT using a variety of anti-viral agents specific for the virus kinase and not recognized by the human enzyme. They enter cells and become phosphorylated and trapped intracellularly only in HSV1-tk-transfected cells. Compounds such as FIAU (5-iodo-2-fluoro-2-deoxy-1-D-arabino-furanosyl-uracil), FEAU (2-fluoro-2-deoxyarabinofuranosyl-5-ethyluracil) or acycloguanosine derivatives (e.g., FPCV: fluoropenciclovir, FHBG: 9-[4-fluoro-3-(hydroxymethyl) butyl] guanine) may be labeled with ^{18}F and used for *in vivo* PET imaging. Sensitivity may be improved by using a mutated gene, HSV1-sr39tk, that codes for a more potent enzyme. HSV1-sr39tk may be used with [^{18}F]-FHBG as a tracer (33).

In a similar approach to the transfection of cells with viral thymidine kinase, animals may be engineered to express thymidine kinases in specific cells. As an example, Rosa26-mT/sr39tk mice were generated and HSV1-sr39tk expression in platelets, T lymphocytes or cardiomyocytes was induced. Longitudinal PET imaging and quantification of T-cell homing during inflammation and cardiomyocyte viability after myocardial infarction could then be monitored using [^{18}F]-FHBG, a cell-permeable tracer that is phosphorylated by HSV1-tk and retained inside the cells (34).

Alternatively, cells may be transfected to express cell-surface receptors for peptides as, for instance, the human glucagon-like peptide 1 receptor gene and imaged with the peptide labeled with fluorine-18 (35). A similar approach was used to detect transplanted pancreatic islet cells that express glucagon-like peptide 1 receptor (GLP-1R) by PET imaging after the injection of ^{64}Cu-DO3A-VS-Cys40-Exendin-4, showing persistent and specific uptake in the mouse pancreas (36). The mutated version of the dopamine receptor, D2R80A, that internalize ^{18}F-Fallypride, has also been proposed for imaging mesenchymal stem cells (37, 38).

Magnetic resonance imaging

Reporter-gene transfection has been proposed for MRI. The transferrin receptor has been used to capture transferrin-conjugated SPIO particles (39). Dendritic cells transfected with the ferritin gene show increased iron uptake that may be detected by MRI (40, 41). A very similar approach to the NIS system may be used for MRI, by transfecting cells with the Divalent Metal Transporter 1 (DMT1) that can import manganese (42). In the same setting, radioactive manganese (^{52}Mn), may be used for PET imaging (43).

Optical imaging

Bioluminescence imaging (BLI) consists in the use of a luciferase enzyme, which reacts with its substrate, luciferin, and emits light between 480 and 600 nm, depending on the type of enzyme (firefly, Renilla, or bacterial) and substrate (44). This method implies the insertion of the luciferase gene inside the genome of the tracked cells by cell transfection during *in vitro* culture or by engineering mice to express the luciferase in target cells. In this later case, the mouse itself allow for visualizing intrinsic cells during the development of a pathology. In the case of adoptive cellular therapy, the cells can be isolated from the mouse before the adoptive transfer without need for *in vitro* transfection. Although the insertion and expression of luciferase is stable, so far adoptively transferred cells have only been followed up to a week, due to the decay of the signal. This may be linked to the death of transferred cells (45). However, after the disappearance of the BLI signal, mice were sacrificed, and histology or flow cytometry was performed. It has been reported that, although the cells are still present and express luciferase, the BLI signal is no more detectable (46). Metabolic changes may be suspected as luciferases need energy and cofactors. Due to this lack of sensitivity, BLI is very often associated with another reporter gene, like Green Fluorescent Protein (GFP), which allow the *ex vivo* detection by flow cytometry or immunostaining of the organs.

Indeed, these reporter genes are most of the times not used alone but in association, either to enhance the signal (39) or to confirm its specificity by a different imaging approach (47, 48). Most of these proteins are endogenous and not toxic (dopamine receptor, NIS, ferritin). They can be expressed naturally in some organs of the human body, limiting their use. On the other side, inducing their expression in cells implies a possible impact on the functions of the cells.

Animals may also be made to express fluorescent proteins or luciferase in specific cells. This approach has been extensively developed for many different studies, including oncogenesis and cancer therapy (49). For instance, the photoconvertible fluorescent protein Kikume green-red protein was used to track dendritic cells *in vivo*. The KikGR protein changes its color from green to red upon UV illumination. Then, migration of dendritic cells, specifically CD103^{+} dendritic cells, from the skin to lymph nodes could be monitored after UV illumination of the skin of knock-in mice expressing the protein (50).

Metabolically Engineered Cells and Click Chemistry

Metabolic engineering and click chemistry (also known as bio-orthogonal chemistry) takes advantage of fast and high yield chemical reactions that may take place in aqueous media and even *in vivo*. A variety of chemical reagents have been developed that allow for highly specific reactions that are not hindered by biological conditions. Cells of interest were labeled by glycoengineering and bioorthogonal click chemistry by incubation *in vitro* with tetra-acetylated N-azidoacetyl-D-mannosamine to generate unnatural sialic acids with azide groups on their surface. The cells may then be injected *in vivo* and detected by the second click chemistry reagent, coupled to a fluorochrome such as dibenzyl cyclooctyne-conjugated Cy5 (DBCO-Cy5) for near-infrared fluorescence imaging or to iron-loaded nanoparticles for MRI (51). This approach was shown to improve labeling efficacy and to reduce false signals generated by macrophage phagocytosis of *in vitro* labeled cell debris. It does not require genetic modifications. So far, this approach has only been used for near-Infrared fluorescence (NIR) with stem cells and tumor cells (52, 53). Although NIR imaging is non-toxic and cheap, its limited spatial resolution and poor penetration through tissue complicate its use in clinical imaging.

Indirect Methods: Labeled Antibodies and Tracers

Labeled antibodies may be used to detect cells *in vivo* by SPECT, PET, or NIR fluorescence. They have mainly been used for tumor diagnosis, staging or tumor response monitoring (54). It has been reported that labeled antibodies allow the tracking of T cells *in vivo* (55).

The first step is to choose the target antigen. Ideally, this antigen should be exclusively expressed on target cells, but most of the time other tissue also express it. For T lymphocytes, many targets have been tested, e.g., CD3, CD8, CD2, and CD7 (56–58).

Once the target is chosen, the antibody must be radiolabeled. Ideally, the radionuclide has a half-life compatible with the biological half-life of the antibody. In human, ^{89}Zr and ^{64}Cu,

with half-lives of 78.4 and 12.7 h, respectively, have been used for PET imaging. The radiolabeling method also has an important impact on the quality of the images, since free radionuclide can lead to enhanced background noise, or worse, false positive signal in normal organs, where the target antigen is not expressed. For instance, ^{89}Zr shows a natural tropism to the bone (59) that can impede the tracking of bone marrow cells.

Multistep labeling techniques using antibodies have been developed to improve target to normal tissues ratio. Among these pretargeting approaches, the affinity enhancement system (AES) has been shown to be an excellent method for *in vivo* tumor imaging by SPECT and PET (60). Recently, new pretargeting approaches have been developed. One is based on the *in vivo* formation of an oligonucleotide duplex. A first oligonucleotide analog (e.g., peptide nucleic acid or PNA) is coupled to an antibody or a small binding protein (e.g., an anti-HER2 Affibody) for pretargeting of a radiolabeled complementary oligonucleotide analog (61). Another approach is based on bio-orthogonal chemistry (62). The CC49 antibody recognizing the tag72 antigen derivatized with trans-cyclooctene (TCO) was used for pretargeting ^{111}In-labeled DOTA-dipyridyltetrazine, demonstrating fast and high tumor activity uptake and high tumor to muscle ratio in a mouse model. Using small binding proteins such as diabodies or affibodies instead of intact IgG antibodies improves the pretargeting performances for PET (62, 63). Pretargeting may also be applied to NIR fluorescence imaging (63).

The feasibility of detecting cells *in vivo* using MRI and contrast agents targeted using antibodies or antibody fragments has been tested. Magnetic iron oxide nanoparticles were coated with ethylene oxide polymers and coupled to a ScFv targeting the epidermal growth factor receptor. The product showed a long blood circulation time and low accumulation in liver and spleen. Although *in vitro* binding and internalization was specific, 24 h after administration to mice bearing EGFR-positive breast cancer 4T1 mouse mammary tumors, MRI signal reduction resulting from uptake of the reagents in the tumor was observed but this signal reduction was equivalent for the targeted and the control products (64). More recently, the same approach was improved by site-selective scFv conjugation to SPION PEG nanoparticles. *In vivo*, the decrease of MR signals in HER2$^+$ xenograft tumor was about 30% at 24 h after the injection, while non-targeted SPION PEG nanoparticles showed no effect (65).

Bi(multi)Modal Imaging

Multimodality approaches deserve specific attention, even if they are generally limited to preclinical studies. Not only can they combine various imaging modalities, such as radioactive, MRI or optical imaging, but also *ex vivo* and *in vivo* labeling as well as post-mortem studies. Thus, bimodal systems have emerged that combine magnetic resonance imaging (MRI) or PET with fluorescence or bioluminescence.

Genetically engineered dendritic cells (DC) have been developed for MRI. Proteins which have an affinity for iron compounds may be used as MRI reporters. In a recent study, DC were engineered to express human ferritin heavy chain (FTH), which chelates iron and acts as an endogenous MRI contrast agent, and GFP genes to allow both fluorescence and MRI cell tracking (40). Reporter genes can also be an enzyme like the Drosophila melanogaster 2′-deoxynucleoside kinase (Dm–dNK) that phosphorylates native deoxynucleosides and a wide range of synthetic nucleoside analogs, including fluorescent nucleosides (66). In this study, the fluorescent nucleoside analog, 2′-deoxycytidine (pyrrolo-dC), generated highly specific CEST MRI signal and fluorescence for bimodal imaging (67).

DC can be loaded by phagocytosis of an antigen labeled with an MRI contrast agent (68). It is possible to effectively load DC with multifunctional polymeric nanoparticles. Nanoparticles composed of iron oxide bearing the OVA antigen coupled to a NIR fluorophore (MNP-OVA) allowed the monitoring of the migration of DCs to lymph nodes in DC adoptive transfer immunotherapy using NIR fluorescence imaging and MRI (69).

PET tracking of genetically engineered DC in combination with bioluminescence has also been developed. In a study, DC were made to express both human NIS and effluc genes. DC migration is then made possible by using ^{18}F-tetrafluoroborate (TFB), a substrate for the NIS reporter gene. Bioluminescence imaging is performed to confirm PET results (32). A combination of PET and Cerenkov luminescence has also been described (70).

Non-phagocytic regulatory T cells (Tregs) have been imaged *in vivo* after transduction by human NIS and the fluorescent protein mCherry. NIS expressing Tregs were labeled *in vitro* with technetium-99m pertechnetate ($^{99m}TcO4^-$) and imaged *in vivo* in C57BL/6 mice by SPECT/CT. After 24 h, Tregs were detected in the spleen and the bimodal labeling confirmed their localization by organ biodistribution studies and flow cytometry (71). In a similar way, bone marrow stem cells were labeled with gadodiamide (Omniscan), a non-ionic complex of gadolinium, using the fluorescent Arrest-In transfection reagent (72).

Nanoparticle systems can integrate therapeutic and imaging agents in a single formulation. They may be particularly useful as multimodal imaging agents. They have been used to deliver these agents through passive or active targeting to cells *in vitro* and *in vivo*. The different kinds of such nanoparticles, which include polymeric nanoparticles, micelles, liposomes and dendrimers and their potential applications in cancer immunotherapy, and immune cell tracking have been reviewed in detail (73).

CELL TRACKING ACHIEVEMENTS: WHAT HAPPENED IN CELL TRACKING OVER THE LAST TEN YEARS?

New methods have been developed, but has *in vivo* cell tracking advanced (cancer) immunotherapy? *In vivo* imaging has the potential to contribute as a drug development tool to improve the understanding of complex mechanisms of action, as a tool to improve efficacy, for example, by stratifying patients as possible responders or non-responders, and as a non-invasive treatment response biomarker to guide immunotherapy and recognize early signs of loss of efficacy. In cell therapy, a series of questions are asked about the delivery of the cells, their viability, differentiation of proliferation, as well as about the immune responses they may trigger. At this point, preclinical studies have been numerous,

but transfer to the clinic remains quite limited (74). This part of the review aims at providing a non-exhaustive survey of achievements in cell tracking using the current tracking methods summarized in **Table 1**.

Investigating the Tumor and Its Microenvironment

The evaluation of tumor volume and demonstration of tumor shrinkage remains the basis for tumor response assessment with the so-called RECIST criteria. It can be easily performed by CT-scans or MRI when the lesions are measurable, which is by far not always the case. In addition, tumor shrinkage may be delayed and some effective treatments (e.g., some kinase inhibitors) do not result in prominent tumor volume changes. Alternative response criteria, PERCIST, have been proposed (86). In addition, new imaging technologies offer possibilities to look at tumor lesions not as a non-descript mass of tumor cells, but as a complex body of interacting cells of different origins.

Imaging Tumor Cellular Composition

Measuring the relative number of tumor cells in the tumor lesion before and after treatment, may be useful in response assessment. Highly specific markers are needed. For instance, compounds that target melanin biosynthesis (benzamides) (87) and metallopeptides (88) binding to melanocortin type 1 receptor (labeled MSH analogs) have been used in melanoma, but many other labeled molecules, including antibodies, labeled for SPECT and PET, have shown high imaging performances in terms of sensitivity and specificity (89, 90).

Imaging TILs

Monitoring the phenotype and function of tumor infiltrating lymphocytes has long been recognized to be important in adoptive tumor cell therapy (91). This was achieved, in animals as well as in human, by the administration of radiolabeled tracers, usually antibodies or analogs, and SPECT or PET. For example, ^{64}Cu-labeled diabody specific for CD8 was used to assess CD8 T cell density in tumors in mice and treatment related changes (92). Whole antibodies, labeled with zirconium-89 afford similar results (56). Many target antigens have been tested in animal models (56, 58) and CD7 seems so far to be the best candidate to target T lymphocytes, with the lowest toxicity (56).

Surprisingly, in patients, immuno-PET has not been used to detect lymphocytes in tumors, other than through their expression of immune checkpoints, as discussed below. However, labeled IL-2 has been used to visualize lymphocyte infiltrating tumors (77, 93). In a pilot study, patients with metastatic melanoma receiving ipilimumab (IPI) or pembrolizumab (PEMBRO) were subjected to SPECT/CT imaging with ^{99m}Tc-labeled interleukin-2 in an attempt to detect TILs. In 5 patients (2 treated with IPI and 3 with PEMBRO), metastatic lesions could be visualized with a positive correlation between size and ^{99m}Tc-HYNIC-IL2 uptake, both before and after 12 weeks of therapy (93).

Texture analysis and radiomics may also, without administration of tracer, provide molecular information about infiltration of lymphocytes in tumors. In cancer patients, evidence of for the presence of CD3 T cells in tumors have been obtained by MRI texture analysis (94) and for the presence of CD8 T cells by CT radiomics and Artificial Intelligence analysis (95).

Macrophages

Macrophages are tissue-resident cells of the innate immune systems that perform a variety of functions in host tissue repair and maintenance of homeostasis. Macrophages are associated with auto-immune and inflammatory diseases and, in oncology, one of the tumor escape factors is the presence of pro-tumor macrophage, tumor-associated macrophages (TAM) that support tumor growth (96). *In vivo* studies have analyzed the biological role and migration of macrophages using different imaging methods such as fluorescent imaging (97), PET, MRI, and multimodal imaging. Macrophages migration to the inflammatory site after an induction of inflammation was analyzed by *in vitro* labeling with radioactive iodide-embedded gold nanoparticles (RIe-AuNPs) and PET imaging (76). During inflammatory disease such as arthritis, atherosclerotic plaques, *in vivo* staining of the macrophage with ^{111}In- or ^{64}Cu-labeled antibodies allowed imaging follow-up, evaluation of therapeutic efficacy and therapy adaption (98, 99). For acute or chronic obstructive pulmonary disease, the recruitment of macrophages was monitored by labeling with amine-modified PEGylated dextran-coated SPIO and MRI (81).

In oncology, macrophages are an important part of the tumor microenvironment and thus a therapeutic target. Indeed, the presence of TAM favors tumor escape. In order to assess their presence in tumors and to analyze the efficacy of therapy, these cells were tracked by immuno-SPECT using ^{111}In-labeled anti F4/80 (100) antibody, by MRI using the contrast agents MPIO (82) and ultra-small iron oxide nanoparticles (USPIO) (101), by BLI in transgenic luciferase mice (84) or by multimodal imaging combining MRI and BLI (85). PET imaging using labeled ligands targeting receptors overexpressed in macrophages, such as the Translocator protein (peripheral benzodiazepine receptor), has also been proposed (80).

Imaging Tumor Metabolic Activity

^{18}F-FDG is the most commonly used radiopharmaceutical for imaging tumor metabolism in clinical practice. Its use is based on the increased glycolytic rate in tumors compared to physiologic cells, known as the Warburg effect. However, inflammatory and other metabolically active effector immune cells may contribute to activity uptake in tumor lesions (102). By contrast, lesions with high numbers of proliferative tumor cells are ^{18}F-FDG avid, whereas low ^{18}F-FDG avid lesions have been shown by immunohistology to be infiltrated by activated immune cells. As a result, ^{18}F-FDG is not considered as a marker of immune response and new markers such as amino acids, nucleotides, choline, and receptor ligands have been studied. In hematolymphoid tissues, however, increased levels of deoxycytidine kinase (DCK) expression is found; DCK is the rate-limiting step in the deoxycytidine salvage pathway. The tissue-specific expression of this enzyme allows

TABLE 1 | Current tracking cell methods in pre-clinic, depending on the type of labeling (direct, indirect, and transgene) and the modality of imaging (TEP/SPECT, MRI, BLI/fluorescence, and multimodal imaging).

	Direct labeling			Indirect labeling				Transgene			
	Radioactive/ contrast agent	**Cell type**	**References**	**Radioactive/ contrast agent**	**Targeting molecule**	**Cell type**	**References**	**Transgene**	**Radioactive/ contrast agent**	**Cell type**	**References**
TEP/SPECT	Zirconium 89	Dendritic cells	(10)	Copper-64 and	Radiolabeled antibody anti	Tumor-infiltrated	(56, 77–79)	Transporter NIS	18F -tetra fl uorobora te	Dendritic cells and tumor cells	(31, 32)
		T cell	(10, 14–16, 75)	Zirconium-89	CDS, CD7, PDl, CD3	lymphocytes		GLP-IR	Copper-641abeled peptide	Pancreatic cells	(36)
	Indium-111	Leukocytes	(11)								
	Cuivre-64	Glioma cells	(12)	Inidum-111	anti HER2 affibody	Tumor cells	(61)				
	18-FDG	Cardiac stem cells	(17)		rituximab		(62)	D2R80A	18F-Fallypride	Stem cells	(37, 38)
			(18)				(63)	HSVI-tk	Fluor-18	T cells and cardiomyocytes	(34)
	18F-FLT	HUVECs	(76)	Lutetium-177	anti TAG72 diabody						
	Rie-AuNPs	Macrophages									
				Carbon-11	Diolabeled antibody anti F4	Macrophages	(80)				
MRI	SPIO	Dendritic cells	(22)	Iron nanoparticles	Click chemistry	Stem cells	(53)	Transferrin receptor	SPIO particles	Human Mesenchymal Stem Cells	(39)
		Macrophages	(81)								
		T cells	(24)								
	Gadolinium-DTPA	MSC	(20)					Ferritin	Iron uptake	Dendritic cells	(40, 41)
	MPIO, USPIO	Macrophages	(23, 76, 82)								
	Fluorine-19	NK cells	(27)								
BLI/fluorescence				ManNaz and DBCO	Click chemistry	Stem cells	(52, 53)	Luciferase		Stem cells	(34, 46)
										T cells	(83)
						Tumor cells	(63)			Macrophage	(84, 85)
								Kikume green-red		Dendritic cells	(50)
Multimodal	Fluorescence+ MRI	Dendritics cells :*ex vivo* labeling tumor peptide	(69)					Fluorescence+ MRI: DMdNk protein	CEST MRI	Genetically engineered DC	(66, 67) (32, 70)
								PET+BLI:NIS	18 tetrafluoroborate		
								TEP/IRM: transporteur DMTl	Manganese-52	Human stem cells	(43)
								PET+ fluorescence: NIS and mcherry gene	99mTC04-	Regulatory T cells	(71)

more specific targeting by, for example, ^{18}F—2-fluoro-D-(arabinofuranosyl)cytosine (^{18}F-FAC), which has been shown to accumulate preferentially in CD8^{+} T cells and in innate immune cells in mice (103).

^{18}F-labeled 3-fluoro-3-deoxythymidine (^{18}F-FLT) is trapped intracellularly after phosphorylation by thymidine kinase 1 (TK-1) but is not incorporated into DNA since ^{18}F-FLT-monophosphate is a very poor substrate of thymidylate kinase (TMPK). Imaging with ^{18}F-FLT has been evaluated to show proliferation more specifically (18), but effector immune cells that infiltrate tumors are mostly of a differentiated phenotype and do not proliferate. Thus, ^{18}F-FLT uptake in the lymph nodes of vaccinated patients only increased in the presence of antigen-loaded DC, providing the first clinical demonstration that immune responses induced by antigen-specific therapy can be imaged *in vivo* (102).

In bladder cancer, and presumably in other cancers, correlations have been observed between tumor ^{18}F-FDG uptake and expression of PD-1/PD-L1 (104). Such a correlation may be useful for the selection of appropriate therapeutic strategies.

Immune Checkpoint Inhibitors: Assessment of Immune Status in Tumor Lesions

Immunotherapy agents do not directly attack tumors but re-activate the immune system by targeting adaptive or innate immunity. Immuno-oncology has been revolutionized by the introduction of immune checkpoint inhibitors (ICI) and the approval of ipilimumab in 2011. ICI are monoclonal antibodies targeting immuno-regulatory molecules on the surface of T cells, antigen-presenting cells, and neoplastic cell populations. Clinical success of reagents blocking the CTLA-4 (cytotoxic T lymphocyte-associated protein 4, CD152) and PD-1/PD-L1 checkpoints (programmed cell death protein 1, CD279; programmed death-ligand 1, CD274) has driven rapid regulatory approval for treatment of patients with both solid and hematologic malignancies (105). Patients treated with immune checkpoint inhibitors (ICI) have objective response rates of 20–40% for solid tumors, lymphomas, and malignant melanomas. Thus, 60% of patients do not respond to treatment. It may of course be expected that patients with tumors presenting a higher load of tumor infiltrating lymphocytes (TIL) are more likely to respond to anti-PD-1/PD-L1 check point inhibitors (106).

A detailed understanding of the tumor microenvironment, including the identification and quantification of different immune cell subsets, their spatial context, and the expression of these immune checkpoint markers is obviously required to go further with these new therapies (107). Changes in immune cell infiltration and biomarker expression before and after therapeutic intervention are critical parameters for clinical development (108). Thus, assessment of PD-L1 expression by IHC has emerged as an important predictive biomarker for patients with various cancers including non-small cell lung cancer (NSCLC) and renal cell cancer (78).

Immuno-detection using antibodies labeled with zirconium-89 or copper-64 for PET, as well as indium-111 for SPECT, has been used to assess the CTLA-4 and PD-1 status of TIL *in vivo* and the expression of PD-L1 by tumor cells in order to predict the therapeutic efficacy of the administration of immune checkpoint inhibitors in mice and in human (79, 109–111). This approach was also proposed in the context of anti CTLA-4 therapy (107). Based on tumor biopsies, it appears that some patients with PD-L1-negative tumors show clinical benefit of anti-PD-L1 treatment. Thus, a zirconium-89-labeled anti-PD-L1 antibody (atezolizumab), was used to image 22 cancer patients before atezolizumab therapy. High PET signal was observed in lymphoid tissues and inflammation sites. In tumors, high but heterogeneous and variable across tumors uptake was observed and clinical responses could be better correlated with PET than with immunohistochemistry or other biomarkers (112).

In mice, the presence of CD8+ T-cells was monitored using ^{89}Zr-labeled an anti-CD8 single domain antibody after treatment of B16 melanoma with an anti-CTLA-4, showing that response correlated with the homogeneity of the distribution of CD8+ T-cells through the tumors (58). In mice with B6-F10 syngeneic melanoma, an anti-mouse PD-1 antibody labeled with copper-64 showed tumor uptake (79).

Monitoring the Activation and Expansion of Immune Effector Cells

Activation and expansion of the immune system may be monitored by imaging changes in the expression of various receptors to cytokines and growth factors as well as changes in the amounts of interstitial water resulting from inflammation. Immune cell trafficking is another aspect of immune system activation.

Imaging Immune Cell Activation

Several examples may be found in preclinical and clinical studies. In mice, an antibody against the cytokine IFNγ, which becomes sequestered at the surface of tumor cells after its production by T lymphocytes, was shown to reflect the activation status of cytotoxic T cells (113).

Reactive lymph nodes also express and secrete chemokines that induce immune cells relocation. Among others, the CCR7 chemokine and chemotactic agents, which play a key role in directing cell trafficking, are suitable imaging targets. For example, CXCL12 is a key chemotaxis factor for lymphocytes with expression of the CXCR4 receptor on their cell membrane (114). PET tracers targeting CXCR4 were thus used in cardiovascular disease and infections. Interestingly, Radiolabeled CXCR4 ligands are also very effective for cancer cell imaging (e.g., ^{68}Ga-labeled pentixafor) and CXCR4-trageting therapeutics labeled with ^{177}Lu are currently under clinical development (114).

Activation of the immune system also results in VEGF release and, subsequently, in significant lymph node volume increase. Lymph node volume can be measured using various techniques including MRI, CT, and ultrasound. Ultrasound imaging using targeted microbubbles improves the evaluation of the microvasculature (115). Dynamic contrast-enhanced (DCE)-MRI using gadolinium (Gd) or USPIO-based contrast agents may also be used to monitor angiogenesis: expansion of lymph

node size, total blood flow and blood volume, permeability of perfused capillaries, and total surface of perfused capillaries. MRI measures of vascularity using iron-based contrast agents have been validated against histology, the gold standard in angiogenesis assessment. Diffusion-weighted (DW)-MRI detects metastatic lymph nodes (116) and may be able to image reactive LNs in immune responses.

Imaging the expression of VEGF receptor may also be a way to monitor the activation of endothelial cells in LN resulting from immunotherapy. This was achieved in preclinical models by using anti-VEGFR (bevacizumab) labeled with indium-111 for SPECT (117) or by using RGD peptides labeled with various radionuclides for SPECT and PET imaging (118, 119). These approaches have shown potential in mice, for instance, to image inflammation-induced expansion and regression of lymphatic networks by PET, they have not yet been translated into human.

Changes that occur in the tumor due to an increased immune response can also be imaged using MRI, for example through changes in relaxation times, contrast, or apparent diffusion coefficient (120). These changes have been shown to correlate with conventional histological measures in mice after treatment by transferred cytotoxic T cells that expressed a modified TCR specific for a tumor antigen.

Imaging Trafficking of Immune Effector Cells

Antigen presenting cells (APC) are cells of the immune system that present pathogen peptides linked to class I or class II major histocompatibility complex (MHC) molecules to T lymphocytes (TL) to initiate adaptive immune responses. They are dendritic cells (DC), macrophages, and B lymphocytes. Analyzing antigen capture, migration to the lymph nodes and antigen presentation by APC started with fluorescently labeled cells using *in vivo* intravital optical imaging (121, 122). Regardless of the microscope type used, this system remains an invasive process, limited in depth penetration and restricted to a specific area of the body. Thus, APC trafficking has been monitored mostly by MRI and, more recently, tracking methods using PET have been reported. Either the cells or mice are genetically engineered, or labeled antigens are loaded *in vivo* or *ex vivo* into APC thanks to their phagocytic capacity. DC may be loaded *ex vivo* with pathogen peptides or irradiated tumor cells and reinjected to the patient. As an alternative, vaccination using labeled irradiated tumor cells or inactivated pathogens have been used to quantify antigen capture and delivery to lymph nodes by MRI (123).

Imaging lymphocyte trafficking is most easily achieved with *ex vivo* labeled cells. Transfused cells often traffic initially to the lungs, bone marrow, liver, and spleen. In mice, labeling Th1 cells with ^{64}Cu-PTSM was shown to permit their detection in single LNs and to monitor T-cell homing *in vivo* over 48 h (117). Changes in cell trafficking resulting from treatments with cyclophosphamide or IL-12 may be monitored by *in vivo* imaging. A similar method, using zirconium-89, was used to monitor γδ T-cells homing into tumor lesions in mice (75). IL13Rα2-CAR T cells delivered intraventricularly were detectable by PET for at least 6 days throughout the central nervous system and within intracranial tumors. When intravenously administered, PSCA-CAR T cells also showed tumor tropism, with a nine-fold greater tumor-to-muscle ratio than for CAR-negative T cells. Bone marrow uptake of ^{89}Zr-labeled hematopoietic stem cells could also be monitored in mice (124) and bone marrow cell uptake in acute fractures in mice could be inhibited, rather than accelerated, by a CXCR4 antagonist, plerixafor (125).

The use of reporter gene expression is another way to study cell trafficking, because imaging is independent of factors lifetime and distribution of the tracer and an enzymatic reporter allows for amplification of a weak signal. Antigen-specific T-cells were made to express a viral Tk gene could be tracked in mice, over a period of 3 weeks, using an ^{18}F-tagged probe specific to this variant of Tk. Detection of 10^4 T cells was claimed (67).

Lymphocytes may also be imaged by targeting cell surface markers. ^{99m}Tc-labeled IL-2 was used to detect tumor-infiltrating lymphocytes in melanoma patients (77, 93). Non-depleting ^{111}In-labeled anti-CD4 antibodies have been used to track CD4$^+$ T cells by SPECT in mice with good correlation with pathologic measures (126). *In vivo* ^{19}F MRI was also used to track homing to draining lymph nodes of T cells that were intracellularly labeled *ex vivo* with a perfluoropolyether (PFPE) nanoemulsion (127). Time-lapse ^{19}F MRI was used to calculate the number of T-cells in lymph nodes over 21 days and correlated with *in vitro* fluorescence measurements to compensate for *in vivo* T-cell division. MRI also allowed visualization of CD8$^+$ cytotoxic T cells, regulatory T cells, and myeloid-derived suppressor cells loaded with to monitor the effect of vaccination. Increased recruitment of cytotoxic T cells and decreased recruitment of myeloid-derived suppressor cells and regulatory T cells to the tumor was observed (128).

Cell-Based Therapies

Earlier Results in Cell-Based Therapy

So far, most clinical studies have used ^{99m}Tc or ^{111}In or superparamagnetic iron oxide to label therapeutic cells for *in vivo* cell tracking using SPECT or MRI, as reviewed by Srinivas et al. (129). Adoptive T-cell therapy (ACT) using expanded autologous tumor-infiltrating lymphocytes (TIL) and tumor antigen-specific T cell expanded from peripheral blood are complex but powerful immunotherapies. Clinical trials that included cell tracking have compared various routes of administration, the effect of the number of injected cells or host pretreatment with cyclofosfamide and compared various therapeutic cell preparation and encapsulation methods.

Tracking Antigen-Presenting Cells *in vivo*

DC are the most effective professional antigen presenting cells for the priming of naïve T cells *in vitro* and *in vivo*. These properties are the consequence of constitutive expression of MHC molecules class I and II and co-stimulatory molecules (CD80, CD86, CD40) and of their ability to secrete regulatory cytokines such as interleukin 12 upon recognition by the T cell receptor. In the immature stage, DC have the ability to capture the antigen by phagocytosis or endocytosis, migrate to the lymph nodes where they become mature and prime T lymphocytes

inducing the adaptive immunity. This is the reason why, in recent years, immunotherapy targeting dendritic cells has developed.

Imaging demonstrated the ability of intradermally or subcutaneously administered therapeutic DC to migrate from the sites of injection into lymph nodes with about 4% of DC reaching draining lymph nodes (130). Actual contact of the DC with T-cells cannot be demonstrated by *in vivo* imaging, but *ex vivo* only after lymph node resection. By contrast, intravenously injected mature DC are trapped in the lungs and redistribute to the liver, spleen, and bone marrow. No lymph node localization has been detected so far, which does not mean that DC completely fail to reach the lymph nodes. The techniques may not be sufficiently sensitive to detect the small numbers of cells that do reach the lymph nodes. Direct intranodal administration of therapeutic DC is also common in clinical studies. Then *in vivo* imaging has been used to study the migration of DC from the primary injected node to secondary nodes. The large variability in the fraction of injected cells (from 0 to 84 %) that was shown to migrate cast doubts on the accuracy of intranodal injections. Labeling the antigen to monitor its fate after DC delivery has been proposed in preclinical *in vivo* models. When DTPA was conjugated to the epsilon NH_2 group of the Lys154 residue, MHC binding of the peptide was preserved and could still be recognized by cytotoxic T cells. These studies allowed the non-invasive determination of the behavior of MHC–peptide complexes expressed by DC in cell vaccination (131) but has not yet been reproduced in the clinic.

CAR (Chimeric Antigen Receptor) T-Cell Therapy

CAR T-cell therapy is a fast-growing research field with various therapeutic indications in autoimmunity, allotransplantation, infection and cancer. Enhancing the functionality and the safety of the injected cells is an important aspect of the clinical development of this very potent therapy. Therefore, there is a real need to develop *in vivo* molecular imaging to better visualize, predict and improve the efficiency of this type of immunotherapy (5). However, so far, clinical studies of CAR T-cell tracking have only established proofs of concept of its feasibility (74).

SPECT and PET imaging are two possible modalities for tracking the fate of T-cells injected for therapeutic use. Labeling T-cells has been extensively investigated and radiolabeling is possible with little impact on cell function or migration ability (13). However, the radionuclide half-life is a limitation to track the cells more than for a few days after injection.

A variety of solutions to this limitation have been proposed (132). While multimodal imaging has been shown possible (133), CAR T-cell tracking in animals has demonstrated homing and persistence in the tumors and spleen by *ex vivo* MRI of tissue samples after CAR T-cell labeling with perfluorocarbon (134) and in whole animals by immuno-PET (135). Although the context of CAR T-cell therapy would be appropriate to develop genetic modification of the T-cells to express reporter genes as discussed above, the outcome of therapy remains monitored mostly by functional imaging and especially by MRI (136).

Other Adoptive T-Cell Transfer Therapies

Although BLI is most of the time used to follow tumor and stem cells, T cells could also be monitored thanks to the luciferase gene; for instance, the migration of CD8 T cells toward tumor site was evaluated in a xenograft mouse model (83), and the migration of tumor associated macrophages has been visualized in a transgenic mouse model of ovarian cancer (84). Also, by optical imaging, but using a fluorophore targeted to NIS-transfected cells, tracking of *ex vivo*-expanded NK cells has been performed *in vitro* and *in vivo* showing fast NK cell accumulation in tumors in triple-negative in breast cancer xenografts (137).

^{89}Zr-oxinate labeling was used to track $V_{\gamma 9}V_{\delta 2}$ T cells *in vivo* by PET. In a mouse xenograft model of human breast cancer, the $V_{\gamma 9}V_{\delta 2}$ T cells could be tracked over 1 week and it was shown that injection of PEGylated liposomal alendronate increased homing of the T cells to the tumors, which was confirmed by histology (75).

Stem Cell Therapies

Mesenchymal stem cells (MSC) have been proposed for cardiac regeneration after myocardial infarction (MI). Mesenchymal stem cells derived from rat fetal heart have the potential to differentiate into cardiomyocytes, endothelial cells and smooth muscle cells *in vitro*. These cells were labeled with technetium-99m for *in vivo* tracking that revealed a focal uptake of cells in the anterior mid-ventricular region of the heart in line with subsequent ventricular functional recovery (138). Cardiac stem cells were also loaded with ^{18}F-FDG and imaged by PET to quantify their biodistribution and assess the retention of implanted cells in a model of chronic myocardial infarction in pigs. Acute cell retention was shown not to correlate with cell engraftment, which is improved by IM injection (17).

Stem cells have been tracked in various models with BLI, for instance in acute liver injury or acute kidney injury, to study the migration and persistence of human bone-marrow derived stem cells to the liver and kidney (45, 139). Luciferase-transfected adipose-derived stem cells could be transplanted in liver and brain and monitored *in vivo* by bioluminescence for several days. *Ex vivo*, immunofluorescence detected the continued expression of luciferase for 4 months, demonstrating that the transplanted cells do not dye, even if the bioluminescence signal is lost (46).

In a tumor graft model, the migration of mesenchymal stem cells toward the subcutaneous tumor could also be observed (140). This study took advantage of a different type of luciferase that metabolizes different substrate, allowing them to follow the migration of stem cells with the Firefly Luciferase, and the tumor progression with the Renilla Luciferase.

BLI imaging has allowed to investigate the impact of stem cells injection modalities, showing that the intravenous route often leads to sequestration in the lung (141) preventing the migration of stem cells to other organs, while the intracardiac route seems to prevent this phenomenon.

DISCUSSION

Cell tracking has a long history of routine clinical use in Nuclear Medicine and it serves a purpose in infectious and inflammatory diseases despite its limitations (142). Imaging has an increasing role in the context of personalized medicine, which becomes the approach to take, at least in developed countries. CT-scan,

MRI and ultrasonography are now inescapable and Nuclear Medicine modalities have gained larger recognition, particularly in cancer. However, the number of tracers of frequent, routine use remains quite limited. In addition to bone and thyroid scans, ^{18}F-FDG is certainly the tracer that has the biggest impact in cancer management, with a few other PET tracers for those cancers in which ^{18}F-FDG does not perform so well, such as prostate cancer. In view of the incredible number of preclinical and early clinical studies about cancer imaging, this seems not much. There are many obvious reasons, the major one being the difficulty of demonstrating that a new imaging technique has its place in medicine as compared to all existing ones. If the imaging technique needs an injectable tracer, such as a radiopharmaceutical, the situation is worse, because of the cost of developing a product that has the regulatory status of a drug and by far not the sales and price of a therapeutic compound.

Will immunotherapy change this situation? Most of the very large number of original publications and reviews that deal with immunotherapy advocate for more imaging, especially more specific imaging of receptors, antigens and other biomarkers that characterize the function of cells *in vivo*. With the progress of cellular therapies, whether regenerative or cancer-oriented, many papers call for cell tracking *in vivo* as a way to understand their behavior and mechanisms of action and, by the way, to design improved therapies. Indeed, if not all novel immunotherapies are cell therapies, they all bear upon complex cellular interactions at the tumor sites and in immunologic tissues and better knowledge of the nature of cancer and non-cancer cells residing in tumors, their activation, proliferation and migration in living animals and, of course, in humans, must be a way of progress in therapy.

This realization triggered a lot of developments that made possible better cell labeling, mostly to make them visible by MRI and PET, for longer times after re-injection, as well as improved tracers to target specific biomarkers *in vivo*, using SPECT and PET, but also MRI, not only on tumor cells but on those cells that make the tumor microenvironment, e.g., endothelial cells, infiltrating antigen-presenting cells, lymphocytes, macrophages and other cells of the immune system. New techniques have been developed and the use of reporter genes to make cells detectable any time after their inoculation using specific tracers is a particularly elegant and powerful one. This review has rapidly depicted these approaches and it is expected that it convinces the reader that they are feasible and effective.

There is no best technique, though. It depends on the objective and, obviously, the most powerful one, for instance the use of reporter genes, are associated with complex manipulations, cost and regulatory hurdles. Interestingly, radioactive (SPECT, PET) and non-radioactive (MRI, optical imaging, ultrasonography) methods have been proposed, which all have advantages and drawbacks. Of course, bimodal and even multimodal agents have been developed. Multimodal imaging is clearly the way to go, with SPECT and PET now always associated with CT and PET-MRI systems developing. It is also clear that multimodal imaging experiments in animals that allowed for *in vivo* imaging and *ex vivo* in-depth investigation of the fate of injected cells and confirmation of *in vivo* imaging results are most convincing. However, such studies do not necessarily need bifunctional tracers, which sometimes look more like "tours de force" than candidates for further development.

One question here is: have these developments and studies been useful for the development of immunotherapy? The answer is not obvious. Such studies have pointed out to some problems and they have been mostly confirmatory, when they have not merely been proofs of concept for feasibility. This review has attempted at presenting clinical results in cell tracking and, while it may have missed some, it is in line with other recent reviews on the subject to conclude that the number of clinical studies is quite small. It may be considered that this is only the beginning of a new story and that groundbreaking discoveries in immunotherapy will be made thanks to imaging and that at least some of the approaches reported here will find their application. Very few cell tracking techniques will become routine. The introduction of reporter genes in therapeutic cells is probably the technique with the highest sensitivity for long term monitoring of cell trafficking, proliferation, and persistence. For cell therapies in which the cells are genetically modified, namely CAR-T cells, the addition of a second gene and cell tracking may be considered in the context of clinical trials. Whether this approach will be used in routine clinical practice is not likely. Conversely, tracers for *in vivo* imaging, particularly PET imaging, designed to detect and quantify specific cell populations are being developed and some will find a routine use. It is always difficult to make predictions, but it seems logical that expensive therapies or therapies that may be efficacious but associated with serious side-effects will not be given to patients who have no chance to benefit from them. The imaging of tumor microenvironment may give answers to how the patients will respond to such therapies, especially immunotherapy. Expression of immune checkpoints, like anti-PD-1, is already assessed from biopsies prior to immunotherapy, but the use of PET-imaging or MRI could allow a non-invasive assessment of the immune state of the tumor. This could provide new insights into the prediction of the response to treatment in patients. This is the theragnostic approach, which is not a reality today, but most probably be one in the future. It is also quite probable that future research in immunotherapy will take advantage of all these technological advances, certainly for preclinical studies, but also in the clinic. Indeed, it is time to combine the novel therapeutic approaches, which afford impressive remissions but not yet to all patients and this will call for precise, specific understanding of what is really going on in the living organism.

AUTHOR CONTRIBUTIONS

All authors listed have made a substantial, direct and intellectual contribution to the work, and approved it for publication.

FUNDING

This work was supported in part by grants from the French National Agency for Research called Investissements d'Avenir IRON Labex no ANR-11-LABX-0018-01 and ArronaxPlus Equipex no ANR-11-EQPX-0004.

REFERENCES

1. Baicus A. History of polio vaccination. *World J Virol*. (2012) 1:108. doi: 10.5501/wjv.v1.i4.108
2. Khalil DN, Smith EL, Brentjens RJ, Wolchok JD. The future of cancer treatment: Immunomodulation, CARs and combination immunotherapy. *Nat Rev Clin Oncol*. (2016) 13:273–90. doi: 10.1038/nrclinonc.2016.25
3. Hoos A. Development of immuno-oncology drugs—from CTLA4 to PD1 to the next generations. *Nat Rev Drug Discov*. (2016) 15:235–47. doi: 10.1038/nrd.2015.35
4. Maldini CR, Ellis GI, Riley JL. CAR T cells for infection, autoimmunity and allotransplantation. *Nat Rev Immunol*. (2018) 18:605–16. doi: 10.1038/s41577-018-0042-2
5. Fruhwirth GO, Kneilling M, de Vries IJM, Weigelin B, Srinivas M, Aarntzen EHJG. The potential of *in vivo* imaging for optimization of molecular and cellular anti-cancer immunotherapies. *Mol Imaging Biol*. (2018) 20:696–704. doi: 10.1007/s11307-018-1254-3
6. van Dongen GAMS, Visser GWM, Lub-de Hooge MN, de Vries EG, Perk LR. Immuno-PET: a navigator in monoclonal antibody development and applications. *Oncologist*. (2007) 12:1379–89. doi: 10.1634/theoncologist.12-12-1379
7. Roca M, de Vries EFJ, Jamar F, Israel O, Signore A. Guidelines for the labelling of leucocytes with 111In-oxine. Inflammation/Infection Taskgroup of the European Association of Nuclear Medicine. *Eur J Nucl Med Mol Imaging*. (2010) 37:835–41. doi: 10.1007/s00259-010-1393-5
8. Kircher MF, Gambhir SS, Grimm J. Noninvasive cell-tracking methods. *Nat Rev Clin Oncol*. (2011) 8:677–88. doi: 10.1038/nrclinonc.2011.141
9. Charoenphun P, Meszaros LK, Chuamsaamarkkee K, Sharif-Paghaleh E, Ballinger JR, Ferris TJ, et al. [89Zr]Oxinate4 for long-term *in vivo* cell tracking by positron emission tomography. *Eur J Nucl Med Mol Imaging*. (2014) 42:278–87. doi: 10.1007/s00259-014-2945-x
10. Sato N, Wu H, Asiedu KO, Szajek LP, Griffiths GL, Choyke PL. 89 Zr-Oxine complex PET cell imaging in monitoring cell-based therapies. *Radiology*. (2015) 275:490–500. doi: 10.1148/radiol.15142849
11. McAfee JG, Subramanian G, Gagne G. Technique of leukocyte harvesting and labeling: problems and perspectives. *Semin Nucl Med*. (1984) 14:83–106. doi: 10.1016/S0001-2998(84)80023-9
12. Phelps ME, Walsh J, McCarthy T, Adonai N, Iyer M, Toyokuni T, et al. *Ex vivo* cell labeling with 64Cu-pyruvaldehyde-bis(N4-methylthiosemicarbazone) for imaging cell trafficking in mice with positron-emission tomography. *Proc Natl Acad Sci USA*. (2002) 99:3030–5. doi: 10.1073/pnas.052709599
13. Weist MR, Starr R, Aguilar B, Chea J, Miles JK, Poku E, et al. PET of adoptively transferred chimeric antigen receptor T cells with 89Zr-Oxine. *J Nucl Med*. (2018) 59:1531–7. doi: 10.2967/jnumed.117.206714
14. Brown G, Ellis B, Locatelli P, Jones AKP, Fairclough M, Prenant C, et al. A new technique for the radiolabelling of mixed leukocytes with zirconium-89 for inflammation imaging with positron emission tomography. *J Label Compd Radiopharm*. (2016) 59:270–6. doi: 10.1002/jlcr.3392
15. Gennari A, Boutin H, Alzabin S, Jones AKP, Prenant C, McMahon A, et al. Development of a method for the preparation of zirconium-89 radiolabelled chitosan nanoparticles as an application for leukocyte trafficking with positron emission tomography. *Appl Radiat Isot*. (2017) 130:7–12. doi: 10.1016/j.apradiso.2017.09.004
16. Bansal A, Pandey MK, Demirhan YE, Nesbitt JJ, Crespo-Diaz RJ, Terzic A, et al. Novel 89Zr cell labeling approach for PET-based cell trafficking studies. *EJNMMI Res*. (2015) 5:19. doi: 10.1186/s13550-015-0098-y
17. Collantes M, Pelacho B, García-Velloso MJ, Gavira JJ, Abizanda G, Palacios I, et al. Non-invasive *in vivo* imaging of cardiac stem/progenitor cell biodistribution and retention after intracoronary and intramyocardial delivery in a swine model of chronic ischemia reperfusion injury. *J Transl Med*. (2017) 15:1–11. doi: 10.1186/s12967-017-1157-0
18. MacAskill MG, Tavares AS, Wu J, Lucatelli C, Mountford JC, Baker AH, et al. PET cell tracking using 18F-FLT is not limited by local reuptake of free radiotracer. *Sci Rep*. (2017) 7:44233. doi: 10.1038/srep44233
19. Caravan P, Ellison JJ, McMurry TJ, Lauffer RB. Gadolinium(III) chelates as MRI contrast agents: structure, dynamics, and applications. *Chem Rev*. (1999) 99:2293–352. doi: 10.1021/cr980440x
20. Yang ZX, Cheng X, Jia Y, Geng K, Wu R, Yi M, et al. Tracking of mesenchymal stem cells labeled with gadolinium diethylenetriamine pentaacetic acid by 7T magnetic resonance imaging in a model of cerebral ischemia. *Mol Med Rep*. (2014) 11:954–60. doi: 10.3892/mmr.2014.2805
21. Weissleder R, Cheng HC, Bogdanova A, Bogdanov A Jr. Magnetically labeled cells can be detected by MR imaging. *J Magn Reson Imaging*. 7:258–63. doi: 10.1002/jmri.1880070140
22. Sipe JC, Filippi M, Martino G, Furlan R, Rocca MA, Rovaris M, et al. Method for intracellular magnetic labeling of human mononuclear cells using approved iron contrast agents. *Magn Reson Imaging*. (1999) 17:1521–3. doi: 10.1016/S0730-725X(99)00085-5
23. Foley LM, Hitchens TK, Ho C, Janesko-Feldman KL, Melick JA, Bayir H, et al. Magnetic resonance imaging assessment of macrophage accumulation in mouse brain after experimental traumatic brain injury. *J Neurotrauma*. (2009) 26:1509–19. doi: 10.1089/neu.2008.0747
24. Smirnov P. Cellular magnetic resonance imaging using superparamagnetic anionic iron oxide nanoparticles: applications to *in vivo* trafficking of lymphocytes and cell-based anticancer therapy. *Methods Mol Biol*. (2009) 512:333–53. doi: 10.1007/978-1-60327-530-9_19
25. Ward KM, Aletras AH, Balaban RS. A new class of contrast agents for MRI based on proton chemical exchange dependent saturation transfer (CEST). *J Magn Reson*. (2000) 143:79–87. doi: 10.1006/jmre.1999.1956
26. Winter PM. Magnetic resonance chemical exchange saturation transfer imaging and nanotechnology. *Wiley Interdiscip Rev Nanomed Nanobiotechnol*. (2012) 4:389–98. doi: 10.1002/wnan.1167
27. Bouchlaka MN, Ludwig KD, Gordon JW, Kutz MP, Bednarz BP, Fain SB, et al. 19F-MRI for monitoring human NK cells *in vivo*. *Oncoimmunology*. (2016) 5:1–12. doi: 10.1080/2162402X.2016.1143996
28. Penheiter AR, Russell SJ, Carlson SK. The sodium iodide symporter (NIS) as an imaging reporter for gene, viral, and cell-based therapies. *Curr Gene Ther*. (2012) 12:33–47. doi: 10.2174/156652312799789235
29. Jauregui-Osoro M, Sunassee K, Weeks AJ, Berry DJ, Paul RL, Cleij M, et al. Synthesis and biological evaluation of [18F]tetrafluoroborate: a PET imaging agent for thyroid disease and reporter gene imaging of the sodium/iodide symporter. *Eur J Nucl Med Mol Imaging*. (2010) 37:2108–16. doi: 10.1007/s00259-010-1523-0
30. Youn H, Jeong JM, Chung J-K. A new PET probe, (18)F-tetrafluoroborate, for the sodium/iodide symporter: possible impacts on nuclear medicine. *Eur J Nucl Med Mol Imaging*. (2010) 37:2105–7. doi: 10.1007/s00259-010-1601-3
31. Diocou S, Volpe A, Jauregui-Osoro M, Boudjemeline M, Chuamsaamarkkee K, Man F, et al. [18F]tetrafluoroborate-PET/CT enables sensitive tumor and metastasis *in vivo* imaging in a sodium iodide symporter-expressing tumor model. *Sci Rep*. (2017) 7:946. doi: 10.1038/s41598-017-01044-4
32. Lee SB, Lee HW, Lee H, Jeon YH, Lee S-W, Ahn B-C, et al. Tracking dendritic cell migration into lymph nodes by using a novel PET probe 18F-tetrafluoroborate for sodium/iodide symporter. *EJNMMI Res*. (2017) 7:32. doi: 10.1186/s13550-017-0280-5
33. Collins SA, Hiraoka K, Inagaki A, Kasahara N, Tangney M. PET imaging for gene and cell therapy. *Curr Gene Ther*. (2012) 12:20–32. doi: 10.2174/156652312799789271
34. Thunemann M, Schörg BF, Feil S, Lin Y, Voelkl J, Golla M, et al. Cre/lox-assisted non-invasive *in vivo* tracking of specific cell populations by positron emission tomography. *Nat Commun*. (2017) 8:444. doi: 10.1038/s41467-017-00482-y
35. Pan Y, Lv J, Pan D, Xu Y, Yang M, Ju H, et al. Evaluating the utility of human glucagon-like peptide 1 receptor gene as a novel radionuclide reporter gene: a promising molecular imaging tool. *Appl Microbiol Biotechnol*. (2019) 103:1311–24. doi: 10.1007/s00253-018-9562-8
36. Wu Z, Todorov I, Li L, Bading JR, Li Z, Nair I, et al. *In vivo* imaging of transplanted islets with 64Cu-DO3A-VS-Cys 40 -exendin-4 by targeting GLP-1 receptor. *Bioconjug Chem*. (2011) 22:1587–94. doi: 10.1021/bc200132t
37. Haralampieva D, Betzel T, Dinulovic I, Salemi S, Stoelting M, Kramer SD, et al. Noninvasive PET imaging and tracking of engineered human muscle precursor cells for skeletal muscle tissue engineering. *J Nucl Med*. (2016) 57:1467–73. doi: 10.2967/jnumed.115.170548
38. Schonitzer V, Haasters F, Kasbauer S, Ulrich V, Mille E, Gildehaus FJ, et al. *In vivo* mesenchymal stem cell tracking with PET using the

dopamine type 2 receptor and 18F-fallypride. *J Nucl Med*. (2014) 55:1342–7. doi: 10.2967/jnumed.113.134775
39. Guo R, Li Q, Yang F, Hu X, Jiao J, Guo Y, et al. *In vivo* MR imaging of dual MRI reporter genes and deltex-1 gene-modified human mesenchymal stem cells in the treatment of closed penile fracture. *Mol Imaging Biol*. (2018) 20:417–27. doi: 10.1007/s11307-017-1128-0
40. Kim HS, Woo J, Lee JH, Joo HJ, Choi YS, Kim H, et al. *In vivo* tracking of dendritic cell using MRI reporter gene, ferritin. *PLoS ONE*. (2015) 10:1–13. doi: 10.1371/journal.pone.0125291
41. He X, Cai J, Liu B, Zhong Y, Qin Y. Cellular magnetic resonance imaging contrast generated by the ferritin heavy chain genetic reporter under the control of a Tet-On switch. *Stem Cell Res Ther*. (2015) 6:207. doi: 10.1186/s13287-015-0205-z
42. Bartelle BB, Mana MD, Suero-Abreu GA, Rodriguez JJ, Turnbull DH. Engineering an effective Mn-binding MRI reporter protein by subcellular targeting. *Magn Reson Med*. (2015) 74:1750–7. doi: 10.1002/mrm.25566
43. Lewis CM, Graves SA, Hernandez R, Valdovinos HF, Barnhart TE, Cai W, et al. 52Mn production for PET/MRI tracking of human stem cells expressing divalent metal transporter 1 (DMT1). *Theranostics*. (2015) 5:227–39. doi: 10.7150/thno.10185
44. Kim JE, Kalimuthu S, Ahn B-C. *In vivo* cell tracking with bioluminescence imaging. *Nucl Med Mol Imaging*. (2015) 49:3–10. doi: 10.1007/s13139-014-0309-x
45. Xie P, Hu X, Li D, Xie S, Zhou Z, Meng X, et al. Bioluminescence imaging of transplanted mesenchymal stem cells by overexpression of hepatocyte nuclear factor4α: tracking biodistribution and survival. *Mol Imaging Biol*. (2019) 21:44–53. doi: 10.1007/s11307-018-1204-0
46. Muñoz MF, Argüelles S, Guzman-Chozas M, Guillén-Sanz R, Franco JM, Pintor-Toro JA, et al. Cell tracking, survival, and differentiation capacity of adipose-derived stem cells after engraftment in rat tissue. *J Cell Physiol*. (2018) 233:6317–28. doi: 10.1002/jcp.26439
47. Qin C, Cheng K, Chen K, Hu X, Liu Y, Lan X, et al. Tyrosinase as a multifunctional reporter gene for Photoacoustic/MRI/PET triple modality molecular imaging. *Sci Rep*. (2013) 3:1490. doi: 10.1038/srep01490
48. Sanches PG, Peters S, Rossin R, Kaijzel EL, Que I, Löwik CWGM, et al. Bone metastasis imaging with SPECT/CT/MRI: a preclinical toolbox for therapy studies. *Bone*. (2015) 75:62–71. doi: 10.1016/j.bone.2015.02.002
49. Kocher B, Piwnica-Worms D. Illuminating cancer systems with genetically engineered mouse models and coupled luciferase reporters *in vivo*. *Cancer Discov*. (2013) 3:616–29. doi: 10.1158/2159-8290.CD-12-0503
50. Tomura M, Hata A, Matsuoka S, Shand FHW, Nakanishi Y, Ikebuchi R, et al. Tracking and quantification of dendritic cell migration and antigen trafficking between the skin and lymph nodes. *Sci Rep*. (2015) 4:6030. doi: 10.1038/srep06030
51. Kang S-W, Lee S, Na JH, Yoon HI, Lee D-E, Koo H, et al. Cell labeling and tracking method without distorted signals by phagocytosis of macrophages. *Theranostics*. (2014) 4:420–31. doi: 10.7150/thno.7265
52. Lee SY, Lee S, Lee J, Yhee JY, Yoon HI, Park S-J, et al. Non-invasive stem cell tracking in hindlimb ischemia animal model using bio-orthogonal copper-free click chemistry. *Biochem Biophys Res Commun*. (2016) 479:779–86. doi: 10.1016/j.bbrc.2016.09.132
53. Lee S, Yoon HI, Na JH, Jeon S, Lim S, Koo H, et al. *In vivo* stem cell tracking with imageable nanoparticles that bind bioorthogonal chemical receptors on the stem cell surface. *Biomaterials*. (2017) 139:12–29. doi: 10.1016/j.biomaterials.2017.05.050
54. Bailly C, Gouard S, Lacombe M, Saëc P, Chalopin B, Bourgeois M, et al. Comparison of Immuno-PET of CD138 and PET imaging with 64CuCl2 and 18F-FDG in a preclinical syngeneic model of multiple myeloma. *Oncotarget*. (2018) 9:9061–72. doi: 10.18632/oncotarget.23886
55. McCracken MN, Tavaré R, Witte ON, Wu AM. Advances in PET detection of the antitumor T cell response. *Adv Immunol*. (2016) 131:187–231. doi: 10.1016/bs.ai.2016.02.004
56. Beckford Vera DR, Smith CC, Bixby LM, Glatt DM, Dunn SS, Saito R, et al. Immuno-PET imaging of tumor-infiltrating lymphocytes using zirconium-89 radiolabeled anti-CD3 antibody in immune-competent mice bearing syngeneic tumors. *PLoS ONE*. (2018) 13:e0193832. doi: 10.1371/journal.pone.0193832
57. Mayer KE, Mall S, Yusufi N, Gosmann D, Steiger K, Russelli L, et al. T-cell functionality testing is highly relevant to developing novel immuno-tracers monitoring T cells in the context of immunotherapies and revealed CD7 as an attractive target. *Theranostics*. (2018) 8:6070–87. doi: 10.7150/thno.27275
58. Rashidian M, Ingram JR, Dougan M, Dongre A, Whang KA, LeGall C, et al. Predicting the response to CTLA-4 blockade by longitudinal noninvasive monitoring of CD8 T cells. *J Exp Med*. (2017) 214:2243–55. doi: 10.1084/jem.20161950
59. Abou DS, Ku T, Smith-Jones PM. *In vivo* biodistribution and accumulation of 89Zr in mice. HHS public access. *Nucl Med Biol*. (2011) 3812:675–81. doi: 10.1016/j.nucmedbio.2010.12.011
60. Bailly C, Bodet-Milin C, Rousseau C, Faivre-Chauvet A, Kraeber-Bodéré F, Barbet J. Pretargeting for imaging and therapy in oncological nuclear medicine. *EJNMMI Radiopharm Chem*. (2017) 2:6. doi: 10.1186/s41181-017-0026-8
61. Honarvar H, Westerlund K, Altai M, Sandström M, Orlova A, Tolmachev V, et al. Feasibility of affibody molecule-based PNA-mediated radionuclide pretargeting of malignant tumors. *Theranostics*. (2016) 6:93–103. doi: 10.7150/thno.12766
62. Rossin R, Renart Verkerk P, van den Bosch SM, Vulders RCM, Verel I, Lub J, et al. *In vivo* chemistry for pretargeted tumor imaging in live mice. *Angew Chemie Int Ed*. (2010) 49:3375–8. doi: 10.1002/anie.200906294
63. Zhang X, Wang B, Zhao N, Tian Z, Dai Y, Nie Y, et al. Improved tumor targeting and longer retention time of NIR fluorescent probes using bioorthogonal chemistry. *Theranostics*. (2017) 7:20912. doi: 10.7150/thno.20912
64. Chen H, Wang L, Yu Q, Qian W, Tiwari D, Yi H, et al. Anti-HER2 antibody and ScFvEGFR-conjugated antifouling magnetic iron oxide nanoparticles for targeting and magnetic resonance imaging of breast cancer. *Int J Nanomed*. (2013) 8:3781–94. doi: 10.2147/IJN.S49069
65. Alric C, Hervé-Aubert K, Aubrey N, Melouk S, Lajoie L, Même W, et al. Targeting HER2-breast tumors with scFv-decorated bimodal nanoprobes. *J Nanobiotechnol*. (2018) 16:18. doi: 10.1186/s12951-018-0341-6
66. Li Y, Soni PB, Liu L, Zhang X, Liotta DC, Lutz S. Synthesis of fluorescent nucleoside analogs as probes for 2′-deoxyribonucleoside kinases. *Bioorg Med Chem Lett*. (2010) 20:841–3. doi: 10.1016/j.bmcl.2009.12.097
67. Bar-Shir A, Alon L, Korrer MJ, Lim HS, Yadav NN, Kato Y, et al. Quantification and tracking of genetically engineered dendritic cells for studying immunotherapy. *Magn Reson Med*. (2018) 79:1010–9. doi: 10.1002/mrm.26708
68. van Krieken JH, Oyen WJG, de Vries IJM, Verdijk P, Figdor CG, Barentsz JO, et al. Magnetic resonance tracking of dendritic cells in melanoma patients for monitoring of cellular therapy. *Nat Biotechnol*. (2005) 23:1407–13. doi: 10.1038/nbt1154
69. Noh YW, Jang YS, Ahn KJ, Lim YT, Chung BH. Simultaneous *in vivo* tracking of dendritic cells and priming of an antigen-specific immune response. *Biomaterials*. (2011) 32:6254–63. doi: 10.1016/j.biomaterials.2011.05.013
70. Ahn B-C, Jeong SY, Lee J, Jeong H-J, Ahn SB, Lee SB, et al. Radionuclide-embedded gold nanoparticles for enhanced dendritic cell-based cancer immunotherapy, sensitive and quantitative tracking of dendritic cells with PET and Cerenkov luminescence. *NPG Asia Mater*. (2016) 8:e281. doi: 10.1038/am.2016.80
71. Sharif-Paghaleh E, Ratnasothy K, Sunassee K, Tavaré R, Alhabbab R, Mullen GE, et al. *In vivo* SPECT reporter gene imaging of regulatory T cells. *PLoS ONE*. (2011) 6:e25857. doi: 10.1371/journal.pone.0025857
72. Li YQ, Tang Y, Fu R, Meng QH, Zhou X, Ling ZM, et al. Efficient labeling *in vitro* with non-ionic gadolinium magnetic resonance imaging contrast agent and fluorescent transfection agent in bone marrow stromal cells of neonatal rats. *Mol Med Rep*. (2015) 12:913–20. doi: 10.3892/mmr.2015.3532
73. Conniot J, Gaspar R, Silva LC, Florindo HF, Silva JM, Fernandes JG, et al. Cancer immunotherapy: nanodelivery approaches for immune cell targeting and tracking. *Front Chem*. (2014) 2:1–27. doi: 10.3389/fchem.2014.00105
74. Bulte JWM, Daldrup-Link HE. Clinical tracking of cell transfer and cell transplantation: trials and tribulations. *Radiology*. (2018) 289:604–15. doi: 10.1148/radiol.2018180449
75. Man F, Lim L, Volpe A, Gabizon A, Shmeeda H, Draper B, et al. *In vivo* PET tracking of 89Zr-labeled Vγ9Vδ2 T cells to mouse xenograft breast

tumors activated with liposomal alendronate. *Mol Ther*. (2019) 27:219–29. doi: 10.1016/j.ymthe.2018.10.006
76. Lee SB, Lee HW, Singh TD, Li Y, Kim SK, Cho SJ, et al. Visualization of macrophage recruitment to inflammation lesions using highly sensitive and stable radionuclide-embedded gold nanoparticles as a nuclear bio-imaging platform. *Theranostics*. (2017) 7:926–34. doi: 10.7150/thno.17131
77. Signore A, Annovazzi A, Barone R, Bonanno E, D'Alessandria C, Chianelli M, et al. 99mTc-interleukin-2 scintigraphy as a potential tool for evaluating tumor-infiltrating lymphocytes in melanoma lesions: a validation study. *J Nucl Med*. (2004) 45:1647–52.
78. Patel SP, Kurzrock R. PD-L1 expression as a predictive biomarker in cancer immunotherapy. *Mol Cancer Ther*. (2015) 14:847–56. doi: 10.1158/1535-7163.MCT-14-0983
79. Natarajan A, Mayer AT, Xu L, Reeves RE, Gano J, Gambhir SS. Novel radiotracer for immunoPET imaging of PD-1 checkpoint expression on tumor infiltrating lymphocytes. *Bioconjug Chem*. (2015) 26:2062–9. doi: 10.1021/acs.bioconjchem.5b00318
80. Lanfranca MP, Lazarus J, Shao X, Nathan H, Di Magliano MP, Zou W, et al. Tracking macrophage infiltration in a mouse model of pancreatic cancer with the positron emission tomography tracer [11C]PBR28. *J Surg Res*. (2018) 232:570–7. doi: 10.1016/j.jss.2018.07.015
81. Al Faraj A, Sultana Shaik A, Pureza MA, Alnafea M, Halwani R. Preferential macrophage recruitment and polarization in LPS-induced animal model for COPD: noninvasive tracking using MRI. *PLoS ONE*. (2014) 9:e90829. doi: 10.1371/journal.pone.0090829
82. Valable S, Barbier EL, Bernaudin M, Roussel S, Segebarth C, Petit E, et al. *In vivo* MRI tracking of exogenous monocytes/macrophages targeting brain tumors in a rat model of glioma. *Neuroimage*. (2008) 40:973–83. doi: 10.1016/j.neuroimage.2008.01.005
83. Perez C, Jukica A, Listopad JJ, Anders K, Kühl AA, Loddenkemper C, et al. Permissive expansion and homing of adoptively transferred T cells in tumor-bearing hosts. *Int J Cancer*. (2015) 137:359–71. doi: 10.1002/ijc.29401
84. He H, Kanada M, Contag CH, Krishnan V, Schaar BT, Dorigo O, et al. Imaging of tumor-associated macrophages in a transgenic mouse model of orthotopic ovarian cancer. *Mol Imaging Biol*. (2017) 19:694–702. doi: 10.1007/s11307-017-1061-2
85. Yang R, Sarkar S, Yong VW, Dunn JF. *In vivo* MR imaging of tumor-associated macrophages: the next frontier in cancer imaging. *Magn Reson Insights*. (2018) 11:1178623X1877197. doi: 10.1177/1178623X18771974
86. Wahl RL, Jacene H, Kasamon Y, Lodge MA. From RECIST to PERCIST: evolving Considerations for PET response criteria in solid tumors. *J Nucl Med*. (2009) 50(Suppl. 1):122S−50S. doi: 10.2967/jnumed.108.057307
87. Cammilleri S, Labeille B, Kelly A, Isnardi V, D'Incan M, Tychyj C, et al. 123I-BZA2 as a melanin-targeted radiotracer for the identification of melanoma metastases: results and perspectives of a multicenter phase III clinical trial. *J Nucl Med*. (2013) 55:15–22. doi: 10.2967/jnumed.113.123554
88. Ren G, Liu Z, Miao Z, Liu H, Subbarayan M, Chin FT, et al. PET of malignant melanoma using 18F-labeled metallopeptides. *J Nucl Med*. (2009) 50:1865–72. doi: 10.2967/jnumed.109.062877
89. Lee ST, Burvenich I, Scott AM. Novel target selection for nuclear medicine studies. *Semin Nucl Med*. (2019) 49:357–68. doi: 10.1053/j.semnuclmed.2019.06.004
90. Verhoeff SR, van den Heuvel MM, van Herpen CML, Piet B, Aarntzen EHJG, Heskamp S. Programmed cell death-1/ligand-1 PET imaging. *PET Clin*. (2019) 15:35–43. doi: 10.1016/j.cpet.2019.08.008
91. Hinrichs CS, Turcotte S, Wunderlich JR, Dudley ME, Hogan K, Gros A, et al. Phenotype and function of T cells infiltrating visceral metastases from gastrointestinal cancers and melanoma: implications for adoptive cell transfer therapy. *J Immunol*. (2013) 191:2217–25. doi: 10.4049/jimmunol.1300538
92. Seo JW, Tavaré R, Mahakian LM, Silvestrini MT, Tam S, Ingham ES, et al. CD8+ T-cell density imaging with 64Cu-labeled cys-diabody informs immunotherapy protocols. *Clin Cancer Res*. (2018) 24:4976–87. doi: 10.1158/1078-0432.CCR-18-0261
93. Markovic S, Galli F, Suman VJ, Nevala WK, Paulsen AM, Hung JC, et al. Non-invasive clinical visualization of tumor infiltrating lymphocytes in patients with metastatic melanoma undergoing immune checkpoint inhibitor therapy: a pilot study. *J Clin Oncol*. (2017) 35:3034. doi: 10.1200/JCO.2017.35.15_suppl.3034
94. Narang S, Kim D, Aithala S, Heimberger AB, Ahmed S, Rao D, et al. Tumor image-derived texture features are associated with CD3 T-cell infiltration status in glioblastoma. *Oncotarget*. (2017) 8:101244–54. doi: 10.18632/oncotarget.20643
95. Sun R, Limkin EJ, Vakalopoulou M, Dercle L, Champiat S, Han SR, et al. A radiomics approach to assess tumour-infiltrating CD8 cells and response to anti-PD-1 or anti-PD-L1 immunotherapy: an imaging biomarker, retrospective multicohort study. *Lancet Oncol*. (2018) 19:1180–91. doi: 10.1016/S1470-2045(18)30413-3
96. Mantovani A, Marchesi F, Malesci A, Laghi L, Allavena P. Tumour-associated macrophages as treatment targets in oncology. *Nat Rev Clin Oncol*. (2017) 14:399–416. doi: 10.1038/nrclinonc.2016.217
97. Eisenblatter M, Ehrchen J, Varga G, Sunderkotter C, Heindel W, Roth J, et al. *In vivo* optical imaging of cellular inflammatory response in granuloma formation using fluorescence-labeled macrophages. *J Nucl Med*. (2009) 50:1676–82. doi: 10.2967/jnumed.108.060707
98. Terry SYA, Nayak TK, Oyen WJ, Klein C, Laverman P, Koenders MI, et al. Monitoring therapy response of experimental arthritis with radiolabeled tracers targeting fibroblasts, macrophages, or integrin v 3. *J Nucl Med*. (2015) 57:467–72. doi: 10.2967/jnumed.115.162628
99. Nahrendorf M, Zhang H, Hembrador S, Panizzi P, Sosnovik DE, Aikawa E, et al. Nanoparticle PET-CT imaging of macrophages in inflammatory atherosclerosis. *Circulation*. (2008) 117:379–87. doi: 10.1161/CIRCULATIONAHA.107.741181
100. Terry SYA, Boerman OC, Gerrits D, Franssen GM, Metselaar JM, Lehmann S, et al. 111In-anti-F4/80-A3-1 antibody: a novel tracer to image macrophages. *Eur J Nucl Med Mol Imaging*. (2015) 42:1430–8. doi: 10.1007/s00259-015-3084-8
101. Yang R, Sarkar S, Korchinski DJ, Wu Y, Yong VW, Dunn JF. MRI monitoring of monocytes to detect immune stimulating treatment response in brain tumor. *Neuro Oncol*. (2016) 19:now180. doi: 10.1093/neuonc/now180
102. Aarntzen EHJG, Srinivas M, Radu CG, Punt CJA, Boerman OC, Figdor CG, et al. *In vivo* imaging of therapy-induced anti-cancer immune responses in humans. *Cell Mol Life Sci*. (2013) 70:2237–57. doi: 10.1007/s00018-012-1159-2
103. Radu CG, Shu CJ, Nair-Gill E, Shelly SM, Barrio JR, Satyamurthy N, et al. Molecular imaging of lymphoid organs and immune activation by positron emission tomography with a new [18F]-labeled 2'-deoxycytidine analog. *Nat Med*. (2008) 14:783–8. doi: 10.1038/nm1724
104. Chen R, Zhou X, Liu J, Huang G. Relationship between the expression of PD-1/PD-L1 and 18F-FDG uptake in bladder cancer. *Eur J Nucl Med Mol Imaging*. (2019) 11:12270–7. doi: 10.1007/s00259-018-4208-8
105. Pardoll DM. The blockade of immune checkpoints in cancer immunotherapy. *Nat Rev Cancer*. (2012) 12:252–64. doi: 10.1038/nrc3239
106. Katz SC, Pillarisetty V, Bamboat ZM, Shia J, Hedvat C, Gonen M, et al. T cell infiltrate predicts long-term survival following resection of colorectal cancer liver metastases. *Ann Surg Oncol*. (2009) 16:2524–30. doi: 10.1245/s10434-009-0585-3
107. Ehlerding EB, England CG, Majewski RL, Valdovinos HF, Jiang D, Liu G, et al. ImmunoPET imaging of CTLA-4 expression in mouse models of non-small cell lung cancer. *Mol Pharm*. (2017) 14:1782–9. doi: 10.1021/acs.molpharmaceut.7b00056
108. Buder-Bakhaya K, Hassel JC. Biomarkers for clinical benefit of immune checkpoint inhibitor treatment-a review from the melanoma perspective and beyond. *Front Immunol*. (2018) 9:1474. doi: 10.3389/fimmu.2018.01474
109. Kikuchi M, Clump DA, Srivastava RM, Sun L, Zeng D, Diaz-Perez JA, et al. Preclinical immunoPET/CT imaging using Zr-89-labeled anti-PD-L1 monoclonal antibody for assessing radiation-induced PD-L1 upregulation in head and neck cancer and melanoma. *Oncoimmunology*. (2017) 6:1–13. doi: 10.1080/2162402X.2017.1329071
110. Broos K, Lecocq Q, Raes G, Devoogdt N, Keyaerts M, Breckpot K. Noninvasive imaging of the PD-1: PD-L1 immune checkpoint: embracing nuclear medicine for the benefit of personalized immunotherapy. *Theranostics*. (2018) 8:3559–70. doi: 10.7150/thno.24762

111. Faure M, Rochigneux P, Olive D, Taix S, Brenot-Rossi I, Gilabert M. Hyperprogressive disease in anorectal melanoma treated by PD-1 inhibitors. *Front Immunol.* (2018) 9:797. doi: 10.3389/fimmu.2018.00797
112. Bensch F, van der Veen EL, Lub-de Hooge MN, Jorritsma-Smit A, Boellaard R, Kok IC, et al. 89Zr-atezolizumab imaging as a non-invasive approach to assess clinical response to PD-L1 blockade in cancer. *Nat Med.* (2018) 24:1852–8. doi: 10.1038/s41591-018-0255-8
113. Gibson HM, McKnight BN, Malysa A, Dyson G, Wiesend WN, McCarthy CE, et al. IFNg PET imaging as a predictive tool for monitoring response to tumor immunotherapy. *Cancer Res.* (2018) 78:5706–17. doi: 10.1158/0008-5472.CAN-18-0253
114. Kircher M, Herhaus P, Schottelius M, Buck AK, Werner RA, Wester H-J, et al. CXCR4-directed theranostics in oncology and inflammation. *Ann Nucl Med.* (2018) 32:503–11. doi: 10.1007/s12149-018-1290-8
115. Streeter JE, Gessner RC, Tsuruta J, Feingold S, Dayton PA. Assessment of molecular imaging of angiogenesis with three-dimensional ultrasonography. *Mol Imaging.* (2011) 10:460–8. doi: 10.2310/7290.2011.00015
116. Sui WF, Chen X, Peng ZK, Ye J, Wu JT. The diagnosis of metastatic axillary lymph nodes of breast cancer by diffusion weighted imaging: a meta-analysis and systematic review. *World J Surg Oncol.* (2016) 14:155. doi: 10.1186/s12957-016-0906-5
117. Griessinger CM, Kehlbach R, Bukala D, Wiehr S, Bantleon R, Cay F, et al. *In vivo* tracking of Th1 cells by PET reveals quantitative and temporal distribution and specific homing in lymphatic tissue. *J Nucl Med.* (2014) 55:301–7. doi: 10.2967/jnumed.113.126318
118. Sancey L, Ardisson V, Riou LM, Ahmadi M, Marti-Batlle D, Boturyn D, et al. *In vivo* imaging of tumour angiogenesis in mice with the αvβ3 integrin-targeted tracer 99mTc-RAFT-RGD. *Eur J Nucl Med Mol Imaging.* (2007) 34:2037–47. doi: 10.1007/s00259-007-0497-z
119. Jin Z-H, Furukawa T, Claron M, Boturyn D, Coll J-L, Fukumura T, et al. Positron emission tomography imaging of tumor angiogenesis and monitoring of antiangiogenic efficacy using the novel tetrameric peptide probe 64Cu-cyclam-RAFT-c(-RGDfK-)4. *Angiogenesis.* (2012) 15:569–80. doi: 10.1007/s10456-012-9281-1
120. Galbán CJ, Hoff BA, Chenevert TL, Ross BD. Diffusion MRI in early cancer therapeutic response assessment. *NMR Biomed.* (2017) 30:e3458. doi: 10.1002/nbm.3458
121. Pham W, Xie J, Gore JC. Tracking the migration of dendritic cells by *in vivo* optical imaging. *Neoplasia.* (2007) 9:1130–7. doi: 10.1593/neo.07586
122. Muccioli M, Pate M, Omosebi O, Benencia F. Generation and labeling of murine bone marrow-derived dendritic cells with Qdot nanocrystals for tracking studies. *J Vis Exp*. (2011) e2785. doi: 10.3791/2785
123. Long CM, van Laarhoven HWM, Bulte JWM, Levitsky HI. Magnetovaccination as a novel method to assess and quantify dendritic cell tumor antigen capture and delivery to lymph nodes. *Cancer Res.* (2009) 69:3180–7. doi: 10.1158/0008-5472.CAN-08-3691
124. Asiedu KO, Koyasu S, Szajek LP, Choyke PL, Sato N. Bone marrow cell trafficking analyzed by 89 Zr-oxine positron emission tomography in a murine transplantation model. *Clin Cancer Res.* (2017) 23:2759–68. doi: 10.1158/1078-0432.CCR-16-1561
125. Asiedu KO, Ferdousi M, Ton PT, Adler SS, Choyke PL, Sato N. Bone marrow cell homing to sites of acute tibial fracture: 89Zr-oxine cell labeling with positron emission tomographic imaging in a mouse model. *EJNMMI Res.* (2018) 8:109. doi: 10.1186/s13550-018-0463-8
126. Kanwar B, Gao DW, Hwang AB, Grenert JP, Williams SP, Franc B, et al. *In vivo* imaging of mucosal CD4+ T cells using single photon emission computed tomography in a murine model of colitis. *J Immunol Methods.* (2008) 329:21–30. doi: 10.1016/j.jim.2007.09.008
127. Srinivas M, Turner MS, Janjic JM, Morel PA, Laidlaw DH, Ahrens ET. *In vivo* cytometry of antigen-specific T cells using 19F MRI. *Magn Reson Med.* (2009) 62:747–53. doi: 10.1002/mrm.22063
128. Tremblay M-L, Davis C, Bowen CV, Stanley O, Parsons C, Weir G, et al. Using MRI cell tracking to monitor immune cell recruitment in response to a peptide-based cancer vaccine. *Magn Reson Med.* (2018) 80:304–16. doi: 10.1002/mrm.27018
129. Srinivas M, Aarntzen EHJG, Bulte JWM, Oyen WJ, Heerschap A, de Vries IJM, et al. Imaging of cellular therapies. *Adv Drug Deliv Rev*. (2010) 62:1080–93. doi: 10.1016/j.addr.2010.08.009
130. Verdijk P, Aarntzen EHJG, Lesterhuis WJ, Boullart ACI, Kok E, van Rossum MM, et al. Limited amounts of dendritic cells migrate into the T-cell area of lymph nodes but have high immune activating potential in melanoma patients. *Clin Cancer Res.* (2009) 15:2531–40. doi: 10.1158/1078-0432.CCR-08-2729
131. Laverman P, de Vries IJM, Scharenborg NM, de Boer A, Broekema M, Oyen WJG, et al. Development of 111In-labeled tumor-associated antigen peptides for monitoring dendritic-cell-based vaccination. *Nucl Med Biol.* (2006) 33:453–8. doi: 10.1016/j.nucmedbio.2006.02.005
132. Emami-Shahri N, Papa S. Dynamic imaging for CAR-T-cell therapy. *Biochem Soc Trans.* (2016) 44:386–90. doi: 10.1042/BST20150257
133. Bhatnagar P, Alauddin M, Bankson JA, Kirui D, Seifi P, Huls H, et al. Tumor lysing genetically engineered T cells loaded with multi-modal imaging agents. *Sci Rep.* (2014) 4:4502. doi: 10.1038/srep04502
134. Chapelin F, Gao S, Okada H, Weber TG, Messer K, Ahrens ET. Fluorine-19 nuclear magnetic resonance of chimeric antigen receptor T cell biodistribution in murine cancer model. *Sci Rep.* (2017) 7:17748. doi: 10.1038/s41598-017-17669-4
135. Mall S, Yusufi N, Wagner R, Klar R, Bianchi H, Steiger K, et al. Immuno-PET imaging of engineered human T cells in tumors. *Cancer Res.* (2016) 76:4113–23. doi: 10.1158/0008-5472.CAN-15-2784
136. Wang S, O'Rourke DM, Chawla S, Verma G, Nasrallah MP, Morrissette JJD, et al. Multiparametric magnetic resonance imaging in the assessment of anti-EGFRvIII chimeric antigen receptor T cell therapy in patients with recurrent glioblastoma. *Br J Cancer*. (2019) 120:54–6. doi: 10.1038/s41416-018-0342-0
137. Uong TNT, Lee KH, Ahn SJ, Kim KW, Min JJ, Hyun H, et al. Real-time tracking of *ex vivo*-expanded natural killer cells toward human triple-negative breast cancers. *Front Immunol.* (2018) 9:1–14. doi: 10.3389/fimmu.2018.00825
138. Garikipati VNS, Jadhav S, Pal L, Prakash P, Dikshit M, Nityanand S. Mesenchymal stem cells from fetal heart attenuate myocardial injury after infarction: an *in vivo* serial pinhole gated SPECT-CT study in rats. *PLoS ONE.* (2014) 9:1–10. doi: 10.1371/journal.pone.0100982
139. Schubert R, Sann J, Frueh JT, Ullrich E, Geiger H, Baer PC. Tracking of adipose-derived mesenchymal stromal/stem cells in a model of cisplatin-induced acute kidney injury: comparison of bioluminescence imaging vs. qRT-PCR. *Int J Mol Sci.* (2018) 19:1–12. doi: 10.3390/ijms19092564
140. Kalimuthu S, Zhu L, Oh JM, Gangadaran P, Lee HW, Baek SH, et al. Migration of mesenchymal stem cells to tumor xenograft models and *in vitro* drug delivery by doxorubicin. *Int J Med Sci.* (2018) 15:1051–61. doi: 10.7150/ijms.25760
141. Scarfe L, Taylor A, Sharkey J, Harwood R, Barrow M, Comenge J, et al. Non-invasive imaging reveals conditions that impact distribution and persistence of cells after *in vivo* administration. *bioRxiv [Preprint].* (2018). doi: 10.1101/202101
142. Palestro CJ, Love C, Bhargava KK. Labeled leukocyte imaging: current status and future directions. *Q J Nucl Med Mol Imaging.* (2009) 53:105–23.

Conflict of Interest: The authors declare that the research was conducted in the absence of any commercial or financial relationships that could be construed as a potential conflict of interest.

Advantages of publishing in Frontiers

OPEN ACCESS
Articles are free to read for greatest visibility and readership

FAST PUBLICATION
Around 90 days from submission to decision

HIGH QUALITY PEER-REVIEW
Rigorous, collaborative, and constructive peer-review

TRANSPARENT PEER-REVIEW
Editors and reviewers acknowledged by name on published articles

Frontiers
Avenue du Tribunal-Fédéral 34
1005 Lausanne | Switzerland

Visit us: www.frontiersin.org
Contact us: info@frontiersin.org | +41 21 510 17 00

REPRODUCIBILITY OF RESEARCH
Support open data and methods to enhance research reproducibility

DIGITAL PUBLISHING
Articles designed for optimal readership across devices

FOLLOW US
@frontiersin

IMPACT METRICS
Advanced article metrics track visibility across digital media

EXTENSIVE PROMOTION
Marketing and promotion of impactful research

LOOP RESEARCH NETWORK
Our network increases your article's readership